CHAPTER V

RESULT AND DISCUSSION

5.1 Stochastic Simulation Results

The process of dendritic deposition is very complex and difficult to predict. The particle deposition process has been simulated stochastically using Monte-Carlo technique, under various filtration conditions of convective Brownian diffusion as well as inertial impaction.

5.1.1 Convective Brownian diffusional deposition

The dendritic growth of convective diffusional deposition was simulated using stochastic model for various filtration conditions. The dendrites caused increase in the collection efficiency of a dust-loaded fiber. The positions of particles deposited on the fiber can be obtained by the stochatic simulation. Figures 5.1-5.30 show the configuration of dendrites. The typical dendrites were densely packed when the interception parameter R was small but was more porous when R was large. Furthermore, the configuration of the dendrites was tall and slender at a large Pe. On the other hand, the particles were captured more uniformly over the entire fiber surface at a small Pe.

The particle collection efficiency was evaluated using the Monte-Carlo simulation results. The clean fiber collection efficiency can be obtained from the equation of Stechkina and Fuchs (1966). The collection efficiency raising factor λ listed in Table 5.1 and Table 5.2 shows the difference in λ between the previous stochastic study (Kanaoka et al., 1983) and the present study. According to the previous study, λ values were higher than the present corresponding values for the case of R=0.1 but were nearly equal to those λ for the corresponding case of R=0.2. In the present study, the starting point of an incoming particle was at the generation plane of Kuwabara's cell. But in previous study, they reduced the required

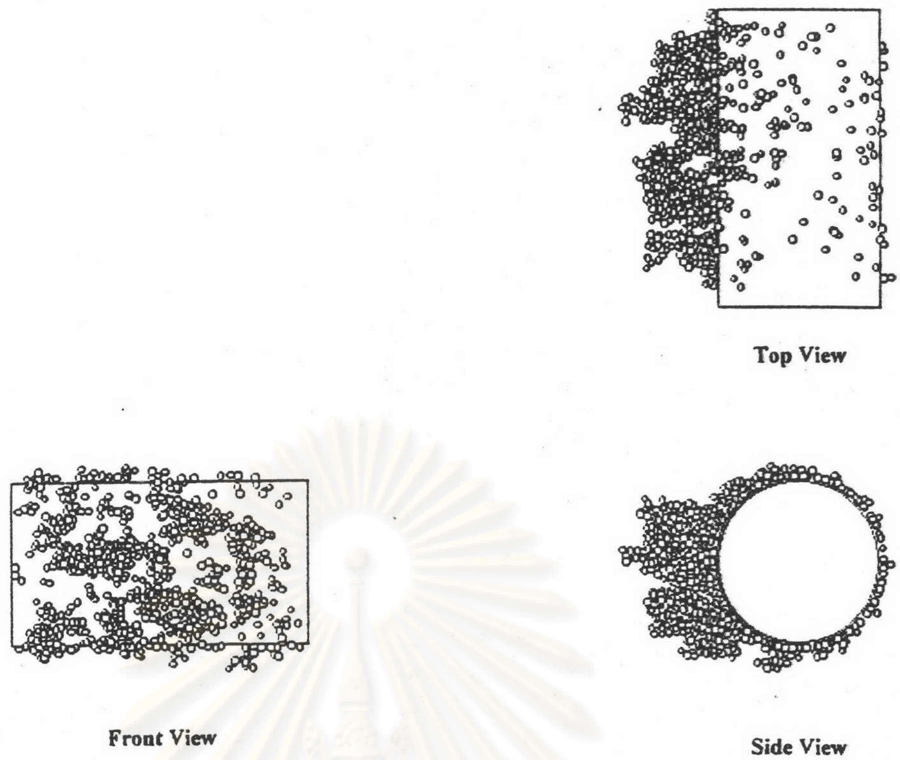

Figure 5.1. Typical configurations of dendrites for R=0.05 and Pe=200

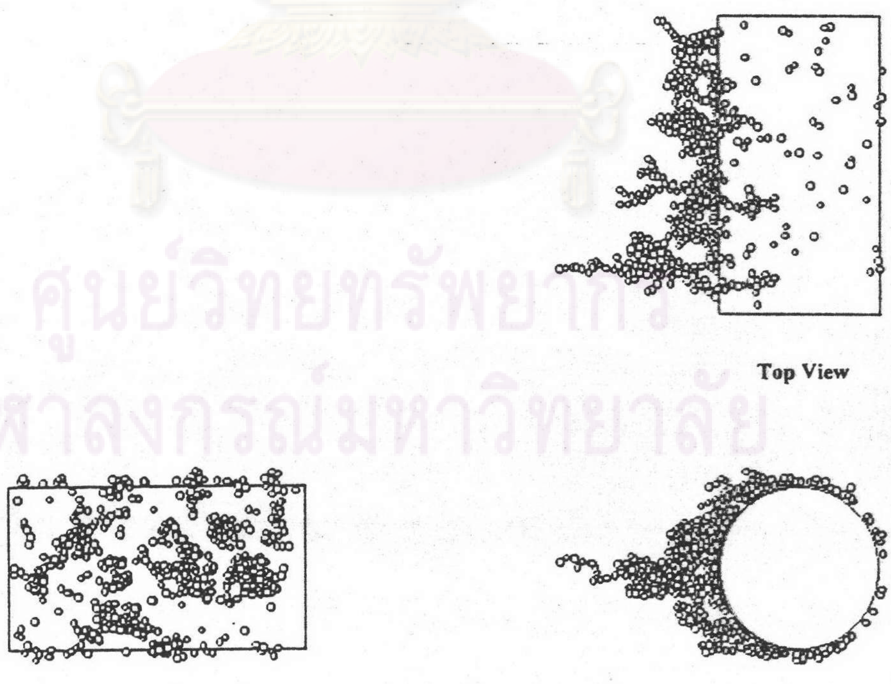

Figure 5.2. Typical configurations of dendrites for R=0.05 and Pe=500

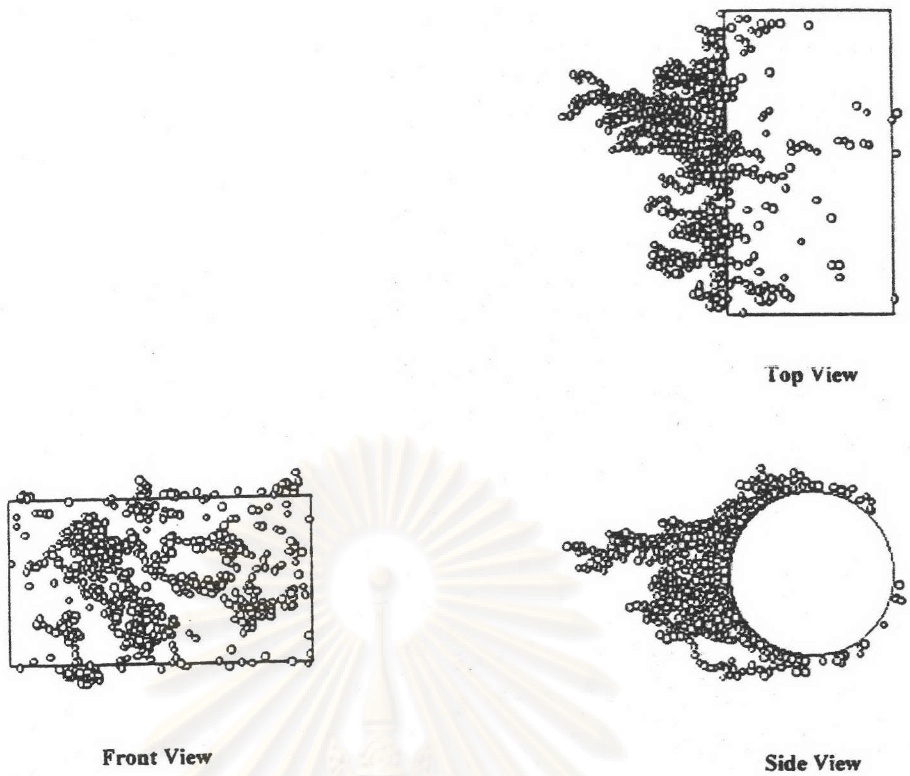

Figure 5.3. Typical configurations of dendrites for R=0.05 and Pe=1000

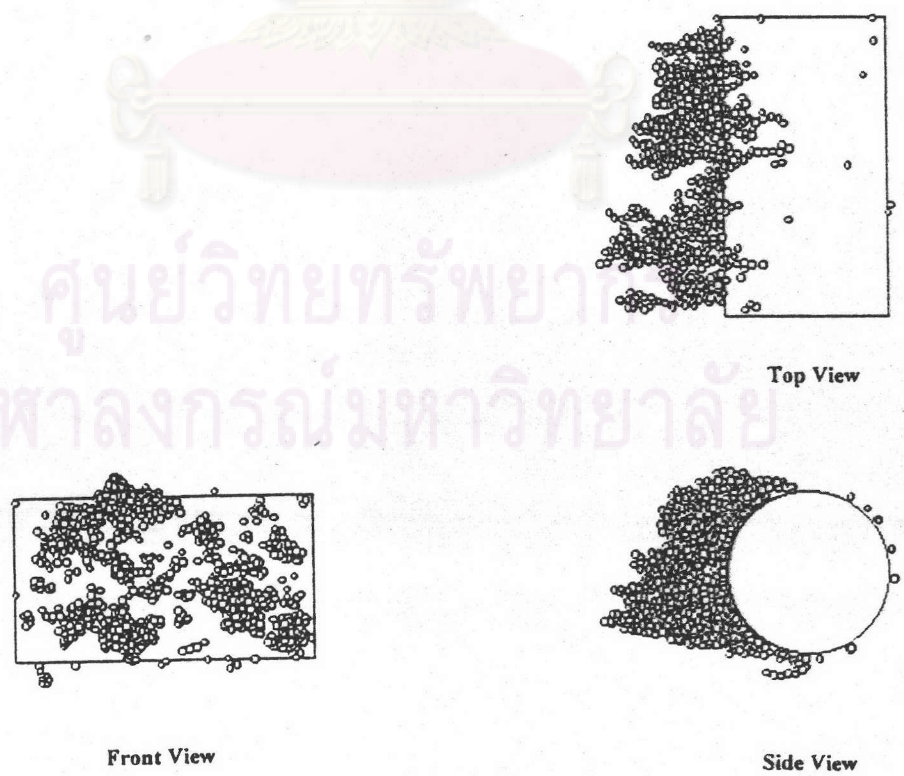

Figure 5.4. Typical configurations of dendrites for R=0.05 and Pe=2500

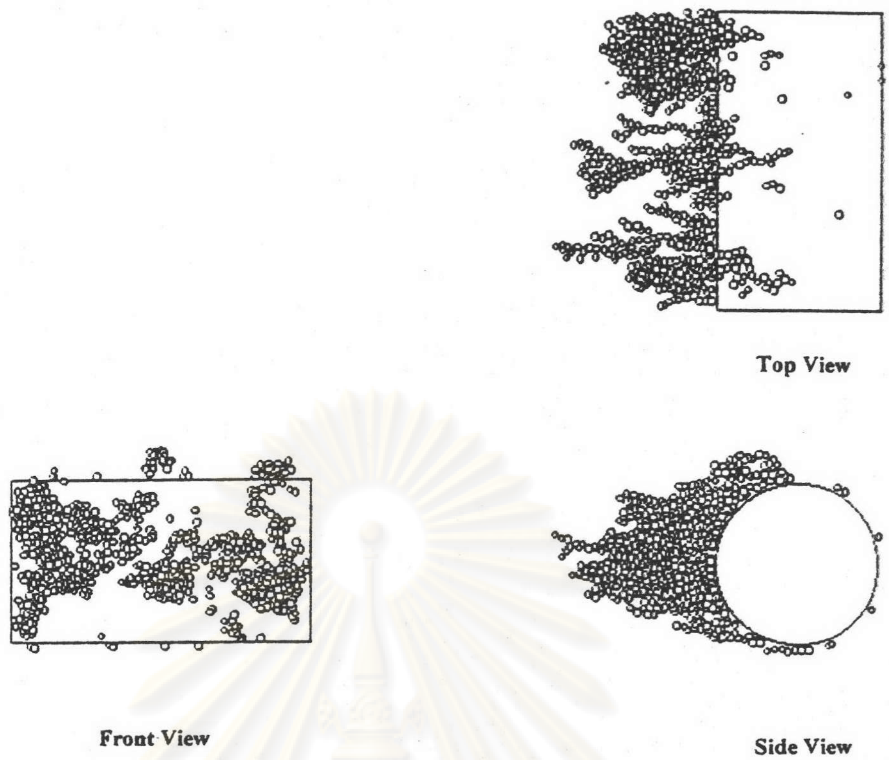

Figure 5.5. Typical configurations of dendrites for R=0.05 and Pe=5000

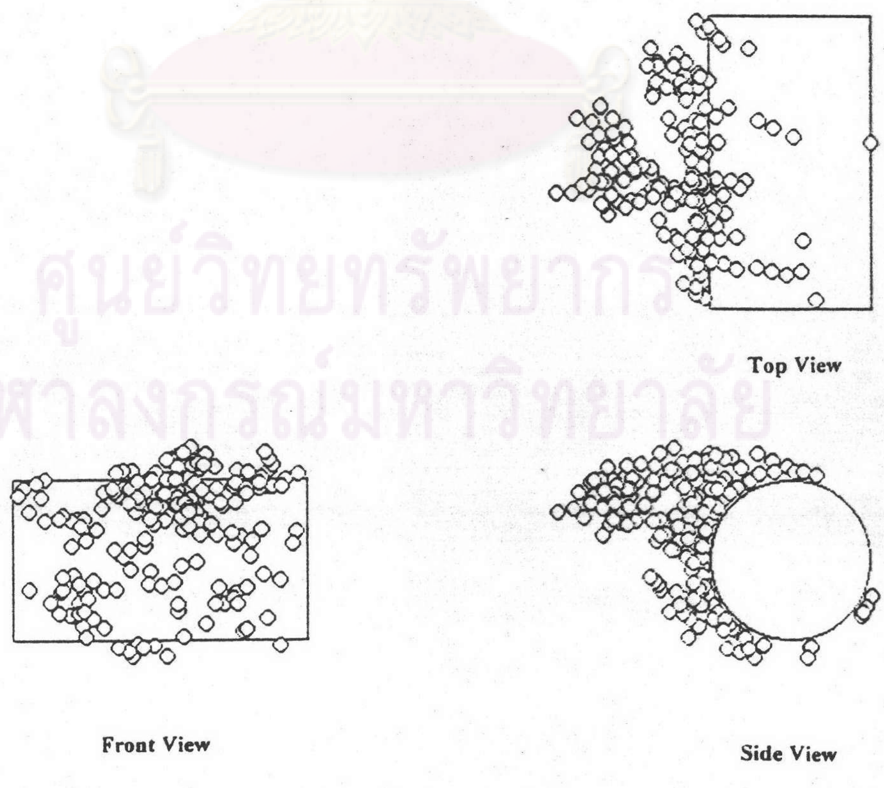

Figure 5.6. Typical configurations of dendrites for R=0.1 and Pe=200

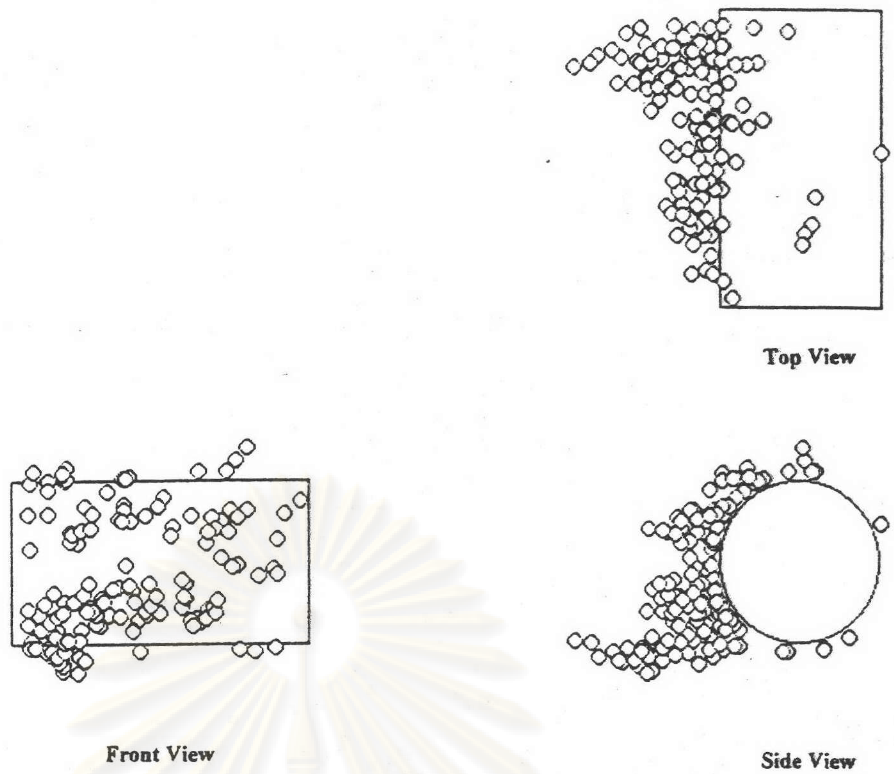

Figure 5.7. Typical configurations of dendrites for R=0.1 and Pe=500

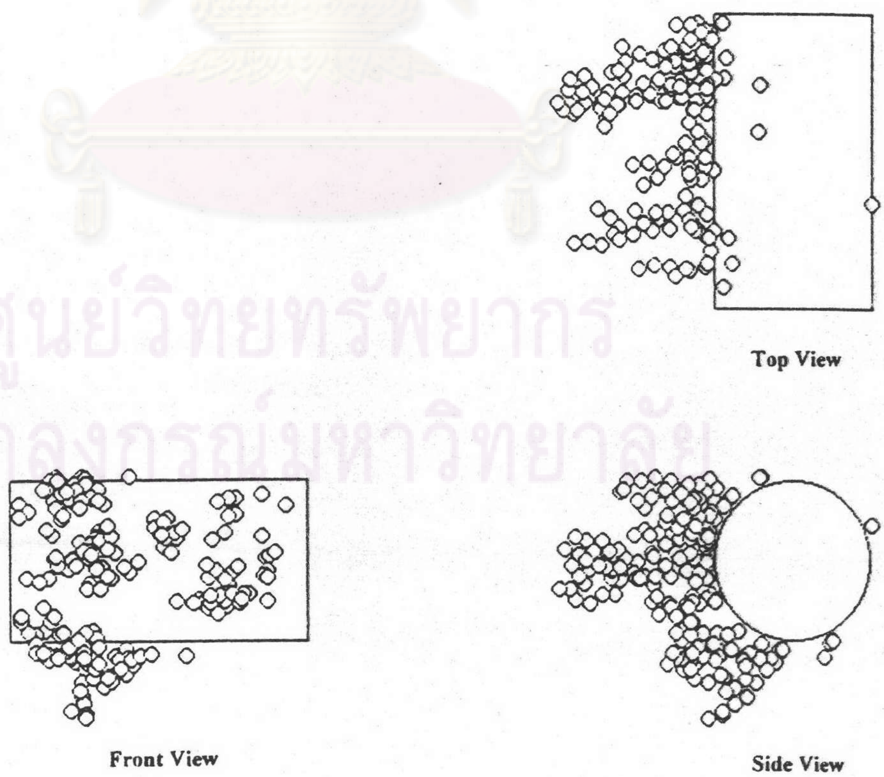

Figure 5.8. Typical configurations of dendrites for R=0.1 and Pe=1000

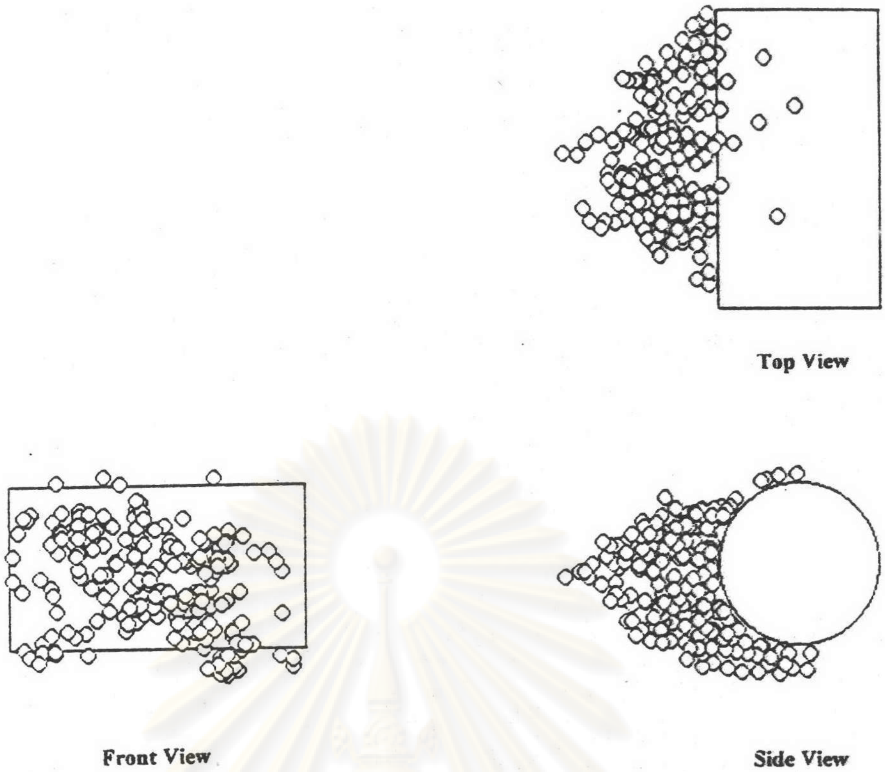

Figure 5.9. Typical configurations of dendrites for R=0.1 and Pe=2500

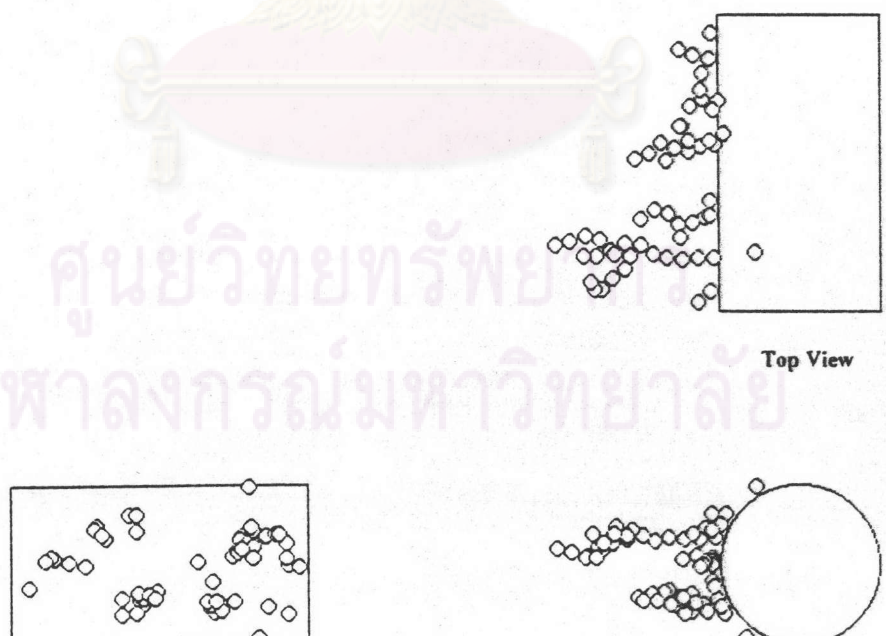

Figure 5.10. Typical configurations of dendrites for R=0.1 and Pe=5000

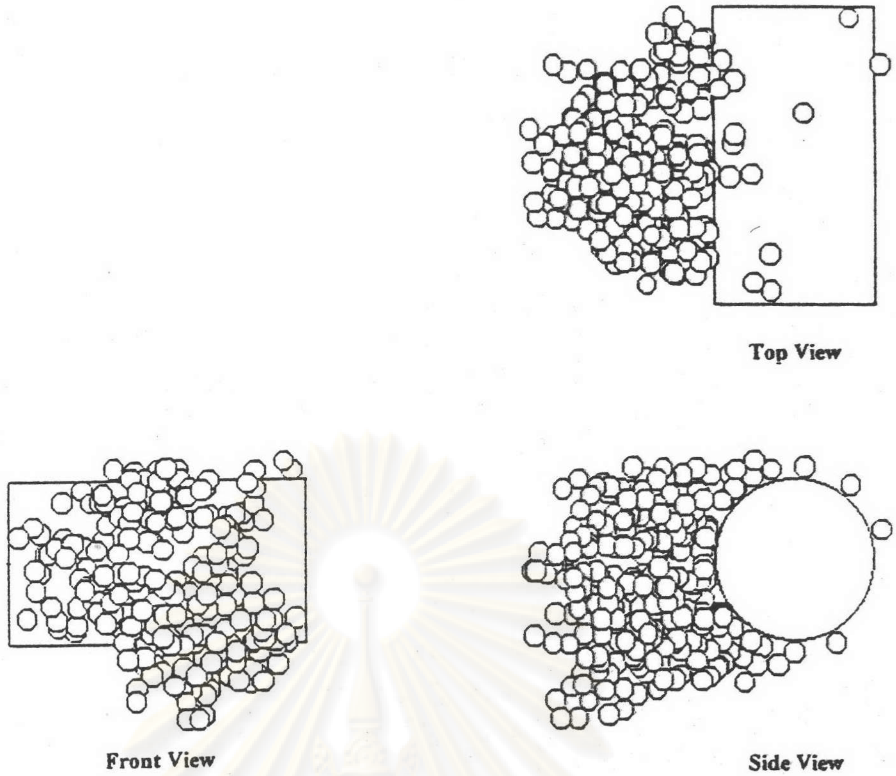

Figure 5.11. Typical configurations of dendrites for R=0.13 and Pe=200

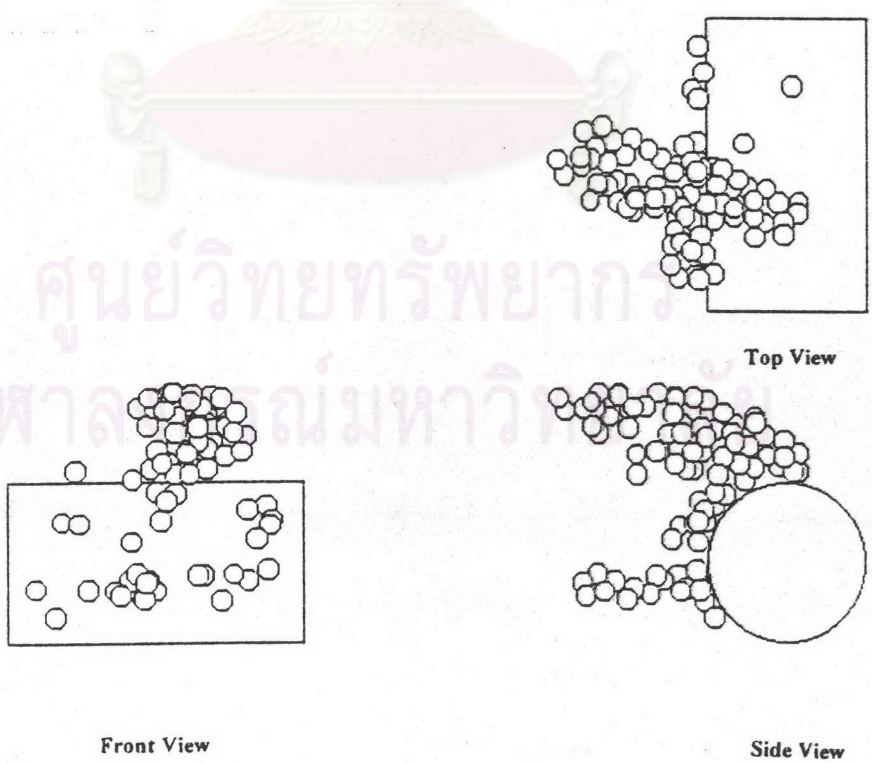

Figure 5.12. Typical configurations of dendrites for R=0.13 and Pe=500

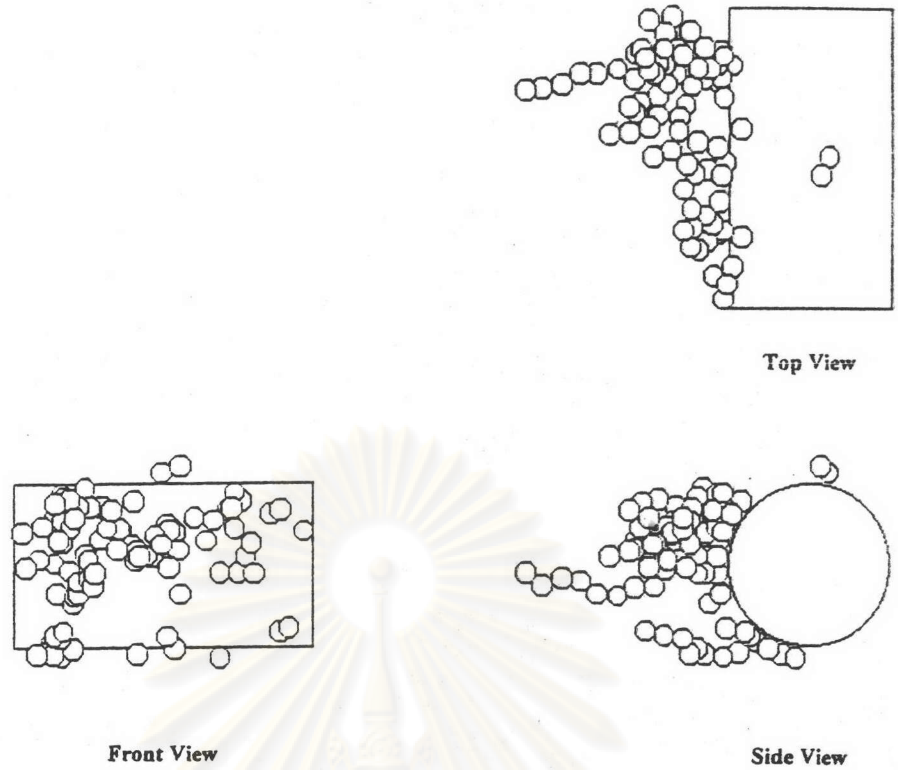

Figure 5.13. Typical configurations of dendrites for R=0.13 and Pe=1000

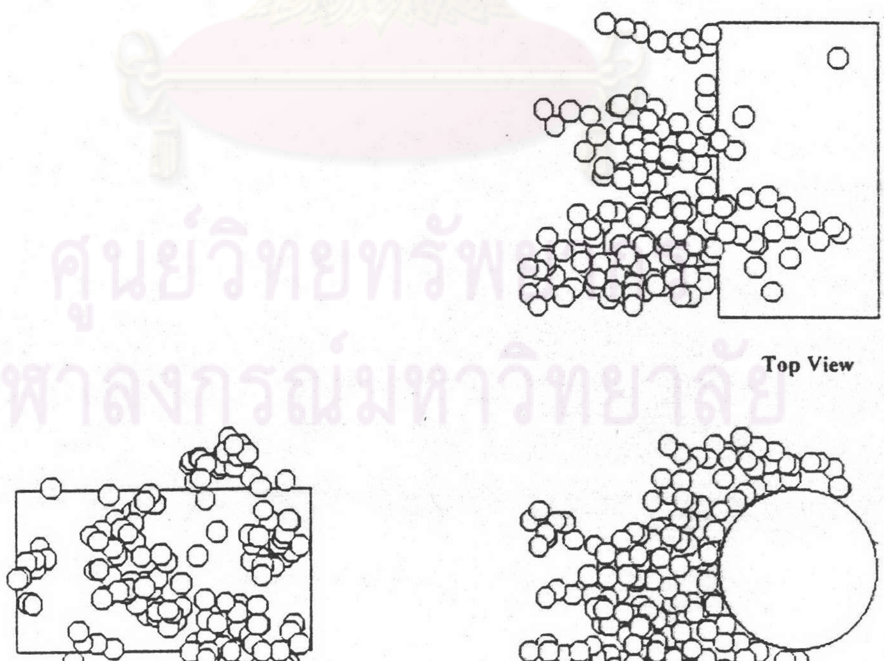

Figure 5.14. Typical configurations of dendrites for R=0.13 and Pe=2500

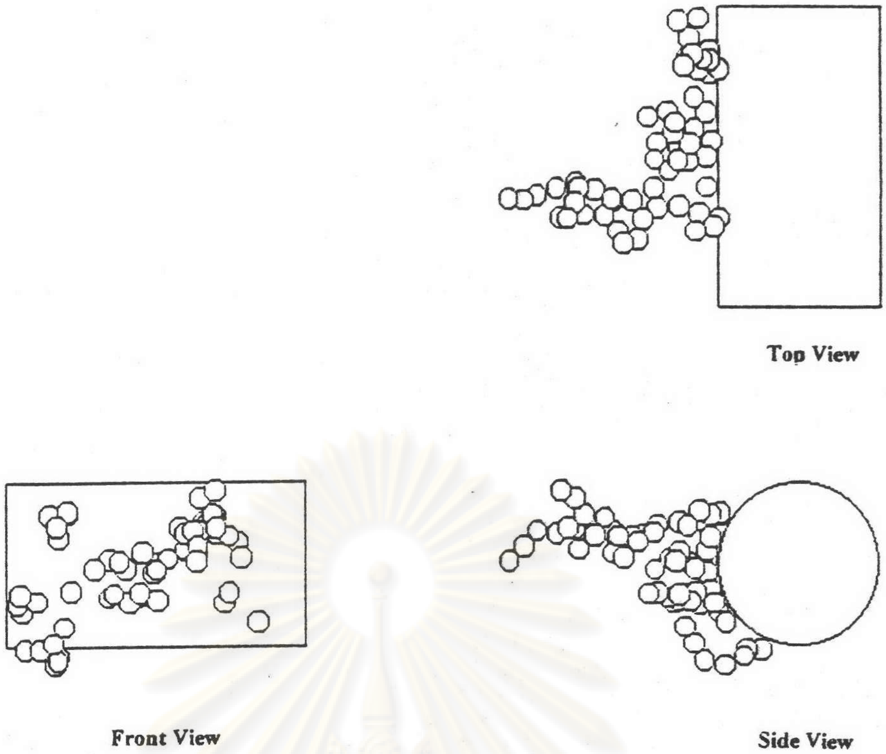

Figure 5.15. Typical configurations of dendrites for R=0.13 and Pe=5000

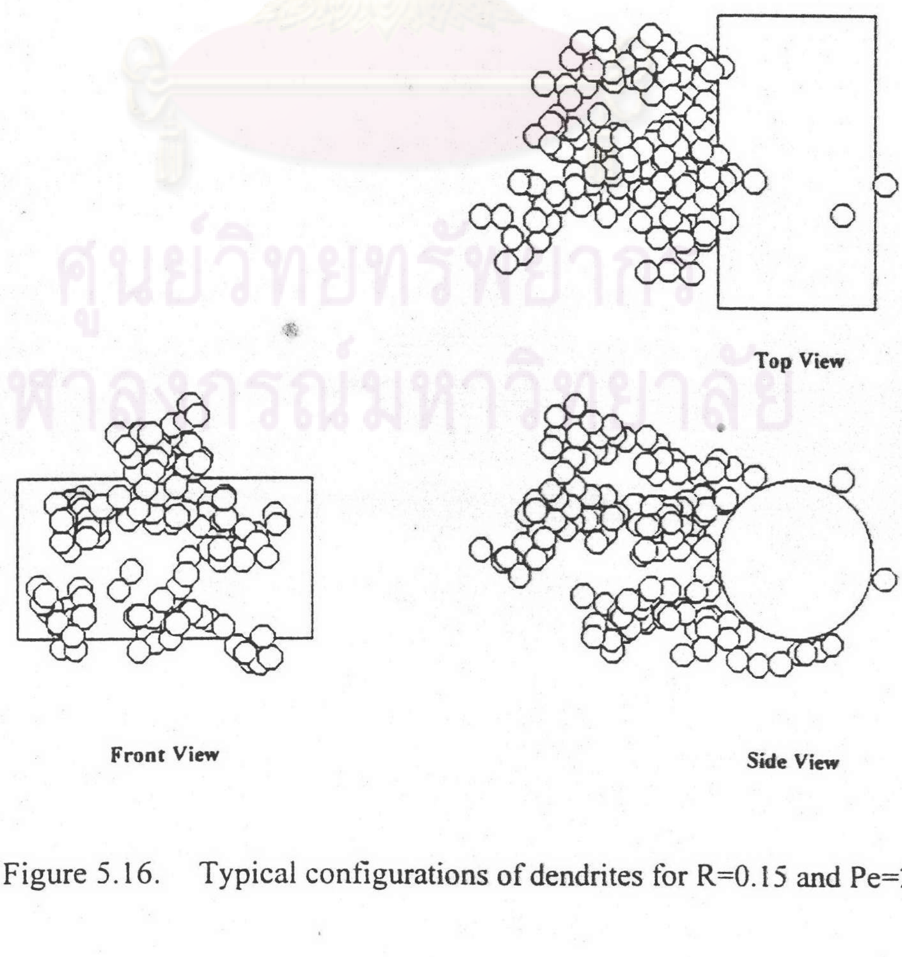

Figure 5.16. Typical configurations of dendrites for R=0.15 and Pe=200

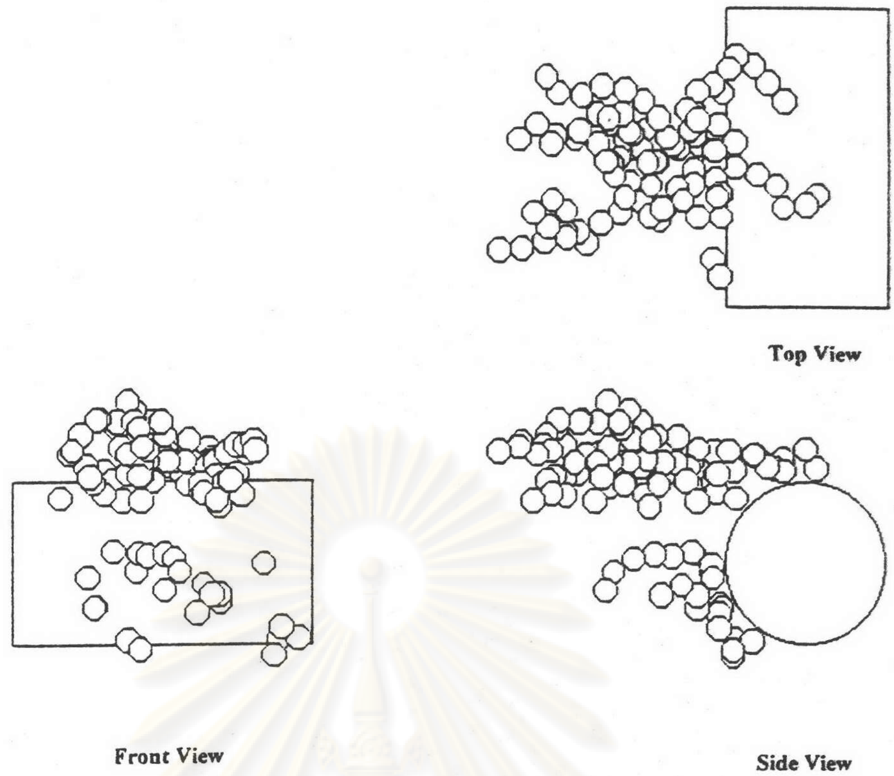

Figure 5.17. Typical configurations of dendrites for R=0.15 and Pe=500

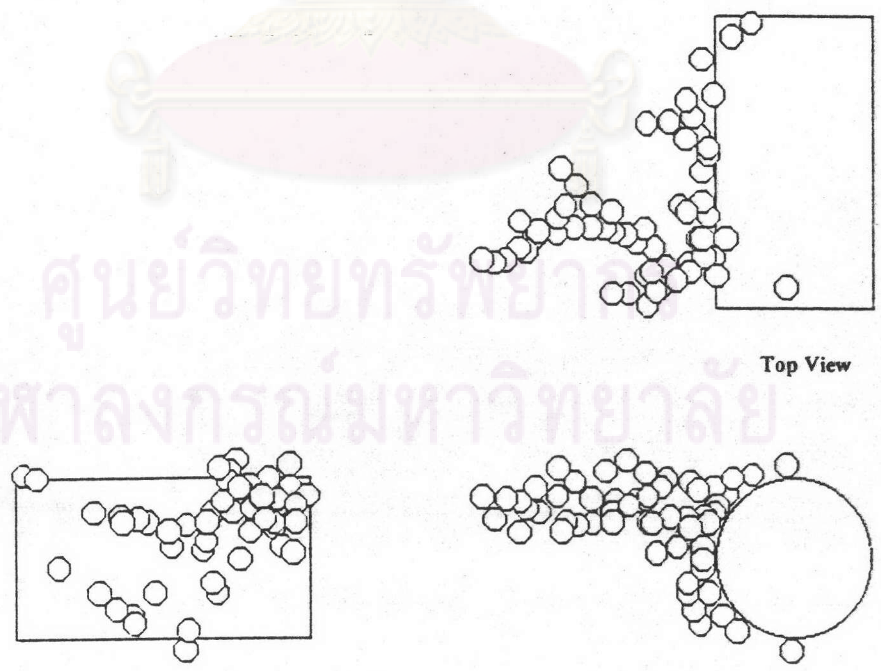

Figure 5.18. Typical configurations of dendrites for R=0.15 and Pe=1000

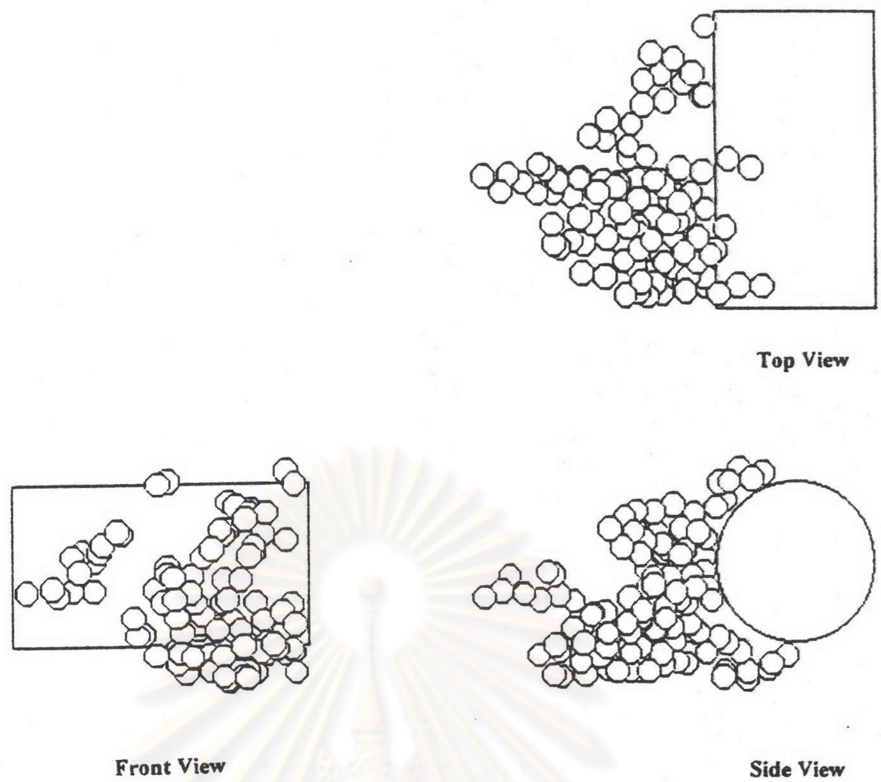

Figure 5.19. Typical configurations of dendrites for R=0.15 and Pe=2500

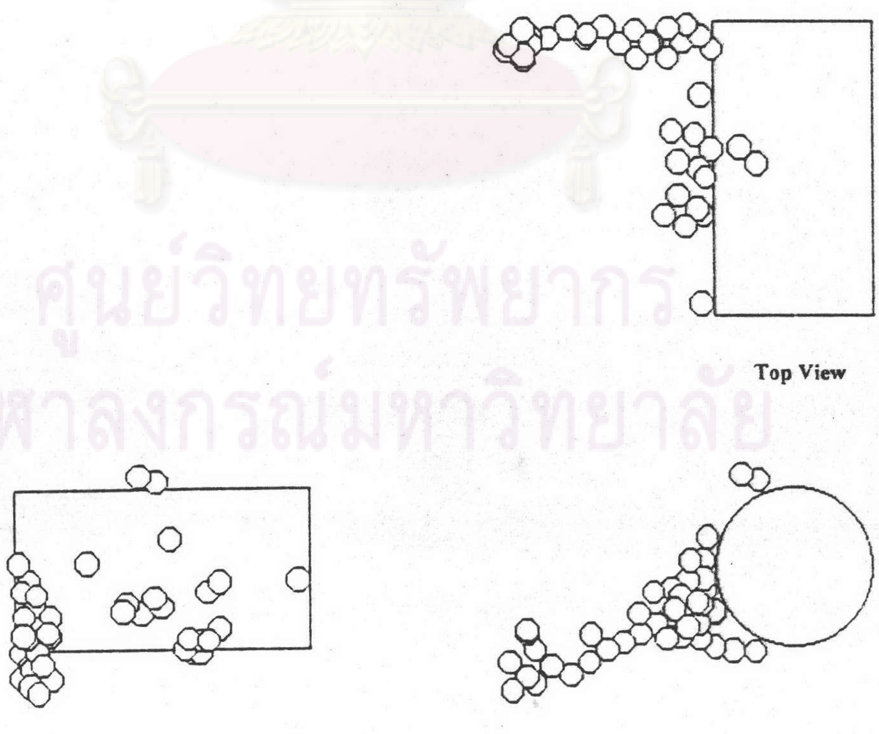

Figure 5.20. Typical configurations of dendrites for R=0.15 and Pe=5000

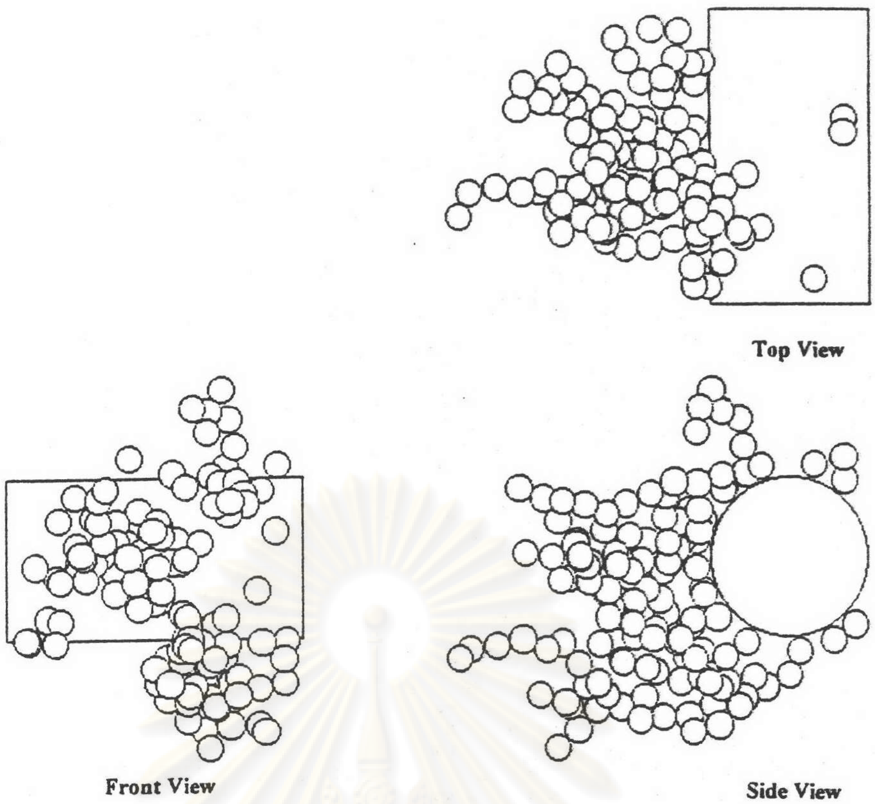

Figure 5.21. Typical configurations of dendrites for R=0.17 and Pe=200

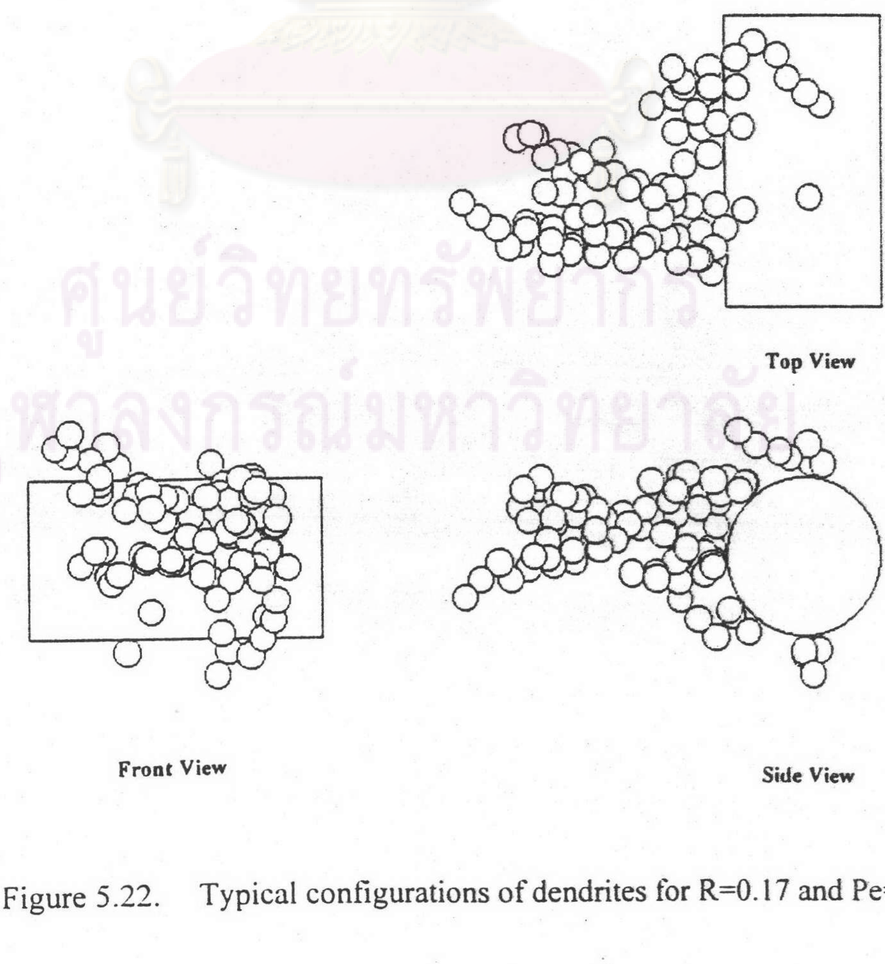

Figure 5.22. Typical configurations of dendrites for R=0.17 and Pe=500

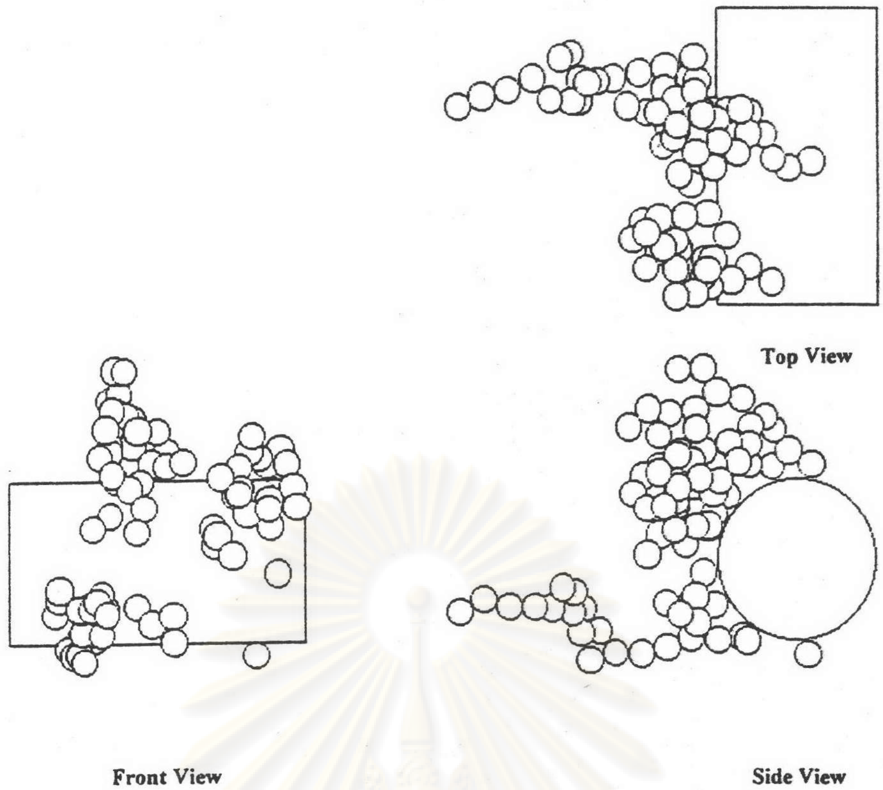

Figure 5.23. Typical configurations of dendrites for R=0.17 and Pe=1000

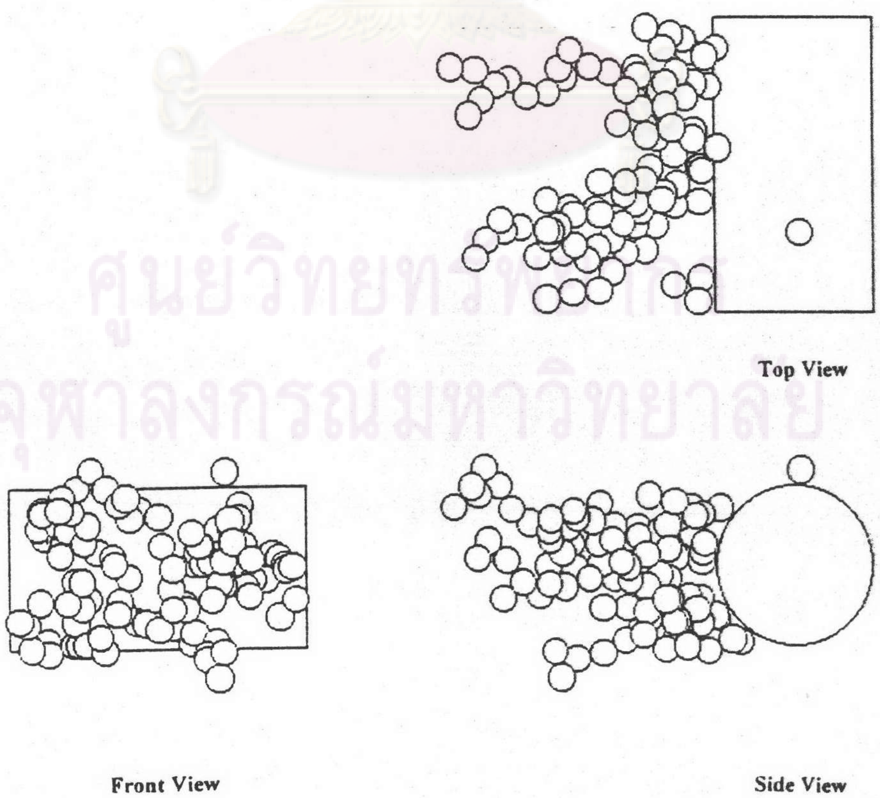

Figure 5.24. Typical configurations of dendrites for R=0.17 and Pe=2500

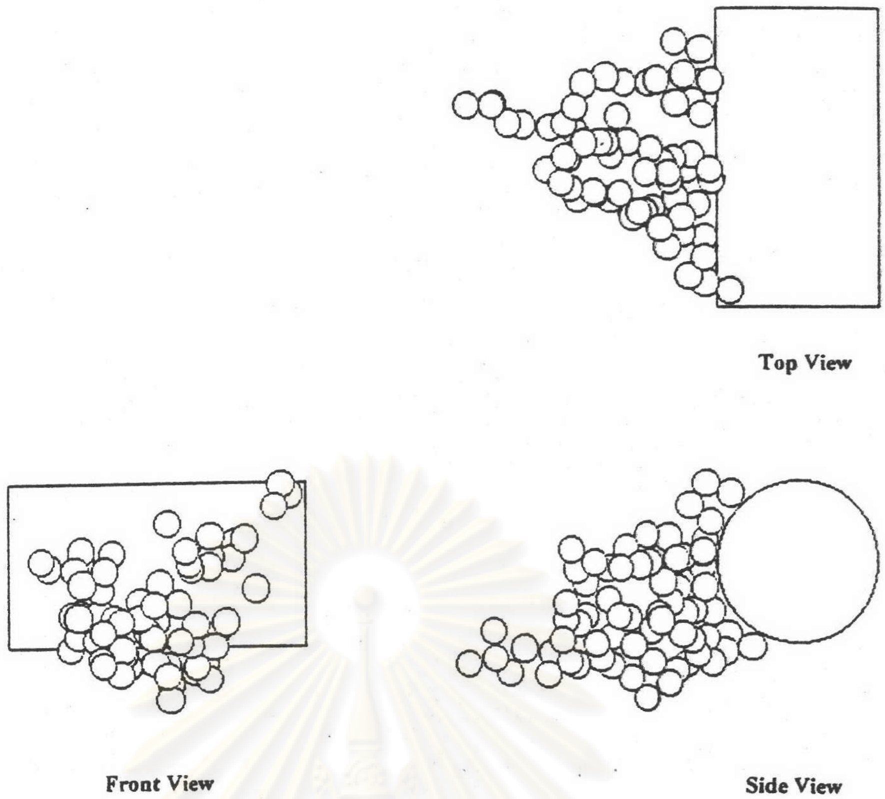

Figure 5.25. Typical configurations of dendrites for R=0.17 and Pe=5000

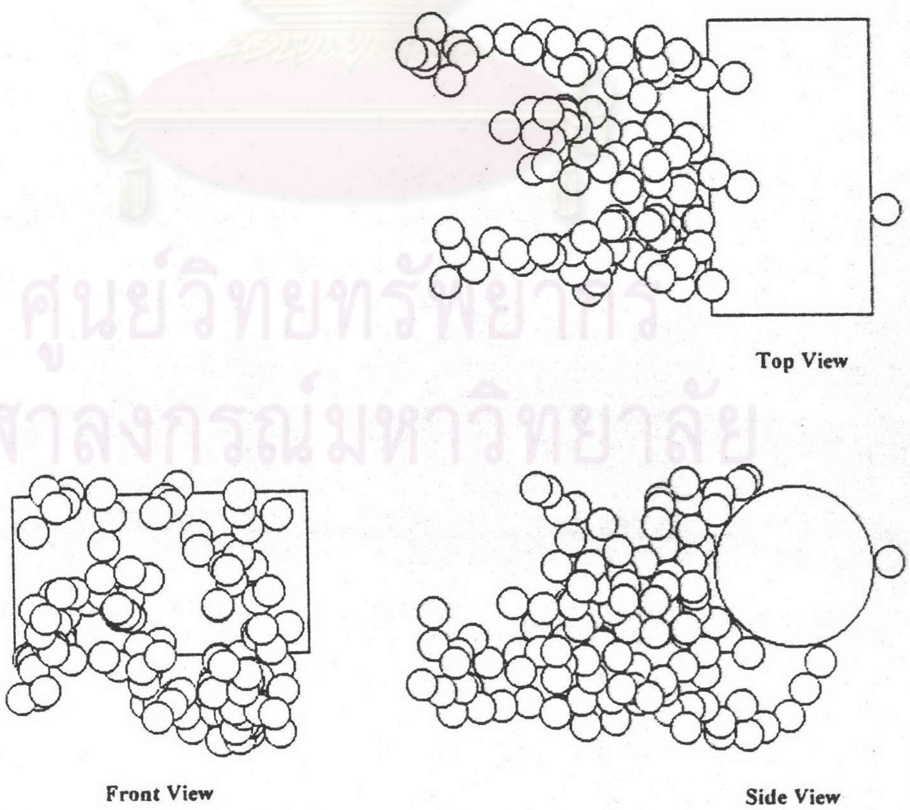

Figure 5.26. Typical configurations of dendrites for R=0.2 and Pe=200

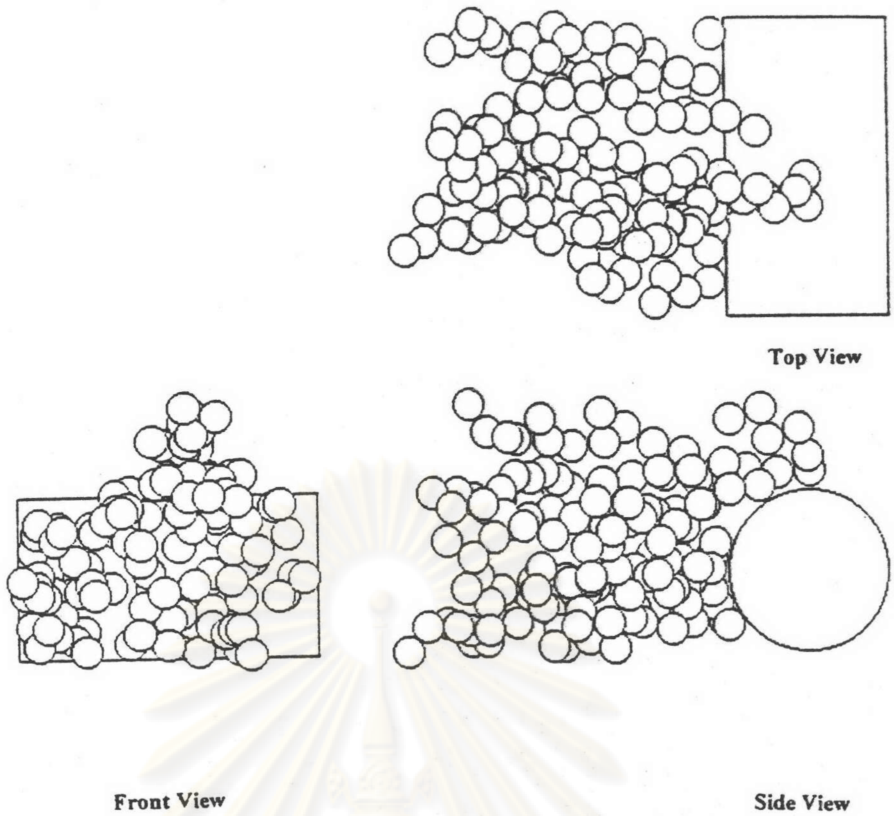

Figure 5.27. Typical configurations of dendrites for R=0.2 and Pe=500

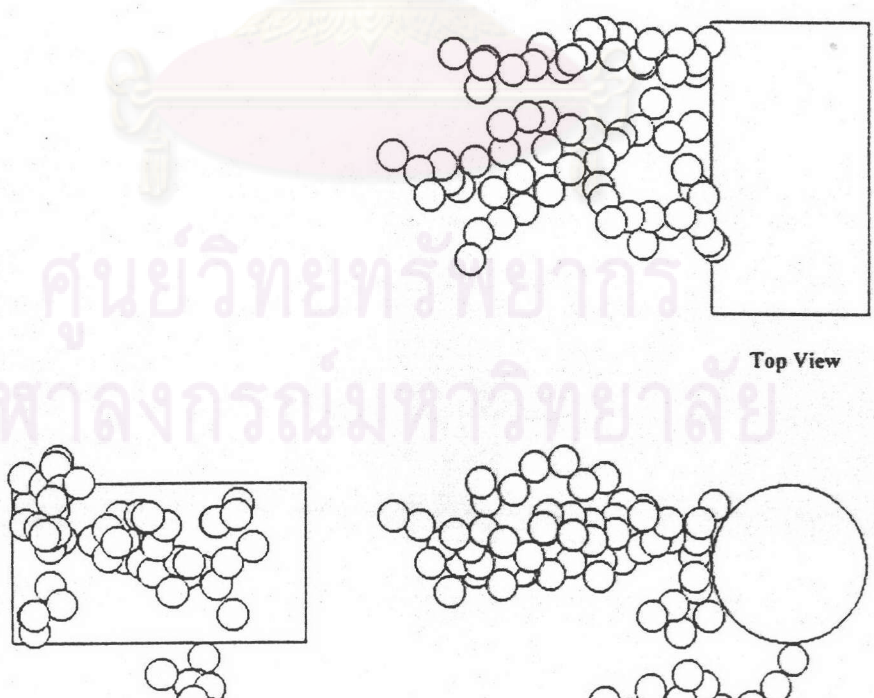

Figure 5.28. Typical configurations of dendrites for R=0.2 and Pe=1000

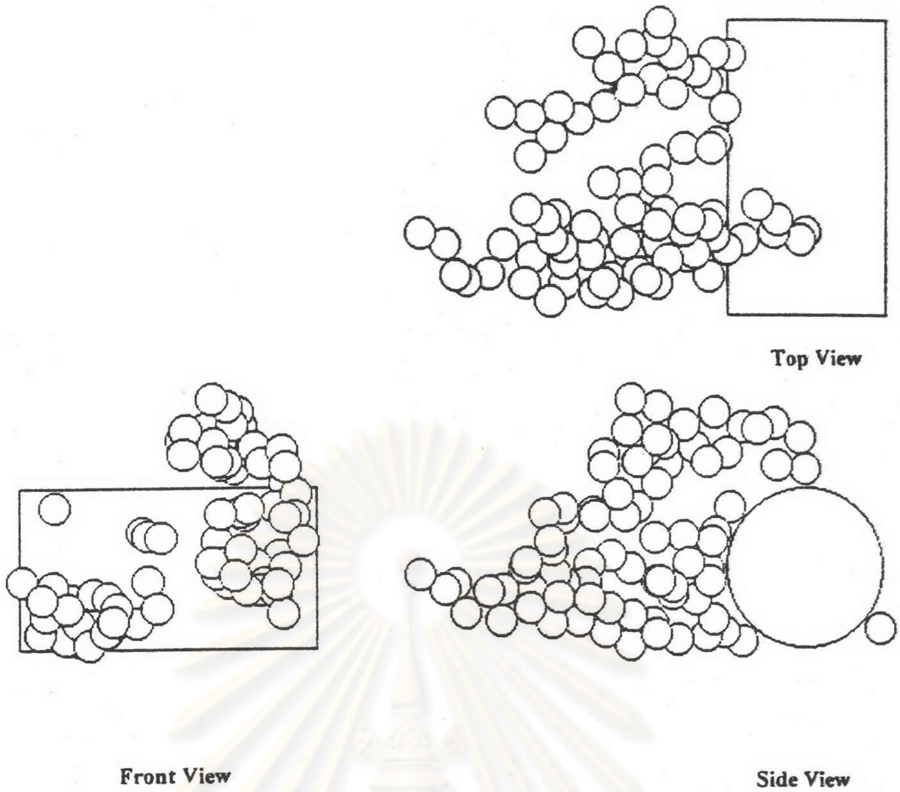

Figure 5.29. Typical configurations of dendrites for R=0.2 and Pe=2500

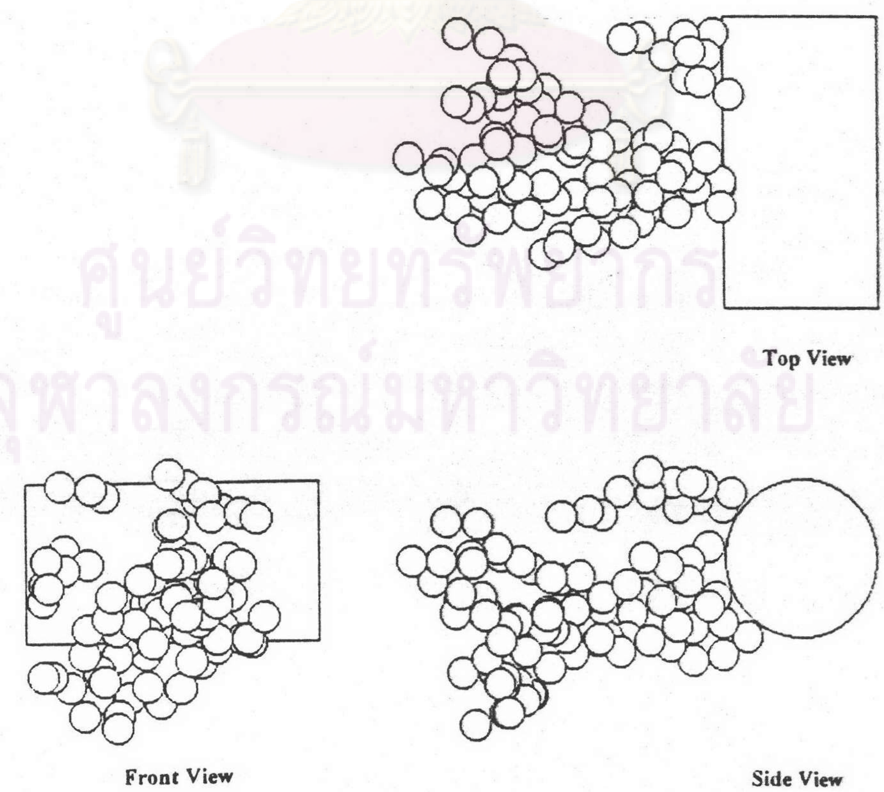

Figure 5.30. Typical configurations of dendrites for R=0.2 and Pe=5000

Table 5.1. Collection efficiency raising factor λ for convective diffusion

Pe	R					
	0.05	0.1	0.13	0.15	0.17	0.2
200		0.789*				0.588*
	0.5210	0.6159	0.6843	0.6272	0.5966	0.5267
500	1.1920	1.0550	1.192	1.0670	0.8668	0.8100
1000		2.19*				1.07*
	2.3870	1.9970	1.472	1.3780	1.258	1.0000
2500	4.6320	3.1190	2.525	1.8080	1.629	1.3870
5000		3.84*				1.42*
	6.2790	3.3570	2.694	1.6540	1.715	1.4840

* Kanaoka et al., 1983

Table 5.2 Difference of λ between the previous study (Kanaoka et.al., 1983) and the present study for convective diffusion (%)

Pe	R	
	0.05	0.1
200	21.94	10.43
1000	8.8100	6.5400
5000	12.5800	4.5100

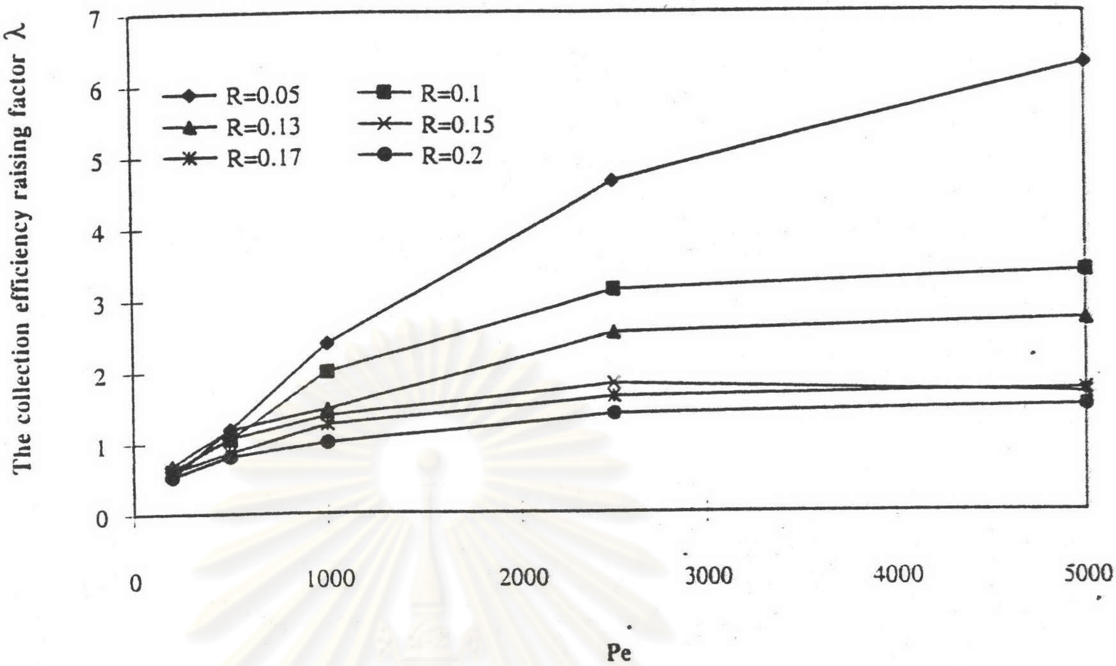

Figure 5.31. Relationship between λ and Pe with R as parameter (Stochastic simulation)

computational time by using only the upper half of Kuwabara's cell. Thus, the present study was more realistic than the previous study.

Figure 5.31 shows the relationship between λ and Pe with R as parameter based on stochastic results. As expected, the value of λ is larger at a large Pe and small R than at a small Pe and large R.

5.1.2 Inertial impactional deposition

The dendritic growth via inertial impaction was also simulated stochastically for various filtration conditions. Figures 5.32-5.61 show the configuration of the dendrites. The particles were captured only on the front surface of the fiber. Similar to convective diffusion, the typical dendrites in the case of inertial impaction were densely packed when the interception parameter R was small but was more porous when R was large. When the mechanism of particle deposition is purely interception (St=0), most particles were captured on upper and lower far sides of the fiber surface and the dendrites was tall. In contrast, many particles were captured around the stagnation point of the fiber surface at small St. Furthermore, the particles were densely packed and the dendrites were shorter length at large St.

The collection efficiency was evaluated from Monte-Carlo simulation results. The clean fiber collection efficiency η_0 was obtained from the limiting trajectory theory. Figures 5.62 and 5.63 show respectively relationship between η_0 and R with St as parameter based on Stechkina's equation (Stechkina et al., 1969), and based on the limiting trajectory theory which integrated equations (3.24) and (3.25) numerically. In the limiting trajectory theory, η_0 increased only slightly at a large St but this was not observed in Stechkina's result, because Stechkina's equation was accurate at St<<1 only.

The resulting collection efficiency raising factor λ for inertial impaction was listed in Table 5.3, including those obtained by Kanaoka et.al.(1980). Table 5.4 shows the difference in λ between the previous stochastic study (Kanaoka et.al., 1980) and the present study. The relative difference never exceeded 30% in all cases. For the majority of the cases, the difference was less than 10%. In the previous study, a three-dimensional mesh network was constructed beforehand for containing captured

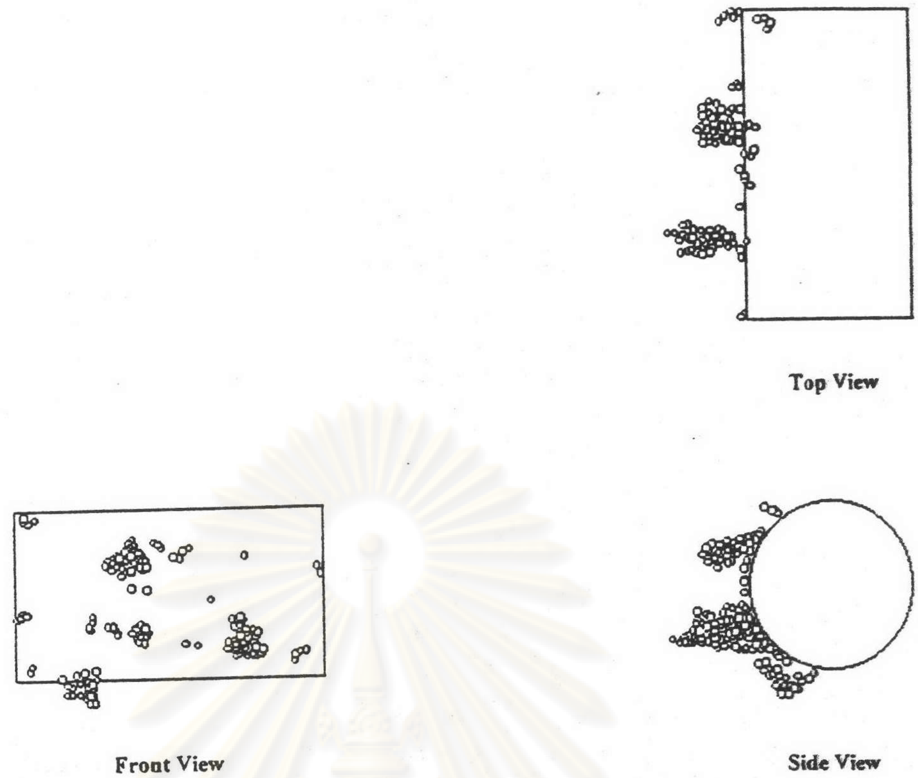

Figure 5.32. Typical configurations of dendrites for R=0.05 and St=0.0

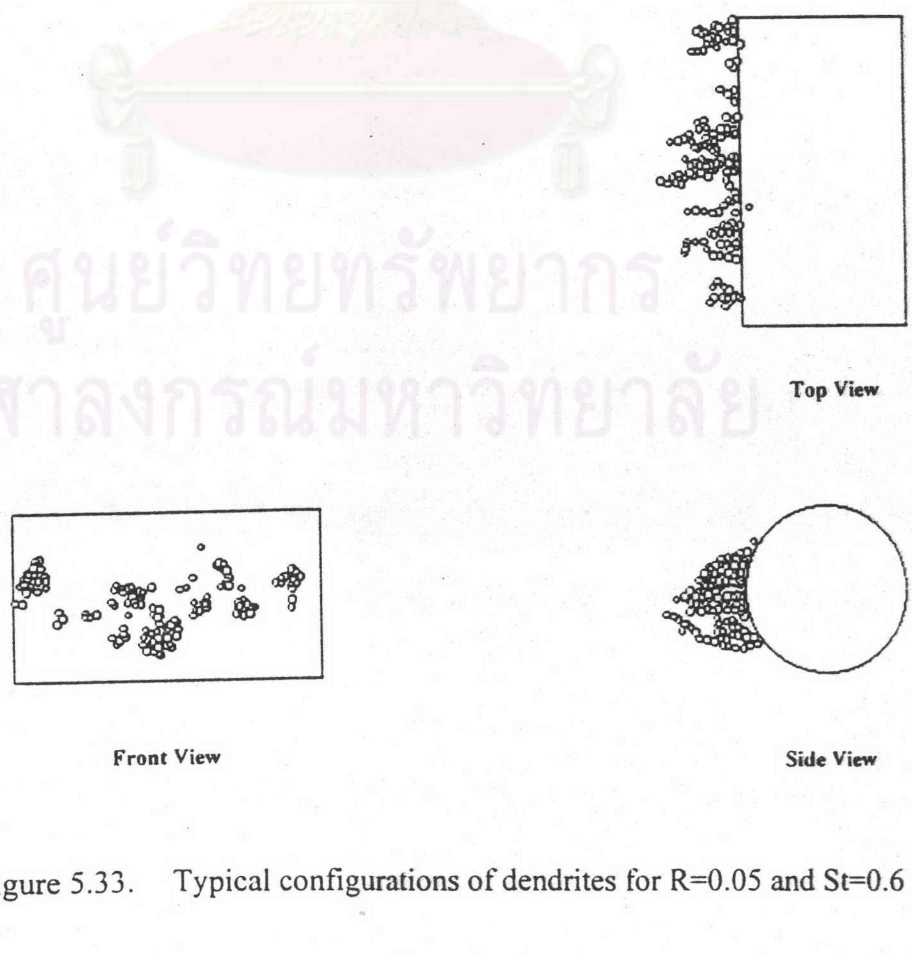

Figure 5.33. Typical configurations of dendrites for R=0.05 and St=0.6

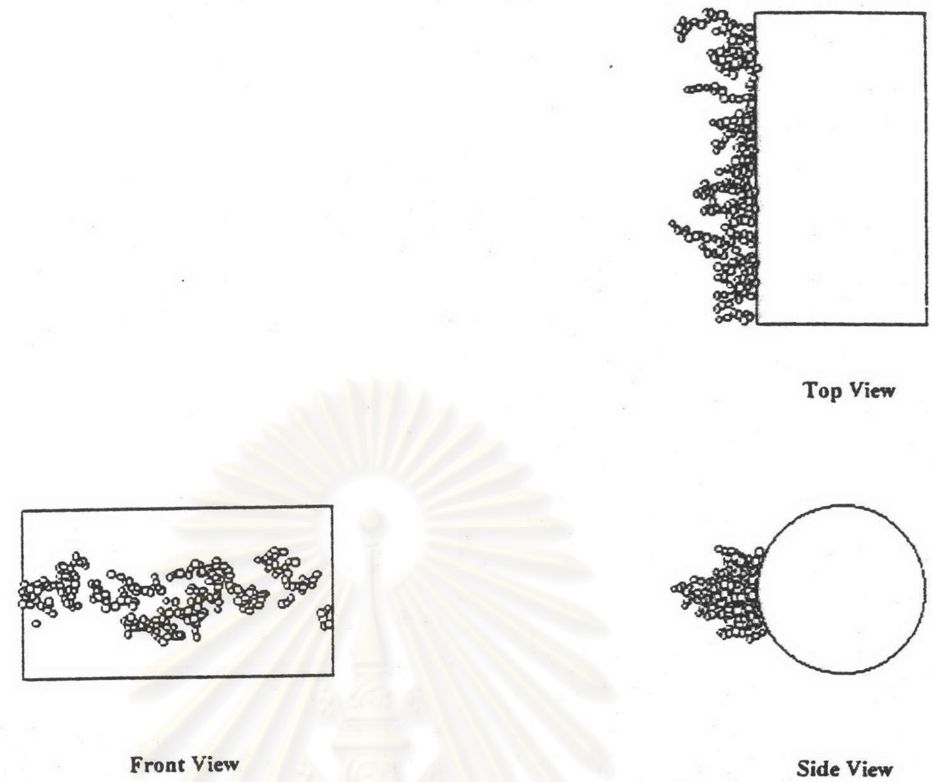

Figure 5.34. Typical configurations of dendrites for R=0.05 and St=1.0

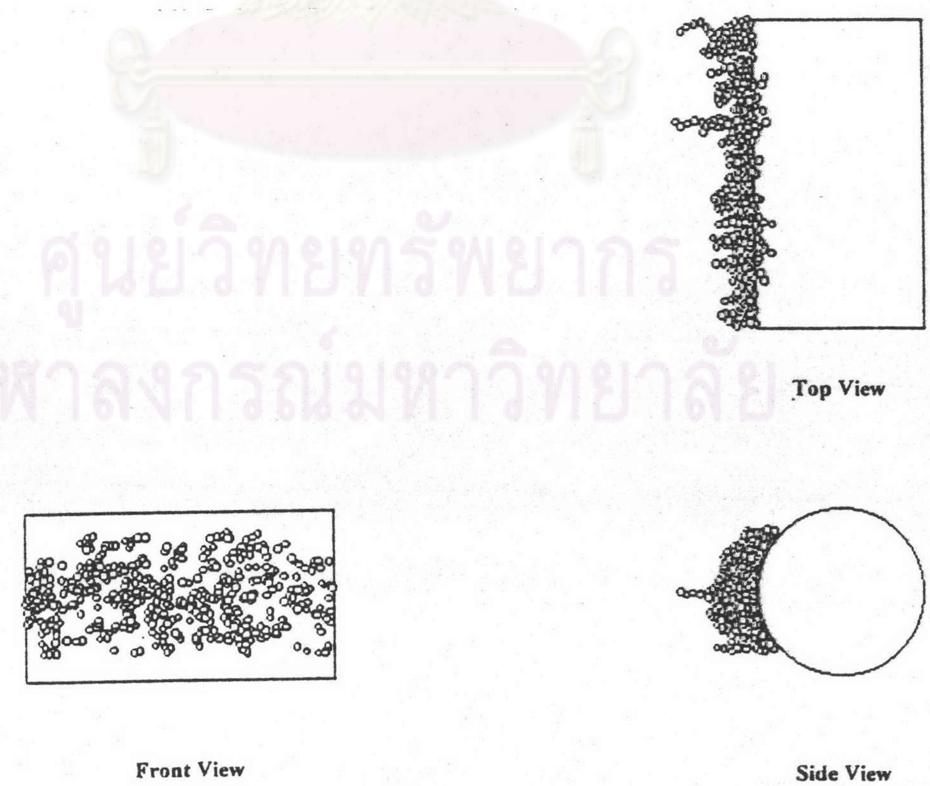

Figure 5.35. Typical configurations of dendrites for R=0.05 and St=1.4

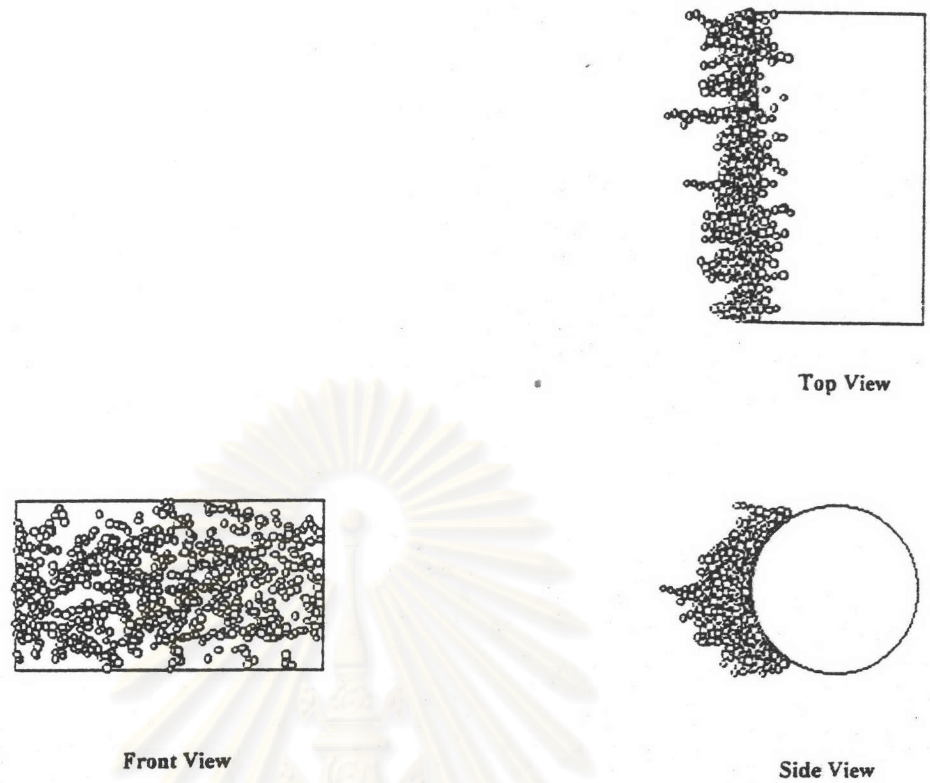

Figure 5.36. Typical configurations of dendrites for R=0.05 and St=2.0

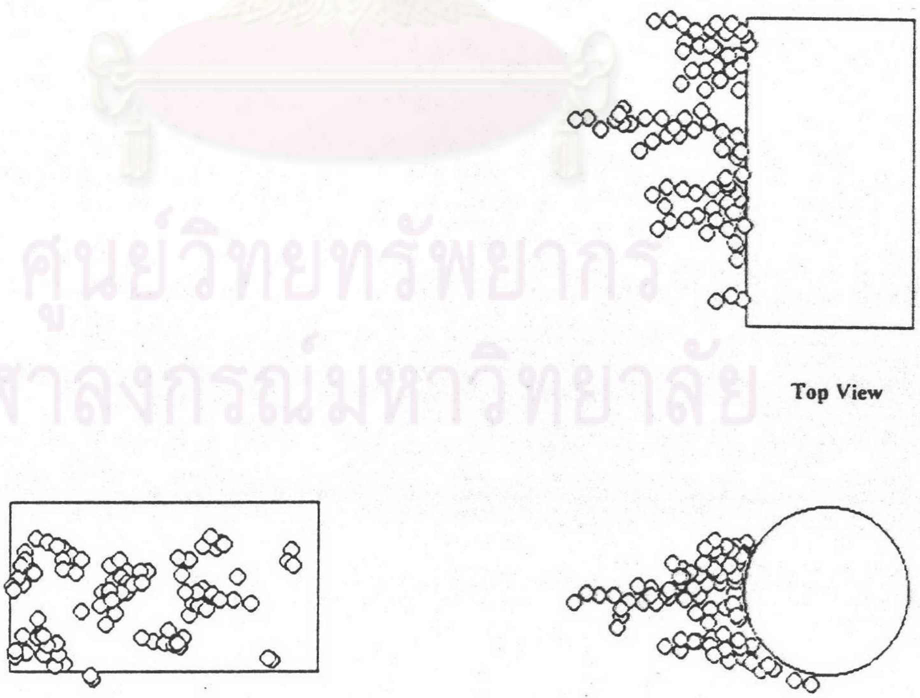

Figure 5.37. Typical configurations of dendrites for R=0.1 and St=0.0

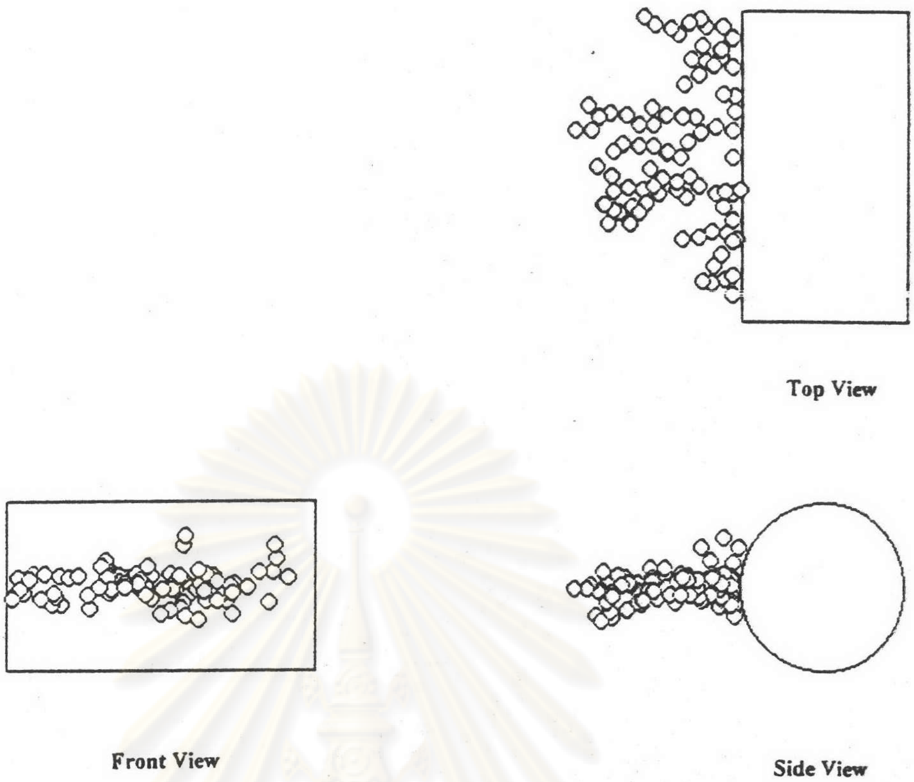

Figure 5.38. Typical configurations of dendrites for R=0.1 and St=0.6

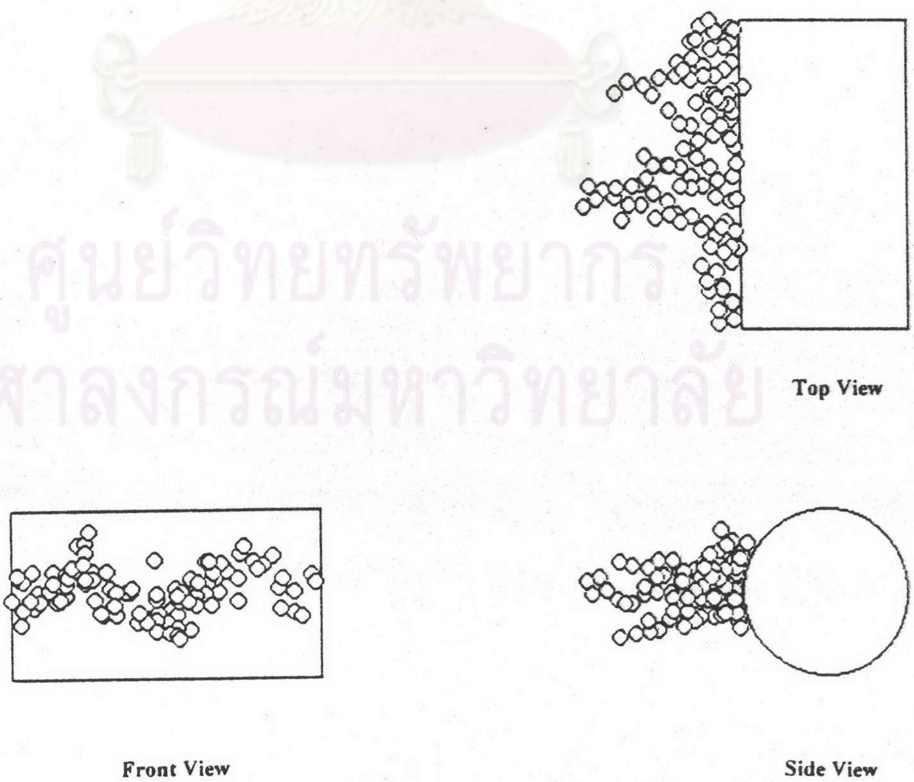

Figure 5.39. Typical configurations of dendrites for R=0.1 and St=1.0

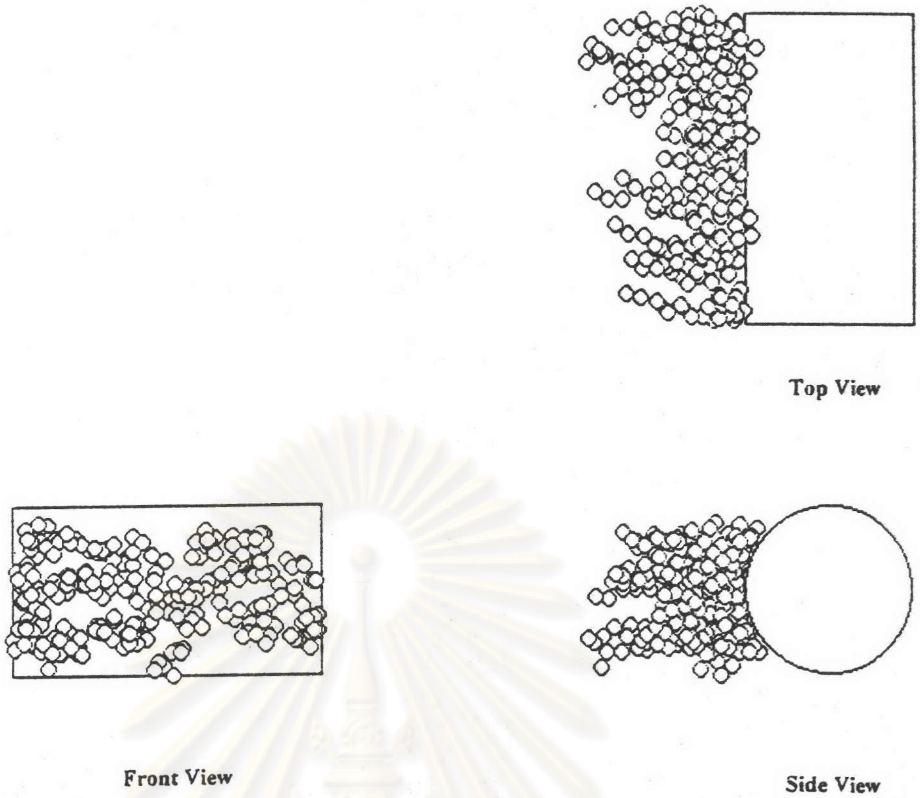

Figure 5.40. Typical configurations of dendrites for R=0.1 and St=1.4

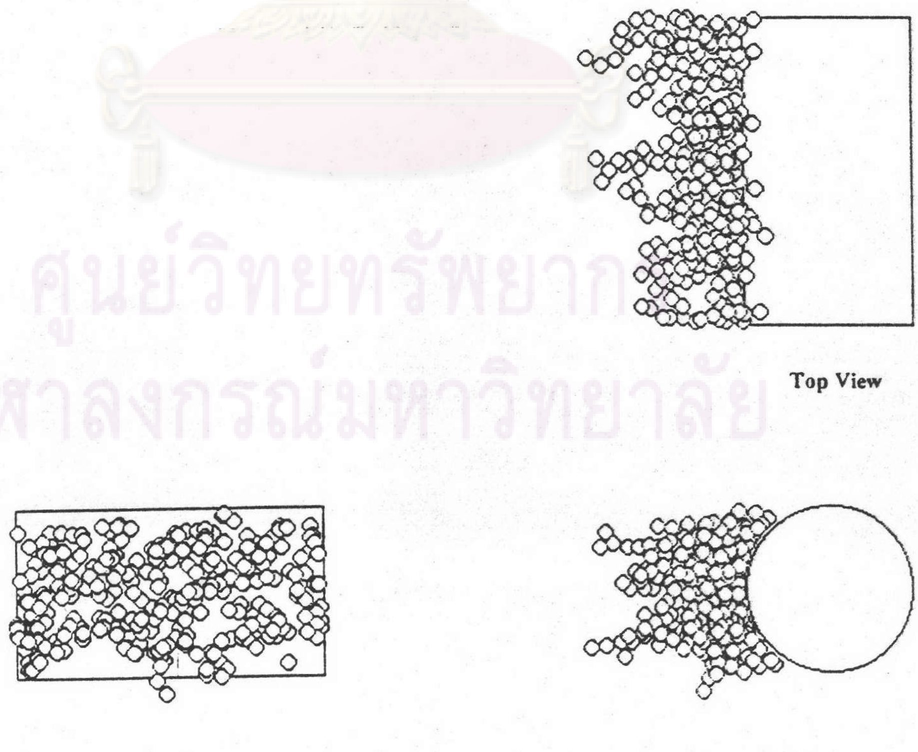

Figure 5.41. Typical configurations of dendrites for R=0.1 and St=2.0

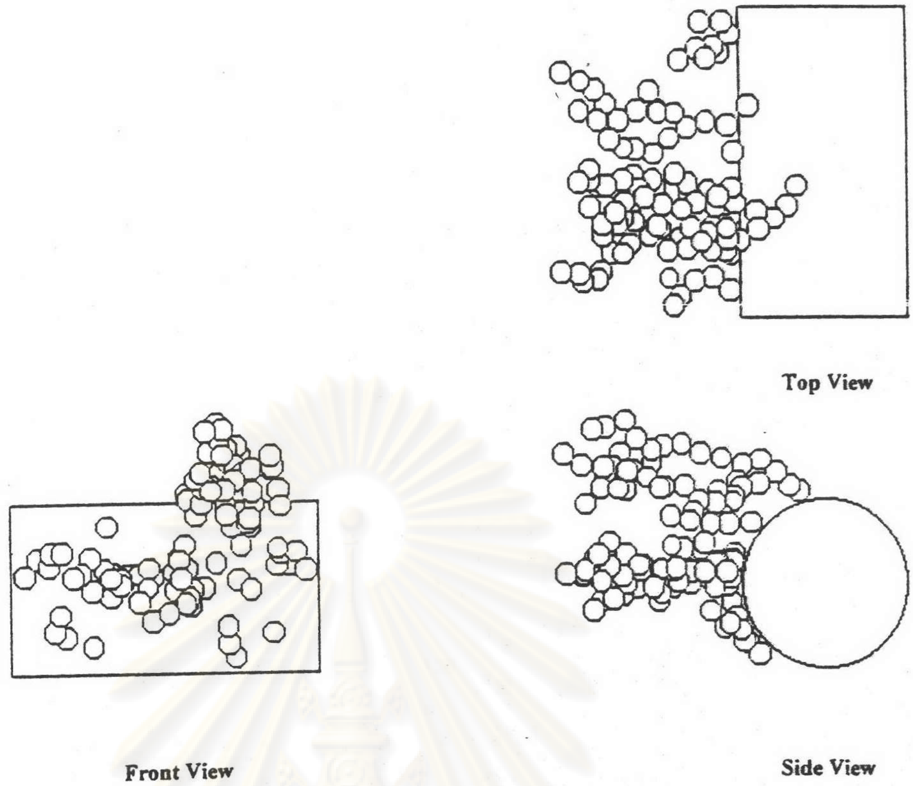

Figure 5.42. Typical configurations of dendrites for R=0.13 and St=0.0

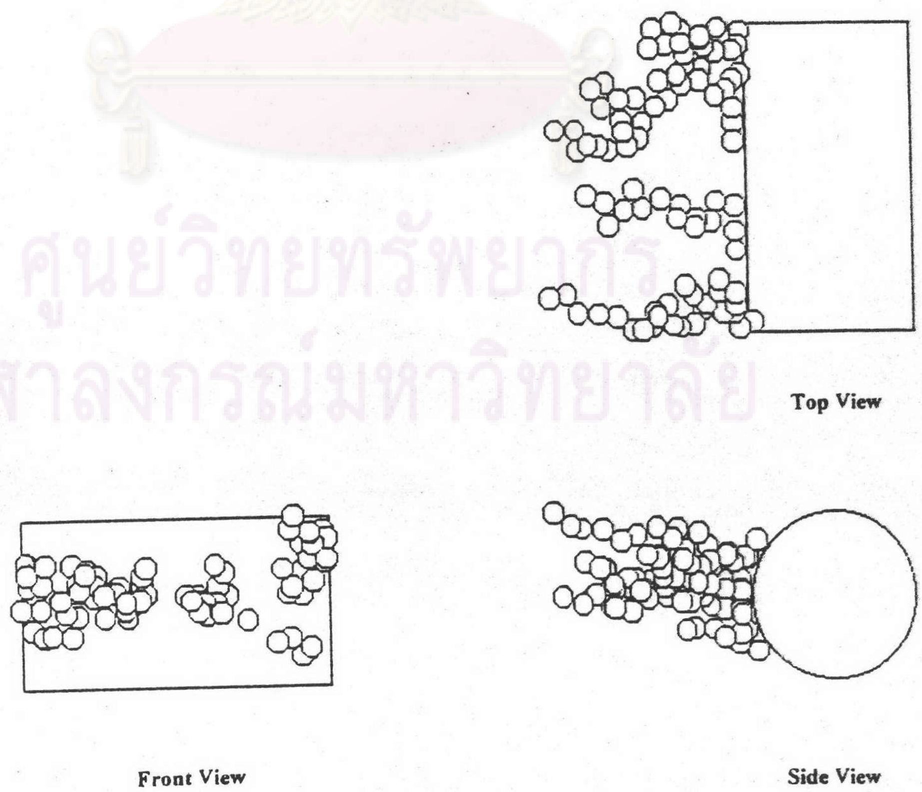

Figure 5.43. Typical configurations of dendrites for R=0.13 and St=0.6

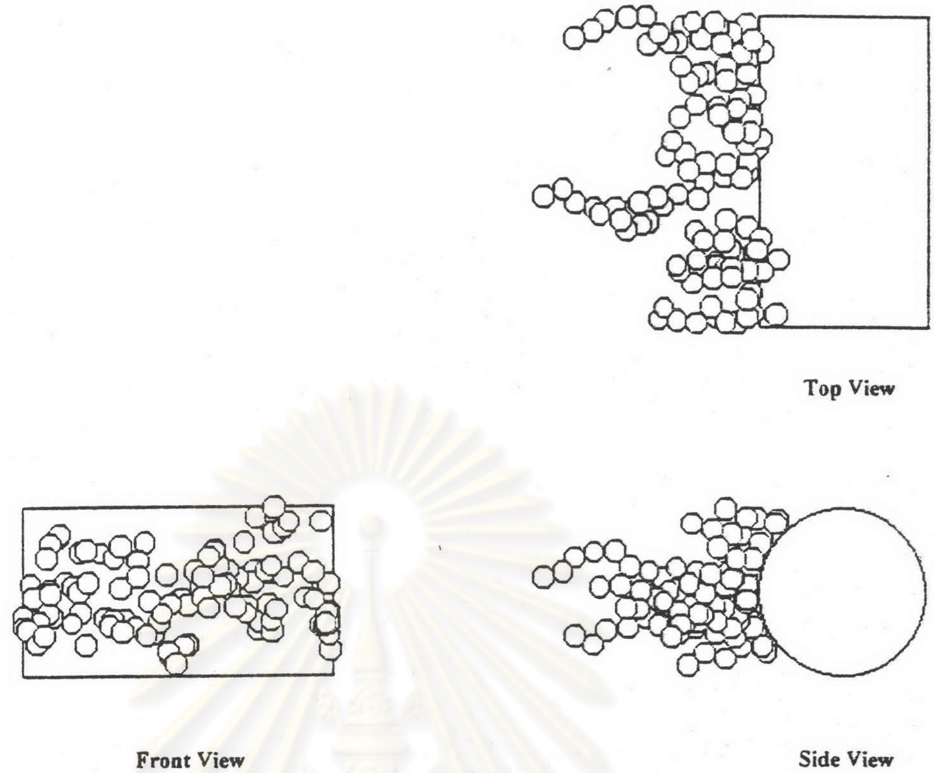

Figure 5.44. Typical configurations of dendrites for R=0.13 and St=1.0

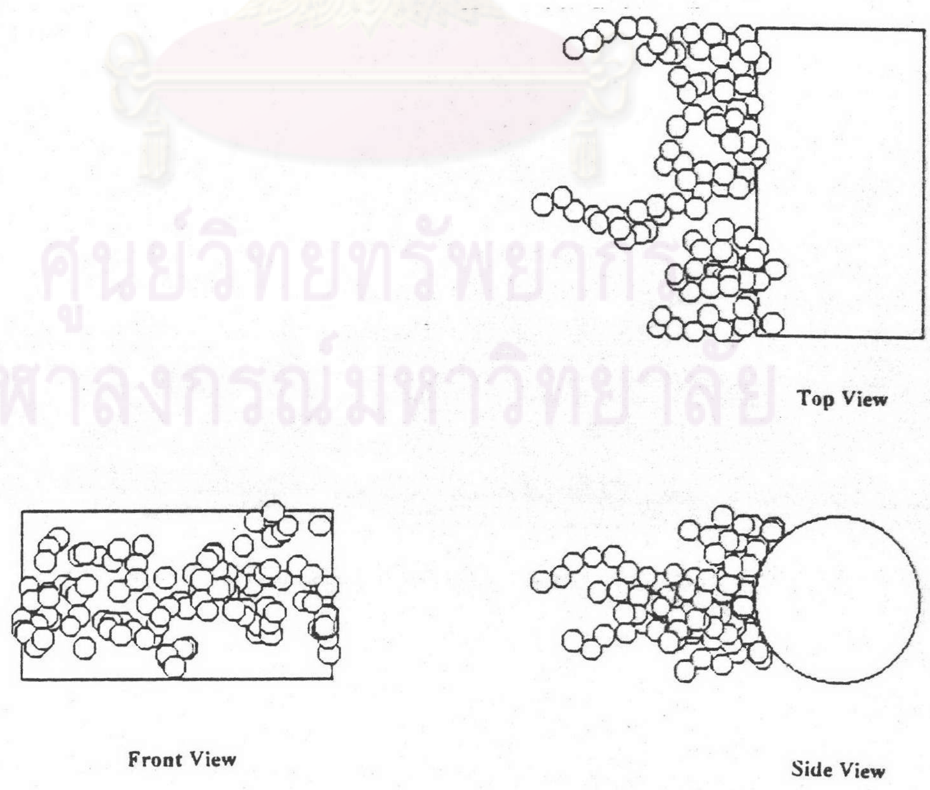

Figure 5.45. Typical configurations of dendrites for R=0.13 and St=1.4

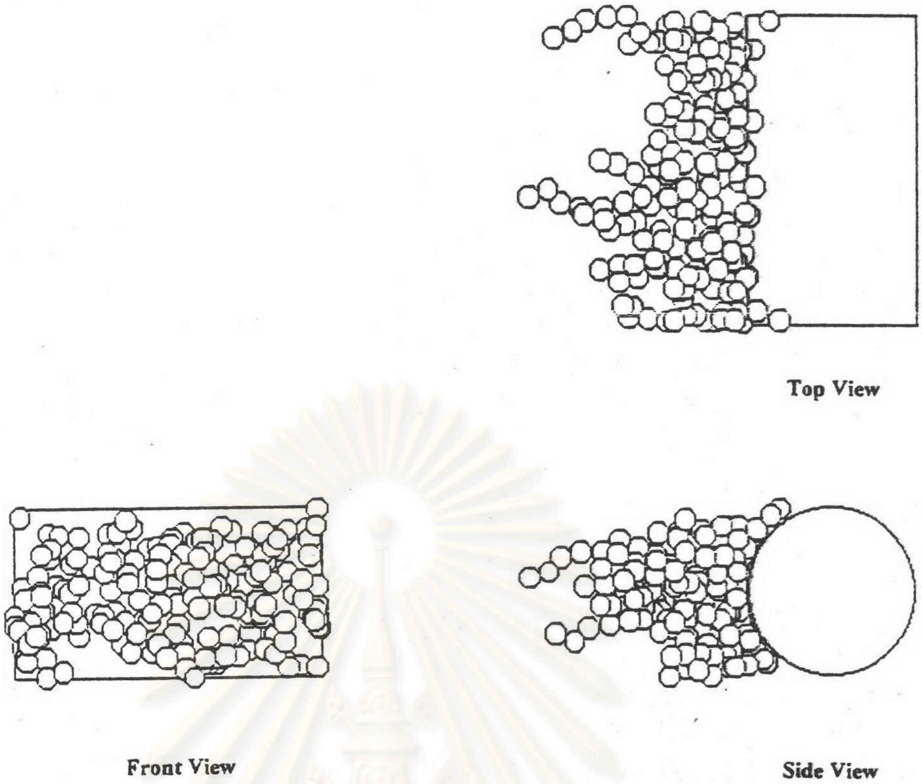

Figure 5.46. Typical configurations of dendrites for R=0.13 and St=2.0

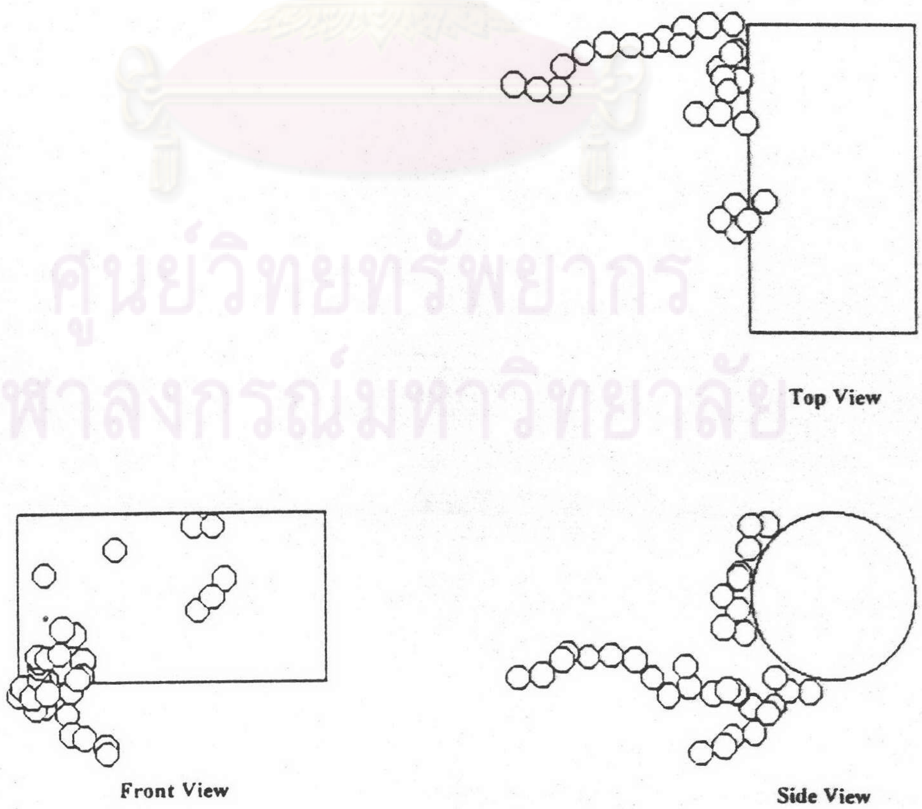

Figure 5.47. Typical configurations of dendrites for R=0.15 and St=0.0

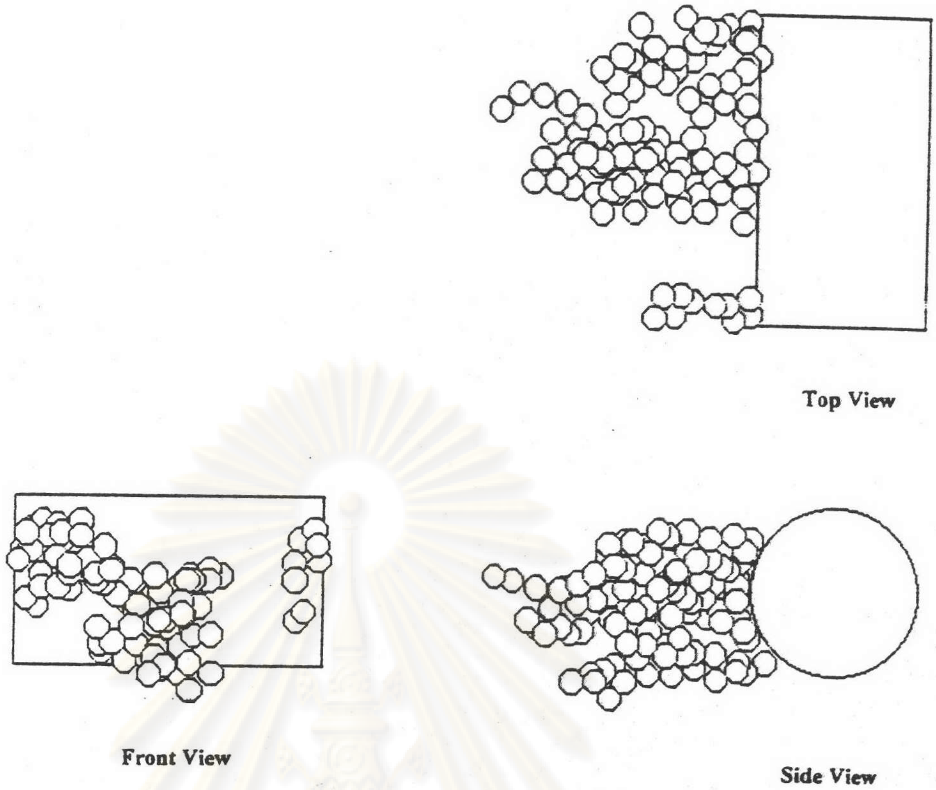

Figure 5.48. Typical configurations of dendrites for R=0.15 and St=0.6

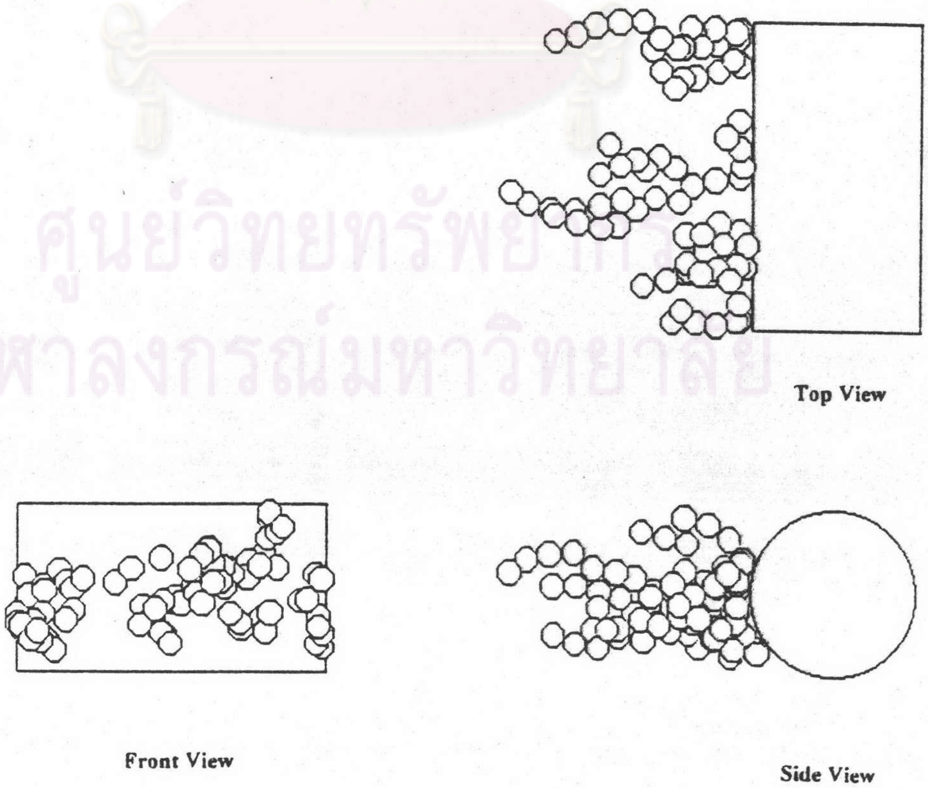

Figure 5.49. Typical configurations of dendrites for R=0.15 and St=1.0

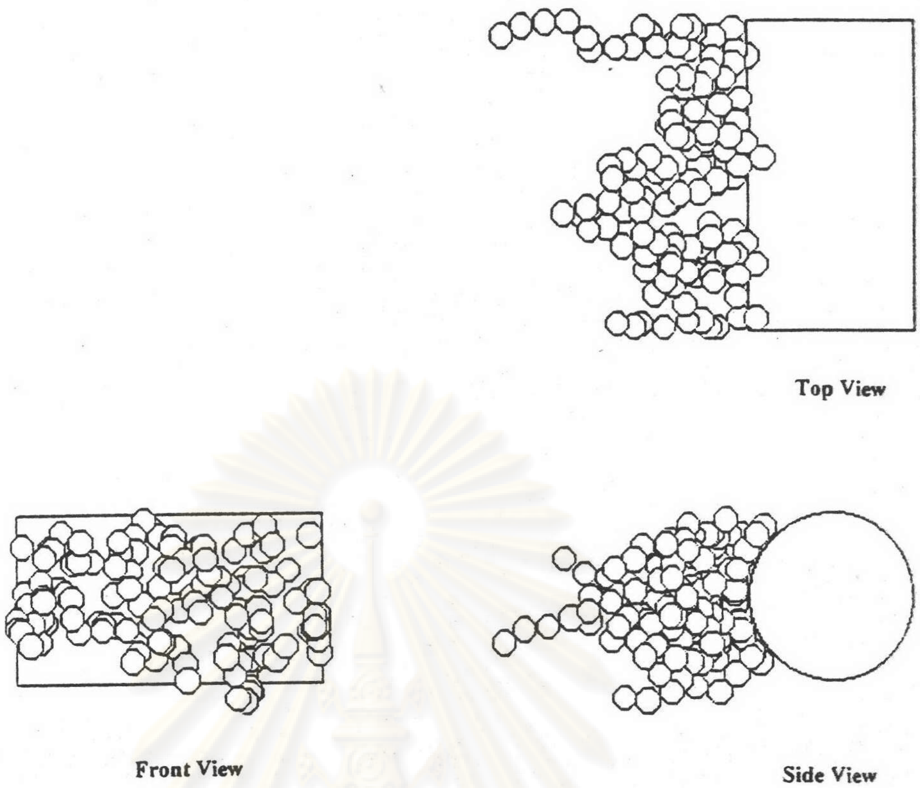

Figure 5.50. Typical configurations of dendrites for R=0.15 and St=1.4

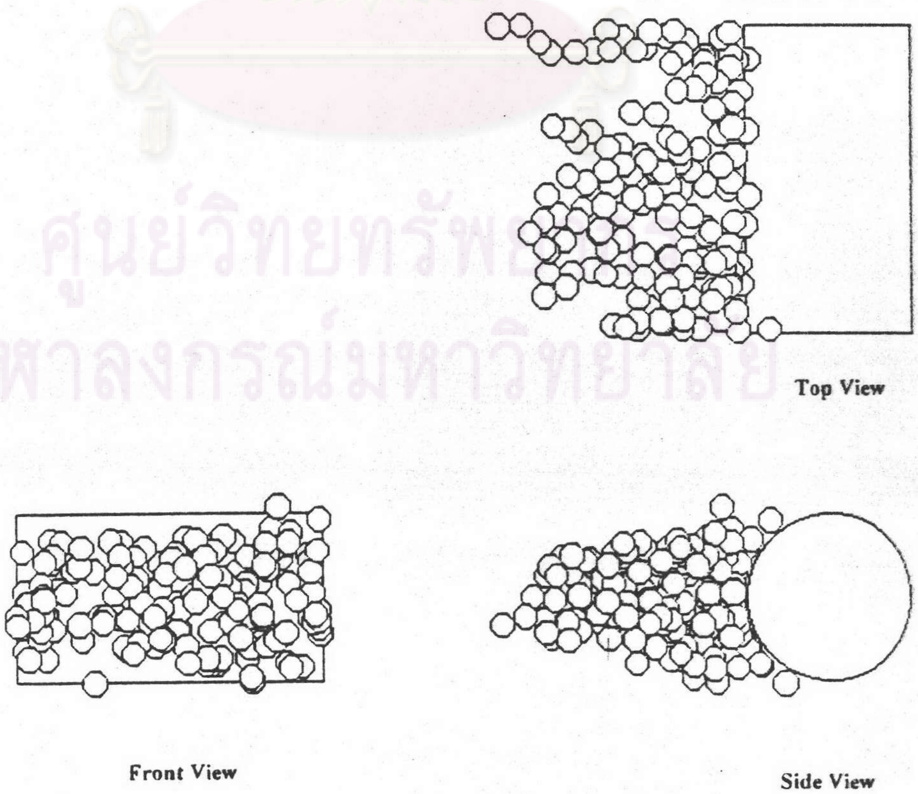

Figure 5.51. Typical configurations of dendrites for R=0.15 and St=2.0

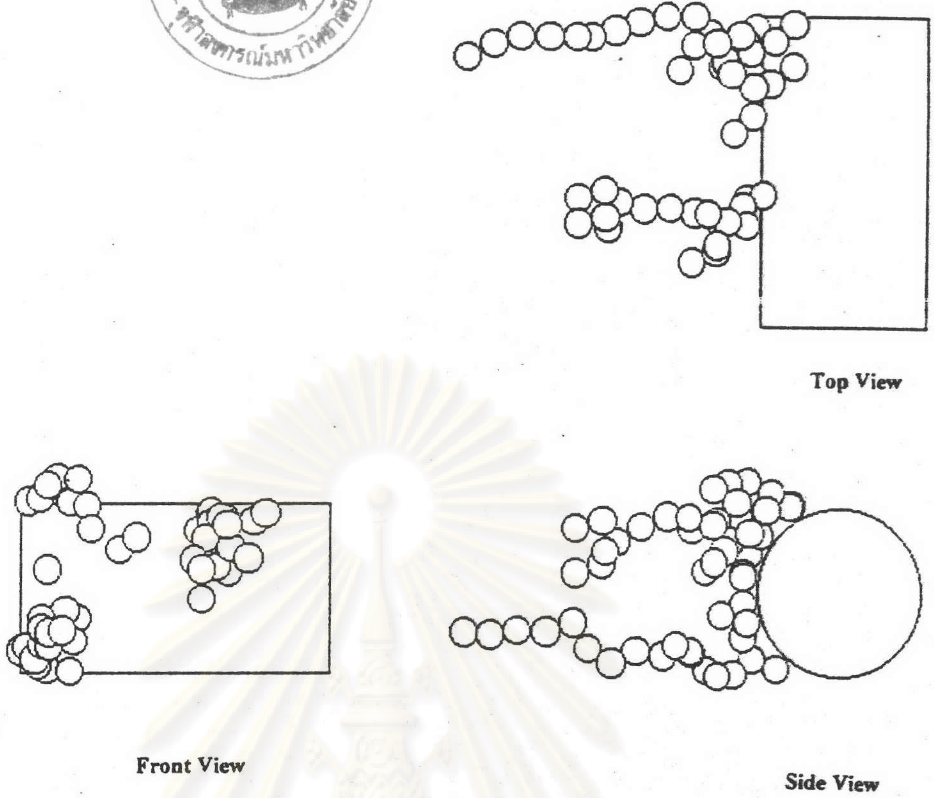

Figure 5.52. Typical configurations of dendrites for R=0.17 and St=0.0

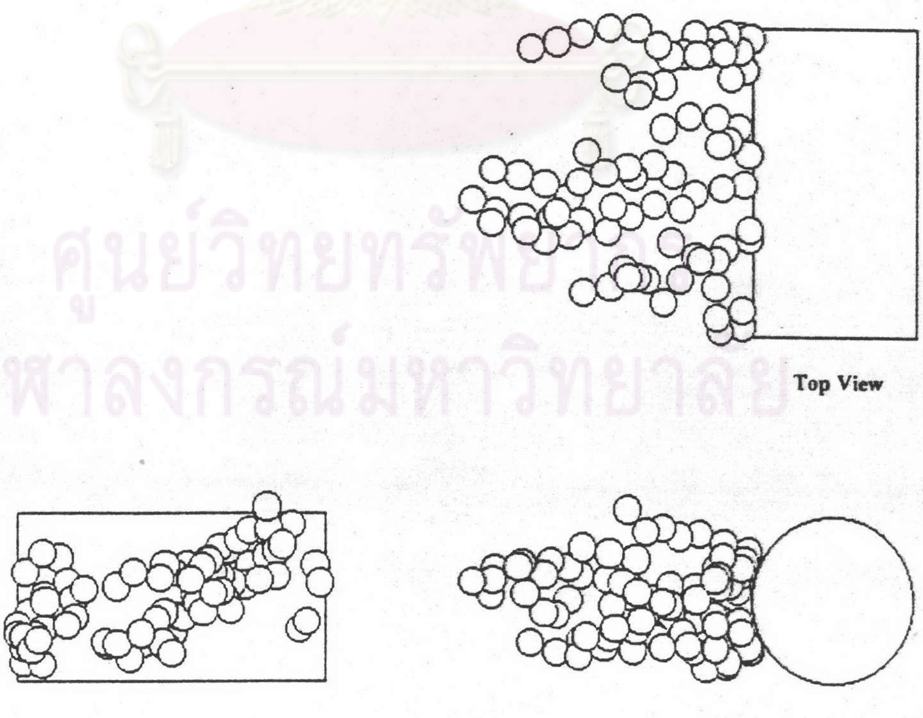

Figure 5.53. Typical configurations of dendrites for R=0.17 and St=0.6

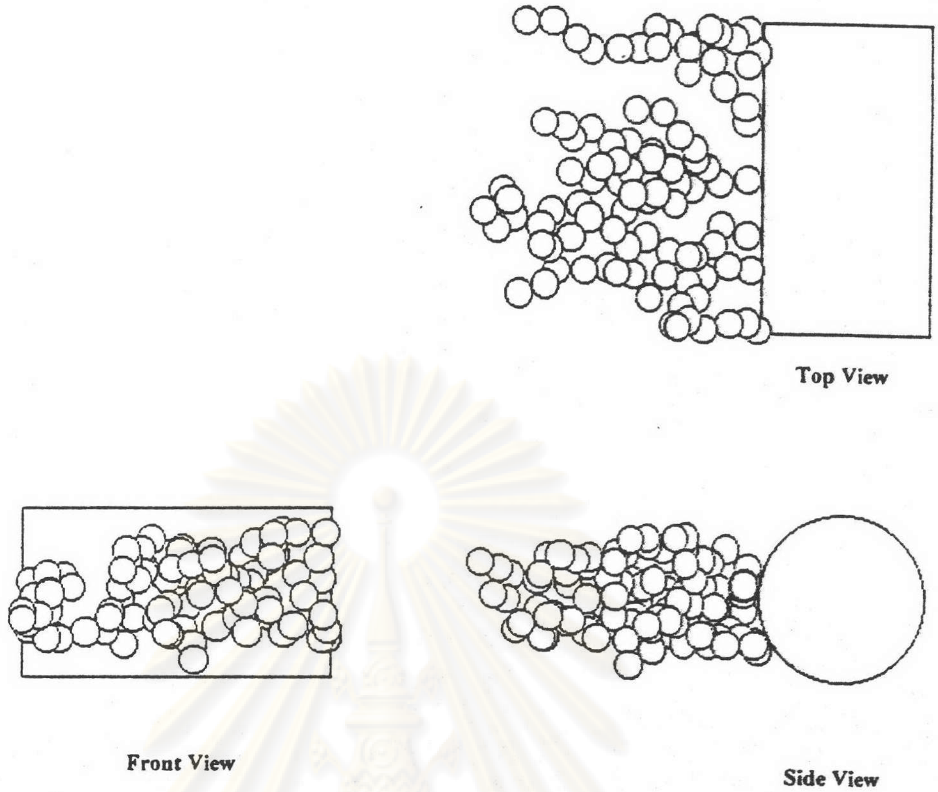

Figure 5.54. Typical configurations of dendrites for R=0.17 and St=1.0

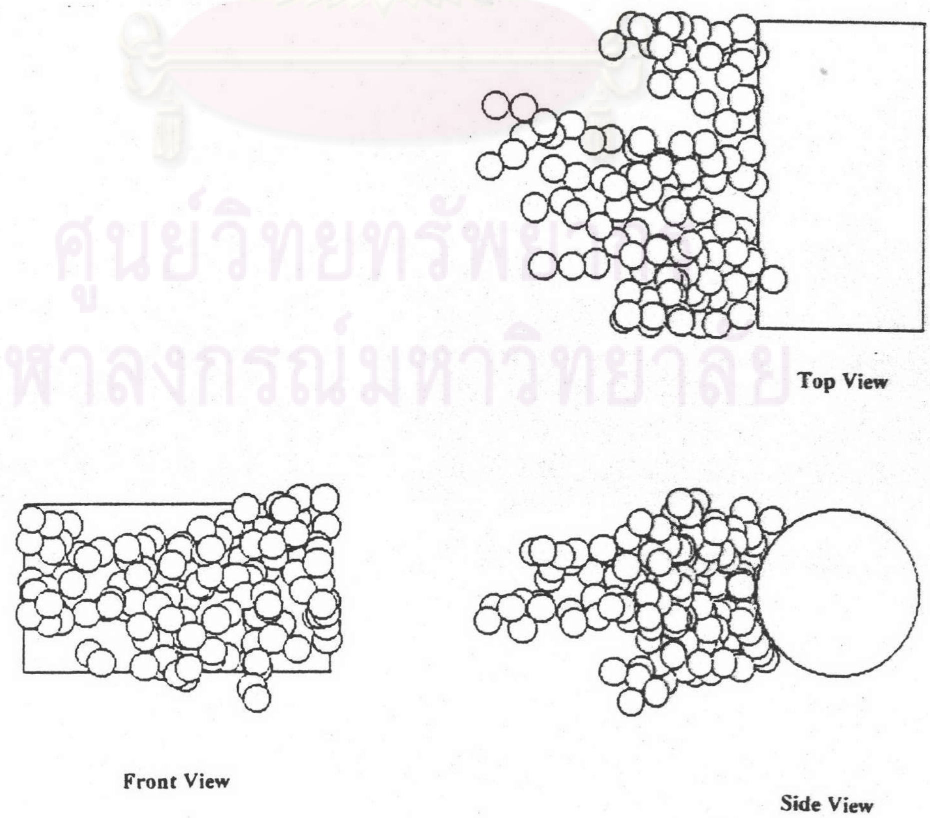

Figure 5.55. Typical configurations of dendrites for R=0.17 and St=1.4

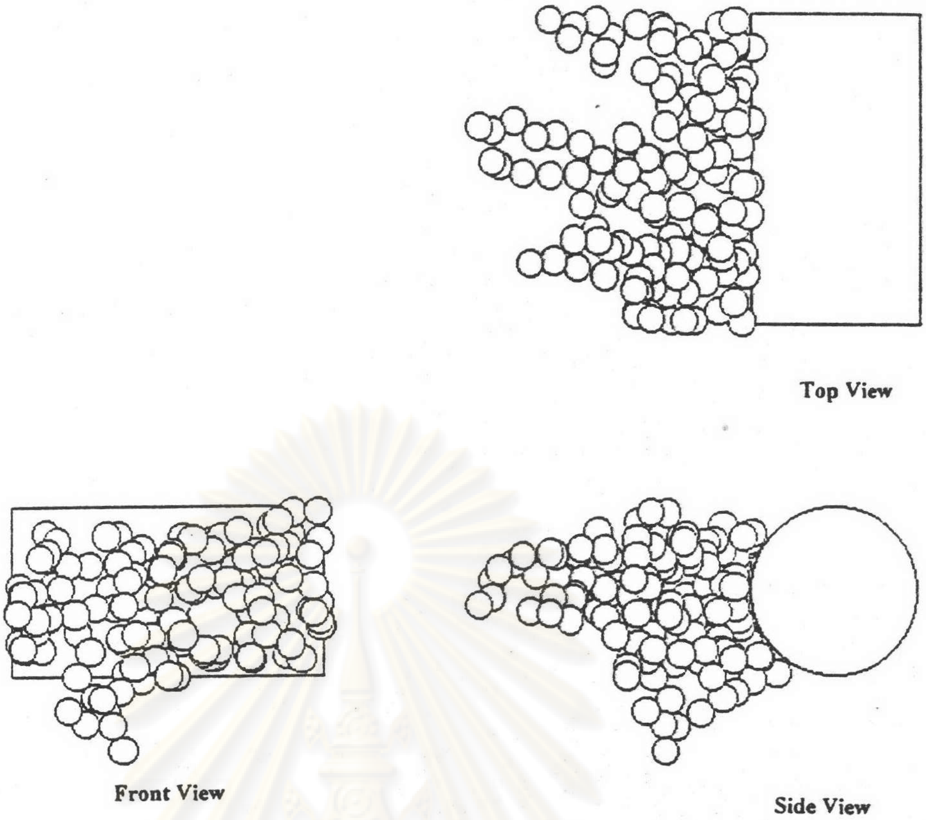

Figure 5.56. Typical configurations of dendrites for R=0.17 and St=2.0

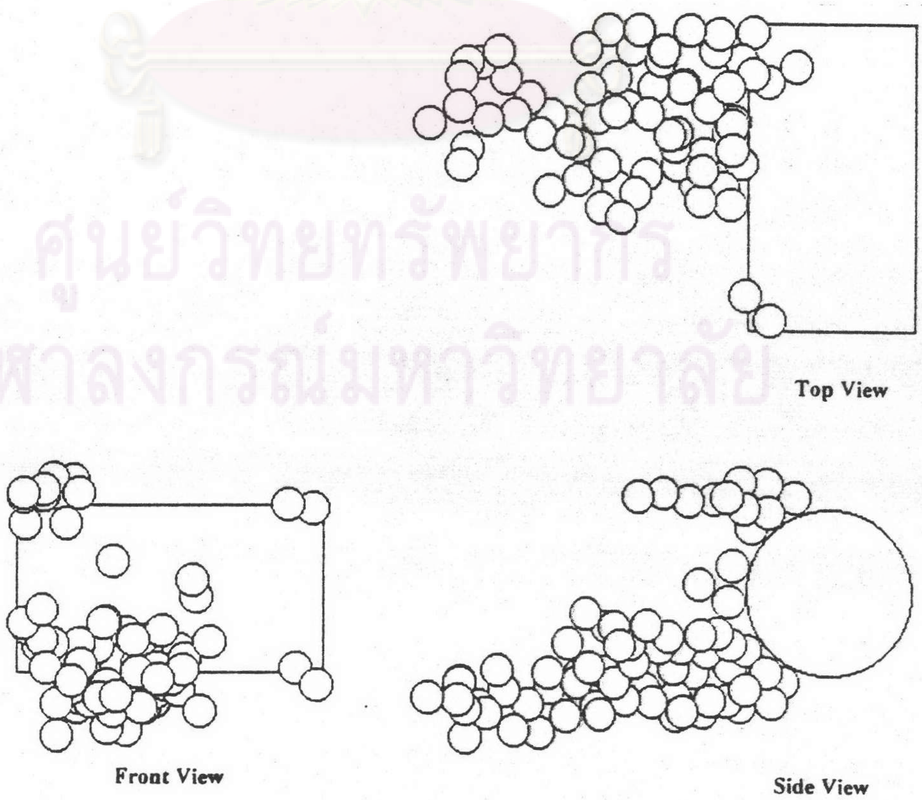

Figure 5.57. Typical configurations of dendrites for R=0.2 and St=0.0

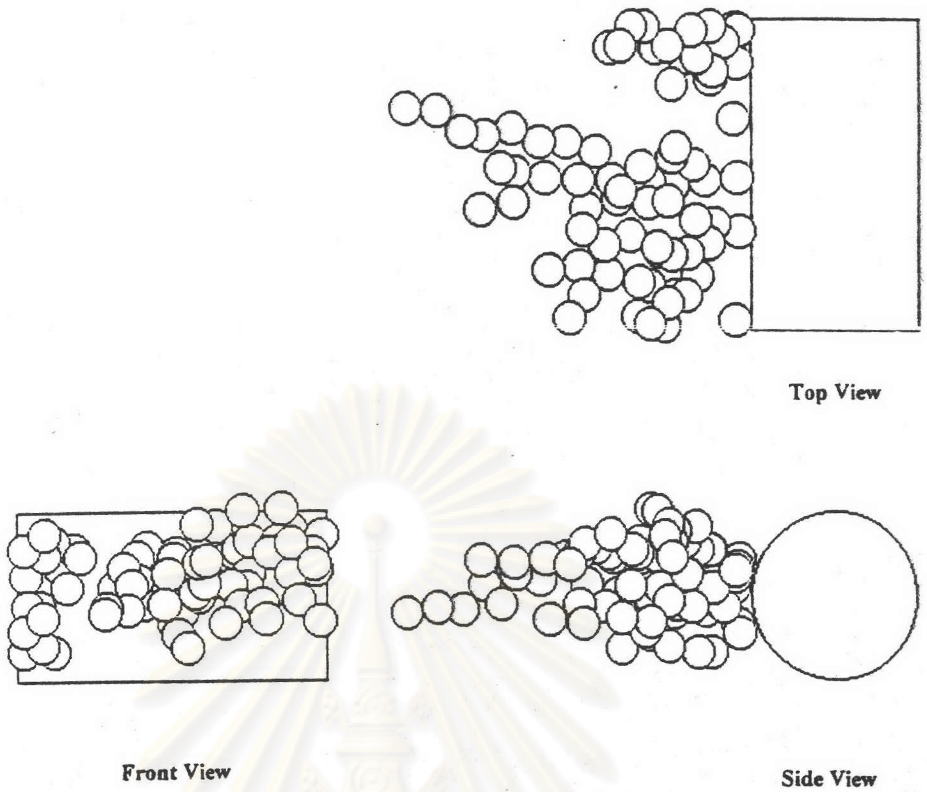

Figure 5.58. Typical configurations of dendrites for R=0.2 and St=0.6

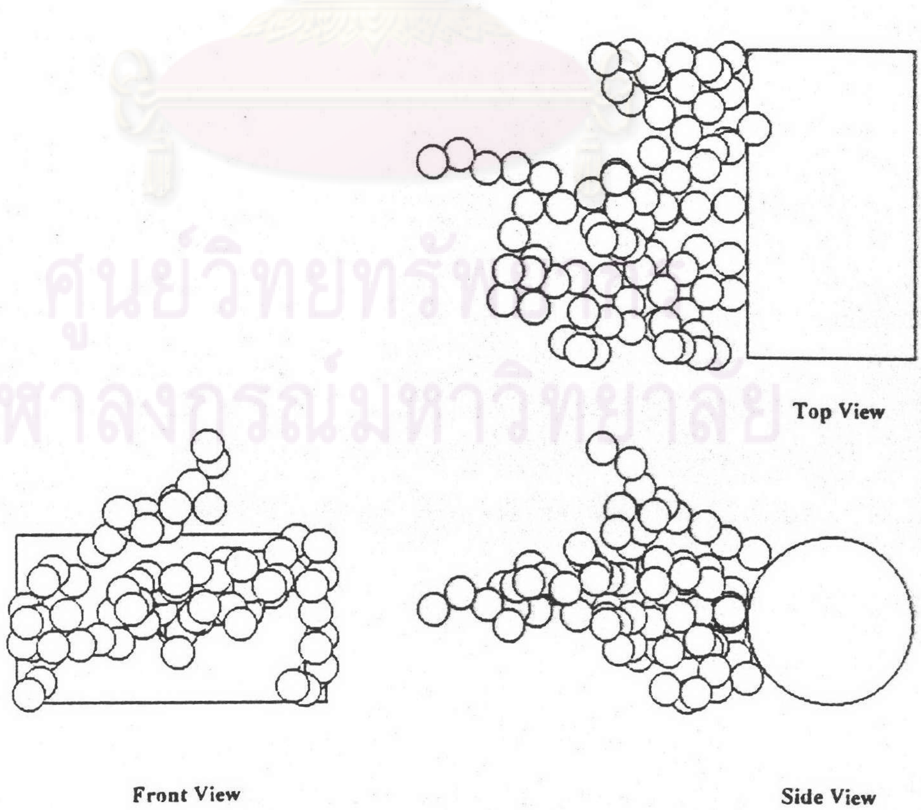

Figure 5.59. Typical configurations of dendrites for R=0.2 and St=1.0

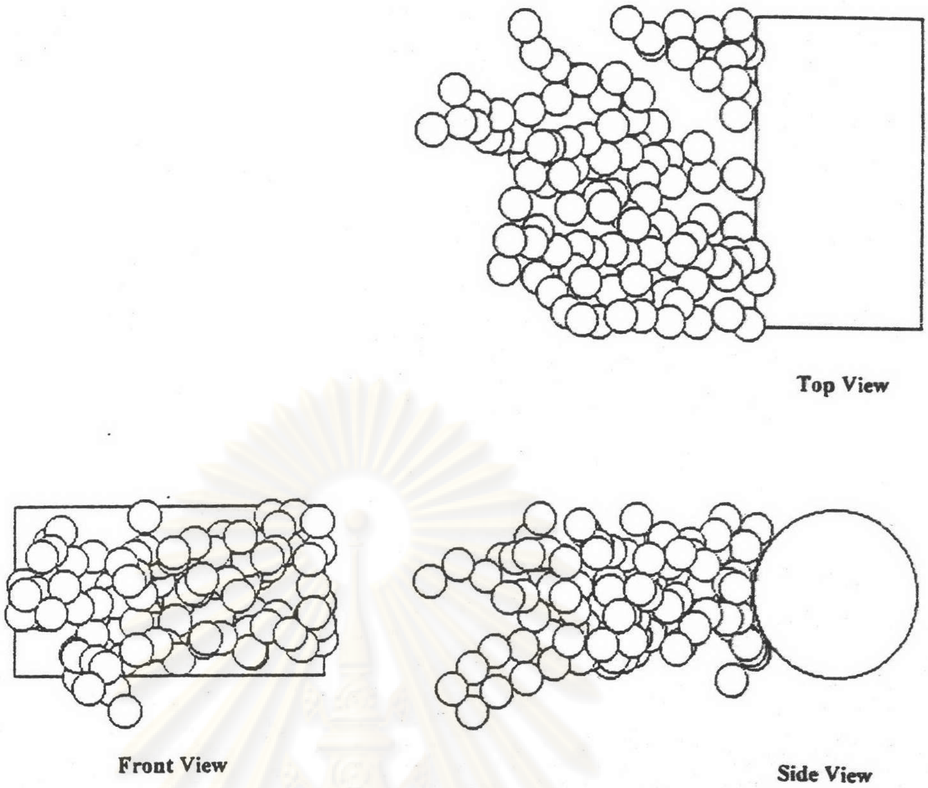

Figure 5.60. Typical configurations of dendrites for R=0.2 and St=1.4

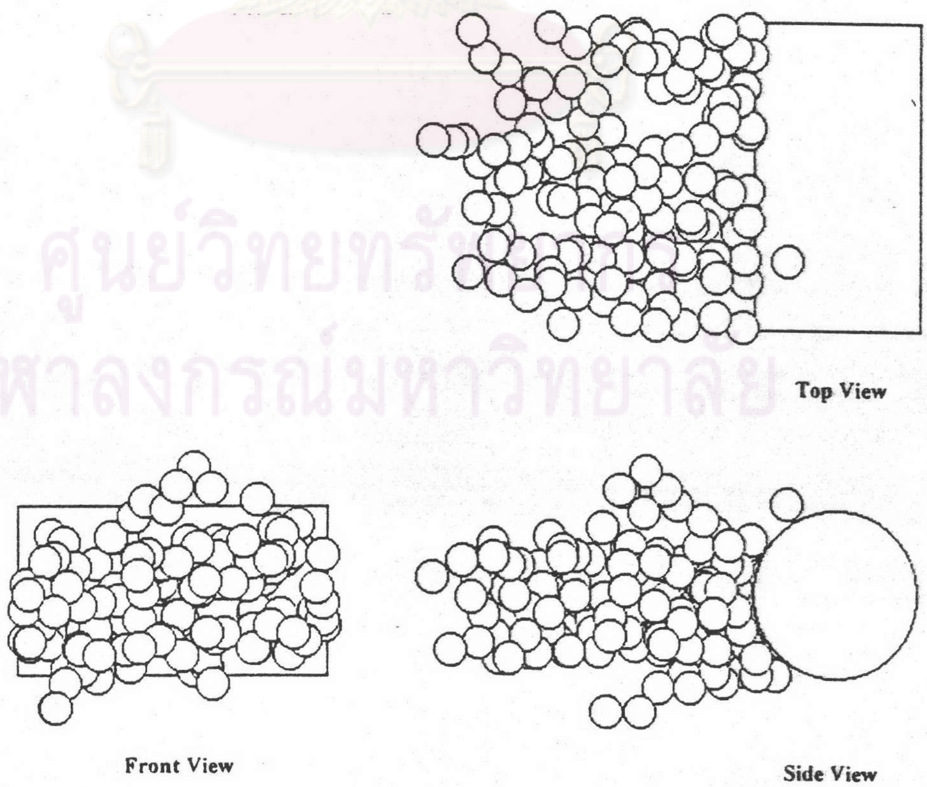

Figure 5.61. Typical configurations of dendrites for R=0.2 and St=2.0

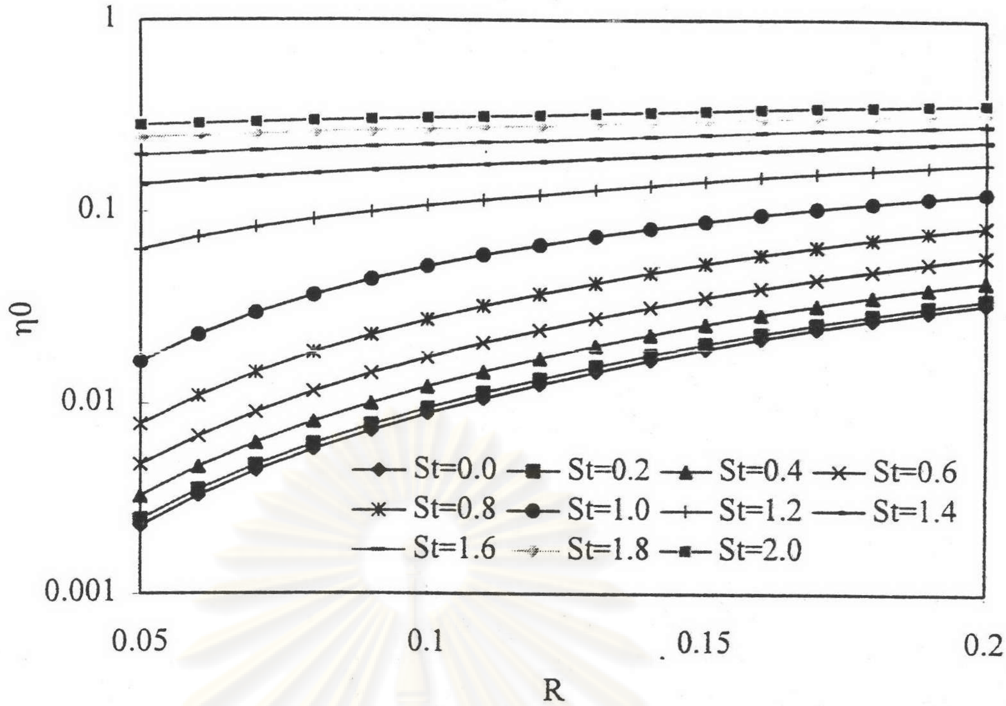

Figure 5.62. Relationship between η_0 and R with St as parameter (Limiting trajectory theory)

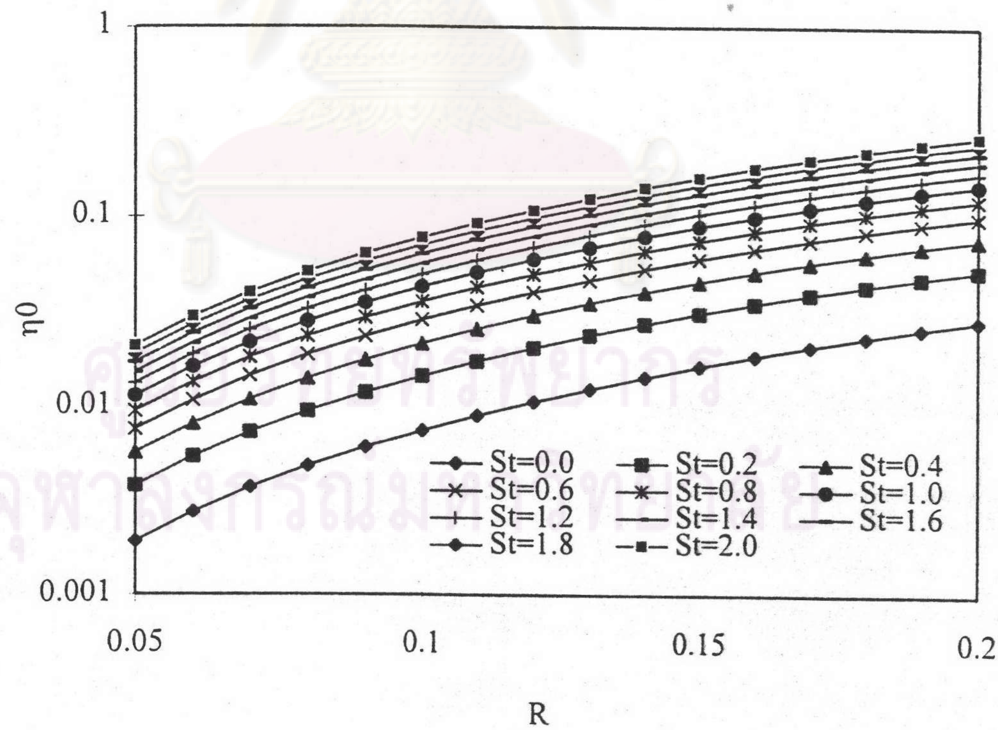

Figure 5.63. Relationship between η_0 and R with St as parameter (Stechkina's equation)

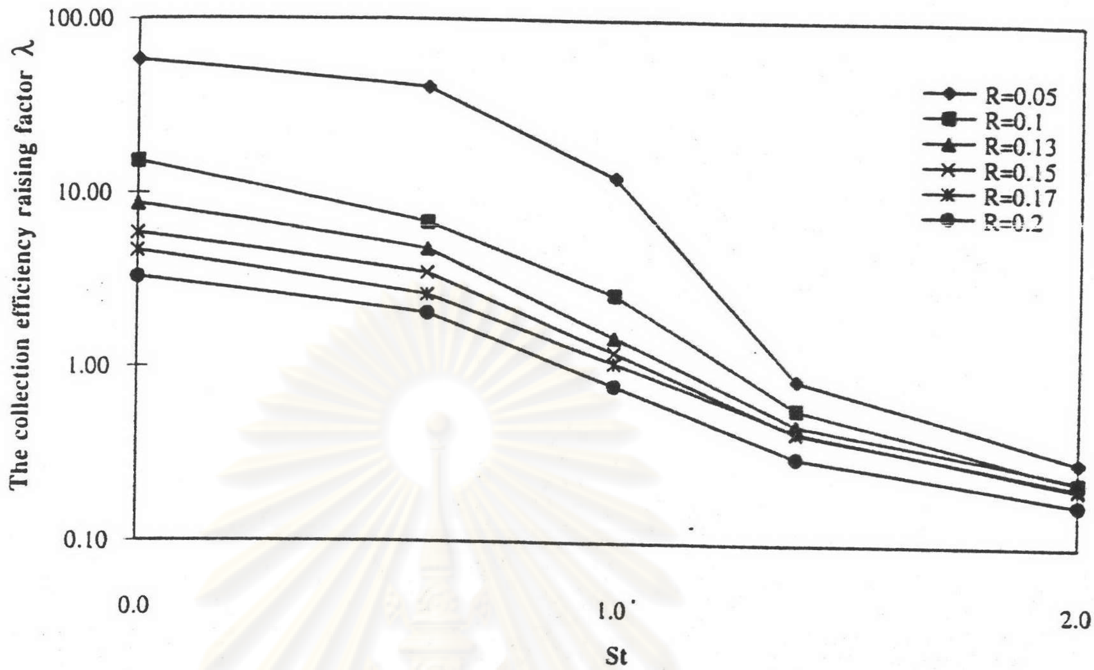

Figure 5.64. Relationship between λ and St with R as parameter (Stochastic simulation)

Table 5.3 Collection efficiency raising factor λ for inertial impaction

St	R					
	0.05	0.1	0.13	0.15	0.17	0.2
0	56.1* 57.770	14.8* 15.180	8.673	5.883	4.664	3.09* 3.307
0.6	45.7* 40.440	6.841	4.811	3.501	2.628	1.82* 2.049
1	16.4* 12.530	2.89* 2.660	1.514	1.234	1.072	0.783* 0.794
1.4	0.874* 0.867	0.594	0.482	0.433	0.441	0.313
2	0.238* 0.306	0.253* 0.236	0.243	0.222	0.216	0.144* 0.176

* Kanaoka et al., 1980

Table 5.4 Difference of λ between another previous study (Kanaoka et al., 1980) and the present study for inertial impaction (%)

St	R		
	0.05	0.1	0.2
0	2.98	2.57	7.02
0.6	11.510	-	12.580
1	23.600	7.960	1.400
1.4	0.800	-	-
2	28.570	6.720	22.220

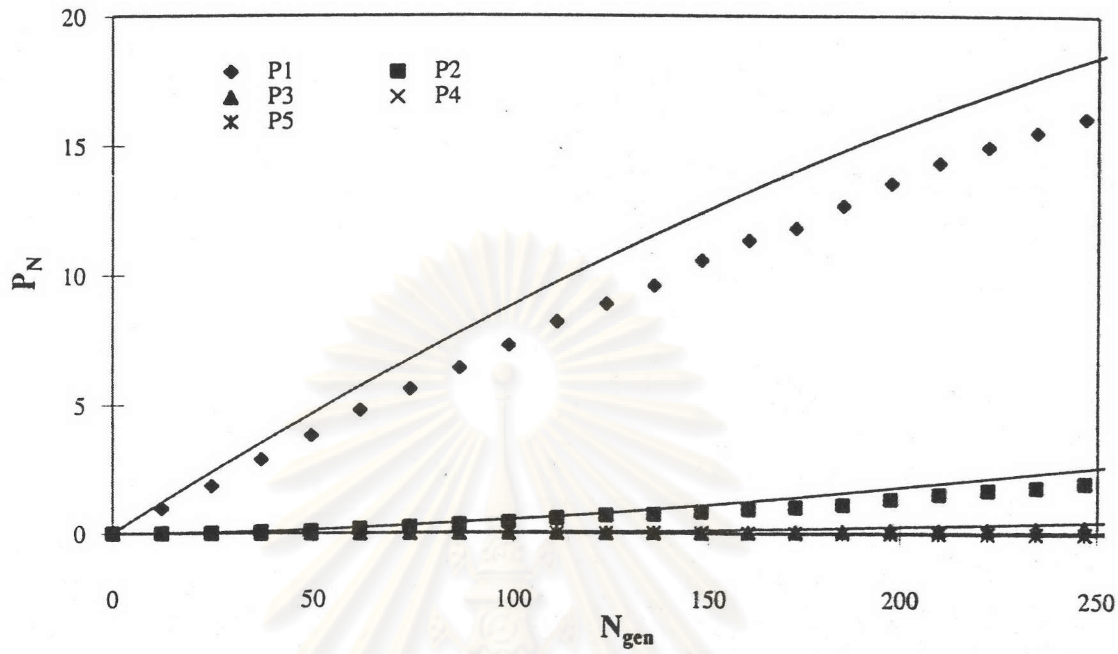

Figure 5.65. Comparison of dendrite distribution between stochastic and simplified model for R=0.05 and Pe=200

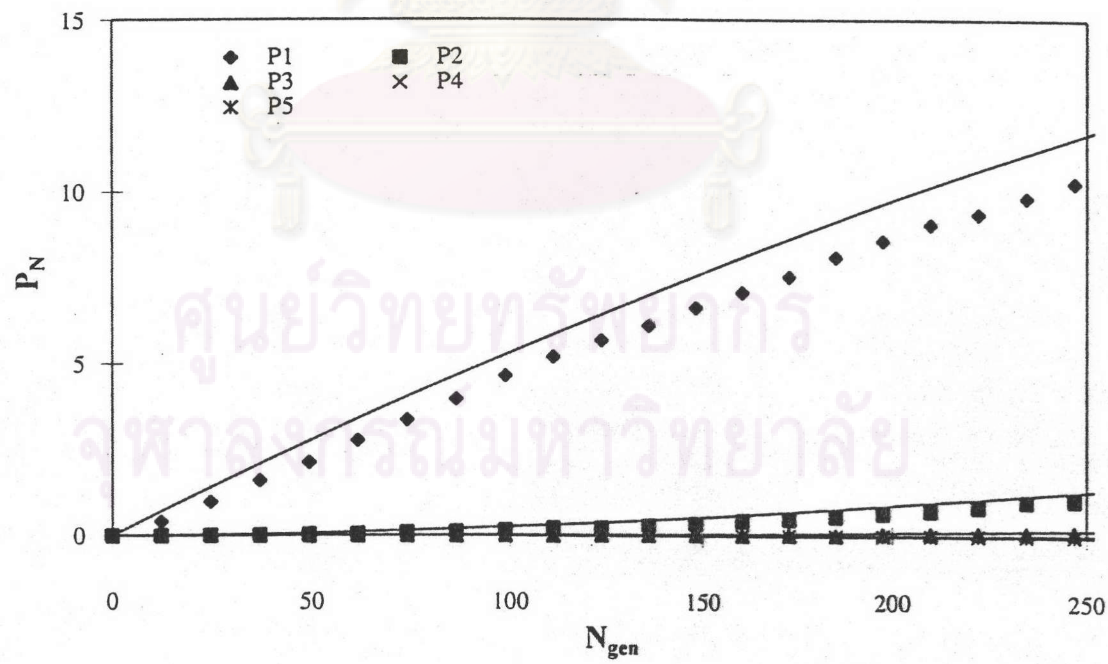

Figure 5.66. Comparison of dendrite distribution between stochastic and simplified model for R=0.05 and Pe=500

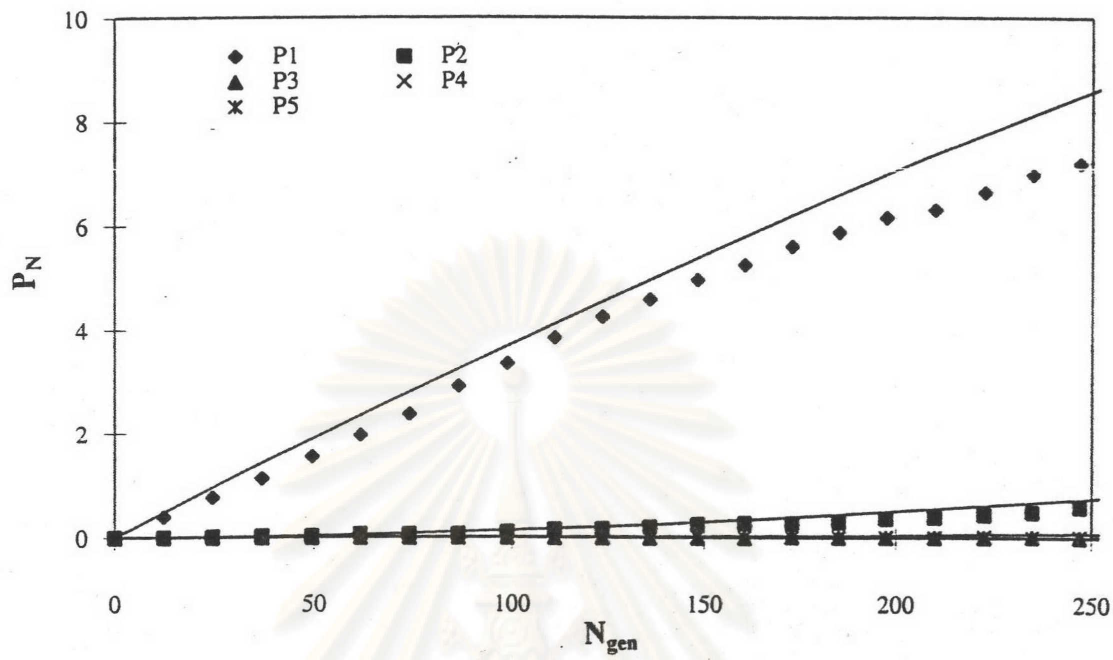

Figure 5.67. Comparison of dendrite distribution between stochastic and simplified model for R=0.05 and Pe=1000

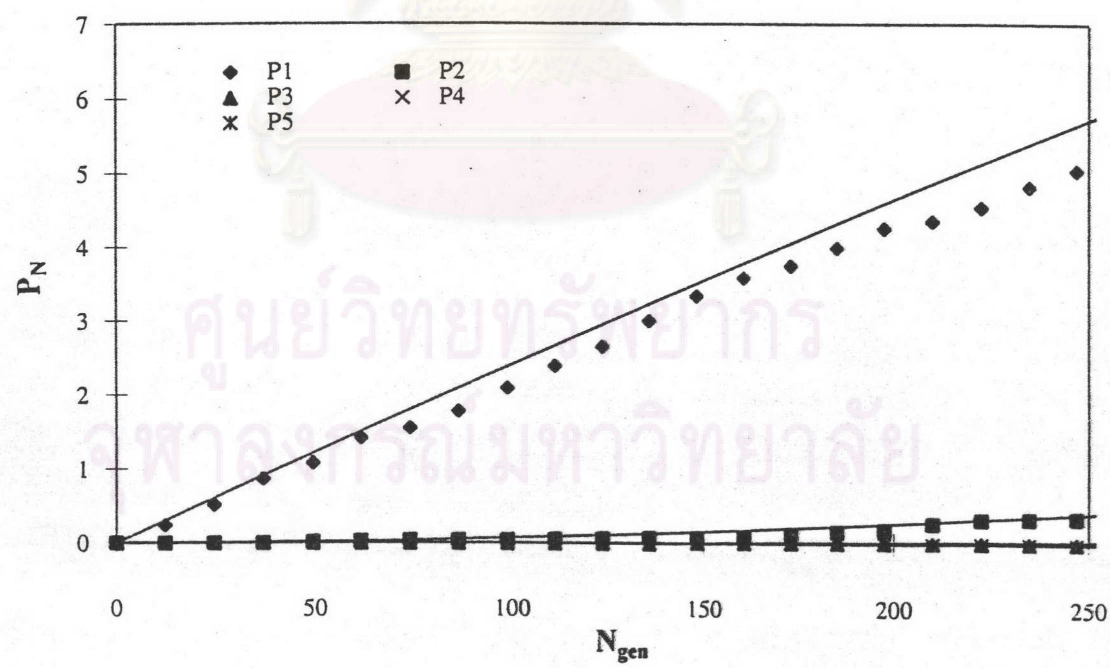

Figure 5.68. Comparison of dendrite distribution between stochastic and simplified model for R=0.05 and Pe=2500

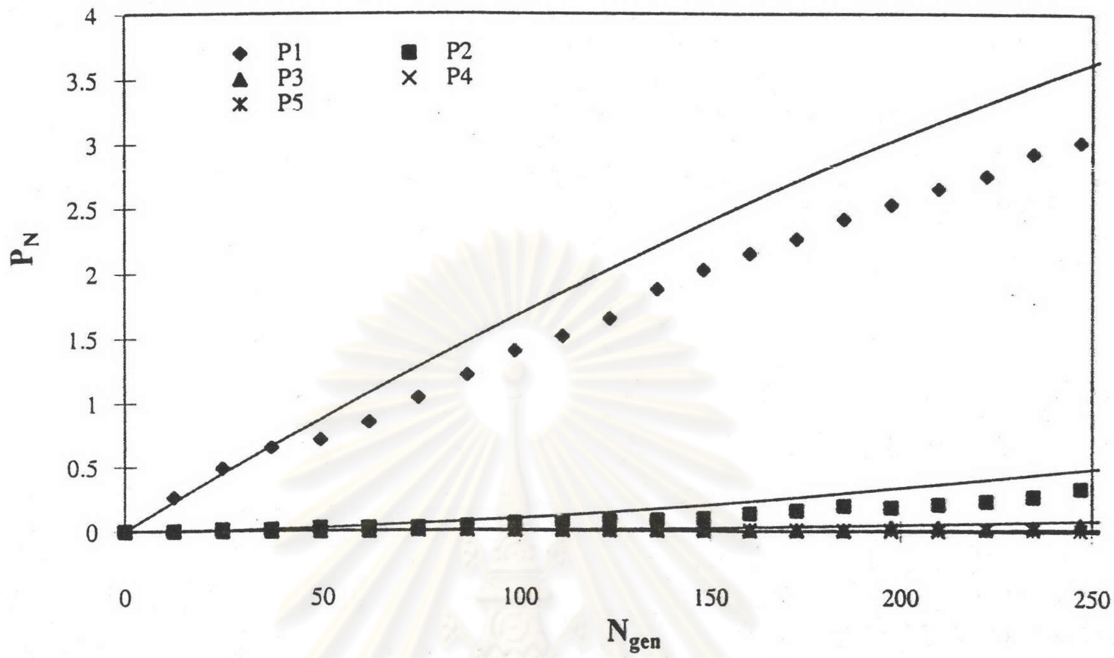

Figure 5.69. Comparison of dendrite distribution between stochastic and simplified model for R=0.05 and Pe=5000

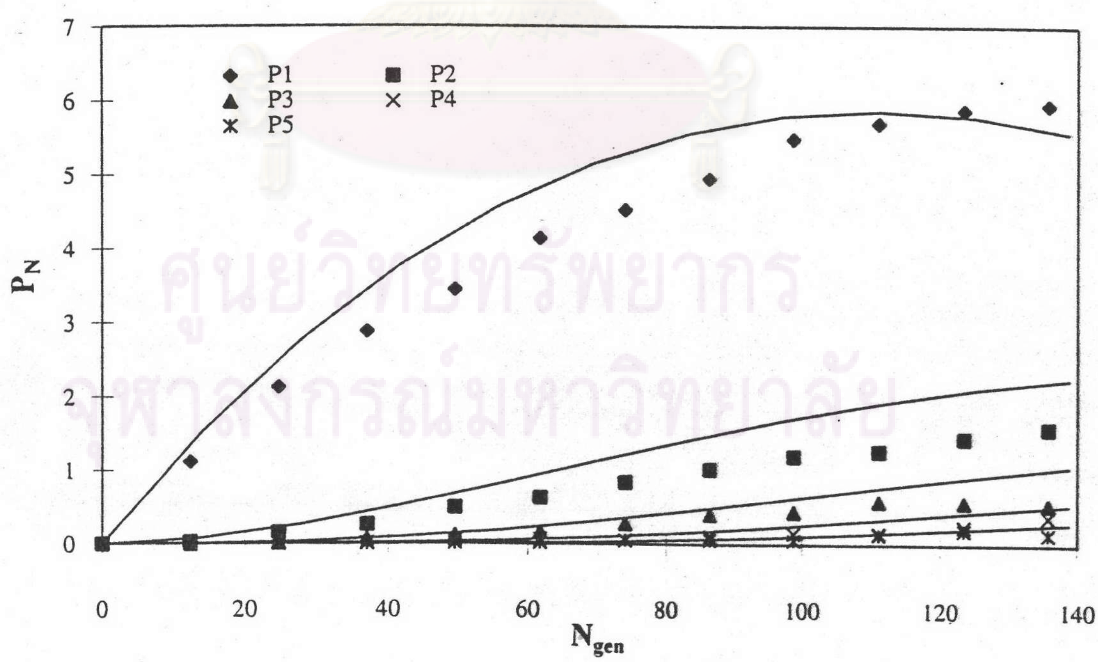

Figure 5.70. Comparison of dendrite distribution between stochastic and simplified model for R=0.1 and Pe=200

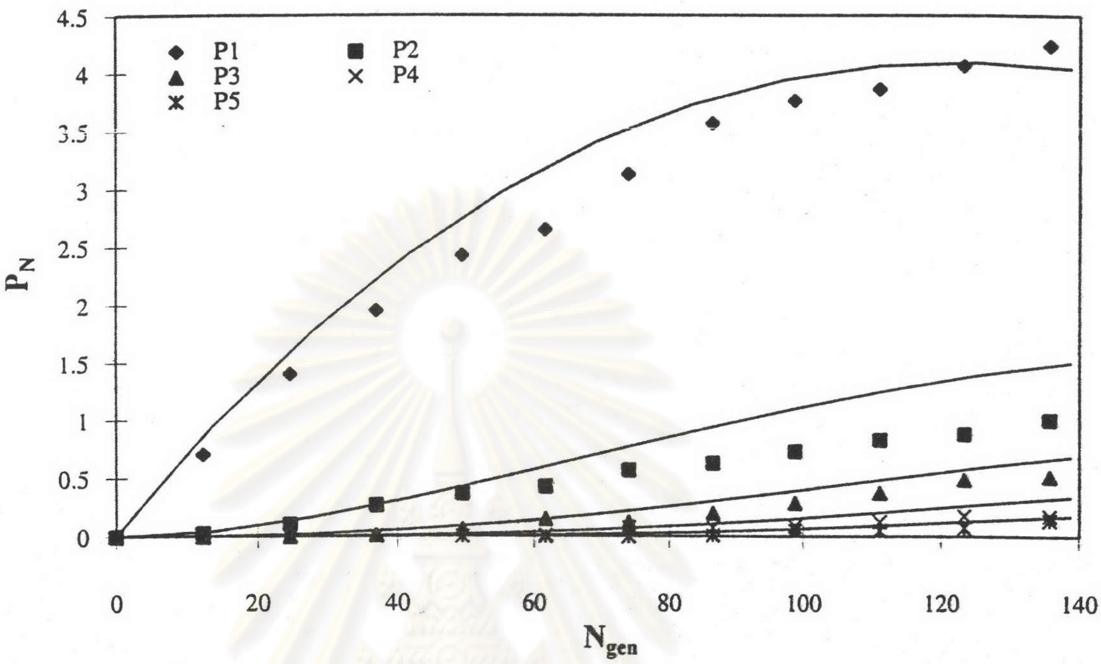

Figure 5.71. Comparison of dendrite distribution between stochastic and simplified model for R=0.1 and Pe=500

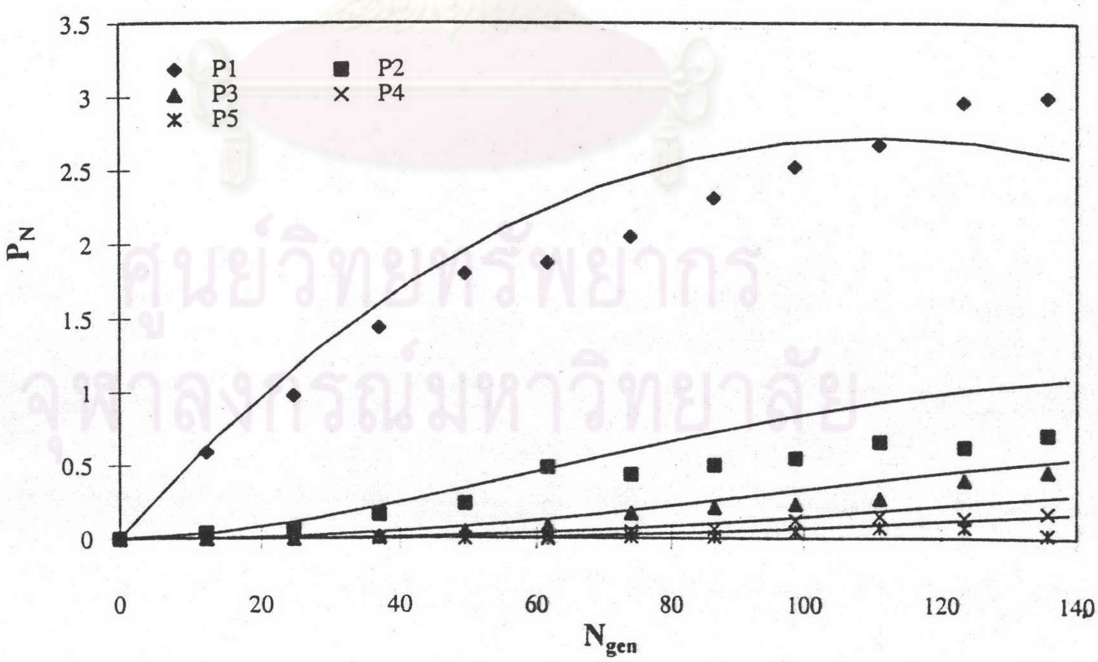

Figure 5.72. Comparison of dendrite distribution between stochastic and simplified model for R=0.1 and Pe=1000

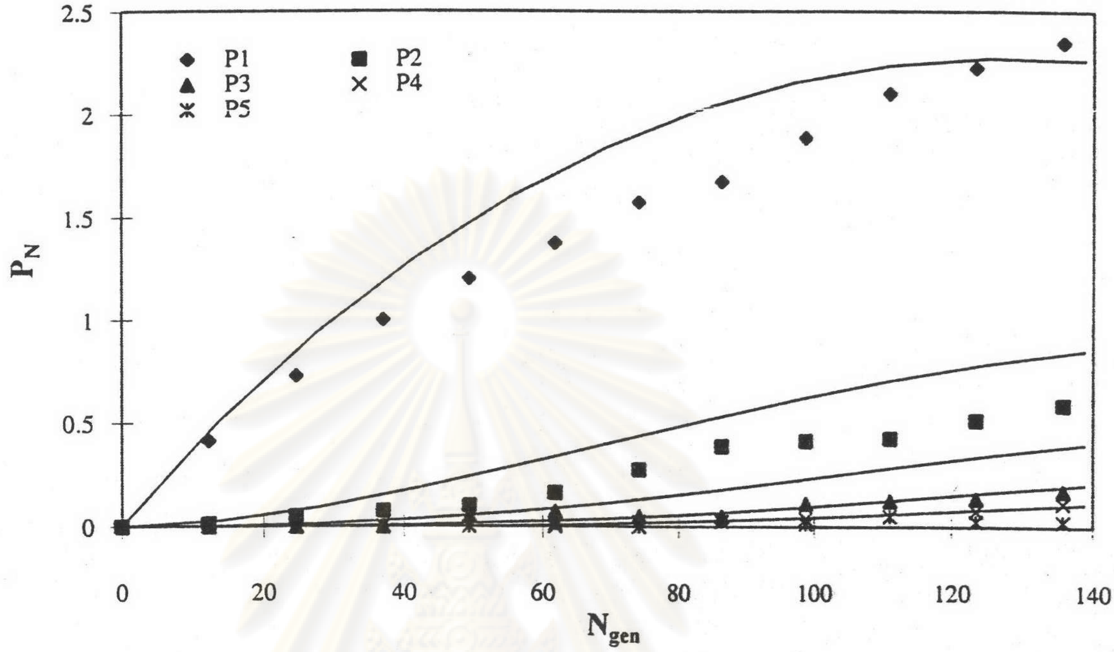

Figure 5.73. Comparison of dendrite distribution between stochastic and simplified model for R=0.1 and Pe=2500

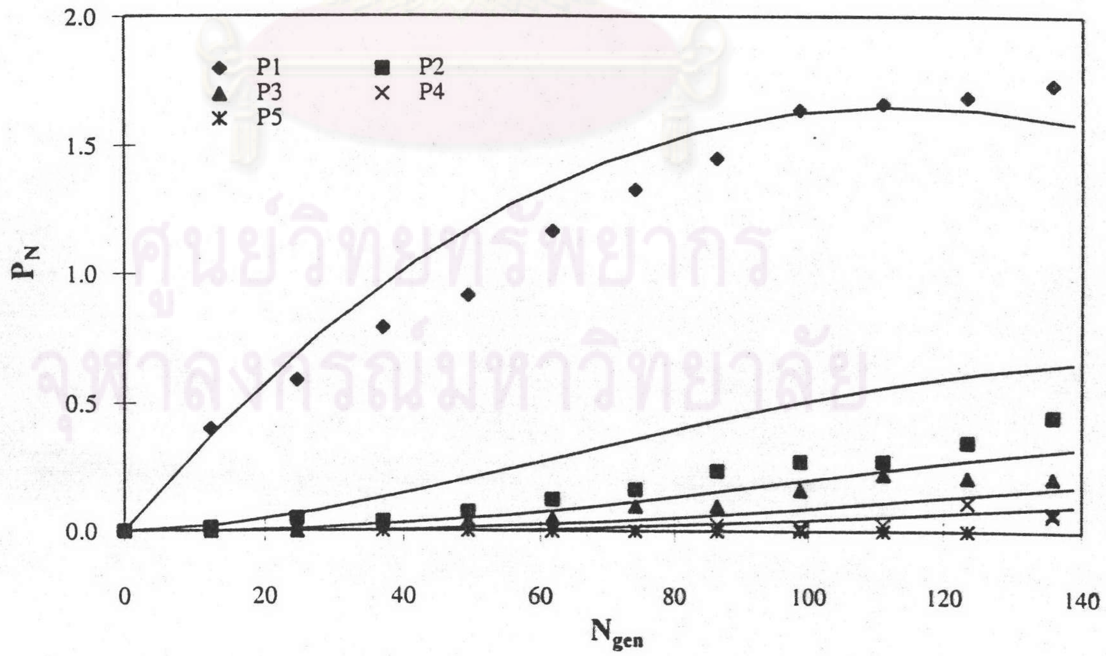

Figure 5.74. Comparison of dendrite distribution between stochastic and simplified model for R=0.1 and Pe=5000

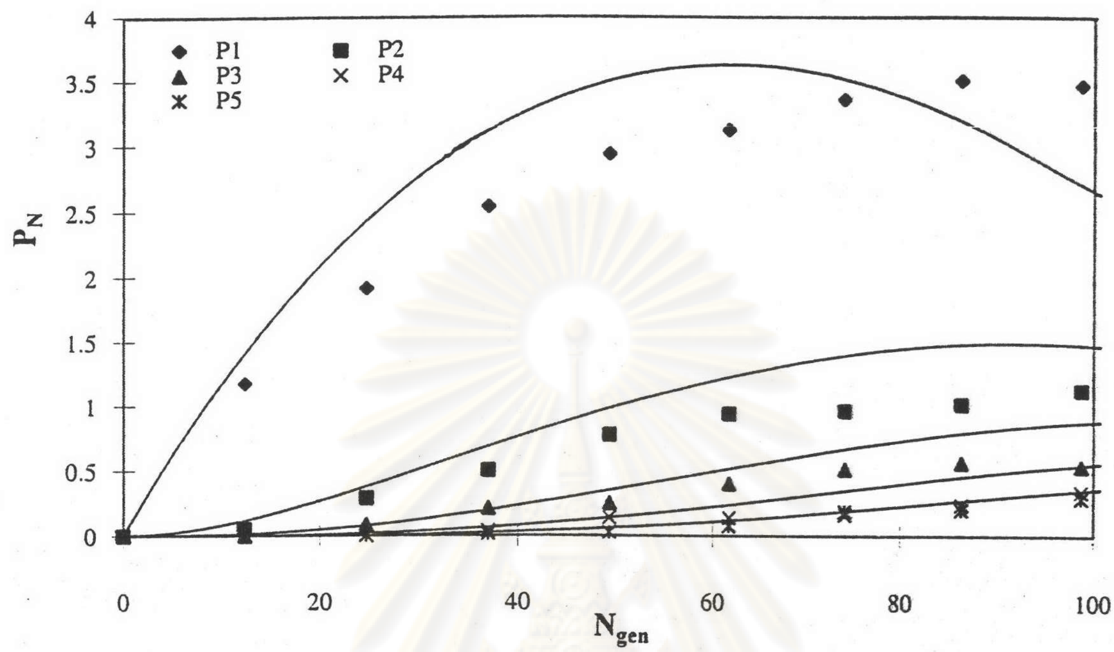

Figure 5.75. Comparison of dendrite distribution between stochastic and simplified model for R=0.13 and Pe=200

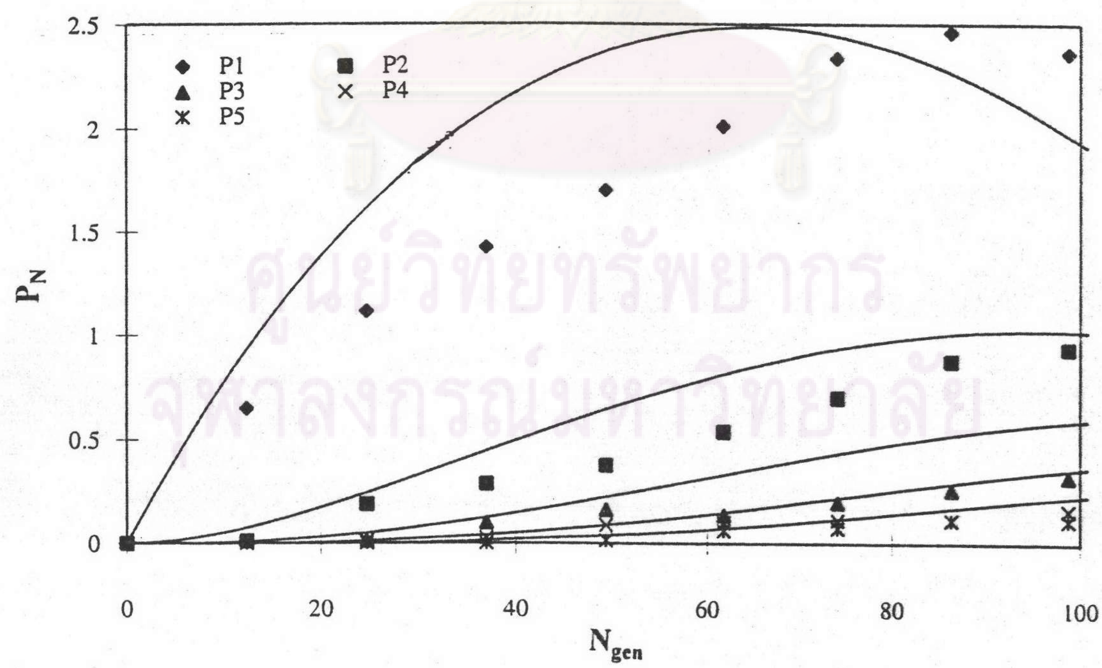

Figure 5.76. Comparison of dendrite distribution between stochastic and simplified model for R=0.13 and Pe=500

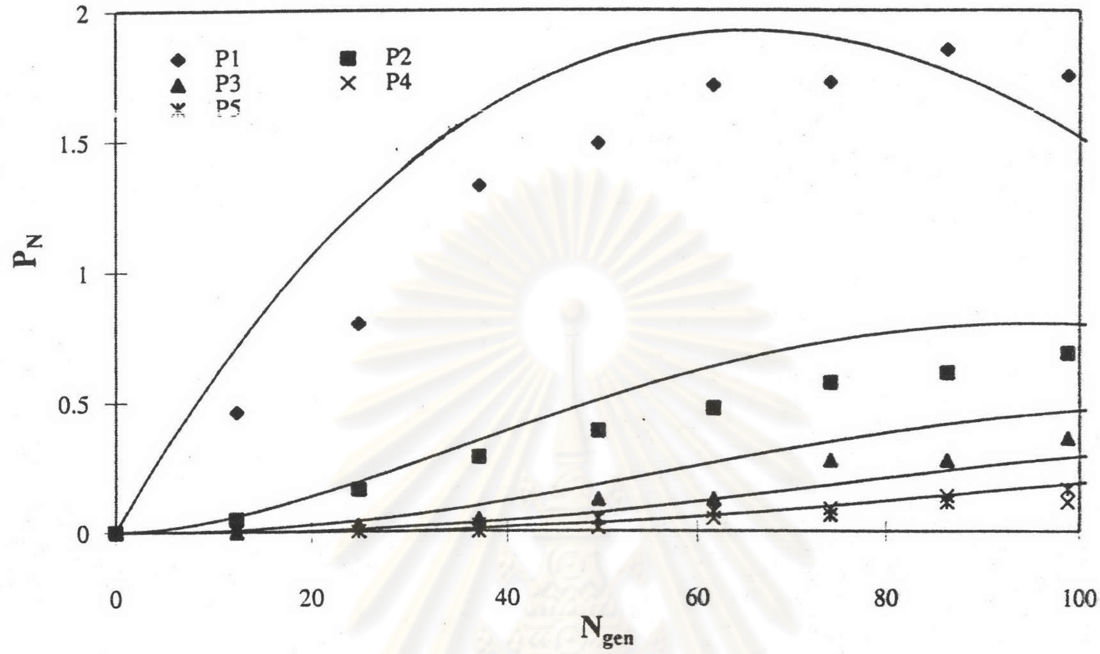

Figure 5.77. Comparison of dendrite distribution between stochastic and simplified model for R=0.13 and Pe=1000

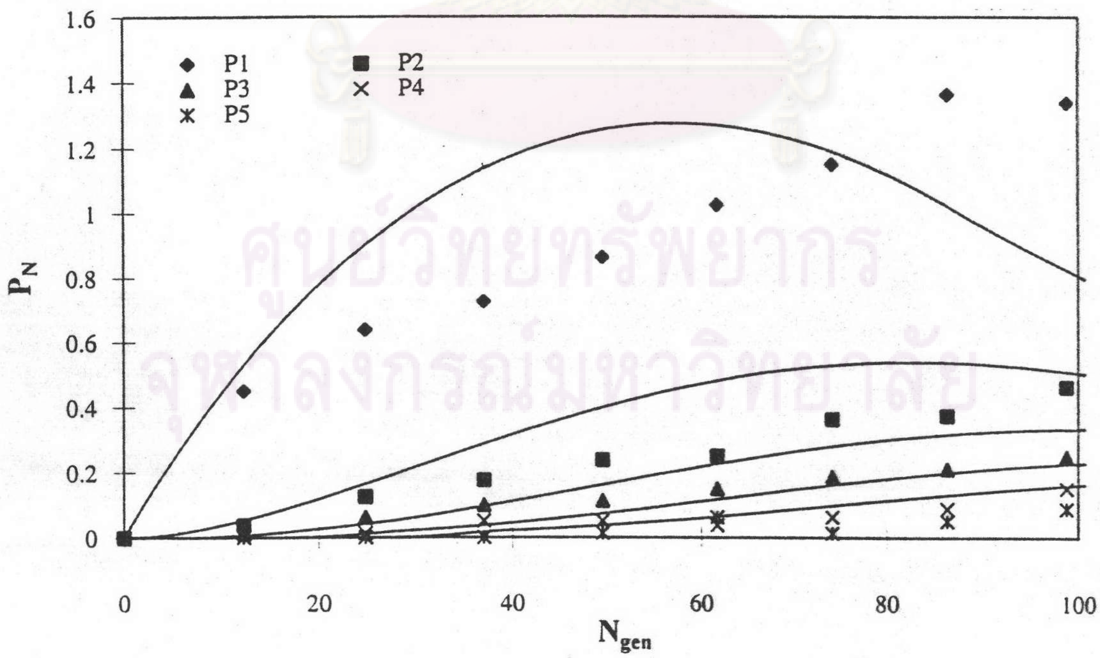

Figure 5.78. Comparison of dendrite distribution between stochastic and simplified model for R=0.13 and Pe=2500

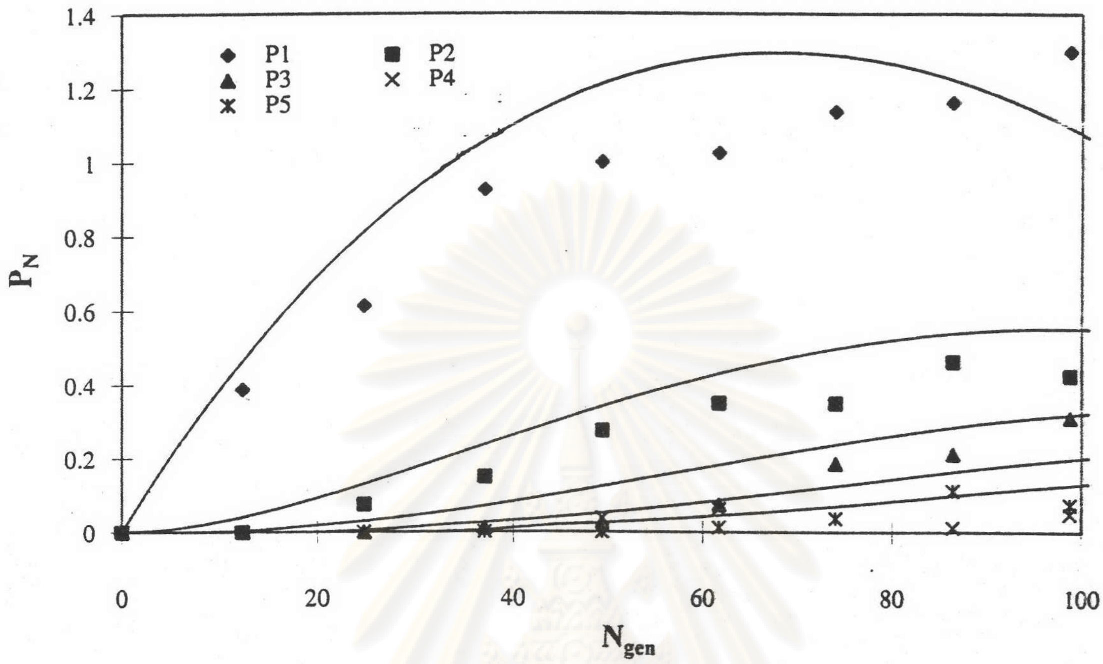

Figure 5.79. Comparison of dendrite distribution between stochastic and simplified model for R=0.13 and Pe=5000

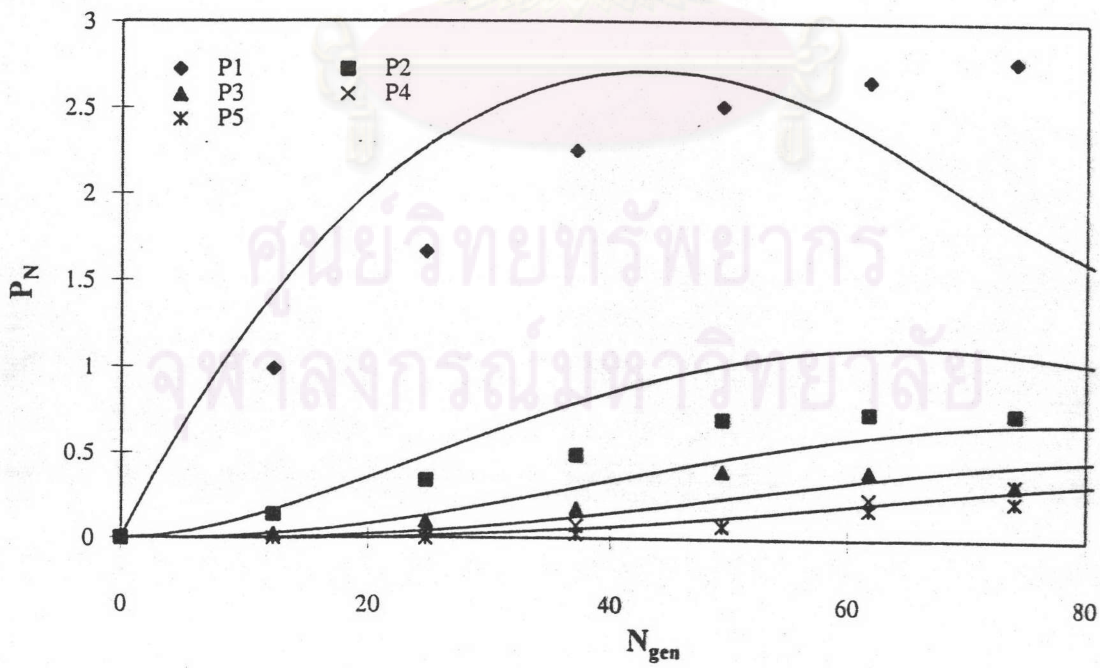

Figure 5.80. Comparison of dendrite distribution between stochastic and simplified model for R=0.15 and Pe=200

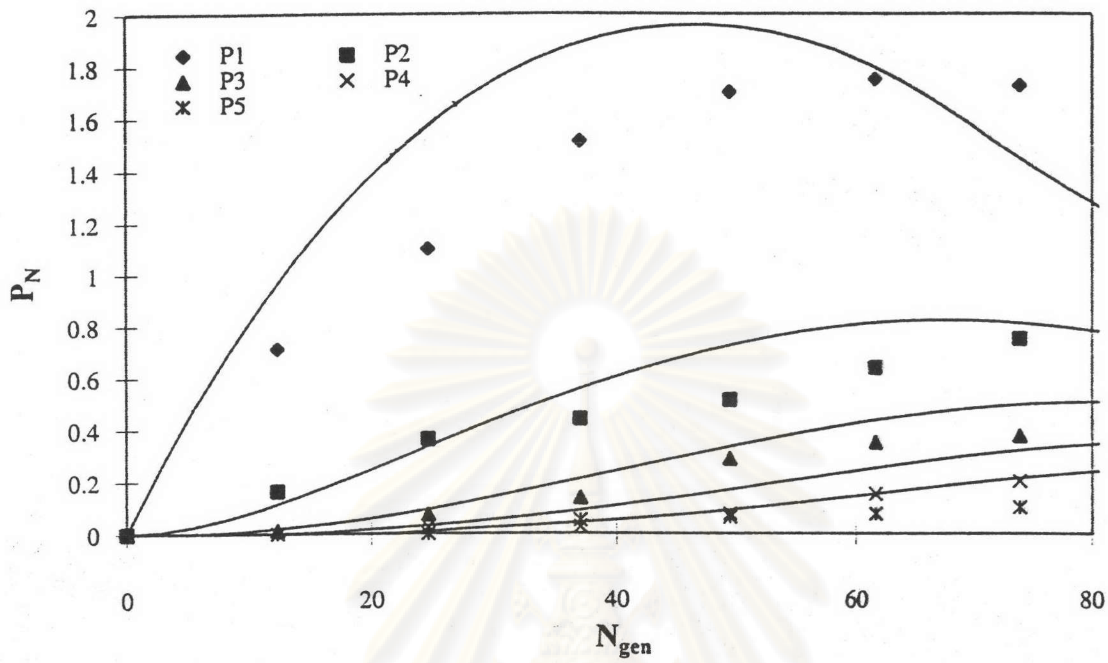

Figure 5.81. Comparison of dendrite distribution between stochastic and simplified model for R=0.15 and Pe=500

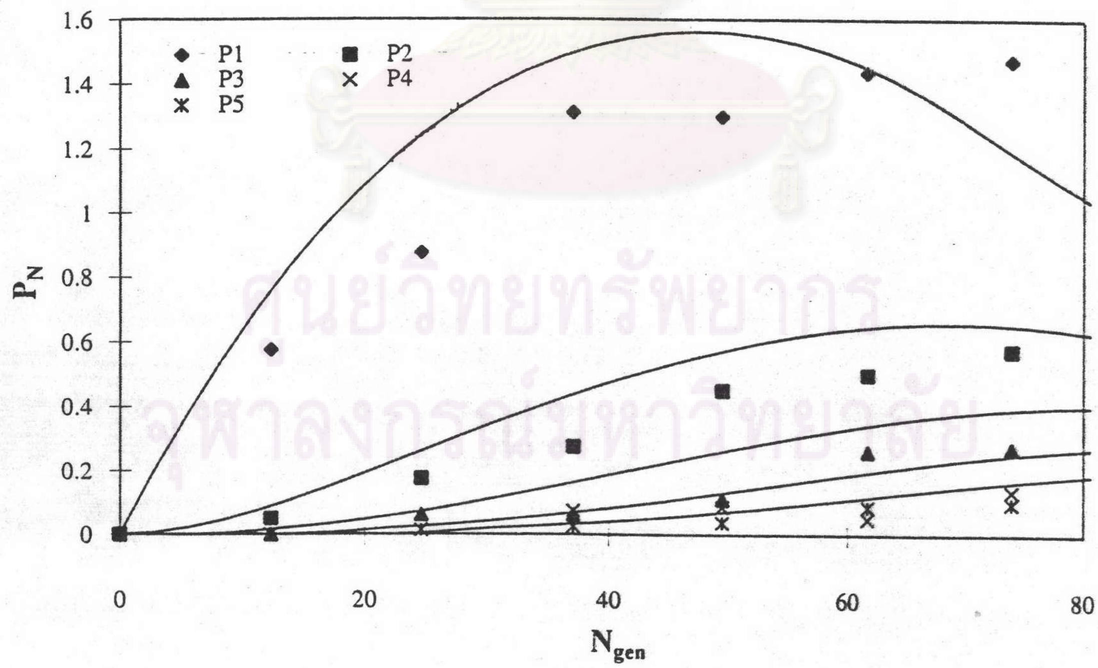

Figure 5.82. Comparison of dendrite distribution betwee stochastic and simplified model for R=0.15 and Pe=1000

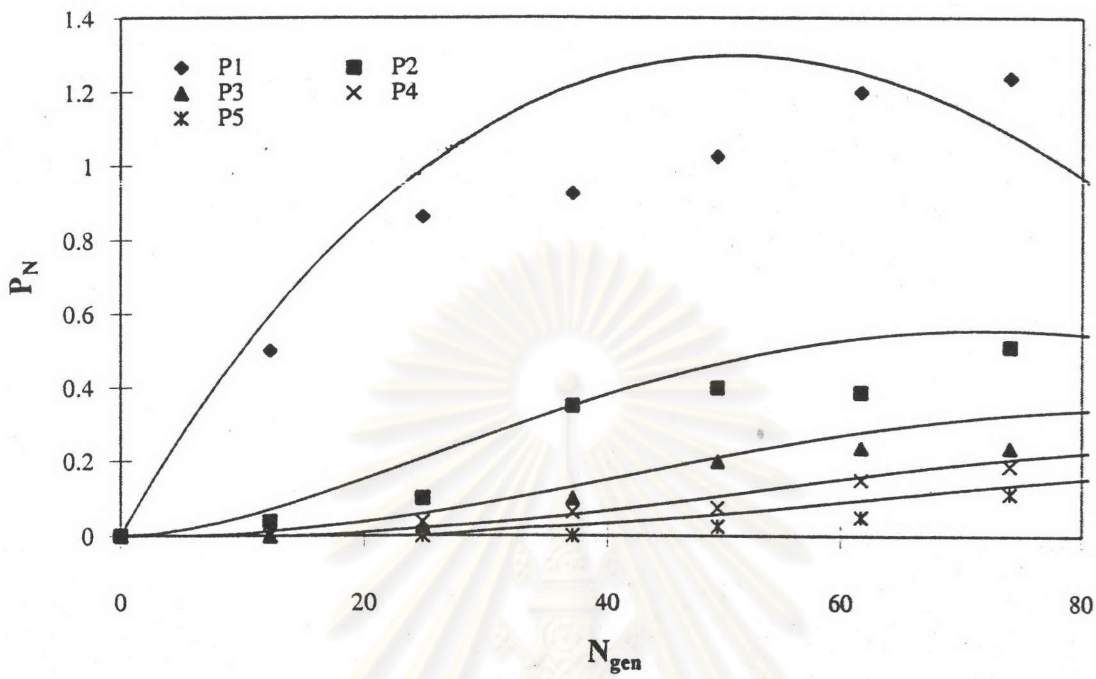

Figure 5.83. Comparison of dendrite distribution between stochastic and simplified model for R=0.15 and Pe=2500

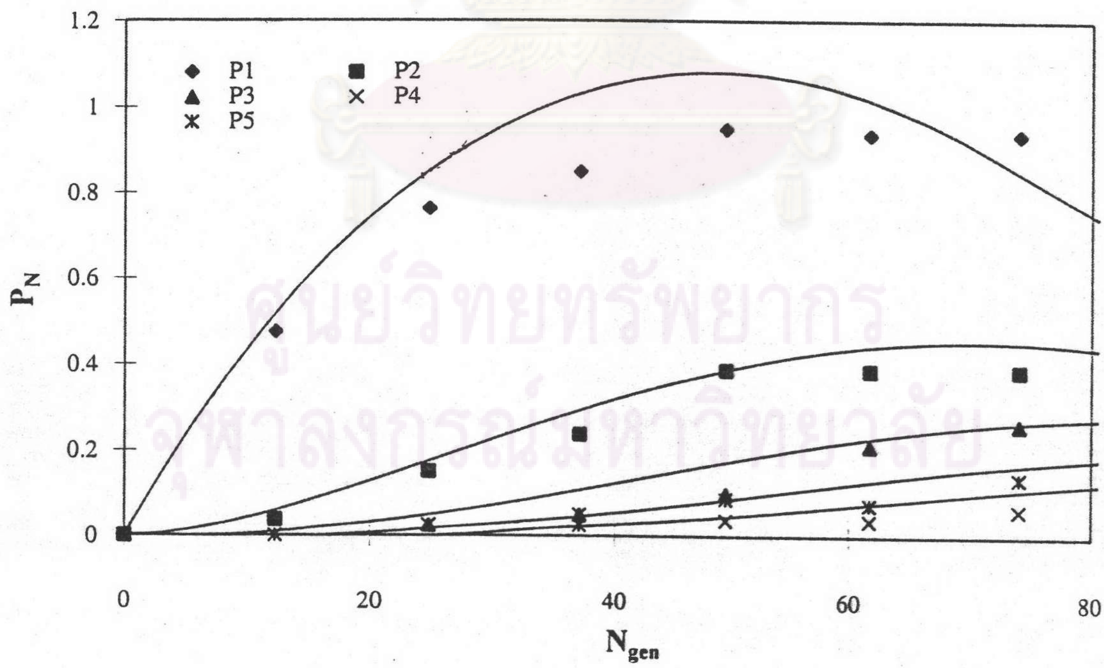

Figure 5.84. Comparison of dendrite distribution between stochastic and simplified model for R=0.15 and Pe=5000

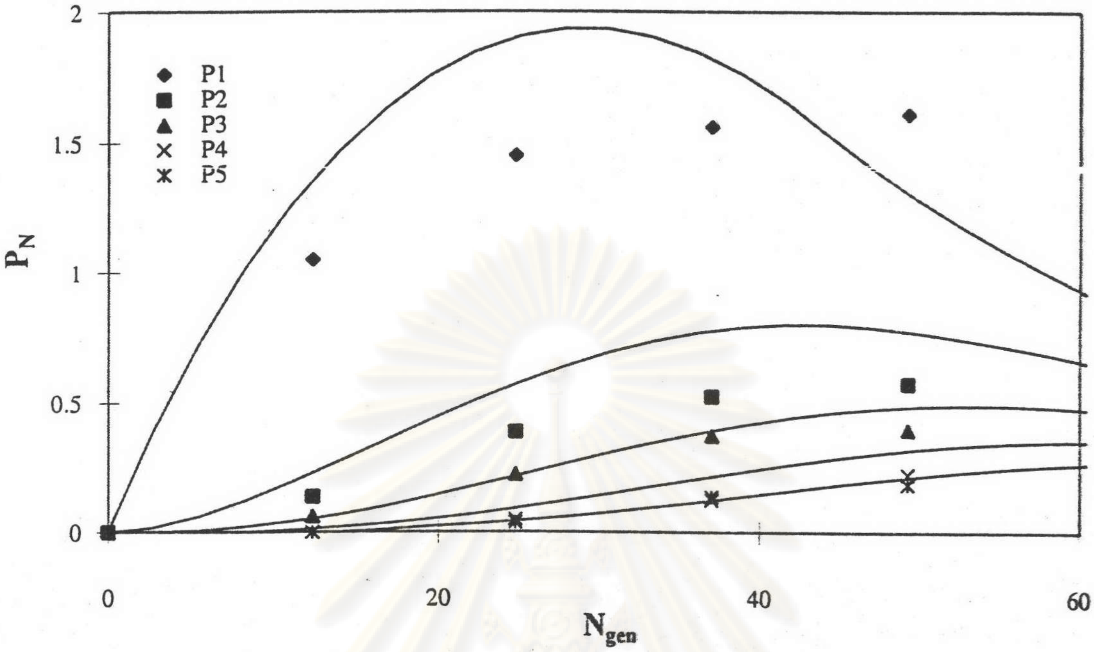

Figure 5.85. Comparison of dendrite distribution between stochastic and simplified model for R=0.17 and Pe=200

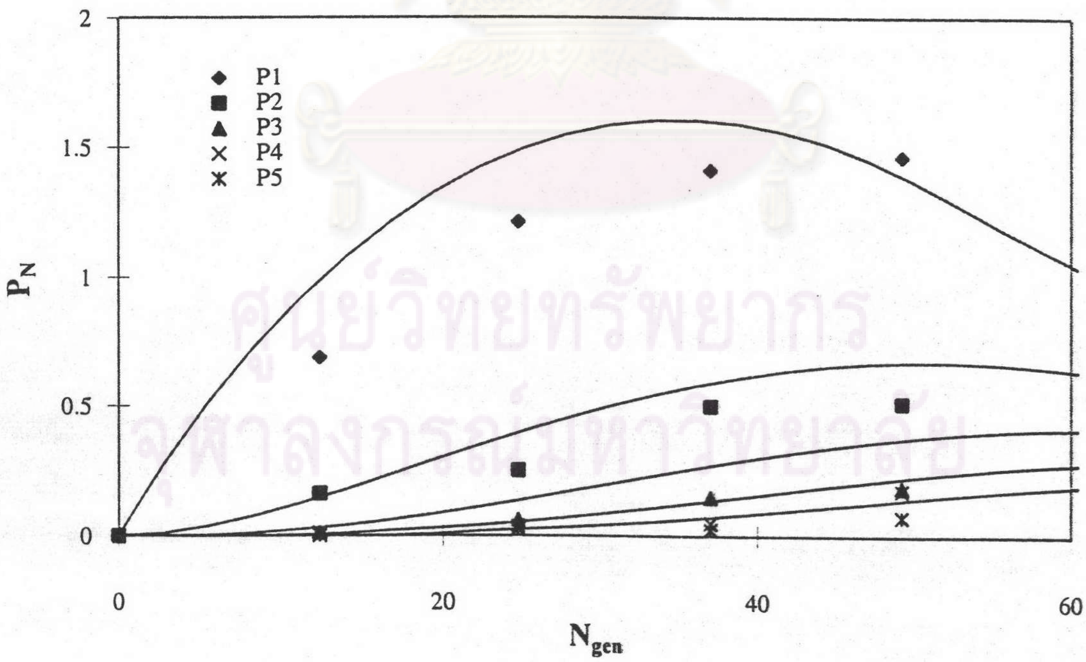

Figure 5.86. Comparison of dendrite distribution between stochastic and simplified model for R=0.17 and Pe=500

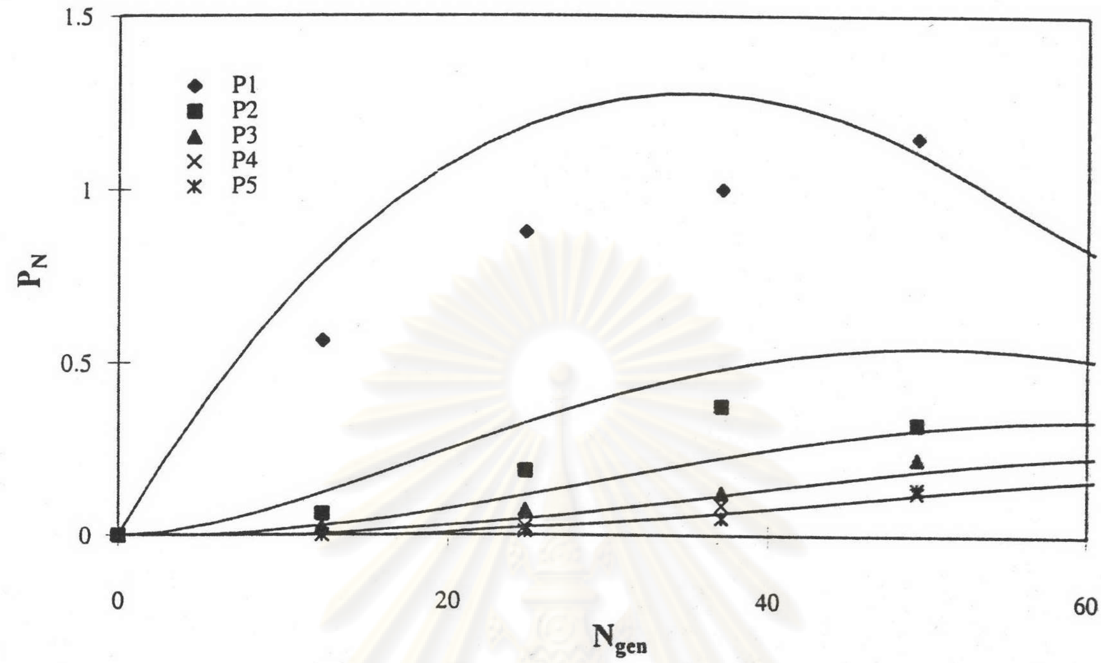

Figure 5.87. Comparison of dendrite distribution between stochastic and simplified model for R=0.17 and Pe=1000

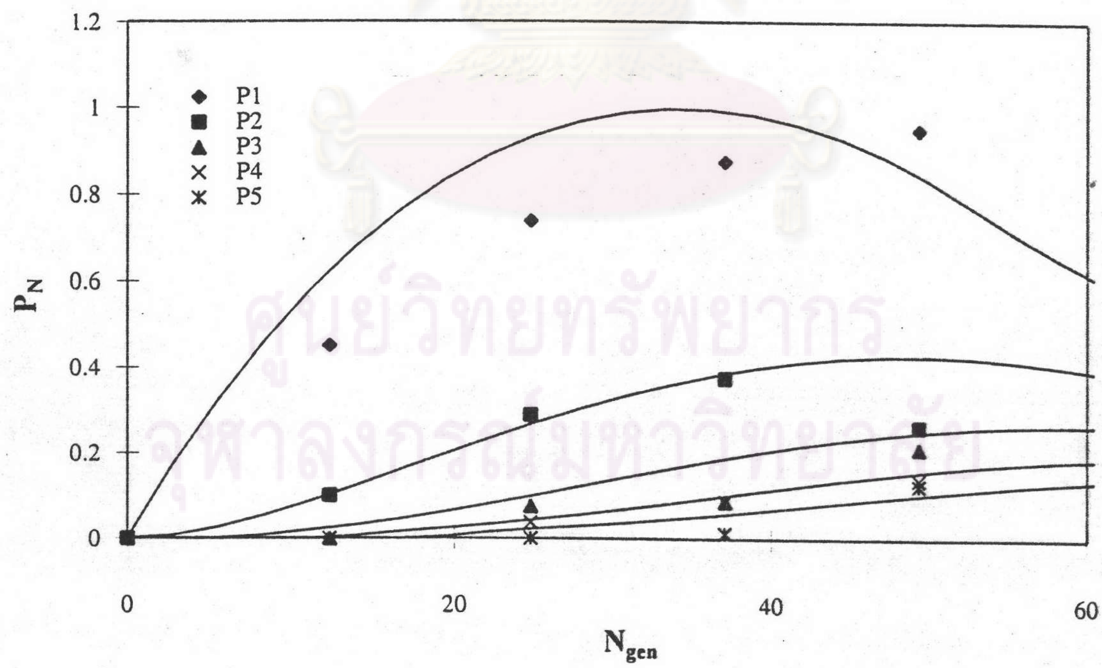

Figure 5.88. Comparison of dendrite distribution between stochastic and simplified model for R=0.17 and Pe=2500

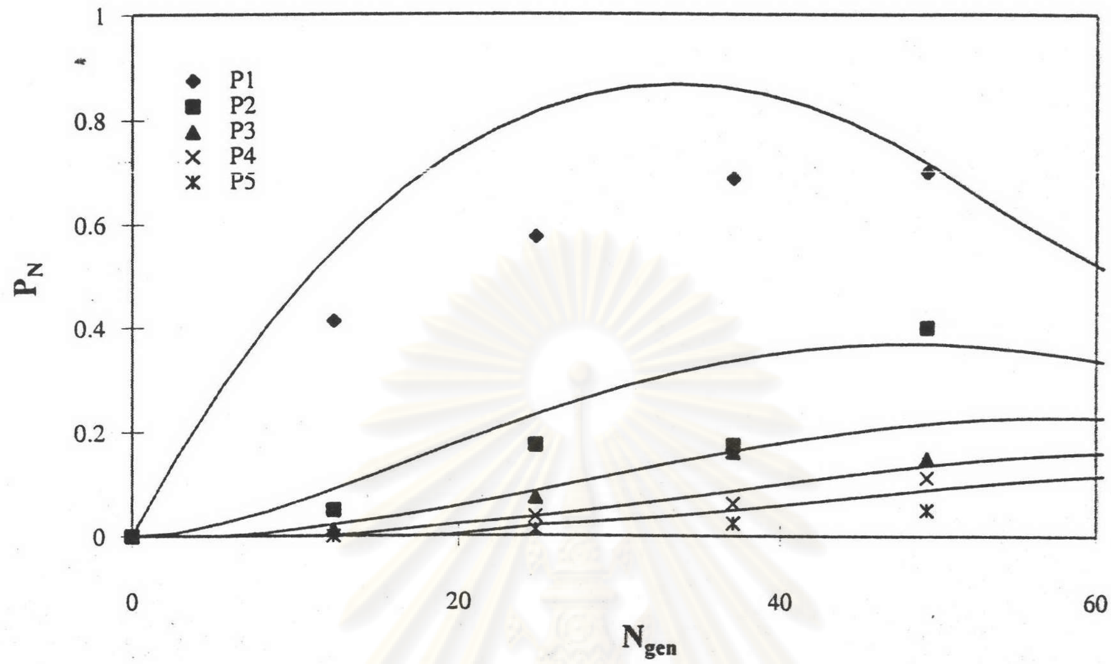

Figure 5.89. Comparison of dendrite distribution between stochastic and simplified model for R=0.17 and Pe=5000

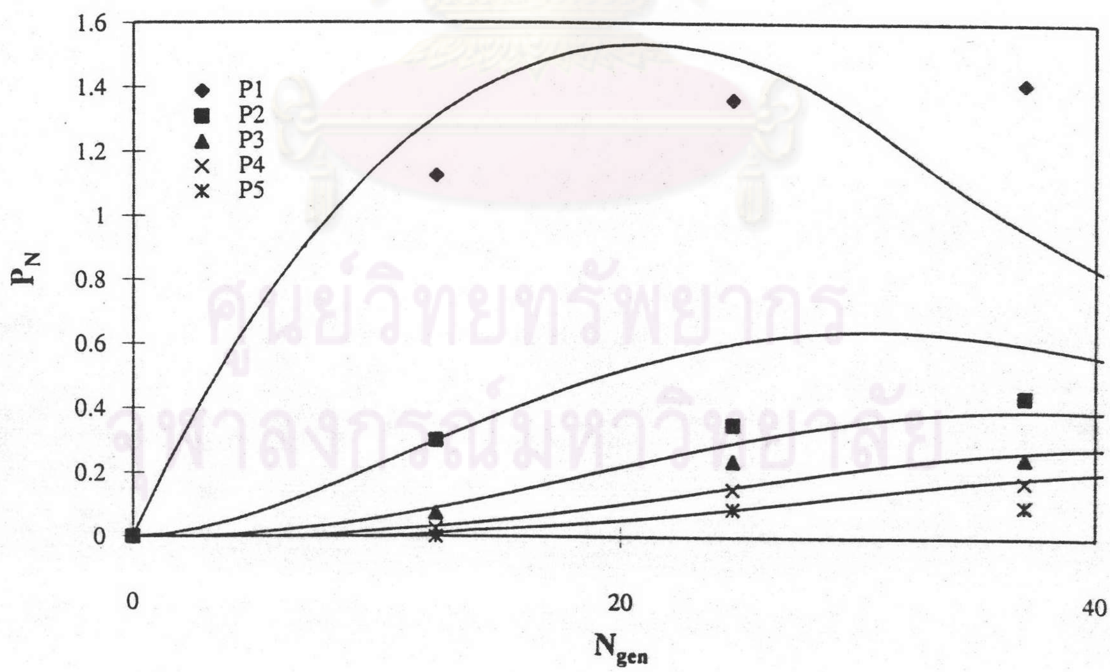

Figure 5.90. Comparison of dendrite distribution between stochastic and simplified model for R=0.2 and Pe=200

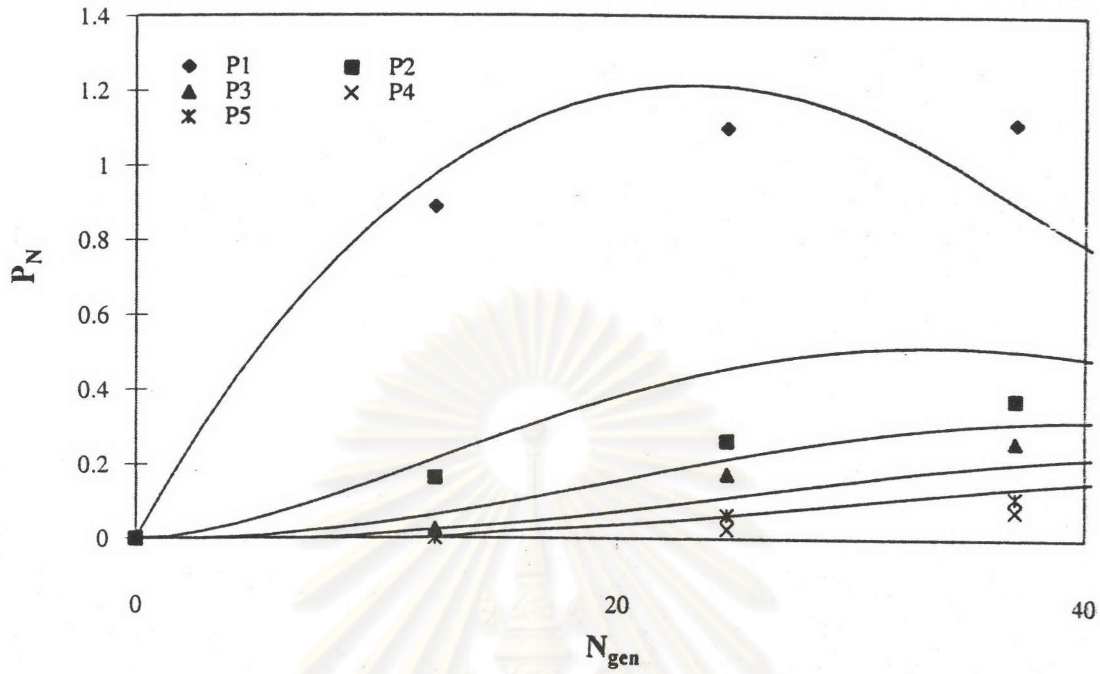

Figure 5.91. Comparison of dendrite distribution between stochastic and simplified model for R=0.2 and Pe=500

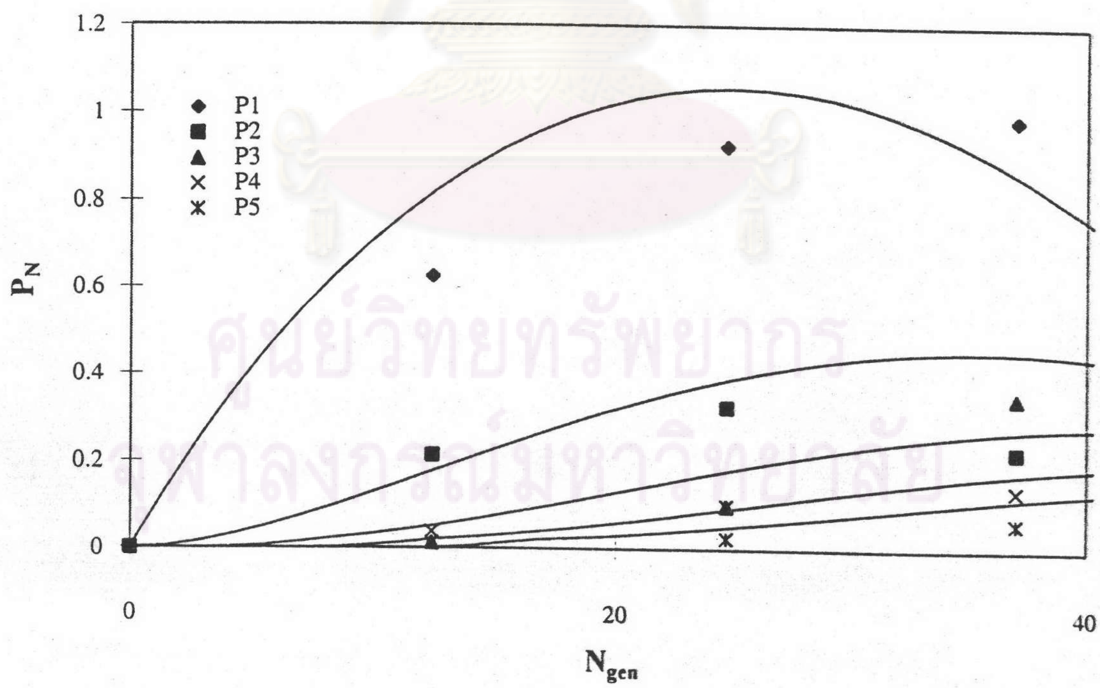

Figure 5.92. Comparison of dendrite distribution between stochastic and simplified model for R=0.2 and Pe=1000

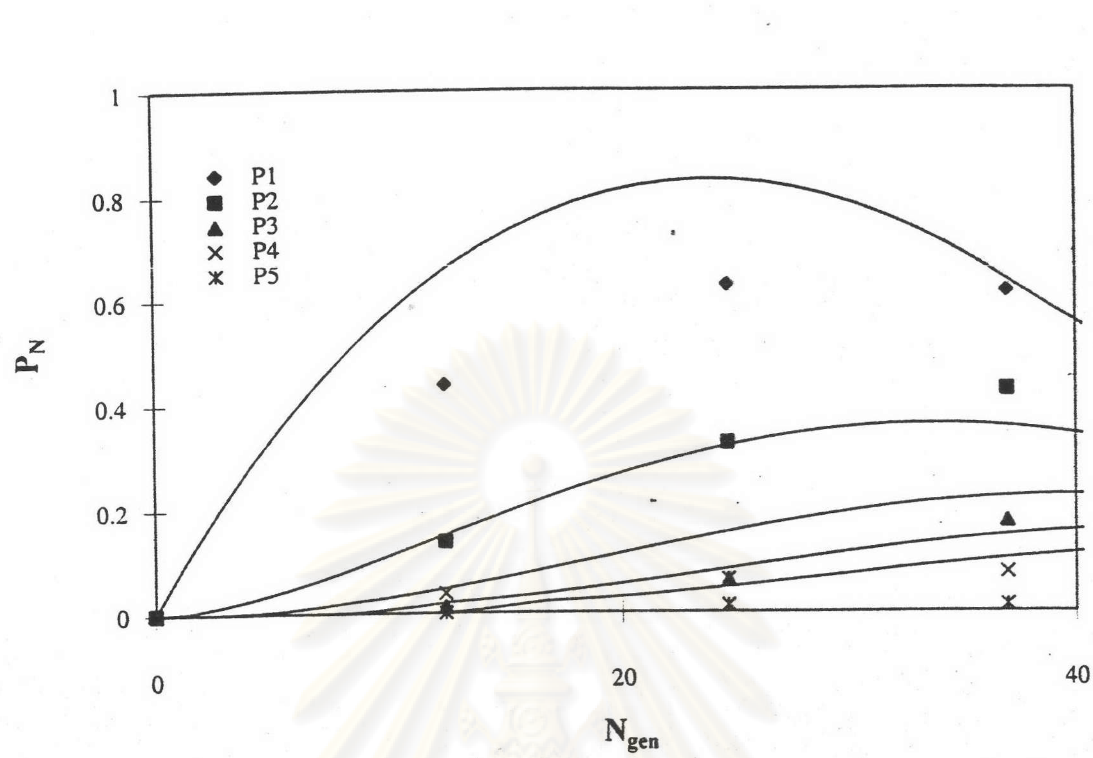

Figure 5.93. Comparison of dendrite distribution between stochastic and simplified model for R=0.2 and Pe=2500

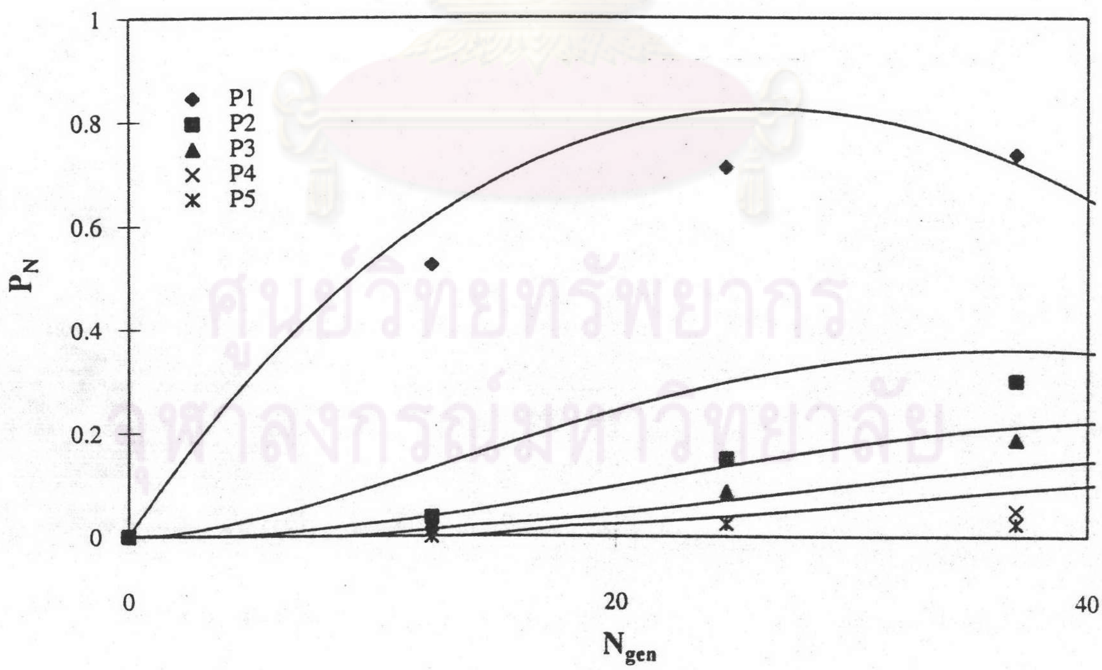

Figure 5.94. Comparison of dendrite distribution between stochastic and simplified model for R=0.2 and Pe=5000

particles, so the locations of deposition was limited in advance. But in the present study, the particles were deposited at their collision points. Furthermore, in the present study the effective fiber length (Z=3.6) was shorter than Kanaoka's (Z=10) because of limitation in personal computer memory.

Figure 5.64 shows the relationship between λ and St with R as parameter based on the stochastic results. The value of λ decreased with increasing St and changed greatly at large St. Moreover, the value of λ was higher value at a smaller R. This means that the collection efficiency increased more rapidly with dust load at small St and R.

At the simulation conditions at Pe=∞ for the case of convective diffusion and at St=0 for the case of inertial impaction, neither the effect of diffusion nor inertia is present in the motion of the aerosol particle in fluid flow. Thus particles are captured on the fiber via interception mechanism only. As seen the figures 5.31 and 5.64, the value of λ at Pe=5000 is slightly smaller than that of λ at St=0 for the same R. It is reasonable to conclude that the values of λ at Pe=∞ equal the corresponding values of λ at St=0.

5.2 Deterministic simulation results

The optimal values of the parameters e_N and e'_N for the deterministic model were estimated by comparison with the stochastic results at each filtration condition for the case of convective diffusion and inertial impaction. The non-linear simplex method was used for estimating the parameters e_N and e'_N by minimizing the objective function shown in Equation (4.2).

5.2.1 Convective diffusional deposition

Figures 5.65-5.94 compare the change with time in the number concetration of dendrites of sizes N=1 to N=5. The solid lines are the results predicted by the present model and the dots belong to the stochastic model. As seen from the figures, the predicted concentration of dendrites of smaller sizes increased faster at the initial stage but dropped faster as N_{gen} increased. Also the predicted concentration of

Table 5.5 Optimal value of the parameters e_N and e'_N for convective diffusion

Pe	R	0.05	0.1	0.13	0.15	0.17	0.2
200	en	2.531	3.159	3.234	3.252	3.644	3.442
	en'	2.022	2.078	1.794	1.803	1.886	1.629
	Lamda	0.510	0.540	0.554	0.483	0.517	0.453
	Obj fun	9.313	4.321	3.951	4.182	2.295	1.282
	Obj fun/pt	0.085	0.079	0.088	0.119	0.077	0.064
500	en	3.411	4.744	4.774	4.928	4.619	4.648
	en'	2.243	2.780	2.583	2.162	2.107	1.835
	Lamda	1.168	0.982	0.843	0.922	0.739	0.703
	Obj fun	4.628	2.250	5.013	1.603	1.982	1.129
	Obj fun/pt	0.042	0.041	0.111	0.046	0.066	0.056
1000	en	3.883	7.499	6.463	6.234	6.115	5.631
	en'	1.533	3.877	3.103	2.670	2.405	1.906
	Lamda	2.350	1.811	1.292	1.188	1.091	0.931
	Obj fun	2.962	1.934	2.052	1.889	1.594	0.697
	Obj fun/pt	0.027	0.035	0.046	0.054	0.053	0.035
2500	en	5.029	9.680	10.272	8.000	8.095	7.424
	en'	0.433	4.088	4.287	2.852	2.912	2.267
	Lamda	4.596	2.796	2.302	1.716	1.524	1.289
	Obj fun	1.278	3.203	2.770	0.713	1.089	0.587
	Obj fun/pt	0.012	0.058	0.062	0.020	0.036	0.029
5000	en	13.238	12.606	10.363	8.817	9.090	7.579
	en'	7.057	6.213	4.016	4.012	3.514	2.211
	Lamda	6.181	3.196	2.441	1.602	1.640	1.342
	Obj fun	2.839	2.394	1.804	0.715	0.949	0.638
	Obj fun/point	0.026	0.044	0.040	0.020	0.032	0.032
	Ngen	1000	500	400	350	300	200
	No. point	110	55	45	35	30	20

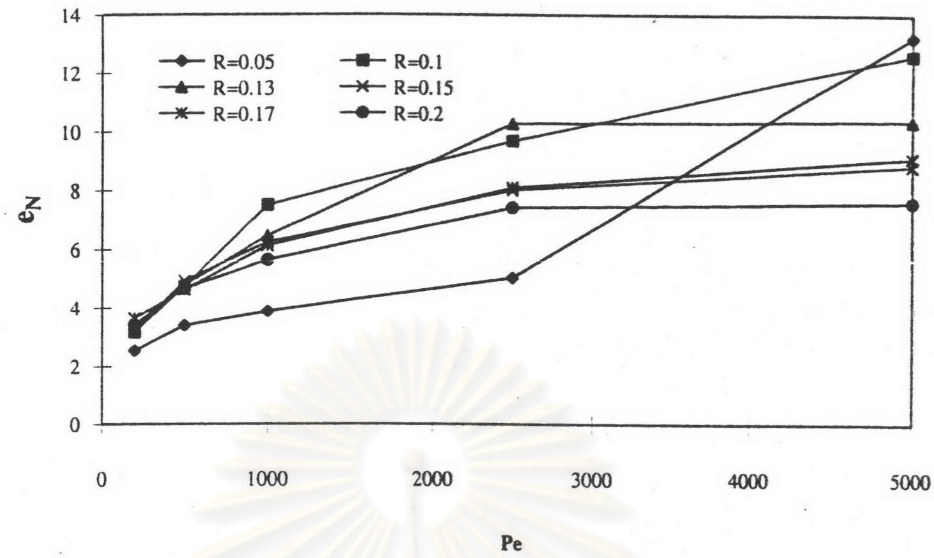

Figure 5.95. Relationship between the parameter e_N and Pe

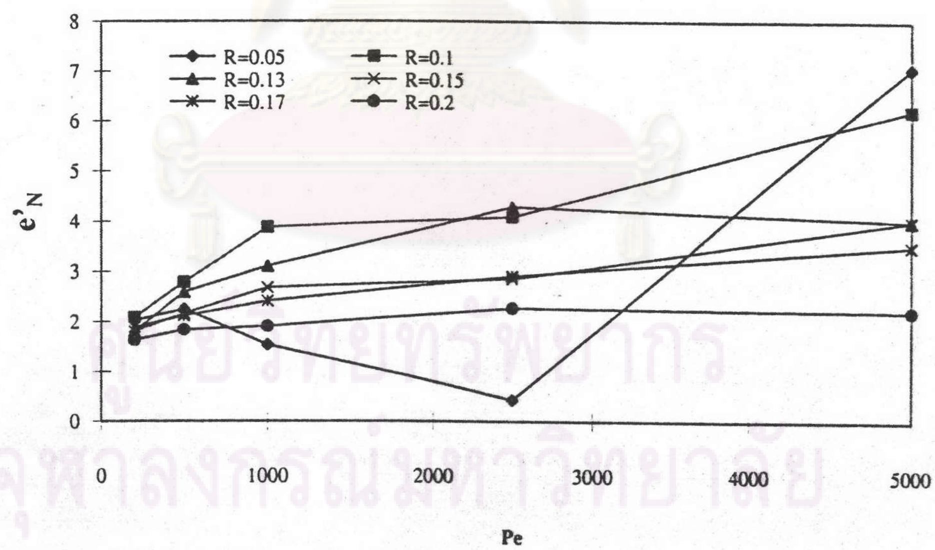

Figure 5.96. Relationship between the parameter e'_N and Pe

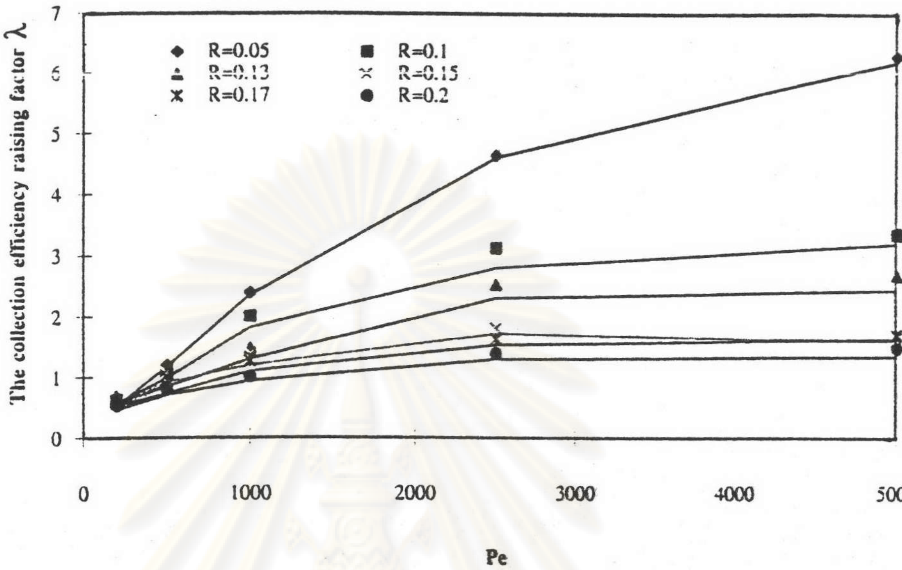

Figure 5.97. Comparison of λ between stochastic and simplified models for convective diffusion

(The dots are stochastic results, the lines are deterministic ones)

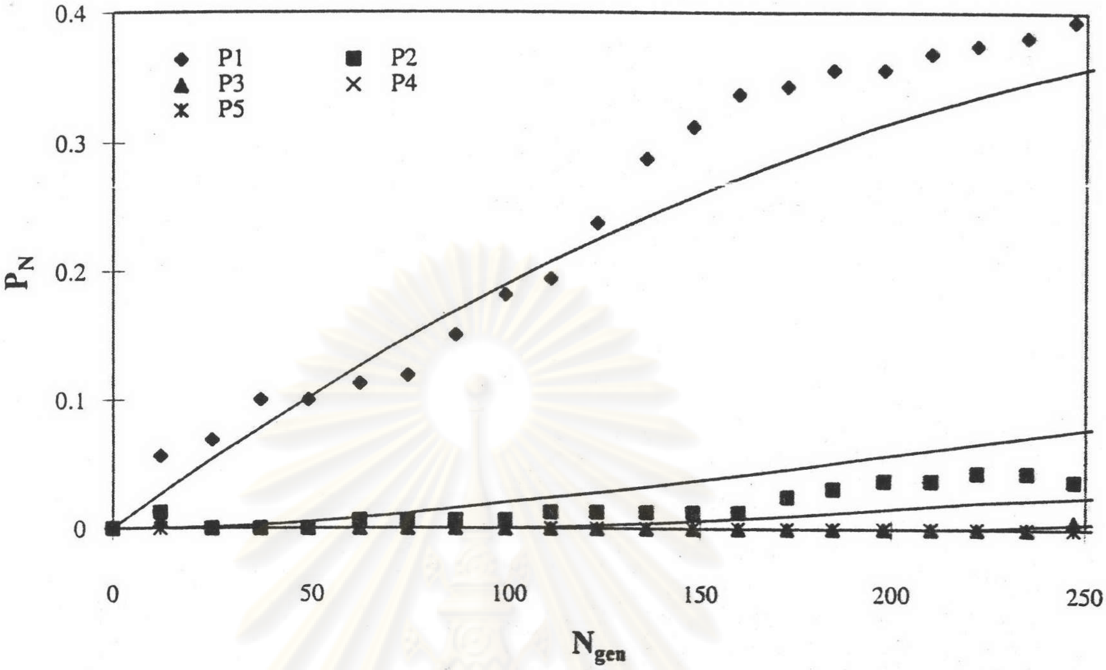

Figure 5.98. Comparison of dendrite distribution between stochastic and simplified model for R=0.05 and St=0.0

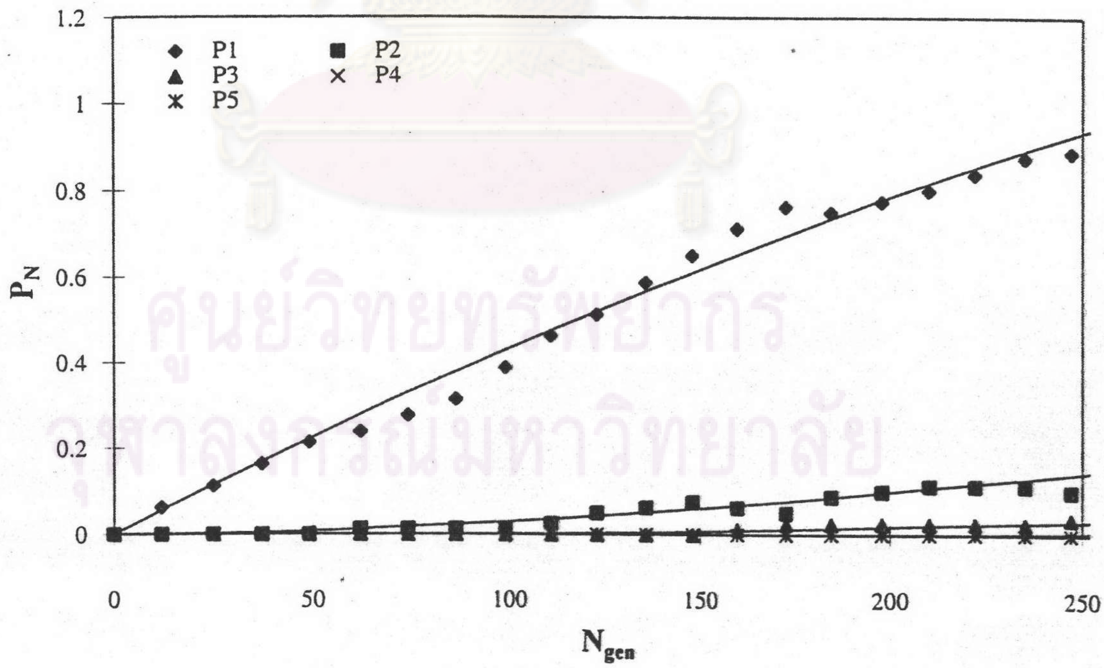

Figure 5.99. Comparison of dendrite distribution between stochastic and simplified model for R=0.05 and St=0.6

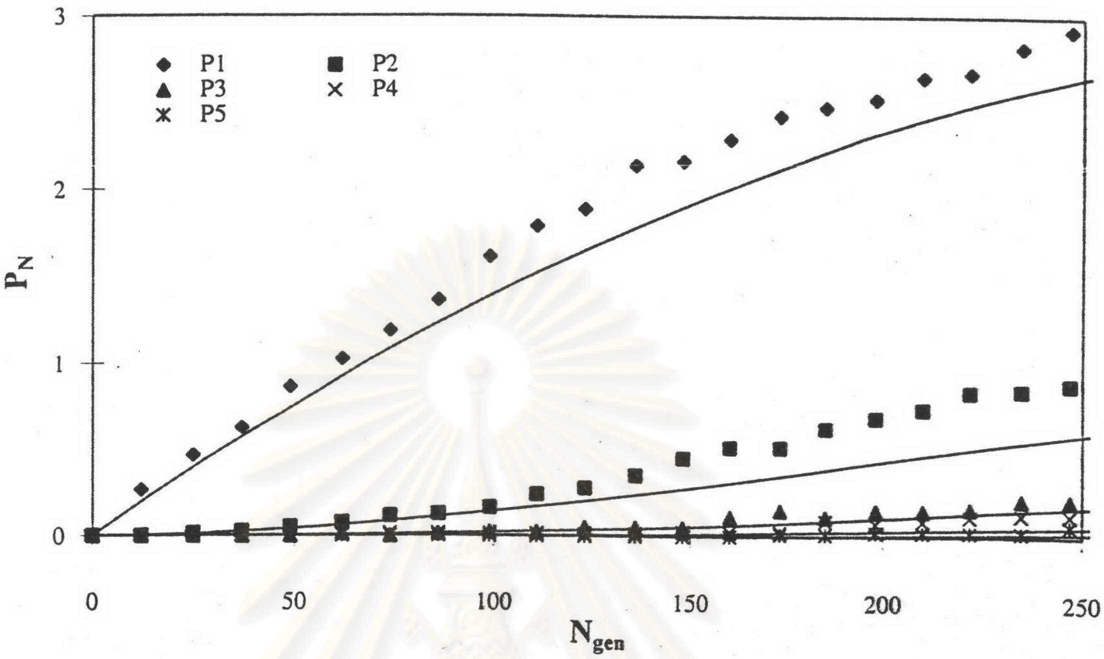

Figure 5.100. Comparison of dendrite distribution between stochastic and simplified model for R=0.05 and St=1.0

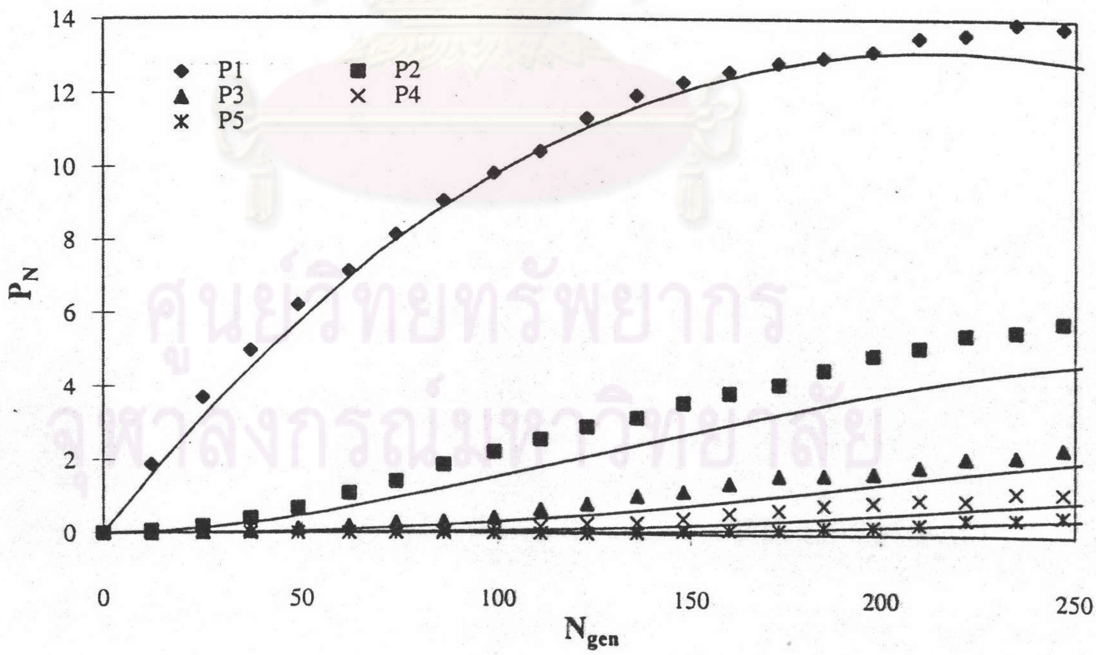

Figure 5.101. Comparison of dendrite distribution between stochastic and simplified model for R=0.05 and St=1.4

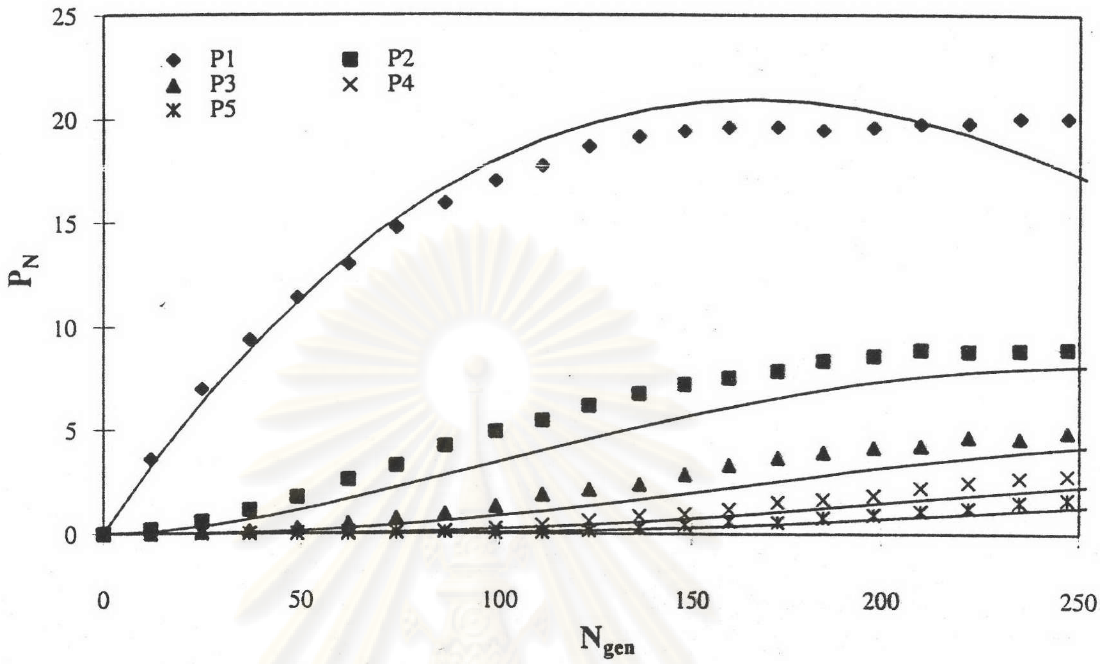

Figure 5.102. Comparison of dendrite distribution between stochastic and simplified model for R=0.05 and St=2.0

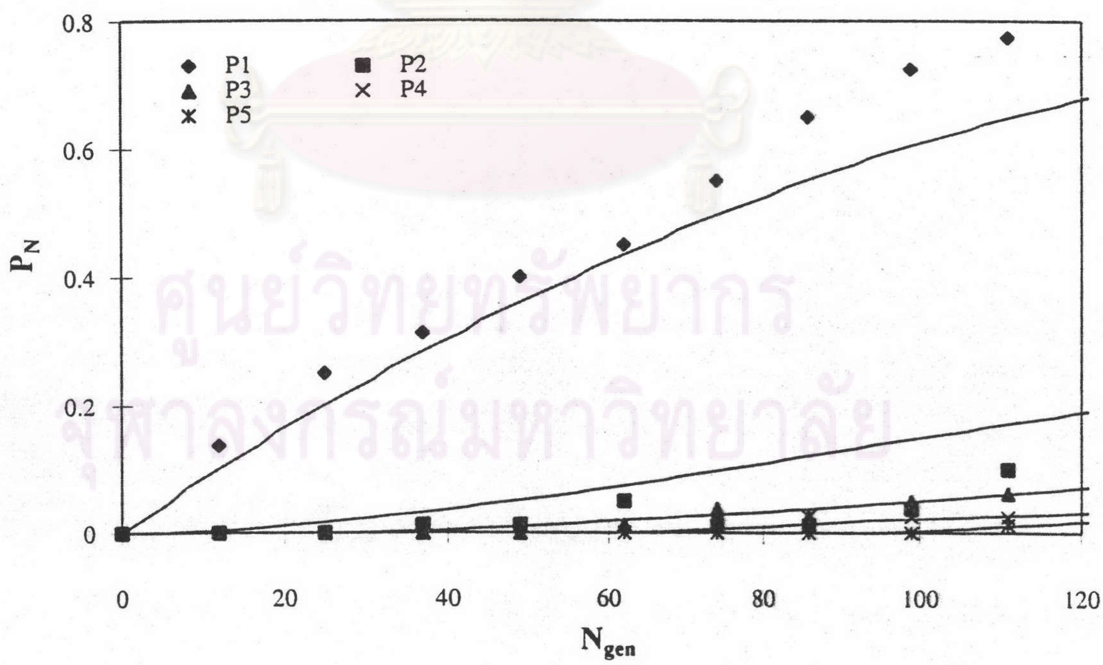

Figure 5.103. Comparison of dendrite distribution between stochastic and simplified model for R=0.1 and St=0.0

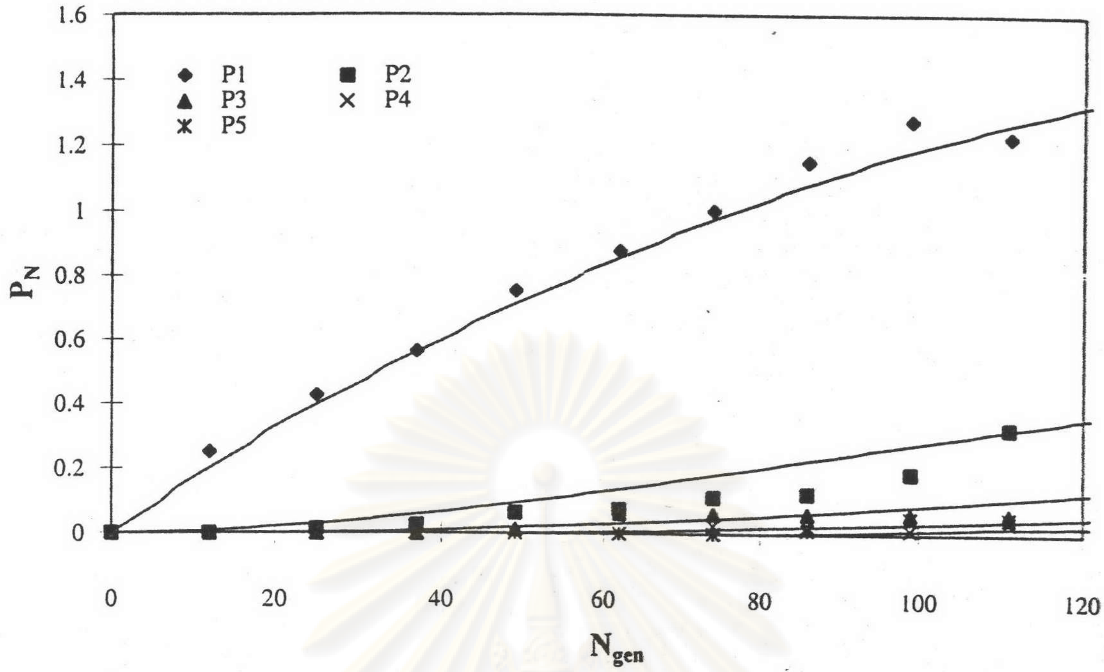

Figure 5.104. Comparison of dendrite distribution between stochastic and simplified model for R=0.1 and St=0.6

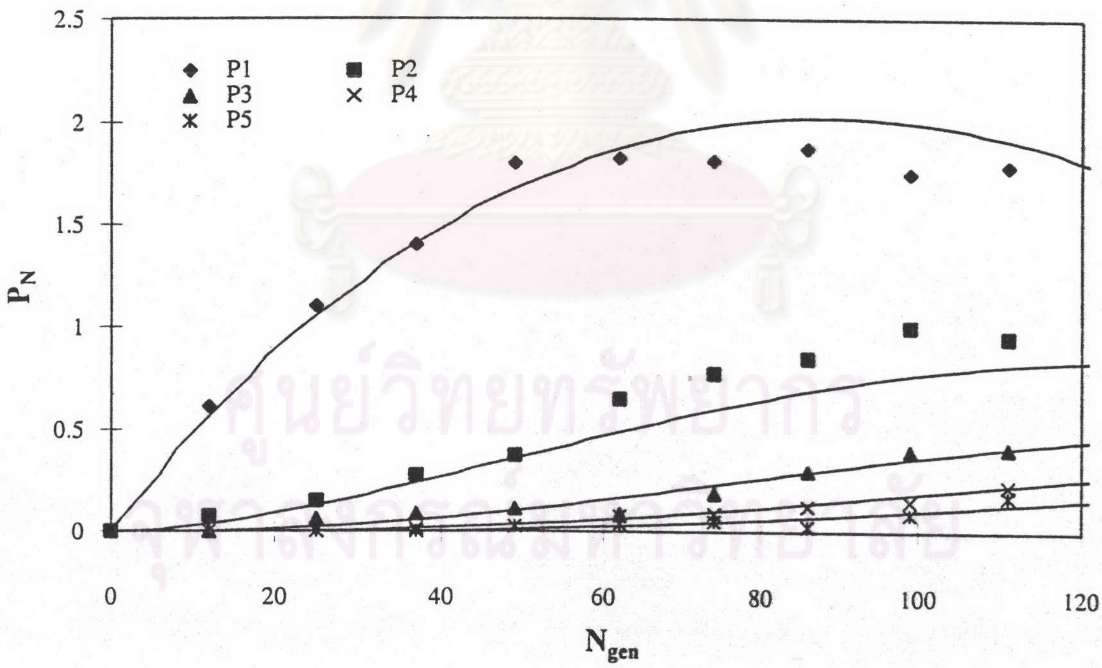

Figure 5.105. Comparison of dendrite distribution between stochastic and simplified model for R=0.1 and St=1.0

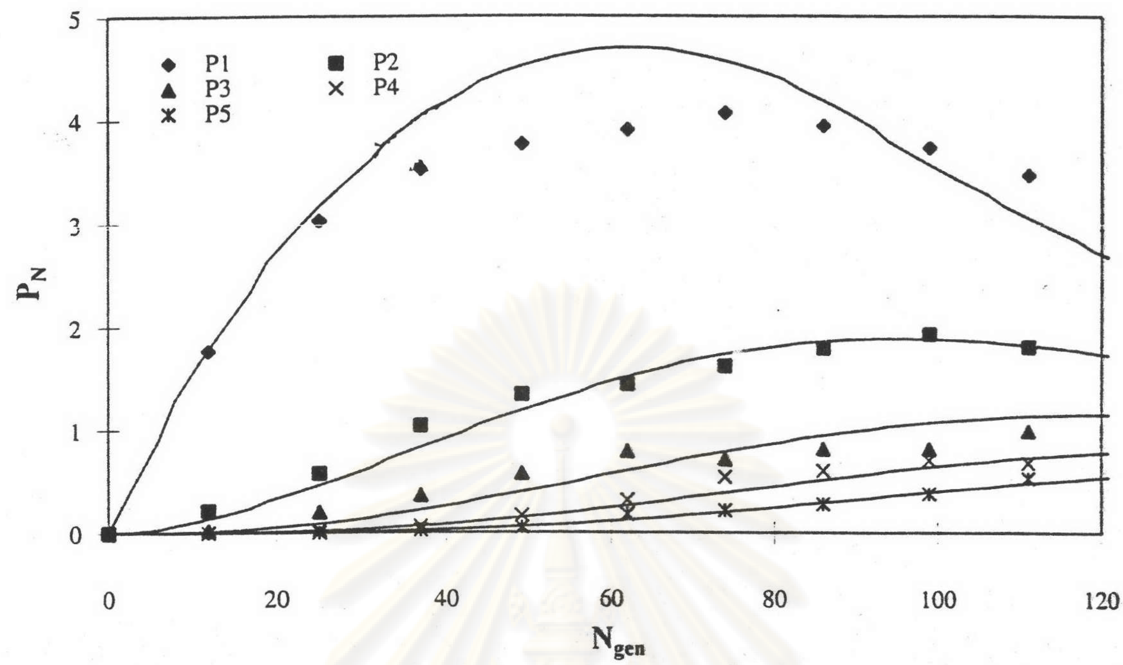

Figure 5.106. Comparison of dendrite distribution between stochastic and simplified model for R=0.1 and St=1.4

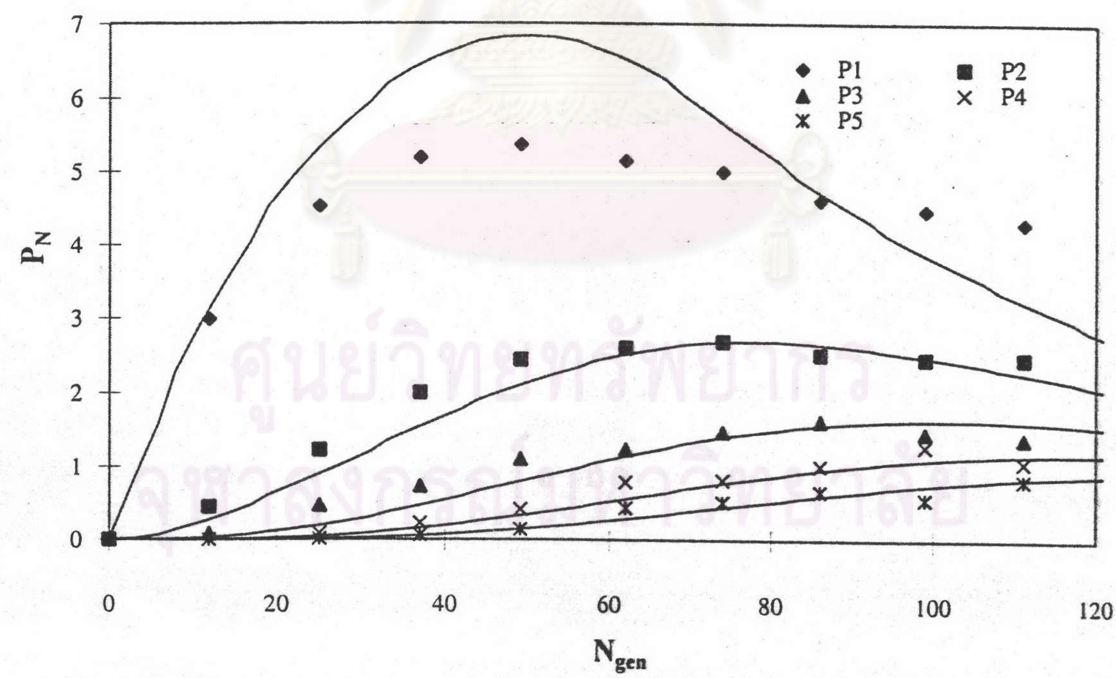

Figure 5.107. Comparison of dendrite distribution between stochastic and simplified model for R=0.1 and St=2.0

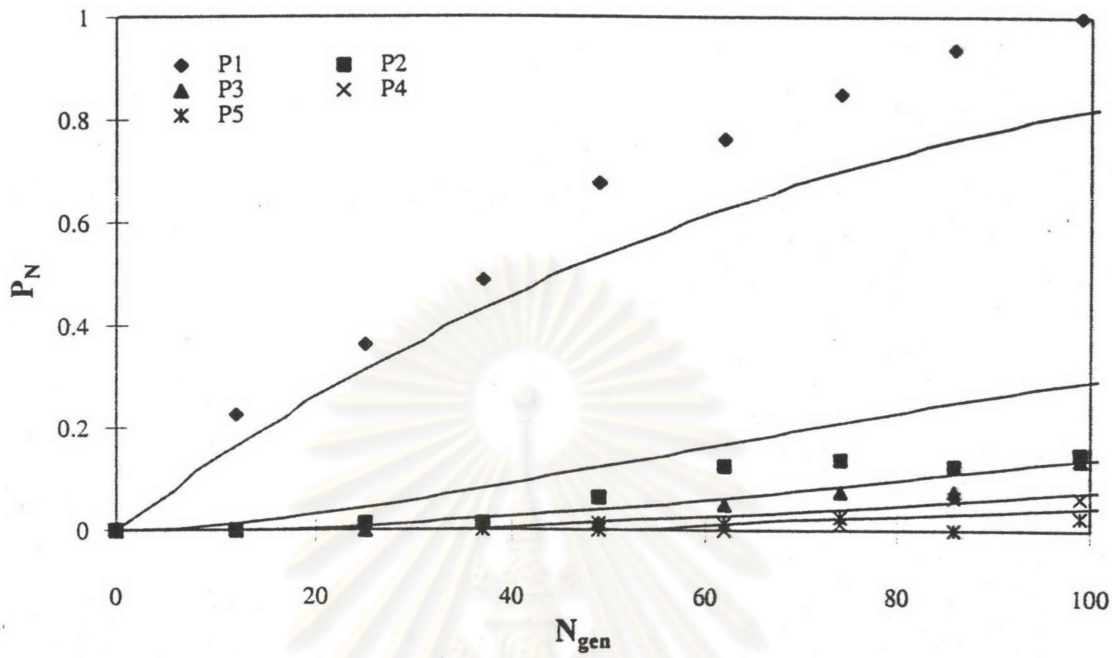

Figure 5.108. Comparison of dendrite distribution between stochastic and simplified model for R=0.13 and St=0.0

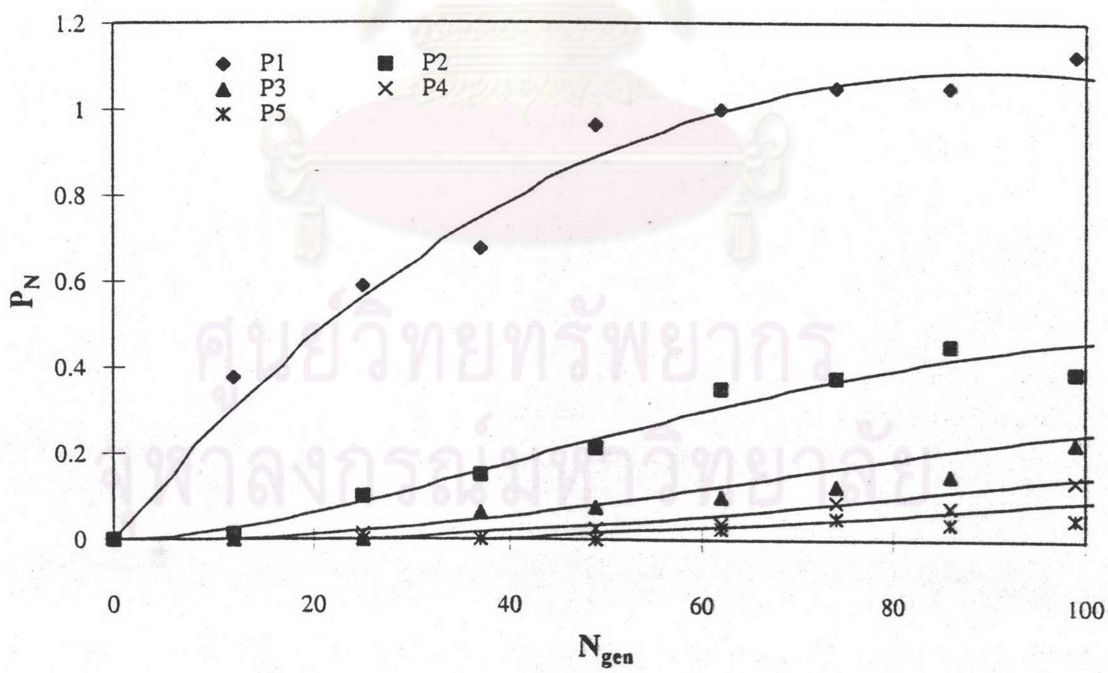

Figure 5.109. Comparison of dendrite distribution between stochastic and simplified model for R=0.13 and St=0.6

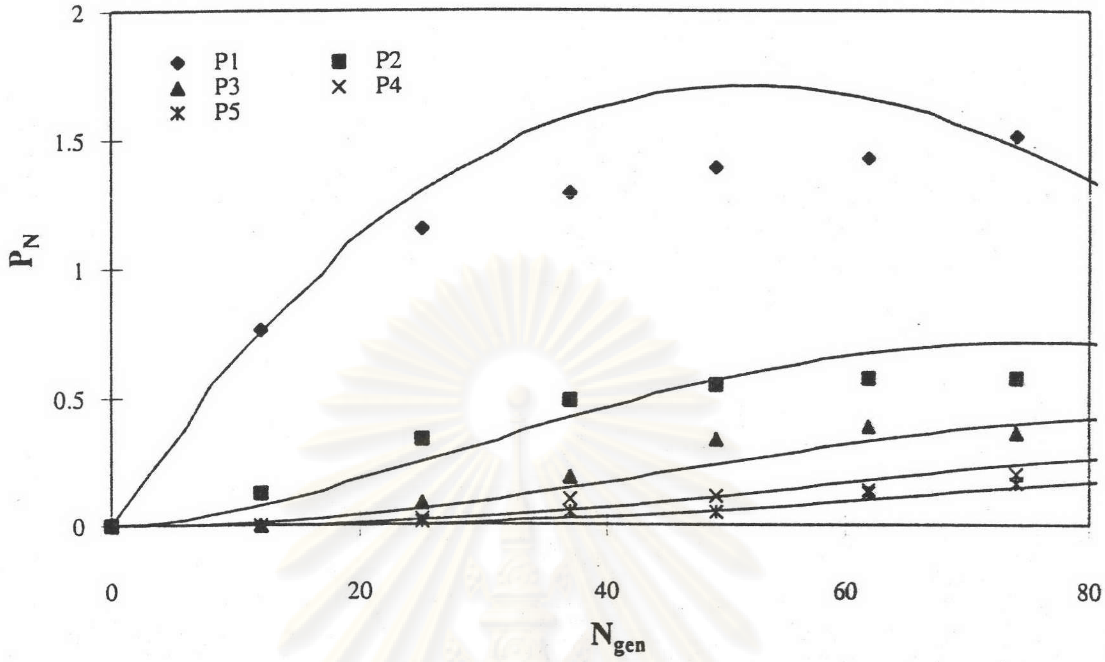

Figure 5.110. Comparison of dendrite distribution between stochastic and simplified model for R=0.13 and St=1.0

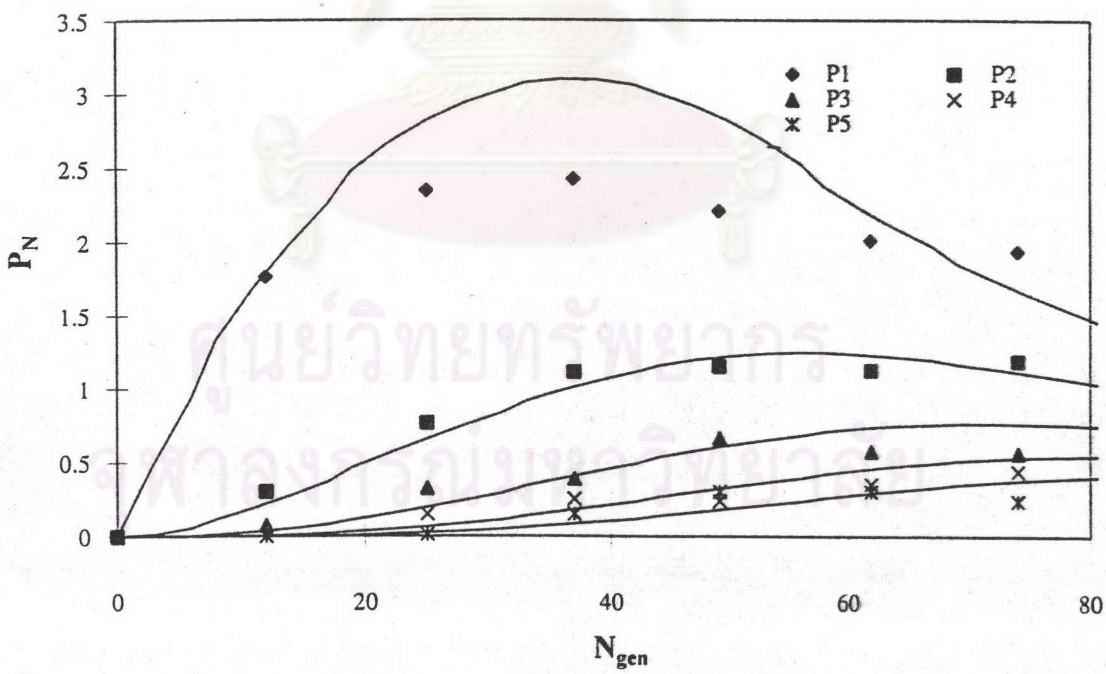

Figure 5.111. Comparison of dendrite distribution between stochastic and simplified model for R=0.13 and St=1.4

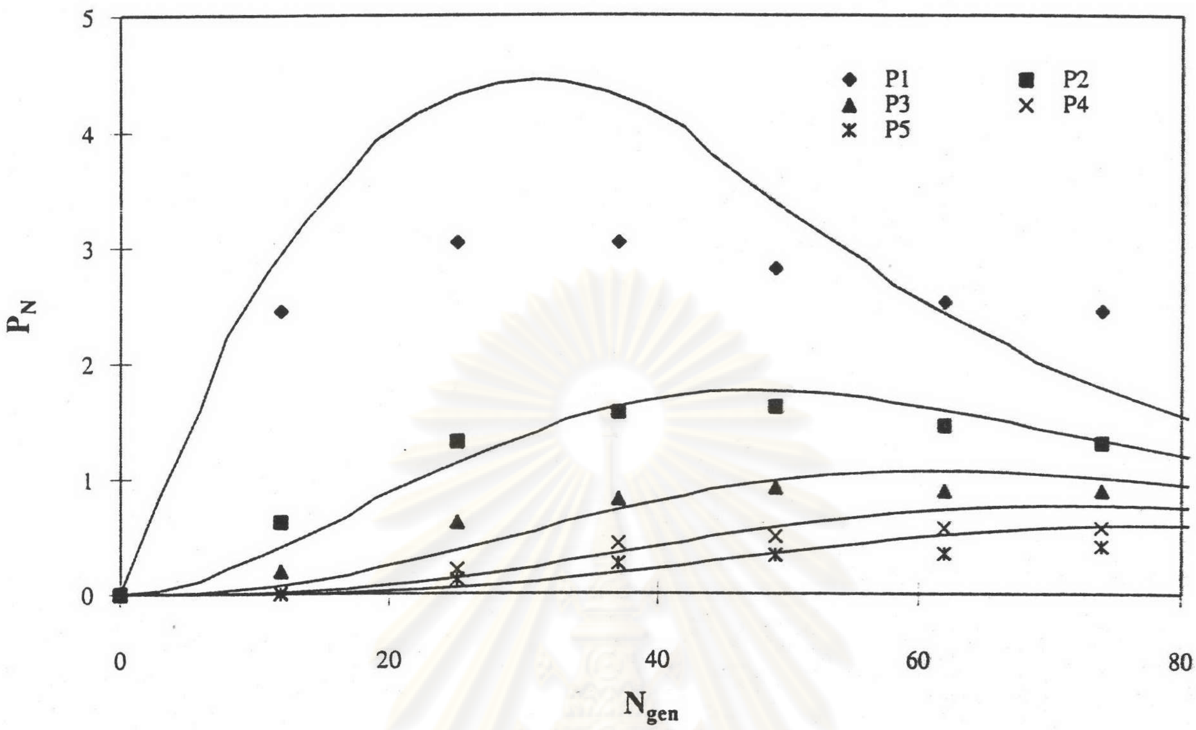

Figure 5.112. Comparison of dendrite distribution between stochastic and simplified model for R=0.13 and St=20

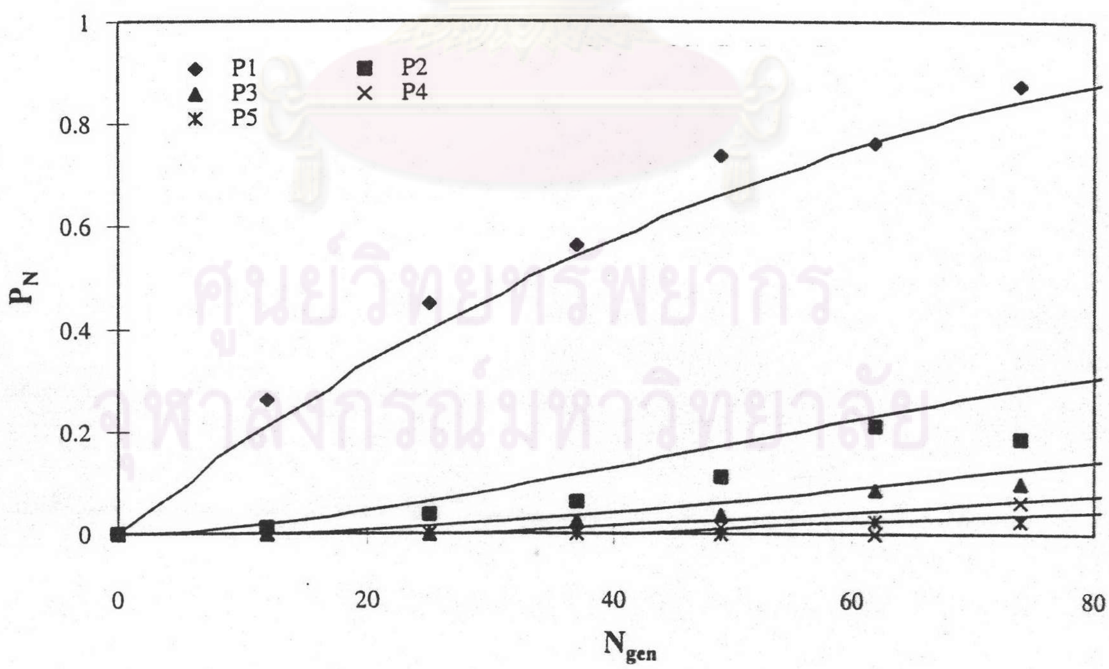

Figure 5.113. Comparison of dendrite distribution between stochastic and simplified model for R=0.15 and St=0.0

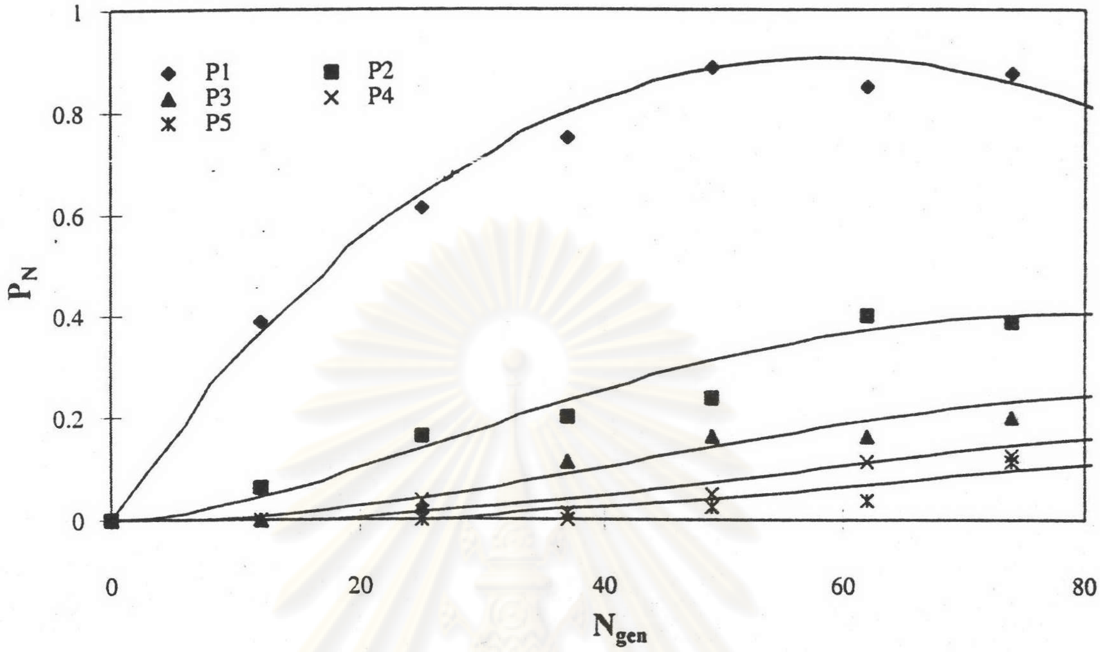

Figure 5.114. Comparison of dendrite distribution between stochastic and simplified model for R=0.15 and St=0.6

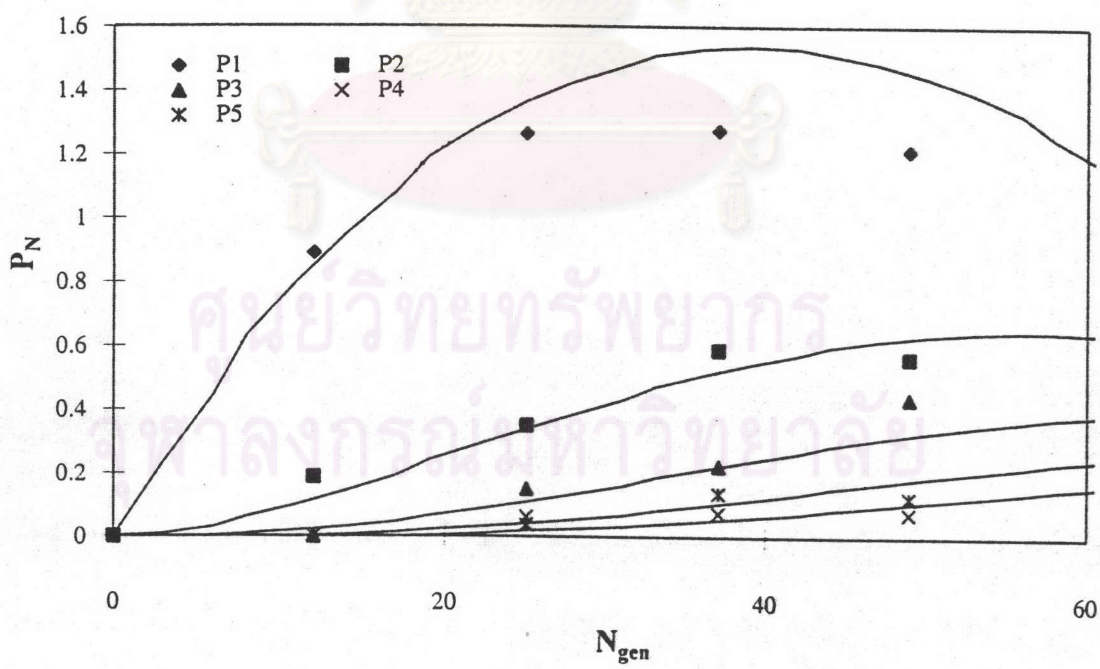

Figure 5.115. Comparison of dendrite distribution between stochastic and simplified model for R=0.15 and St=1.0

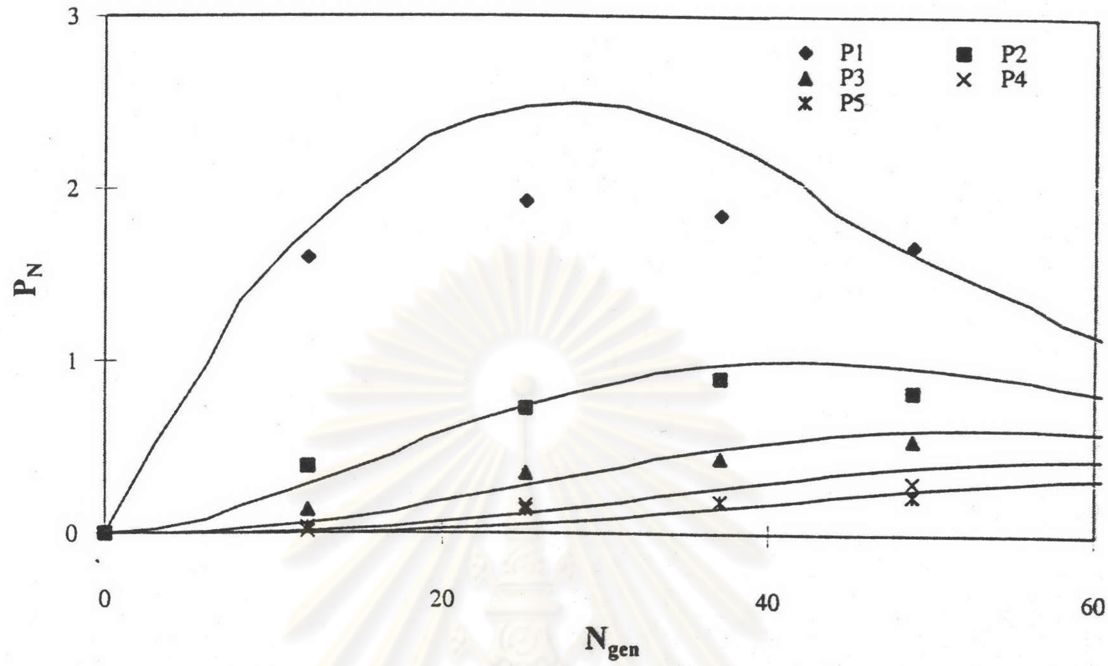

Figure 5.116. Comparison of dendrite distribution between stochastic and simplified model for R=0.15 and St=1.4

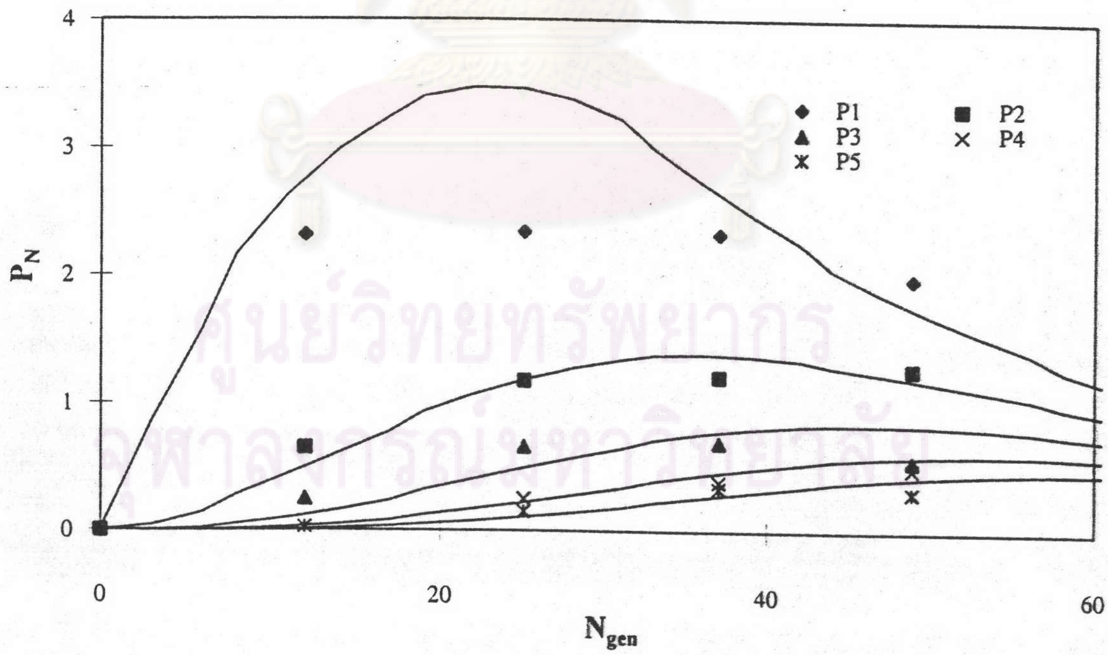

Figure 5.117. Comparison of dendrite distribution between stochastic and simplified model for R=0.15 and St=2.0

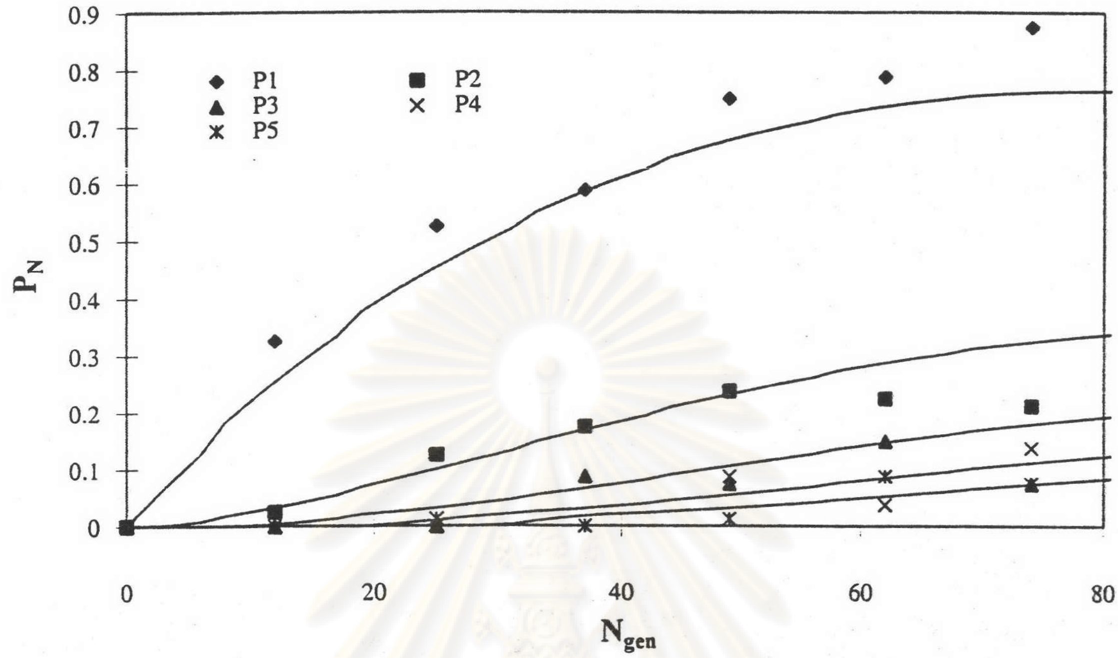

Figure 5.118. Comparison of dendrite distribution between stochastic and simplified model for R=0.17 and St=0.0

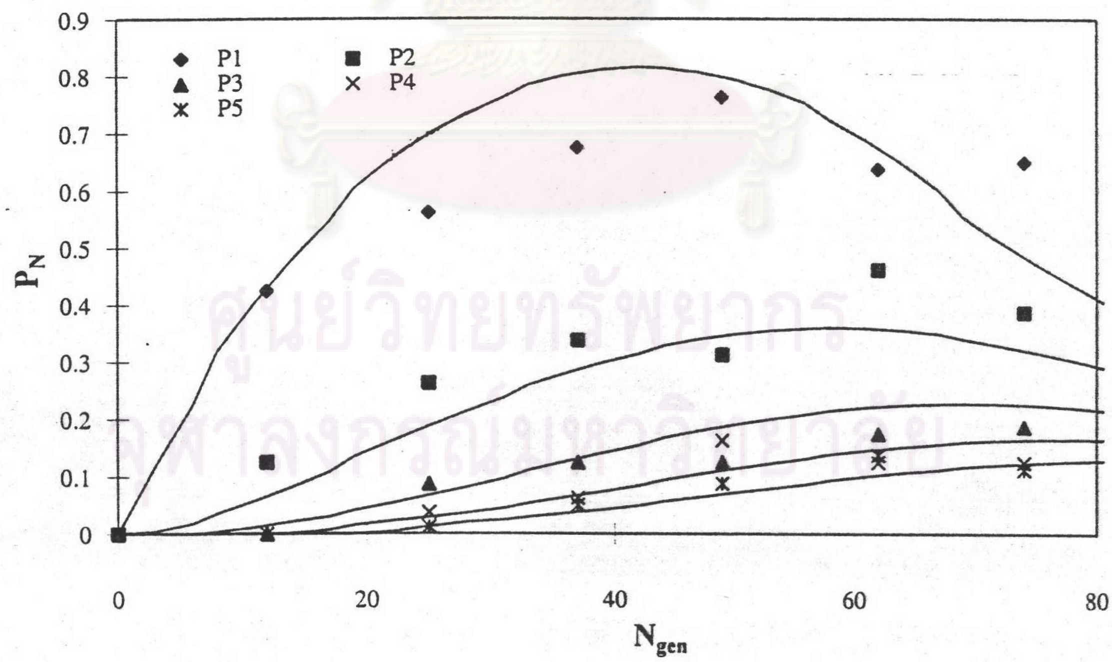

Figure 5.119. Comparison of dendrite distribution between stochastic and simplified model for R=0.17 and St=0.6

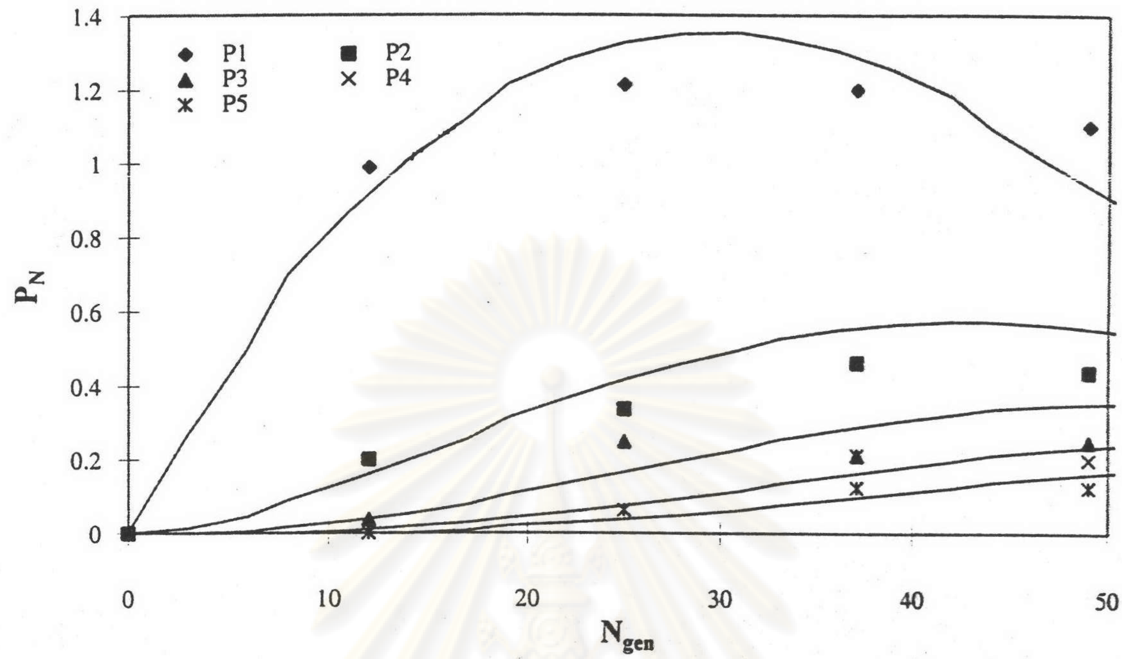

Figure 5.120. Comparison of dendrite distribution between stochastic and simplified model for R=0.17 and St=1.0

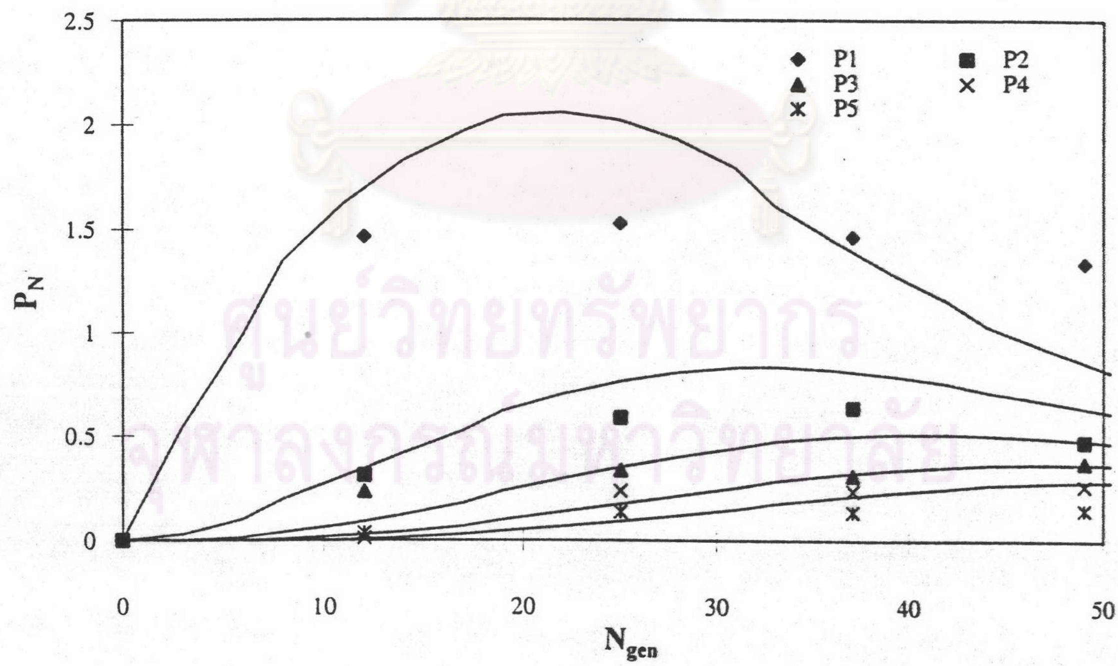

Figure 5.121. Comparison of dendrite distribution between stochastic and simplified model for R=0.17 and St=1.4

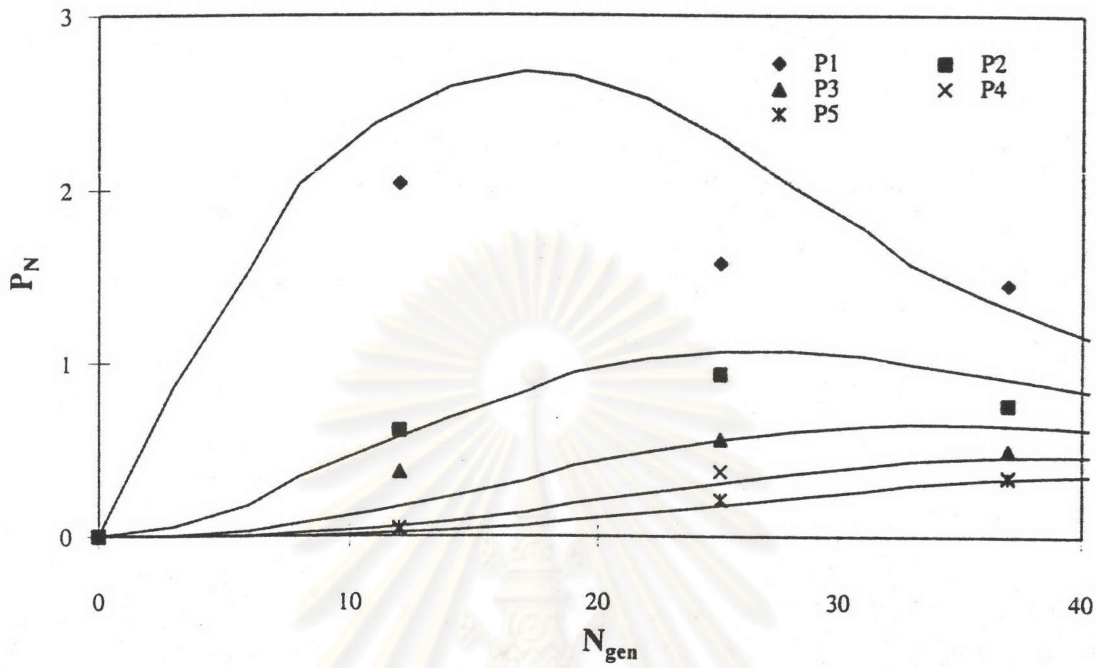

Figure 5.122. Comparison of dendrite distribution between stochastic and simplified model for R=0.17 and St=2.0

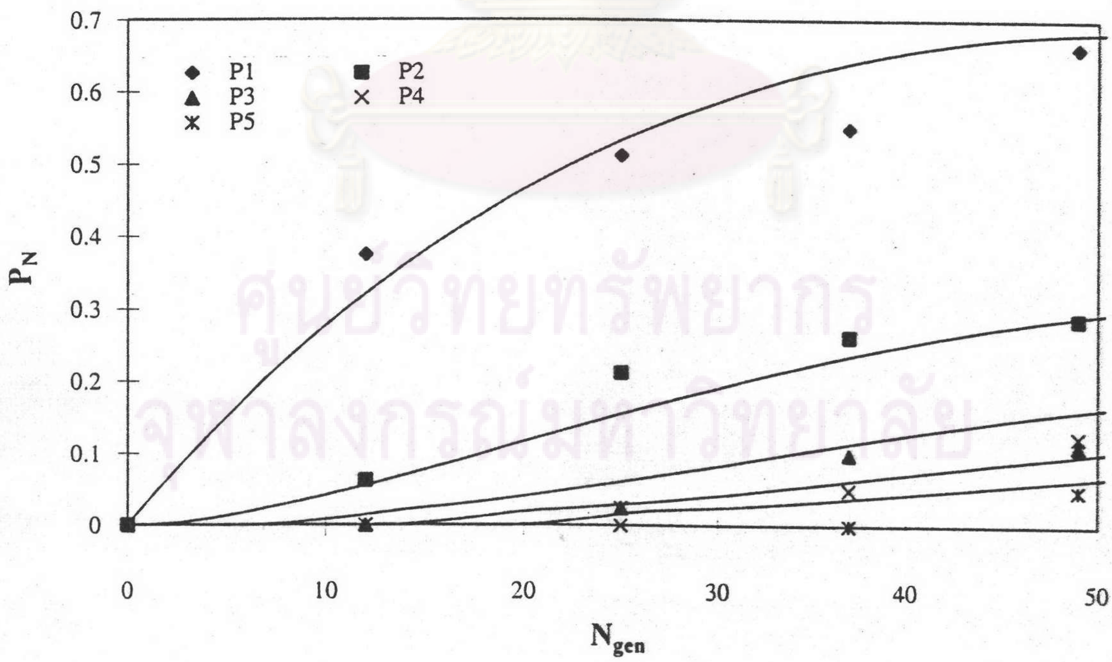

Figure 5.123. Comparison of dendrite distribution between stochastic and simplified model for R=0.2 and St=0.0

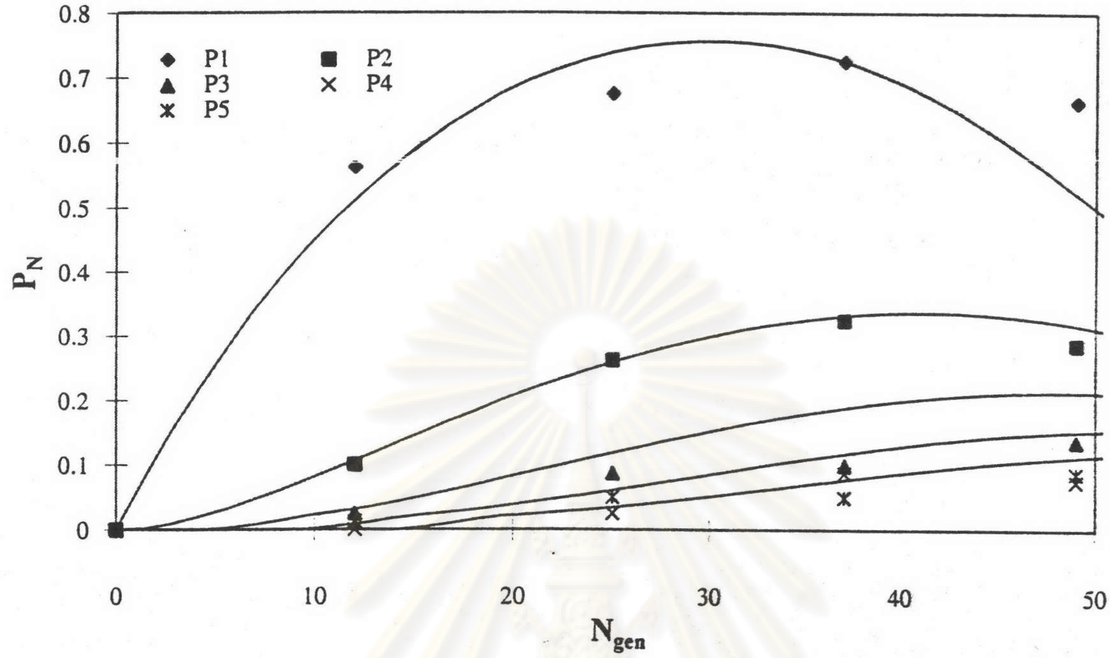

Figure 5.124. Comparison of dendrite distribution between stochastic and simplified model for R=0.2 and St=0.6

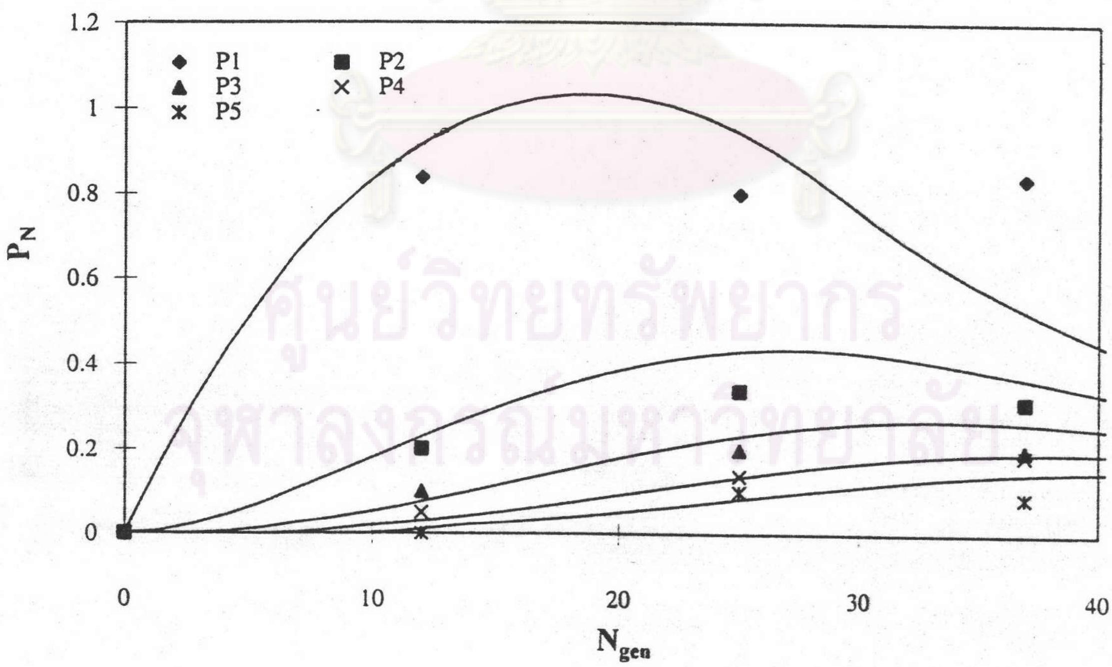

Figure 5.125. Comparison of dendrite distribution between stochastic and simplified model for R=0.2 and St=1.0

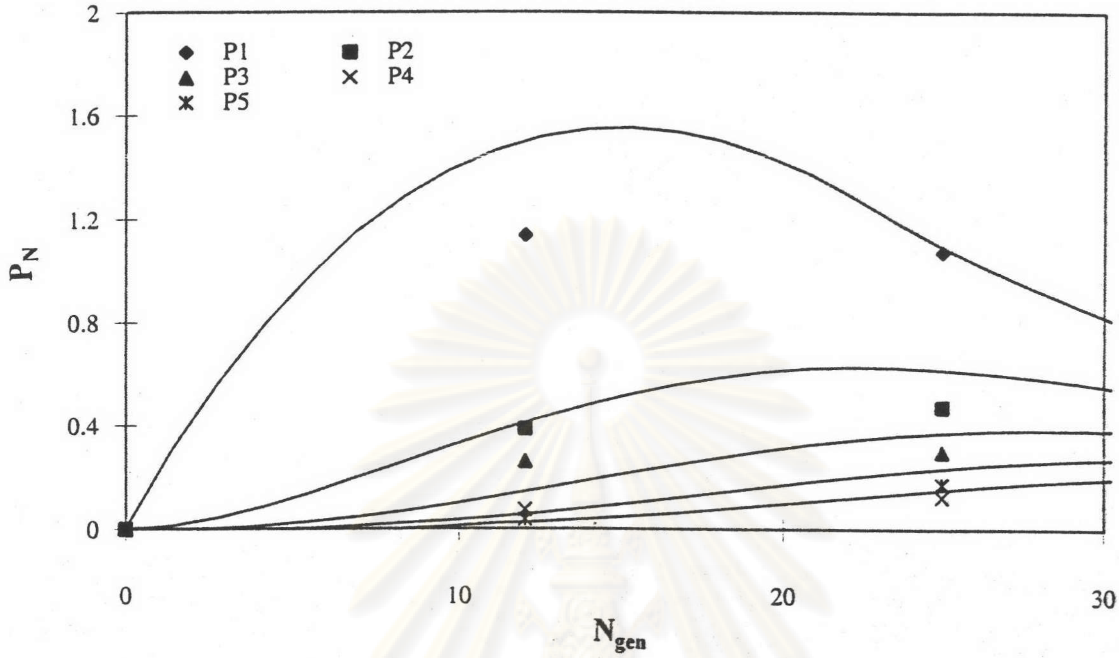

Figure 5.126. Comparison of dendrite distribution between stochastic and simplified model for R=0.2 and St=1.4

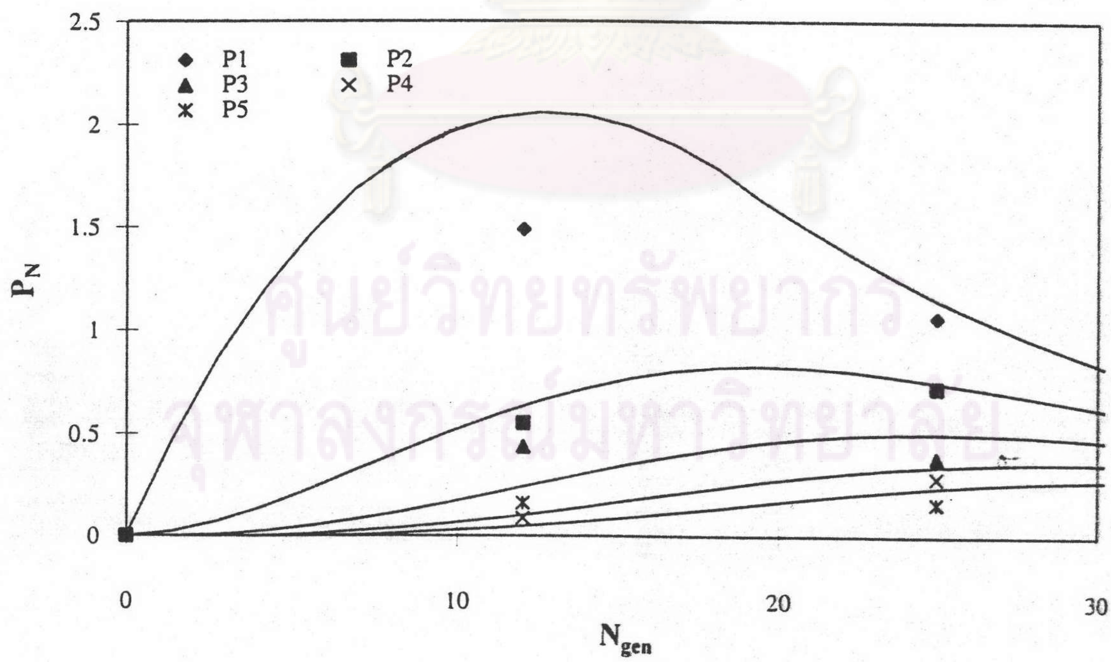

Figure 5.127. Comparison of dendrite distribution between stochastic and simplified model for R=0.2 and St=2.0

dendrites was larger at a small R and Pe than a large R and Pe. The dendritic growth predicted by the present model agreed quite well with that of the stochastic model at a small R and fairly well at a large R.

The values of the parameters e_N and e'_N were summarized in Table 5.5.Figures 5.95 and 5.96 show the relationship between e_N and Pe, and between e'_N and Pe, respectively. The parameters e_N and e'_N increased along with Pe but decreased against R as the dendrites tended to be more slender and densely packed. However, the present results indicated that the trend of the parameters e_N and e'_N for the case R=0.05, differed from the other cases especially at a low Pe. The value of e_N was lower at Pe less than 2500 but became higher at Pe=5000. It could be possible that the relatively tiny particles (R=0.05) was the threshold particle size below which dendritic formation became difficult and nondistinctive. Thus, the particles might be packed very densely on a fiber at low Pe. Therefore, the effective captured area increased at a large Pe and small R. Figure 5.97 compares the relationship between λ and Pe with R as parameter. As seen from the figure, the values of λ agreed well with that of the stochastic model.

5.2.2 Inertial impaction deposition

The dendritic growth of inertial impaction was shown in Figures 5.98-5.127. As seen from the figures, as in the case of convective diffusion, the number concentration of dendrites for inertial impaction predicted by the deterministic model increased faster at the initial stage but them dropped faster at the large N_{gen}. Furthermore, the concentration of dendrites was larger at a small R and large St than at a large R and small St. The dendritic growth of the present agreed quite well with that of the stochastic model at a small R but fairly well at a large R.

The optimal values of the parameters e_N and e'_N were summarized in Table 5.6. Figures 5.128 and 5.129 show the relationship between e_N and St, and between e'_N and St, respectively. The parameter e_N and e'_N decreased along with St and R. Thus the effective capturing area was smaller as St and R increased because the dendrites tended to be shorter and more loosely packed. The relationship of λ vs. η_0 obtained from the present deterministic study is compared with some publishes experimental

Table 5.6 Optimal value of the parameters e_N and e'_N for inertial impaction

St	R	0.05	0.1	0.13	0.15	0.17	0.2
0	en	179.756	37.119	24.832	17.280	16.095	12.795
	en'	121.851	4.863	0.541	0.320	1.038	0.902
	Lamda	57.905	16.128	9.343	5.653	4.429	2.973
	Obj fun	0.266	0.378	0.545	0.460	0.351	0.155
	Obj fun/point	0.002	0.007	0.012	0.013	0.012	0.008
0.6	en	59.434	17.453	15.233	13.597	11.293	9.197
	en'	19.238	3.849	2.992	2.771	2.669	1.853
	Lamda	40.196	6.802	4.708	3.608	2.537	1.836
	Obj fun	0.141	0.467	0.194	0.198	0.310	0.310
	Obj fun/point	0.001	0.008	0.004	0.006	0.010	0.015
1	en	26.316	10.336	7.305	6.299	5.717	5.288
	en'	13.640	5.010	3.460	2.739	2.312	2.287
	Lamda	12.676	2.663	1.479	1.187	1.002	0.750
	Obj fun	2.195	0.597	1.035	0.927	0.870	0.813
	Obj fun/point	0.020	0.011	0.023	0.026	0.029	0.041
1.4	en	5.118	3.853	3.511	3.333	3.244	3.072
	en'	4.214	2.676	2.346	2.148	1.940	1.887
	Lamda	0.903	0.588	0.448	0.395	0.383	0.296
	Obj fun	7.972	1.744	2.791	2.429	2.449	1.322
	Obj fun/point	0.072	0.032	0.062	0.069	0.082	0.066
2	en	3.083	2.475	2.327	2.275	2.311	2.199
	en'	2.761	2.006	1.747	1.644	1.643	1.528
	Lamda	0.322	0.234	0.223	0.210	0.196	0.168
	Obj fun	14.530	4.396	5.271	3.988	3.497	1.679
	Obj fun/point	0.132	0.080	0.117	0.114	0.117	0.084
	Ngen	1000	500	400	350	300	200
	No. point	110	55	45	35	30	20

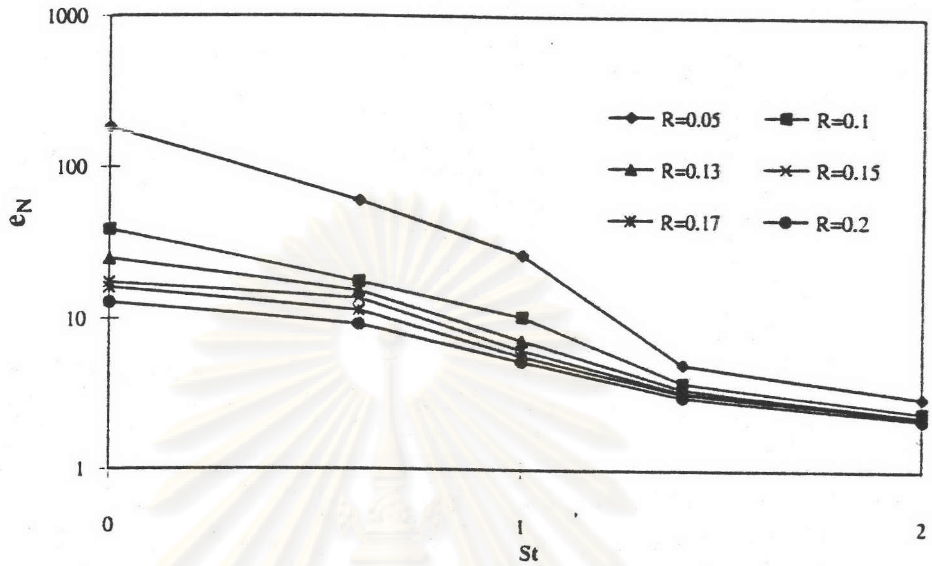

Figure 5.128. Relationshp between the parameter e_N and St

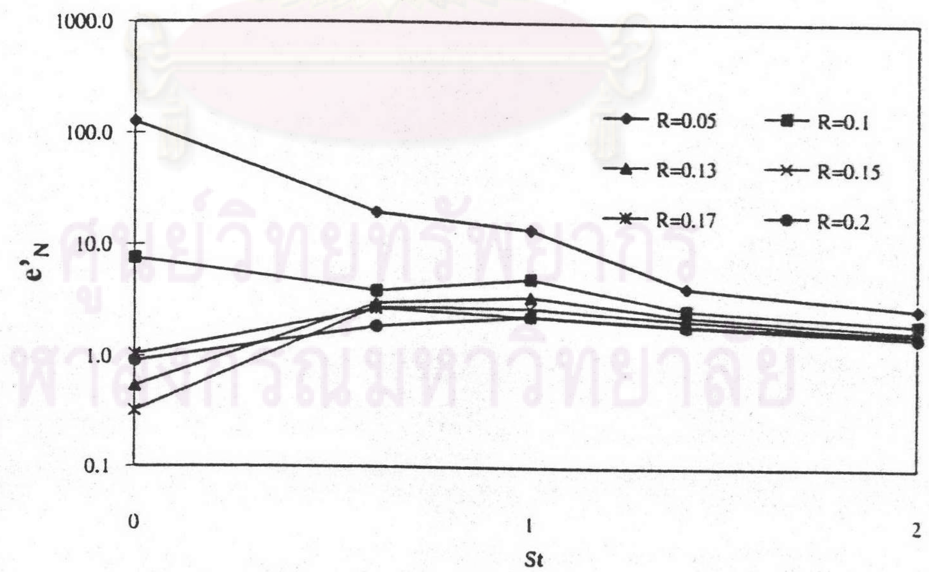

Figure 5.129. Relationshp between the parameter e'_N and St

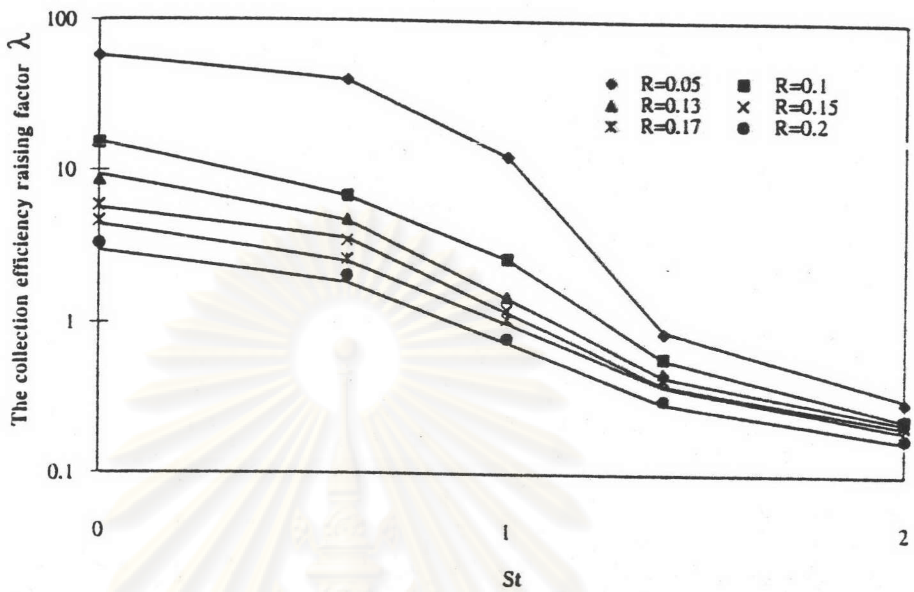

Figure 5.130. Comparison of λ between stochastic and simplified models for inertial impaction

(The dots are stochastic results, the lines are deterministic ones) results (Kimura et al., 1964, Yoshioka et al., 1969,and Myojo et al., 1984), as shown in Figure 5.131 a and b. Clearly the trend of the relationship obtained from this work is quite similar to the experimental one. As seen from Figure 5.131b, λ decreases while η_0 increased as St increases. Table 5.7 reveals certain differences between the experimental results and the deterministic predictions. The predictions are about 103% higher than the experimental results because the configuration of the experimental filter is more complicated than the idealized filter in which all fibers lie parallel to one another. Moreover, re-entrainment and bridging of dendrites between dust-loaded fibers may occured in the experimental study but are not taken into account in the simulation study.

It is obvious that the collection mechanism reduces to pure interception at Pe=∞ or St=0. Therefore the simulation results of Pe=∞ should equal those of St=0. The parameter e_N and λ for Pe=5000 were slightly smaller than their counterparts for at St=0. In contrast, the parameter e'_N for Pe=5000 was higher than that St=0. The reason for this discrepancy is that even at Pe=5000 there remains appreciable diffusion effect. Theoretically speaking, as Pe approaches infinity, the values of e_N and e'_N of both cases should become identical.

The deterministic model has been shown to predict the dendrite distribution and the collection efficiency of the dust-loaded fiber which are in good agreement with the stochastic model for both the case of convective diffusion and inertial impaction. Table 5.8 shows the size of computer memory required to run deterministic and stochastic simulations. Tables 5.9 and 5.10 show the actual simulation times used in stochastic simulation for convective diffusion and inertial impaction, respectively. Tables 5.11 and 5.12 show the actual simulation times required by the simplified model for convective diffusion and inertial impaction, respectively. As seen from the tables, the simplified model required much less computer memory and much shorter computational time than the stochastic model at the same filtration conditions.

5.2.3 The contours of η_0 and λ with respect to particle size and air velocity

The deterministic model was used to predict η_0 and λ under various filtration conditions for the case of convective diffusion and inertial impaction. The

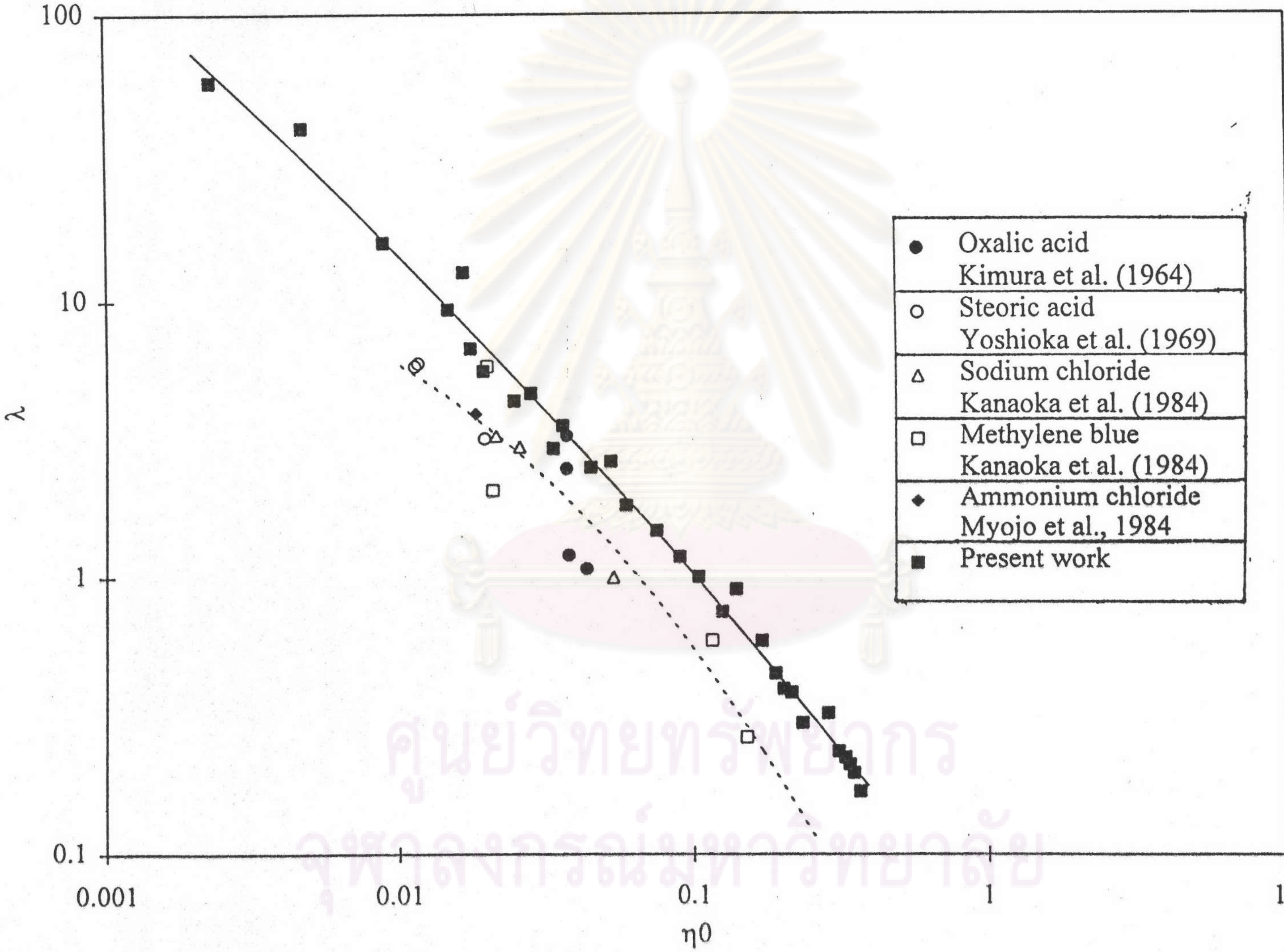

Figure 5.131a Comparison of λ vs. η_0 between the deterministic results and experimental results

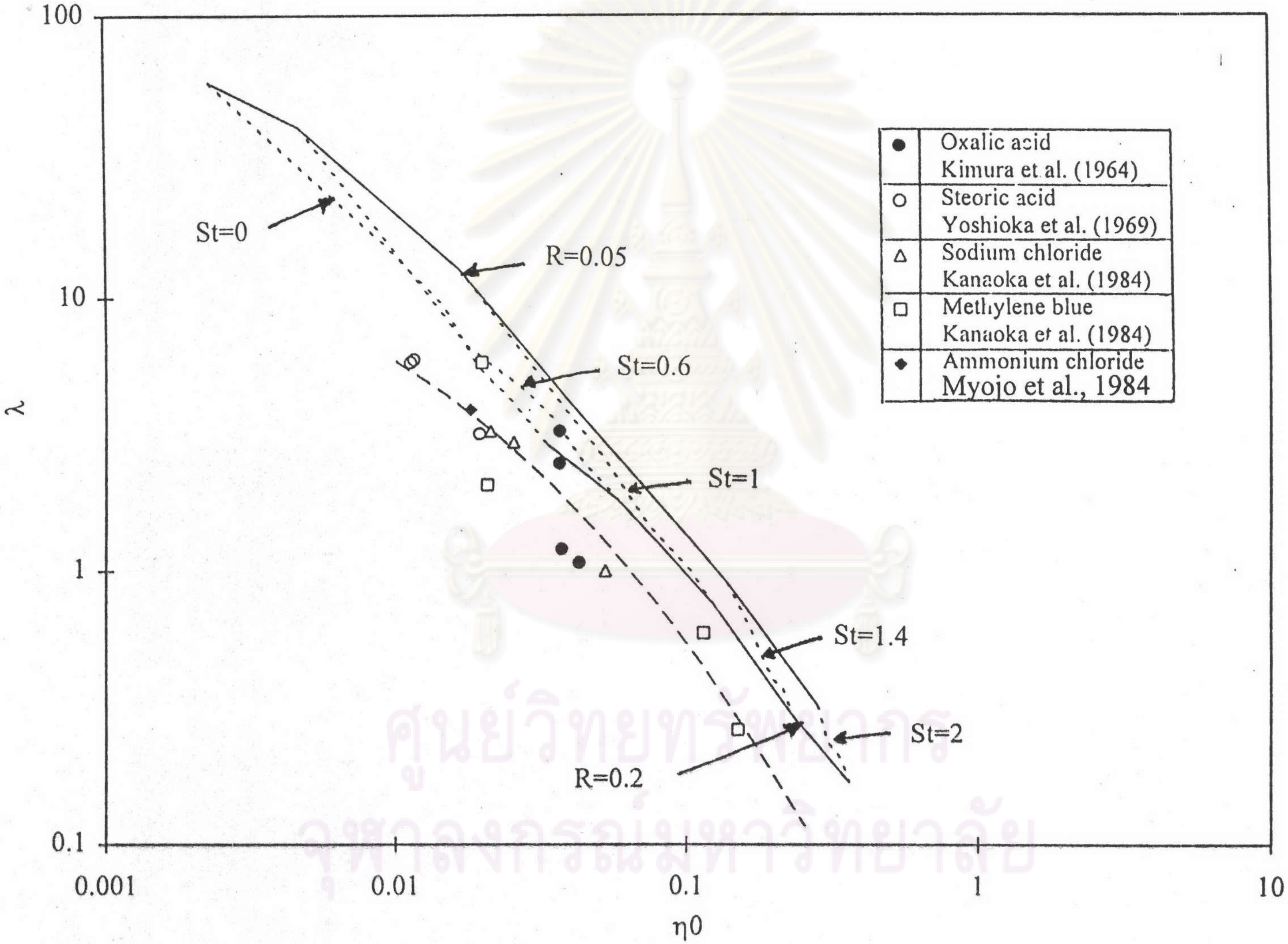

Figure 5.131b Comparison of λ vs. η_0 between the deterministic results and experimental results with St and R as parameters

Table 5.7 Comparison between the experimental and the predicted values of λ

range	$\eta 0$	λ - exp	λ - present	error(%)
1	0.010	5.96	14.40	142
2	0.015	4.50	9.27	106
3	0.023	3.20	5.90	84
4	0.034	2.14	3.71	73
5	0.051	1.35	2.30	71
6	0.076	0.80	1.41	76
7	0.114	0.45	0.86	92
8	0.171	0.23	0.51	119
9	0.256	0.12	0.30	162
			error-avg(%)=	**103**

Table 5.8 Computer memory required to run deterministic and stochastic simulations

Required computer memory			
Deterministic		Stochastic	
181104	bit	49893056	bit
22638	byte	6236632	byte
22	KB	6090	KB

Table 5.9 Actual simulation time used in stochastic simulation (convective diffusion)

Pe	R					
	0.05	0.1	0.13	0.15	0.17	0.2
200	0:24:32	0:02:54	0:01:34	0:01:08	0:00:52	0:01:34
500	0:27:00	0:03:24	0:01:52	0:01:18	0:00:58	0:00:42
1000	0:34:34	0:03:40	0:01:54	0:01:20	0:01:00	0:00:40
2500	0:48:38	0:04:08	0:02:06	0:01:32	0:01:06	0:00:44
5000	0:50:32	0:04:20	0:02:18	0:01:32	0:01:12	0:00:42

Table 5.10 Actual simulation time used in stochastic simulation (inertial impaction)

St	R					
	0.05	0.1	0.13	0.15	0.17	0.2
0.0	1:18:58	0:25:24	0:12:28	0:22:42	0:12:22	0:10:52
0.6	0:25:18	0:18:24	0:09:24	0:16:48	0:12:14	0:08:06
1.0	0:15:24	0:19:06	0:06:48	0:12:40	0:08:24	0:06:10
1.4	0:09:24	0:09:22	0:05:04	0:09:42	0:07:22	0:05:14
2.0	0:05:00	0:07:22	0:04:06	0:08:04	0:06:08	0:04:26

Table 5.11 Actual simulation time used by the simplified model (convective diffusion)

Pe	R					
	0.05	0.1	0.13	0.15	0.17	0.2
200	0:00:15	0:00:08	0:00:08	0:00:08	0:00:08	0:00:06
500	0:00:15	0:00:08	0:00:08	0:00:08	0:00:07	0:00:05
1000	0:00:14	0:00:08	0:00:08	0:00:07	0:00:07	0:00:05
2500	0:00:14	0:00:08	0:00:08	0:00:08	0:00:07	0:00:05
5000	0:00:15	0:00:08	0:00:08	0:00:07	0:00:07	0:00:04

Table 5.12 Actual simulation time used by the simplified model (inertial impaction)

St	R					
	0.05	0.1	0.13	0.15	0.17	0.2
0.0	0:00:17	0:00:10	0:00:08	0:00:06	0:00:06	0:00:05
0.6	0:00:17	0:00:09	0:00:08	0:00:07	0:00:06	0:00:04
1.0	0:00:17	0:00:10	0:00:08	0:00:08	0:00:07	0:00:06
1.4	0:00:18	0:00:11	0:00:09	0:00:10	0:00:08	0:00:06
2.0	0:00:22	0:00:12	0:00:10	0:00:10	0:00:09	0:00:06

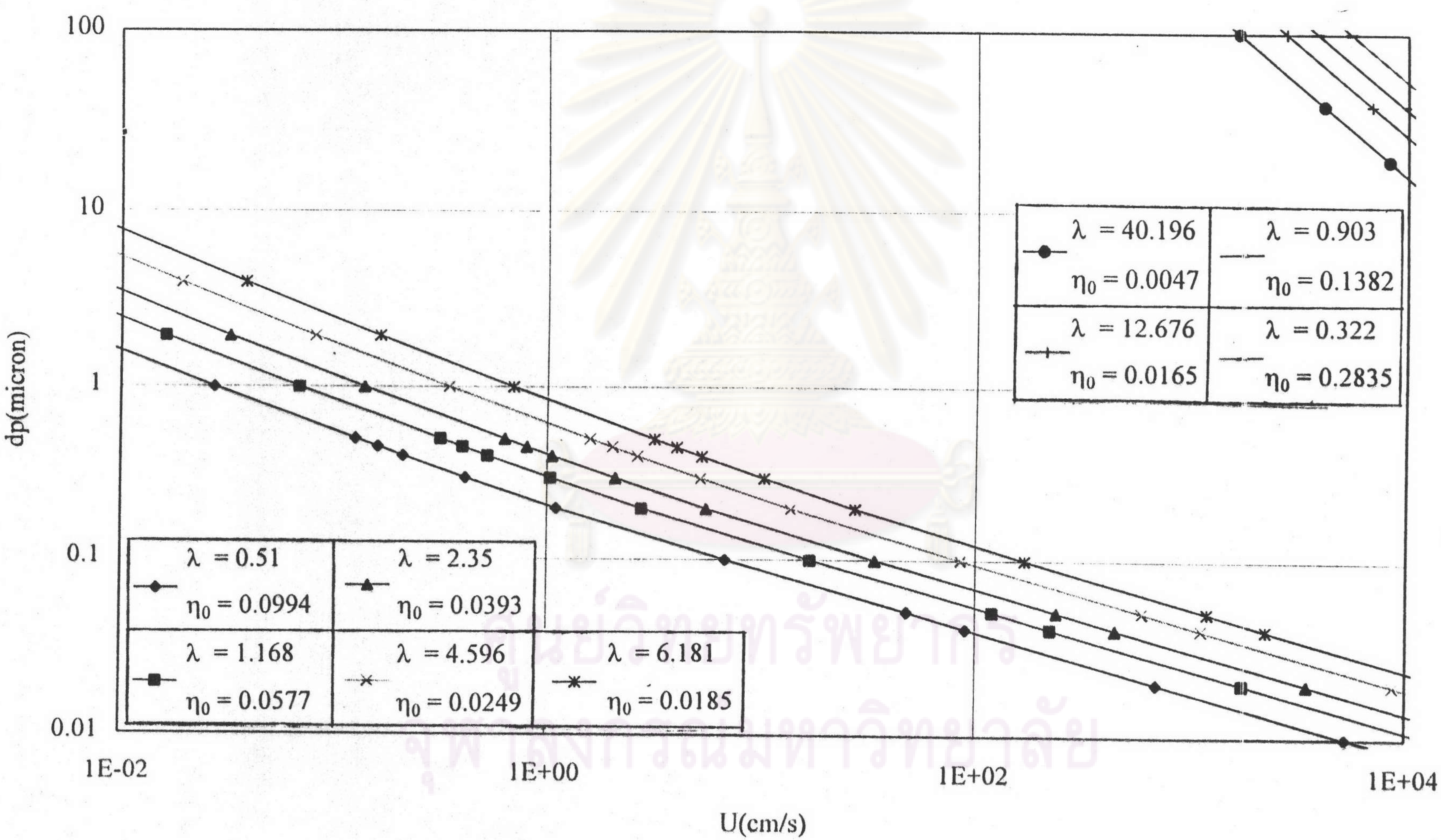

Figure 5.132 Relationship between d_p and U_∞ with η_0 and λ as parameter for R=0.05

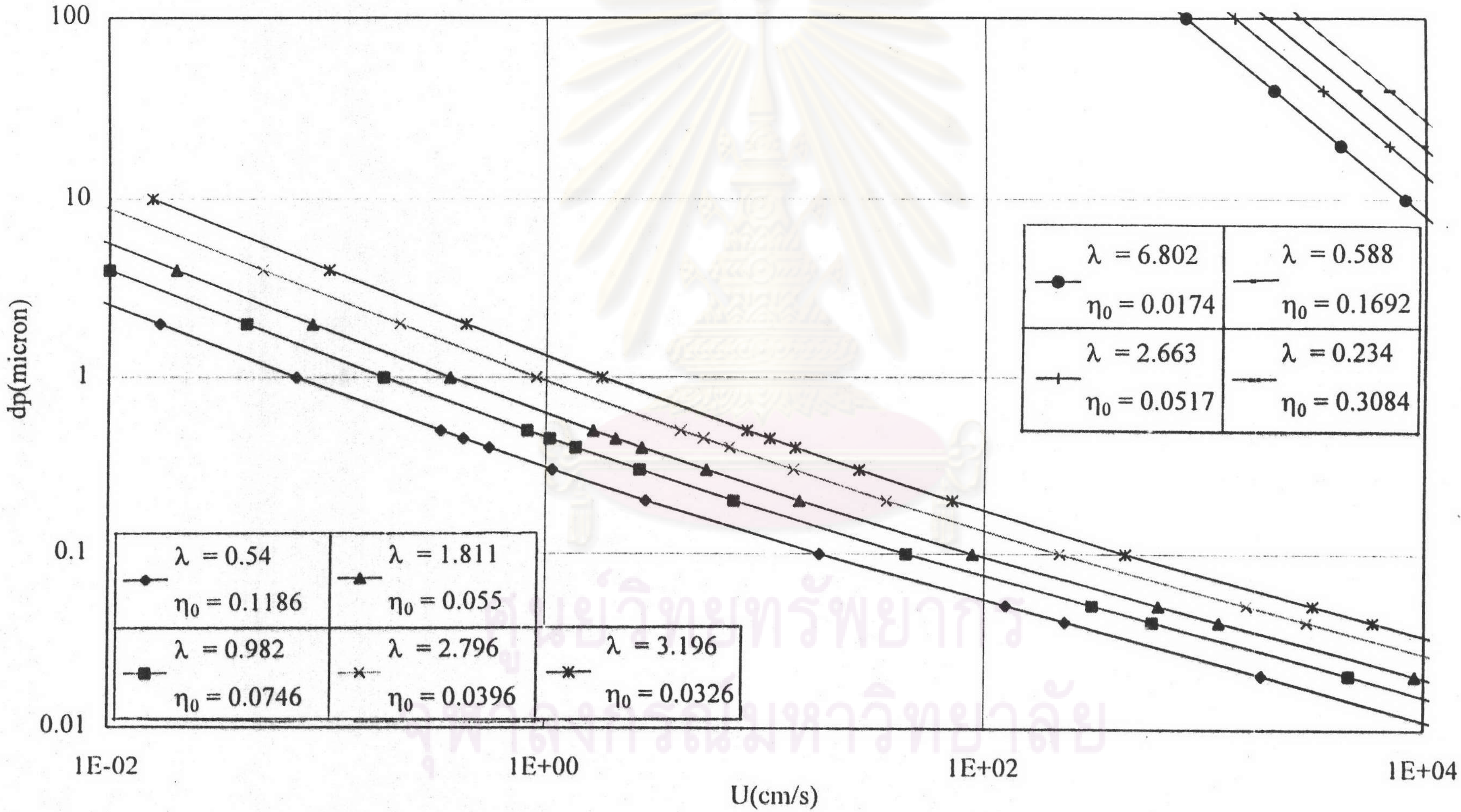

Figure 5.133 Relationship between d_p and U_∞ with η_0 and λ as parameter for R=0.1

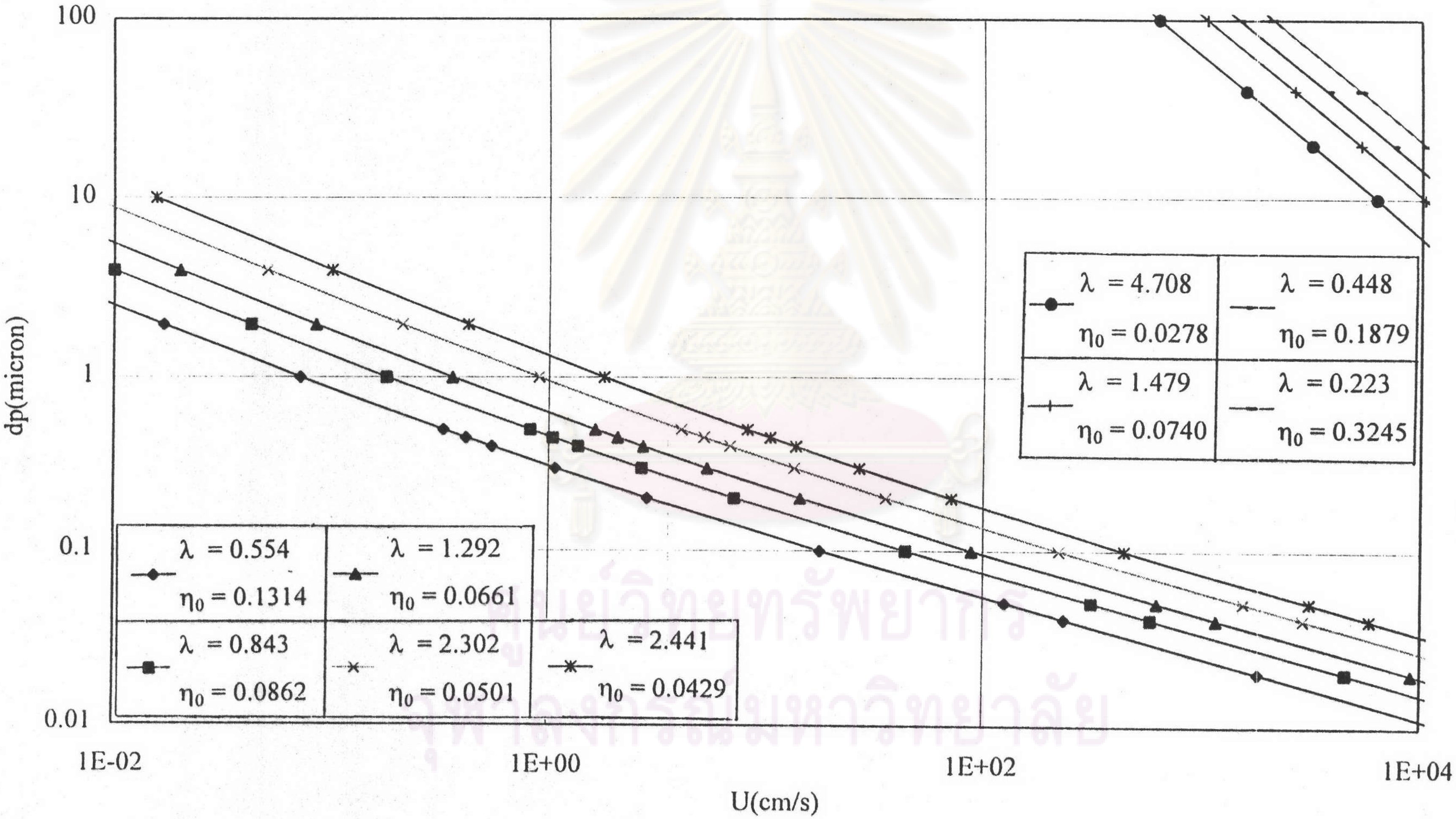

Figure 5.134 Relationship between d_p and U_∞ with η_0 and λ as parameter for R=0.13

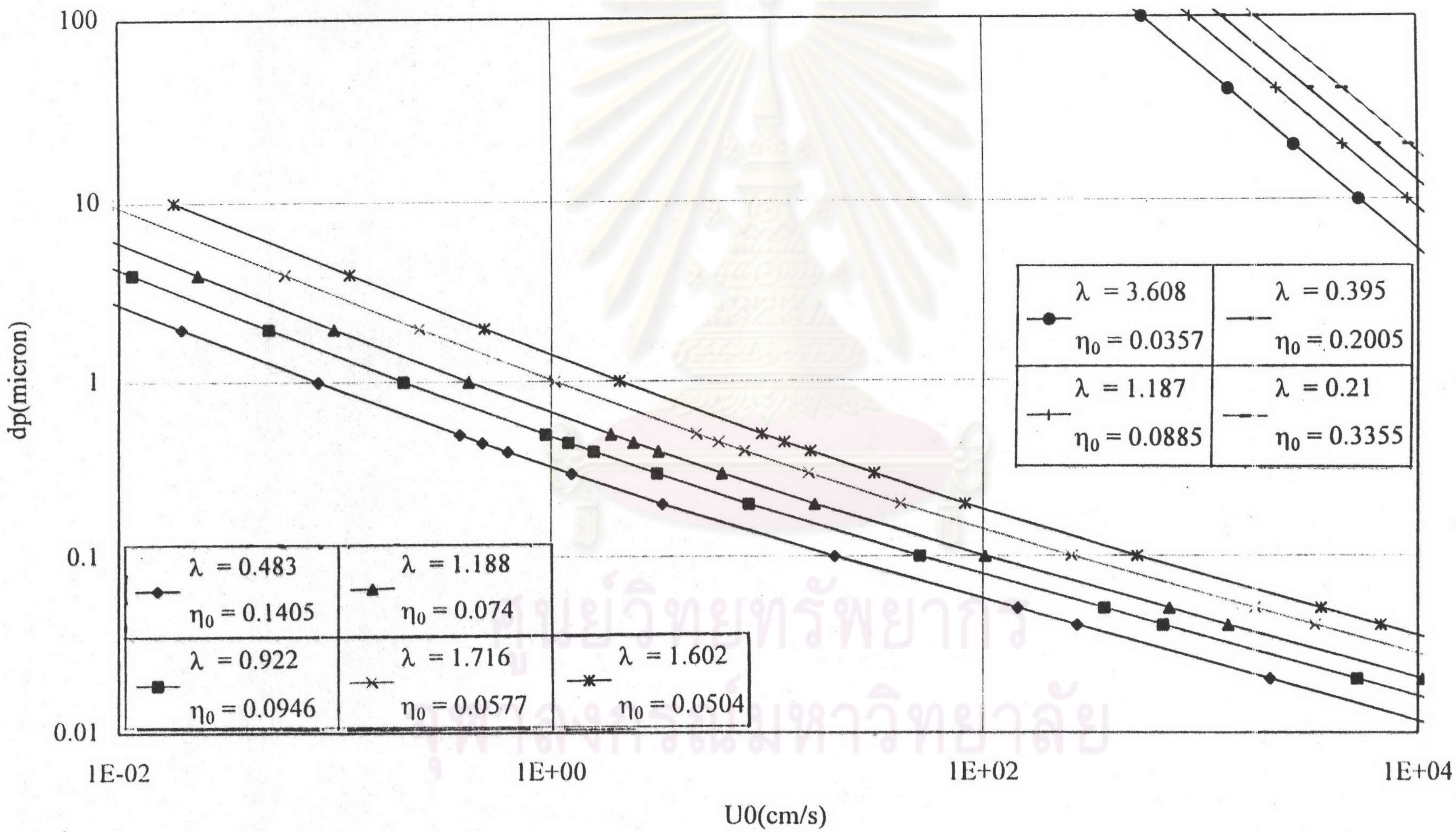

Figure 5.135 Relationship between d_p and U_∞ with η_0 and λ as parameter for R=0.15

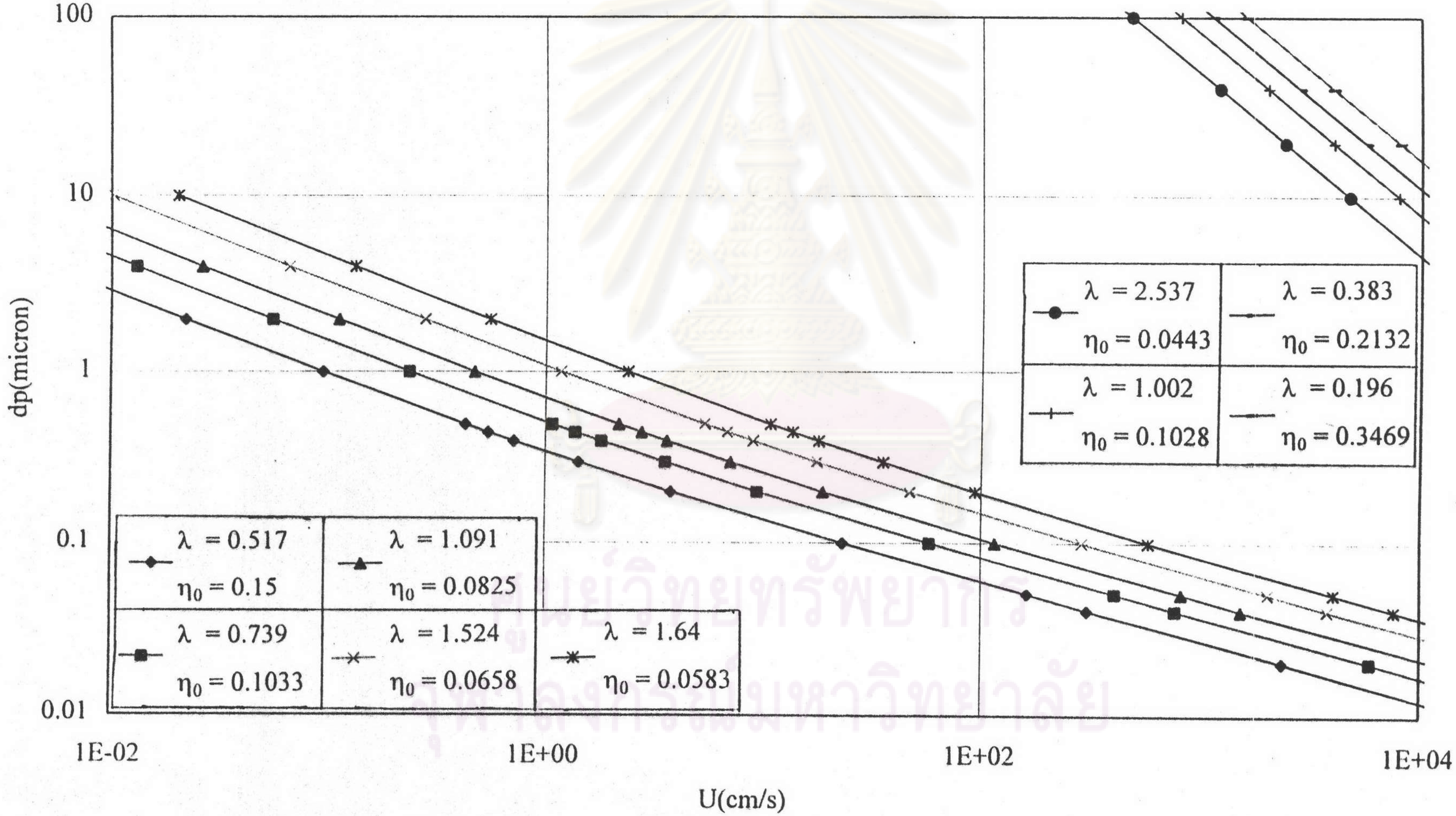

Figure 5.136 Relationship between d_p and U_∞ with η_0 and λ as parameter for R=0.17

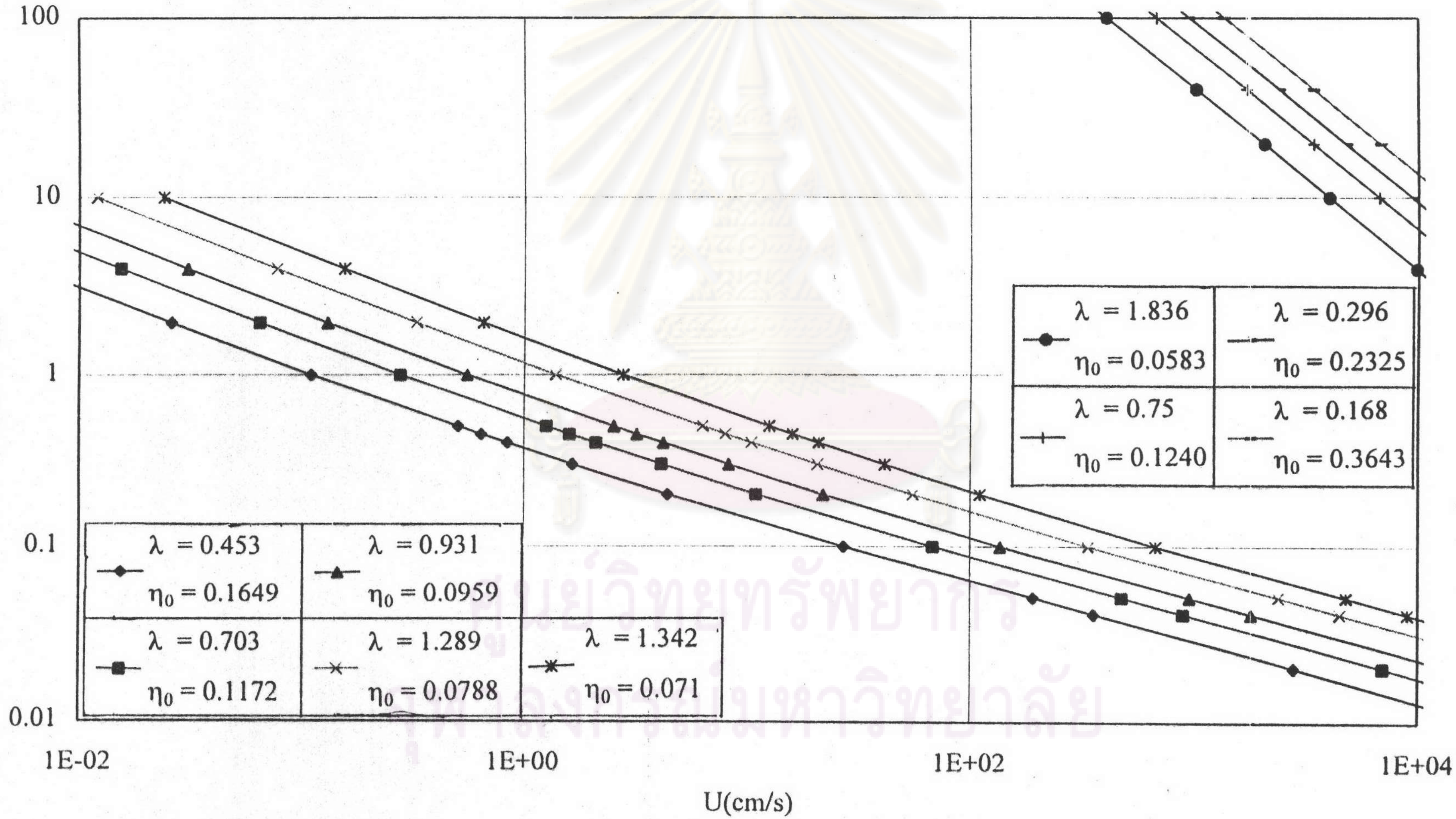

Figure 5.137 Relationship between d_p and U_∞ with η_0 and λ as parameter for R=0.2

dimensionless parameters such as R, Pe and St were rewritten and solved for the air velocity and particle size. Thus the air velocity U_∞ could be expressed in terms the dimensionless variables Pe and St, respectively.

For convective diffusion

$$U_\infty = \frac{PeD_{BM}}{d_f} \tag{5.1}$$

For inertial impaction

$$U_\infty = \frac{9\mu d_f St}{C_m \rho_p d_p^2} \tag{5.2}$$

The contours of the clean fiber collection efficiency η_0 and the collection efficiency raising factor λ were then plotted with respect to d_p and U_∞. The clean fiber collection efficiency calculated from Stechkina and Fuchs's equation for convective diffusion and limiting trajectory theory for inertial impaction, respectively. Figures 5.132-5.137 show the relationships between d_p and U_∞ with η_0 and λ as parameters for various R. As seen from the figures, λ increased but η_0 decreased at a large d_p and U_∞ in the case of convective diffusion. On the other hand, λ increased but η_0 decreased at a small d_p and U_∞ in the case of inertial impaction. Hence λ and η_0 can be estimated quickly from these figures.

5.3 The behavior of the deterministic model

The average dendritic growth was already calculated under various filtration conditions for convective diffusion and inertial impaction by using the deterministic model. To see the individual effect of the parameters e_N and e'_N, as well as the dimensionless groups R, Pe, St, on the model behavior, the dendrite distribution, the average dendrite size, the total population of dendrites, λ, and η were plotted against N_{gen} (corresponding to filtration time) which varying slightly each of the parameters or groups.

5.3.1 Convective diffusion

The effects of the parameters e_N and e'_N, the Peclet number Pe and the interception parameter R on the dendrite distribution, the average dendrite size, the

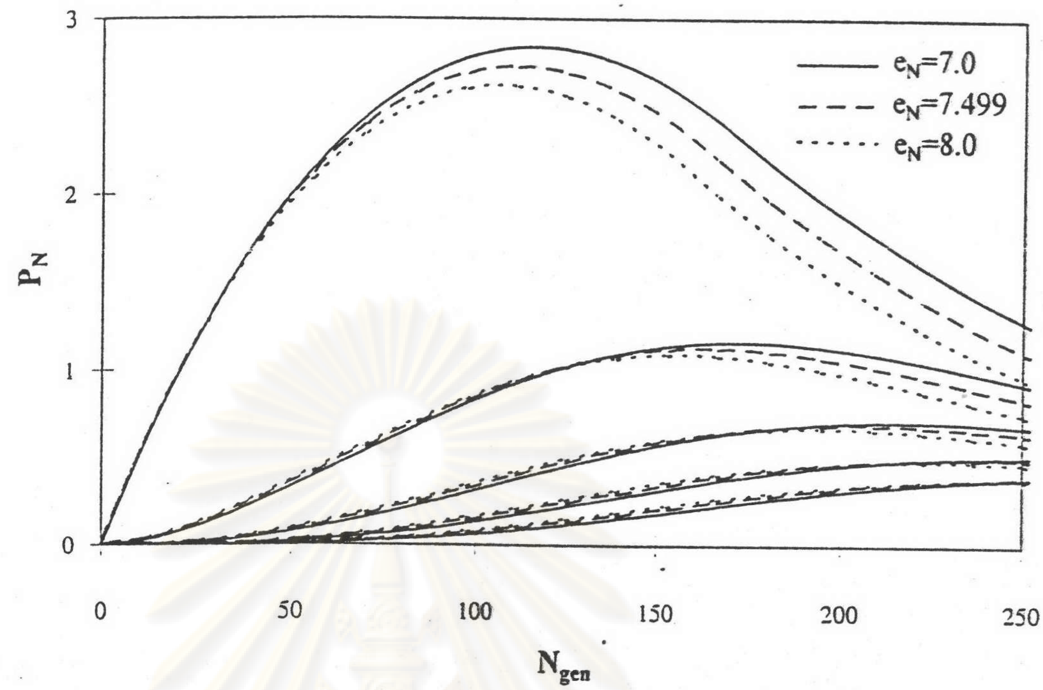

Figure 5.138 Dendrite distribution for convective diffusion of R=0.1, Pe=1000, and e'_N=3.877

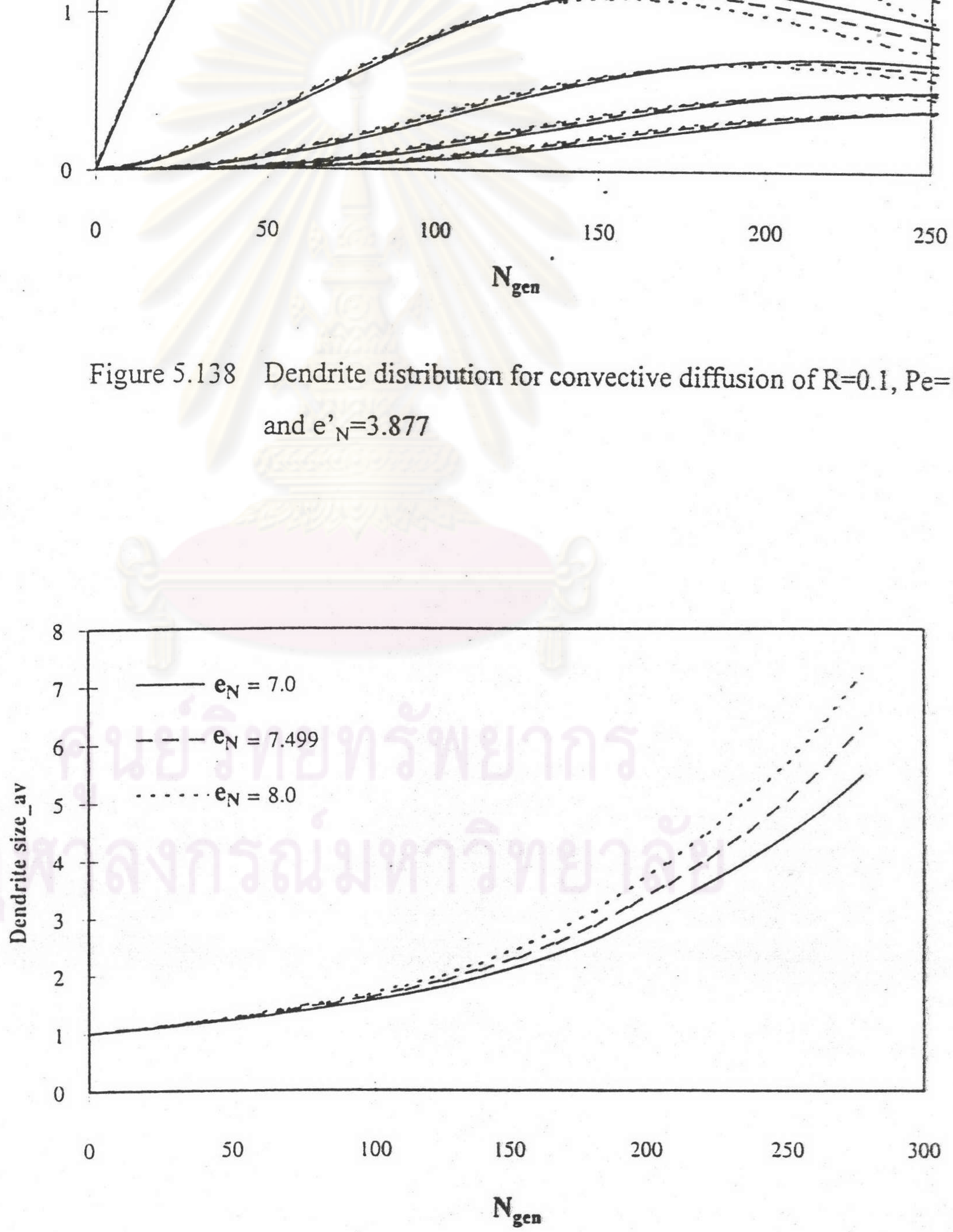

Figure 5.139 Dendrite average size for convective diffusion of R=0.1, Pe=1000, and e'_N=3.877

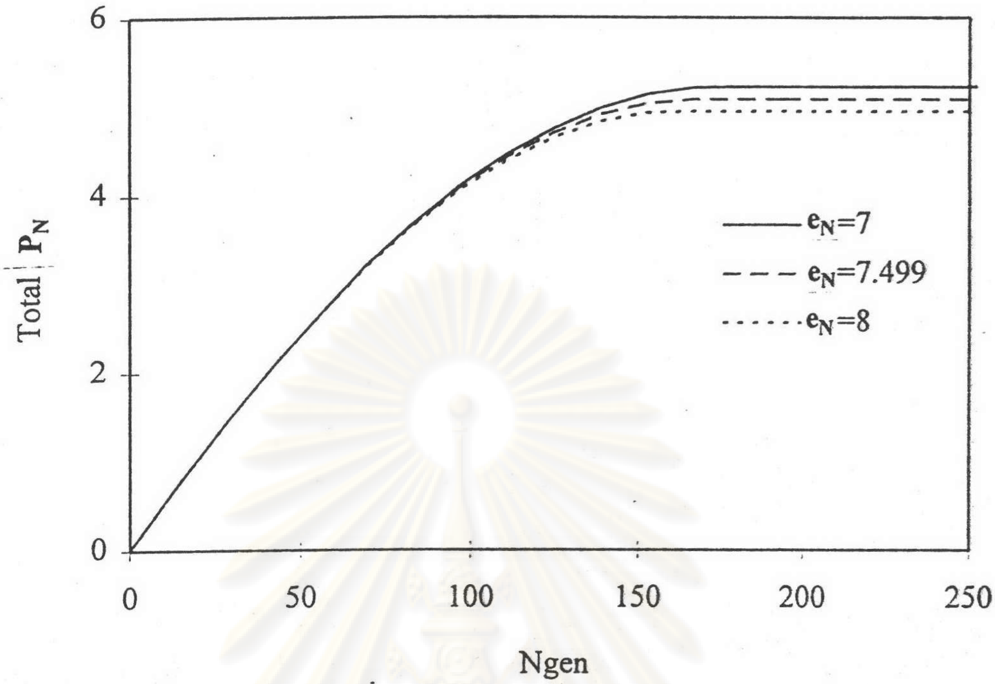

Figure 5.140 Total population of dendrites for convective diffusion ($R=0.1$, $Pe=1000$ and $e'_N=3.877$)

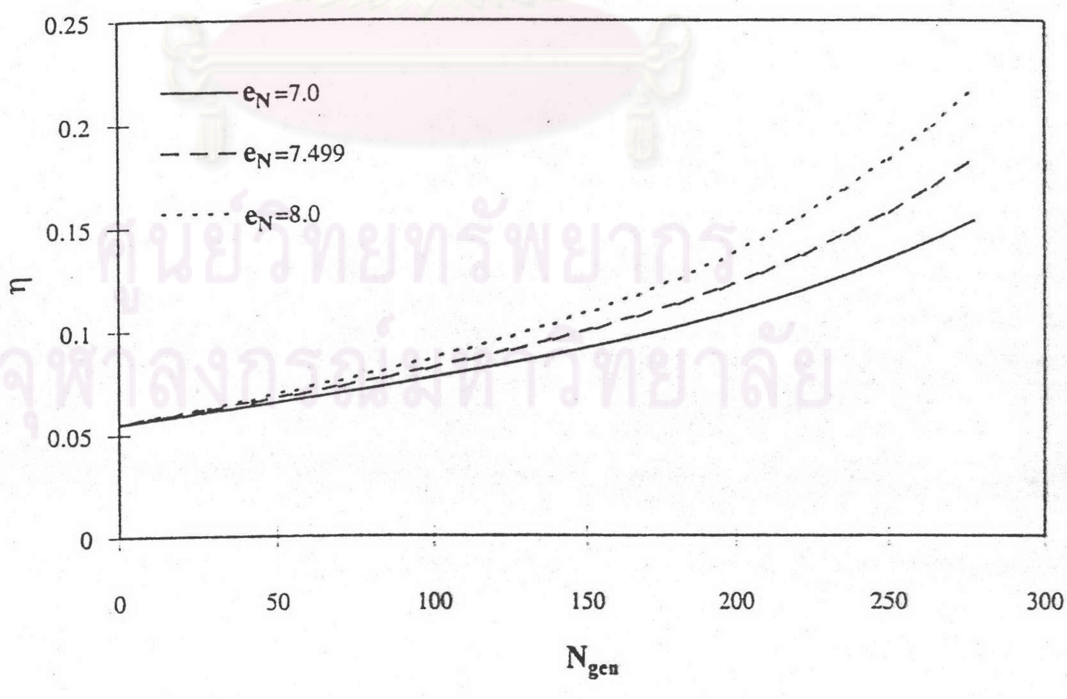

Figure 5.141 Collection efficiency for convective diffusion of $R=0.1$, $Pe=1000$, and $e'_N=3.877$

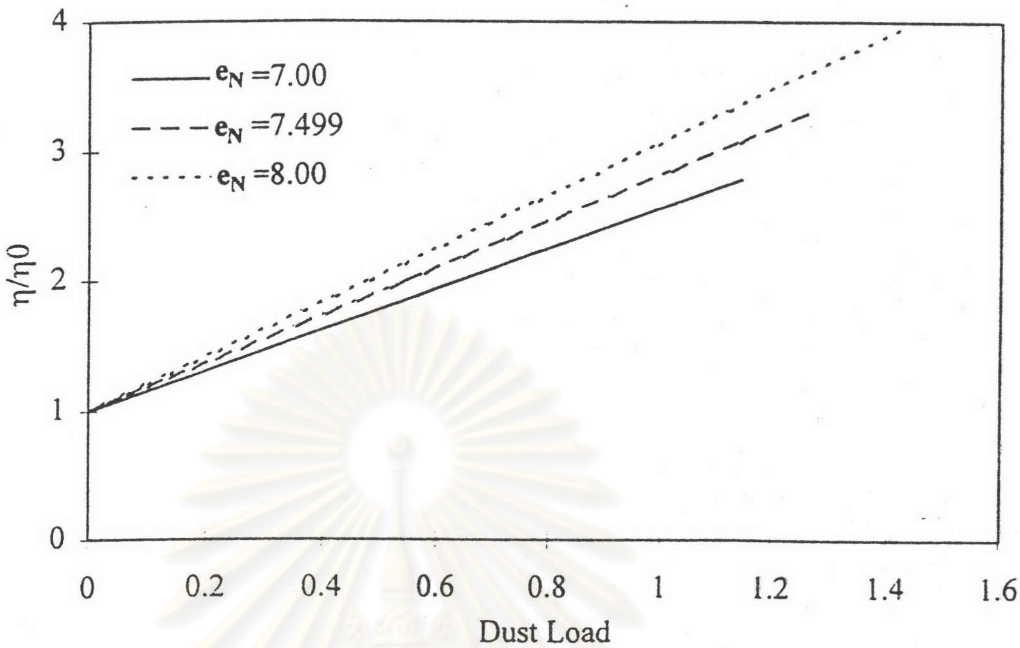

Figure 5.142 Normalized collection efficiency of dust load for R=0.1, Pe=1000, and e'_N=3.877

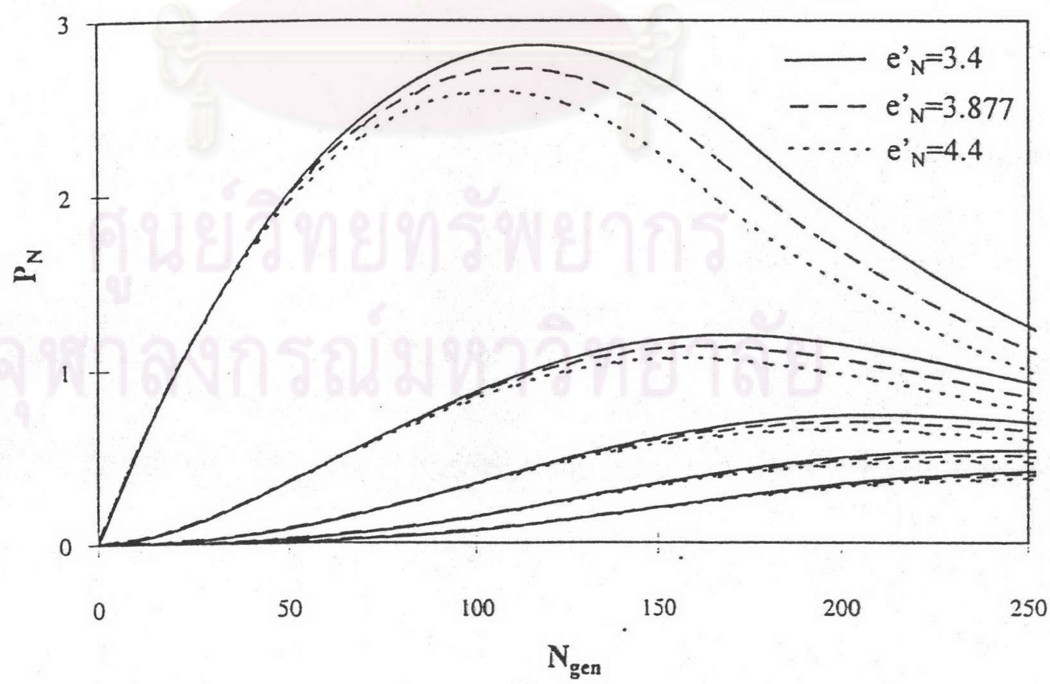

Figure 5.143 Dendrite distribution for convective diffusion of R=0.1, Pe=1000, and e_N=7.499

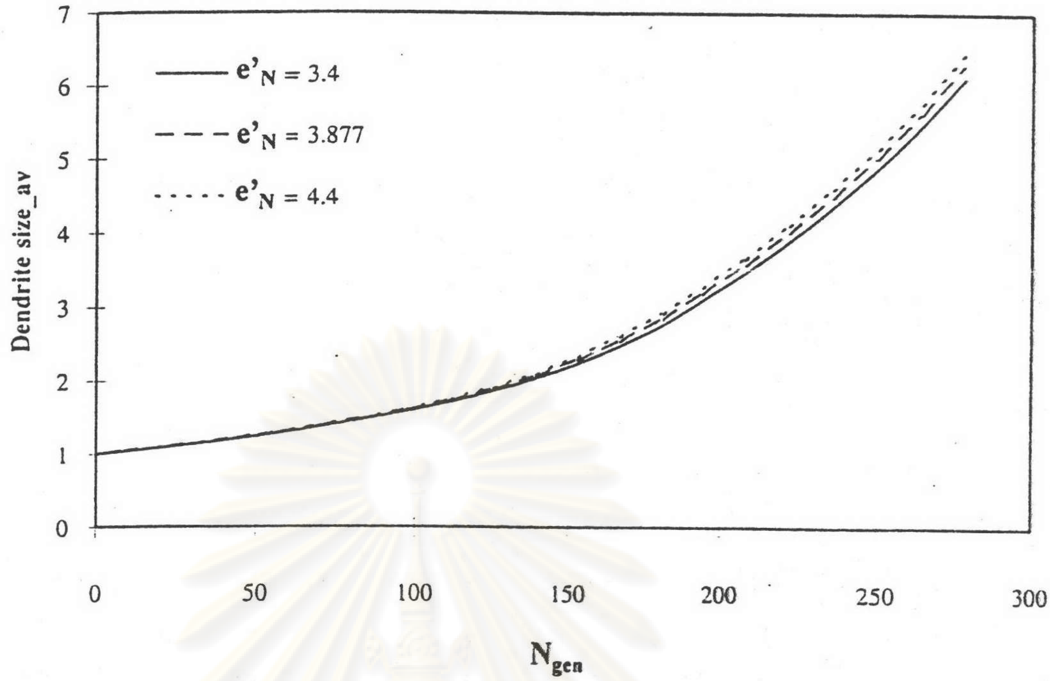

Figure 5.144 Dendrite average size for convective diffusion of R=0.1, Pe=1000, and e_N=7.499

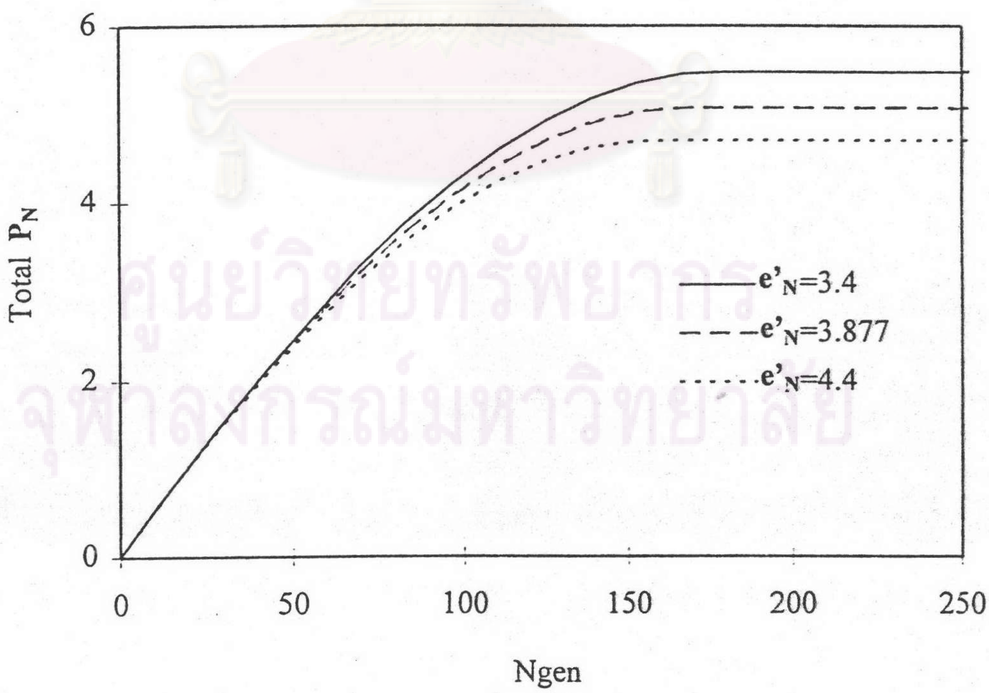

Figure 5.145 Total population of dendrites for convective diffusion (R=0.1, Pe=1000 and e_N=7.499)

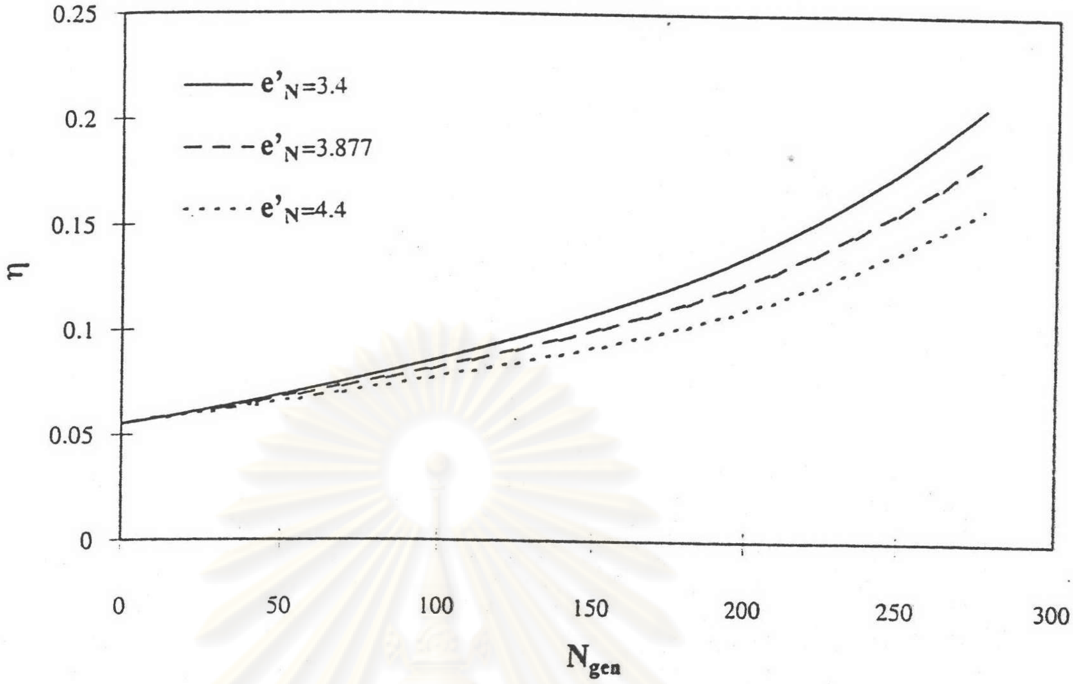

Figure 5.146 Collection efficiency for convective diffusion of R=0.1, Pe=1000, and e_N=7.499

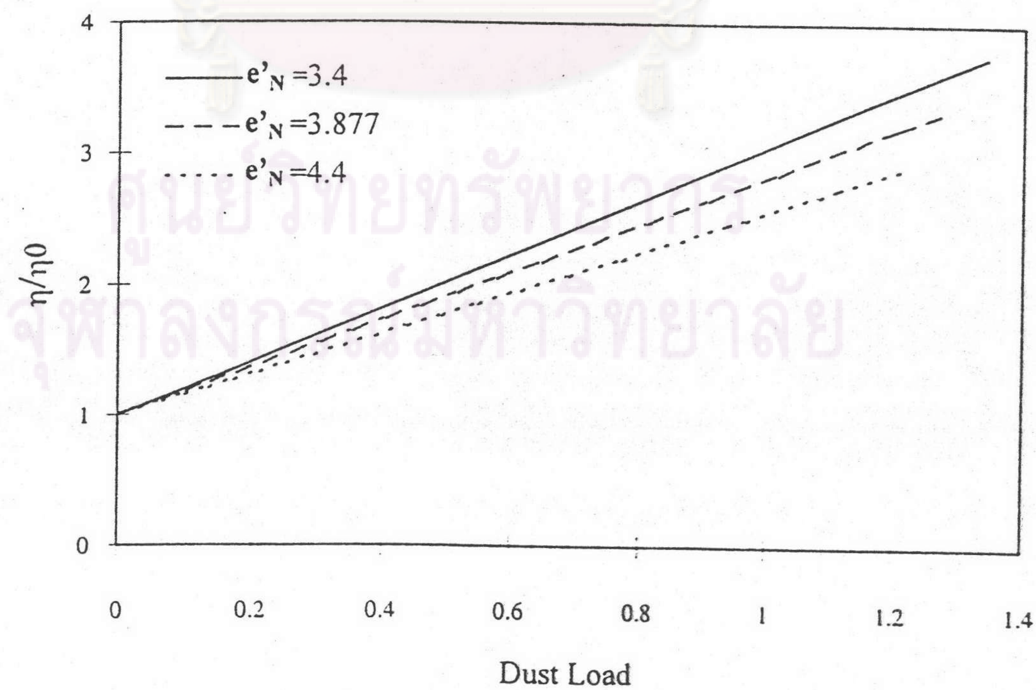

Figure 5.147 Normalized collection efficiency of dust load for R=0.1, Pe=1000, and e_N=7.499

collection efficiency raising factor λ and the collection efficiecny η were investigated in section 5.3.1.

5.3.1.1 Effect of the parameter e_N

The effects of the parameter e_N on the dendrite distribution, the average dendrite size, the total population of dendrites, λ and η were studied at R=0.1, Pe=1000 and e'_N=3.877. Figure 5.138 shows the resulting dendrite distribution with e_N as parameter. As seen from the figure, the number concentration of P_N initially increased slightly faster but subsequently decreased faster as the parameter e_N was increased. Figure 5.139 shows the average dendrite size with e_N as parameter. As seen from the figure, the average dendrite size was bigger when the parameter e_N increased. Figure 5.140 shows the comparative effect of e_N on the total population of dendrites. As seen from the figure, the resulting population of dendrites becomes smaller when e_N increases. Figure 5.141 shows the effect of e_N on η. At a larger e_N, η increased more rapidly with N_{gen} because the effective capture area increased. Table 5.13 shows the effect of e_N on λ. Figure 5.142 shows the effect of e_N on η/η_0 vs. dust-loaded. As seen from the Figure, e_N enhanced the normalized collection efficiency versus dust load.

5.3.1.2 Effects of the parameter e'_N

As above, the effects of e'_N on the dendrite distribution, the average dendrite size, the total population of dendrites, λ, and η at R=0.1, Pe=1000 and e_N=10.336 were investigated. Figure 5.143 shows the effect of e'_N on the dendrite distribution. As seen from the figure, the concentration P_N initially increased barely faster but subsequently decreased singnificantly faster when the parameters e'_N was raised. Figure 5.144 shows the effect of e'_N on the average dendrite size. As seen from the figure, the average dendrite size was almost the same as the parameter e'_N was raised. Figure 5.145 shows the comparative effect of e'_N on the total population of dendrites. As seen from the figure, the total population of dendrites also becomes smaller when e'_N increases. Figure 5.146 shows the effect of e'_N on η. As seen from the figure, e'_N negatively affected η. Table 5.14 lists λ with e'_N as parameter. Again e

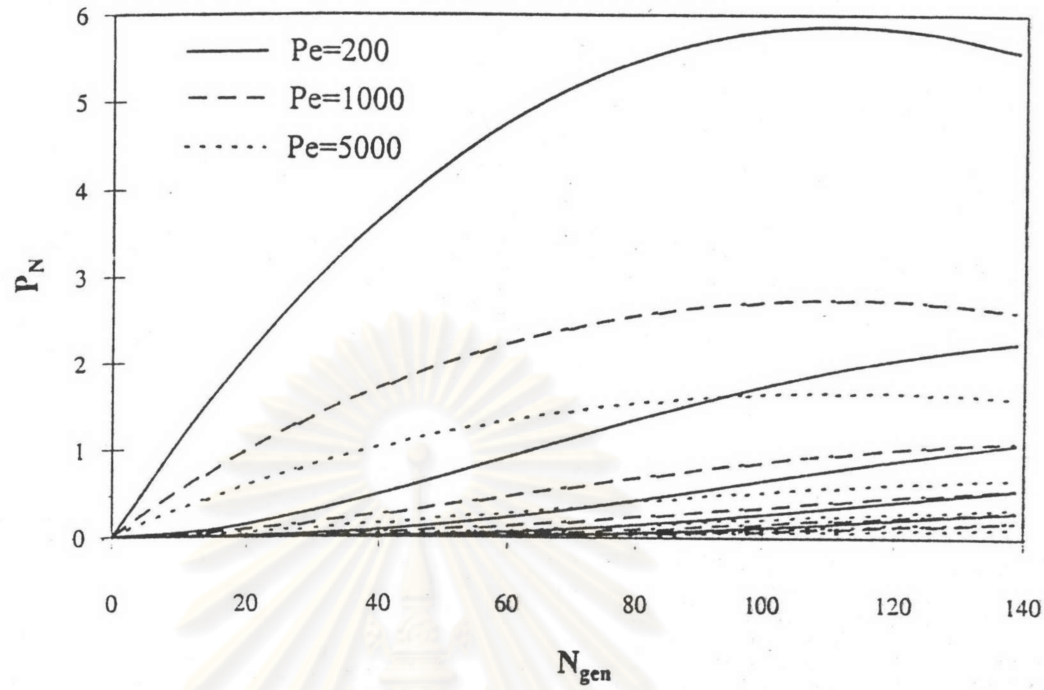

Figure 5.148 Dendrite distribution of convective diffusion with Pe as parameter for R=0.1

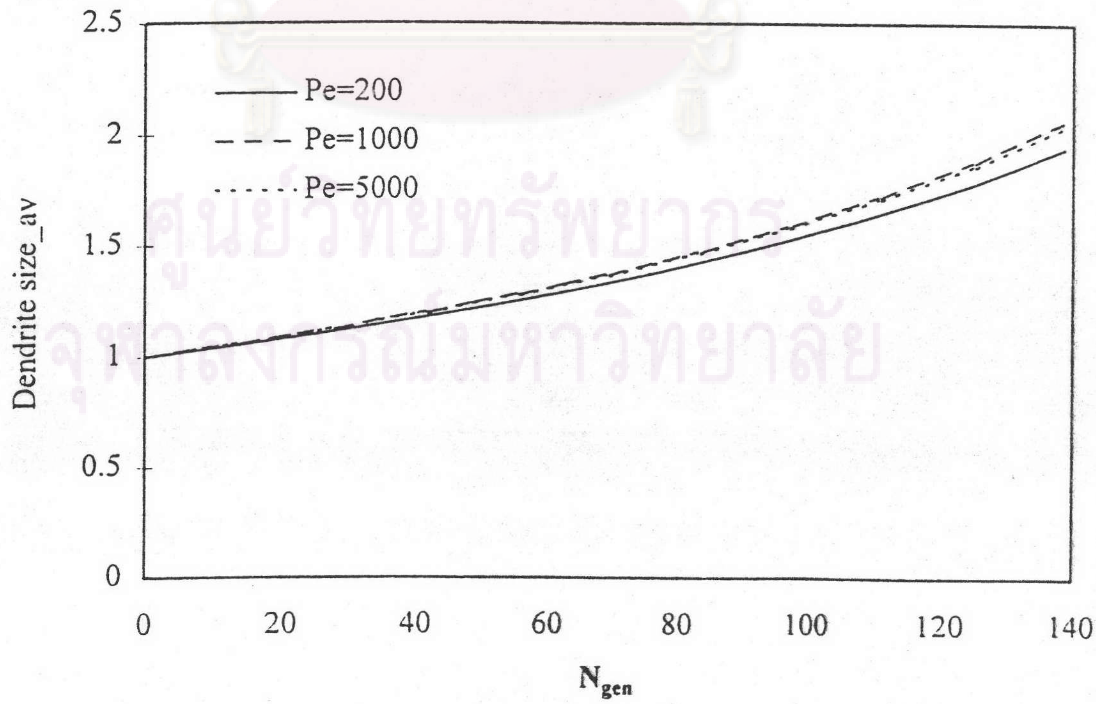

Figure 5.149 Dendrite average size of convective diffusion with Pe as parameter for R=0.1

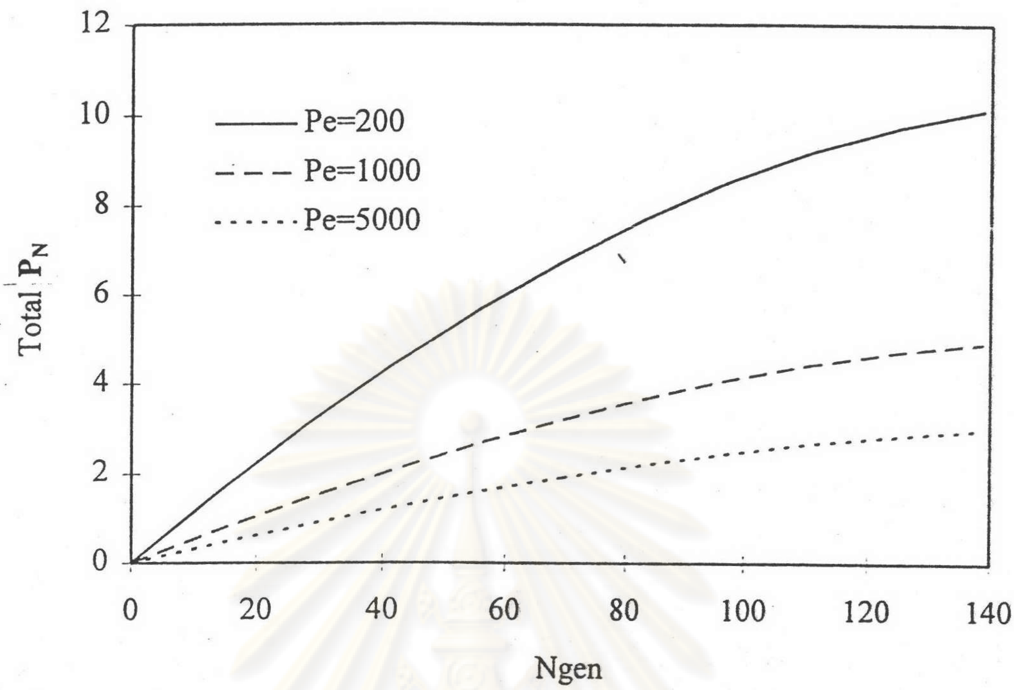

Figure 5.150 Total population of dendrites for convective diffusion (R=0.1)

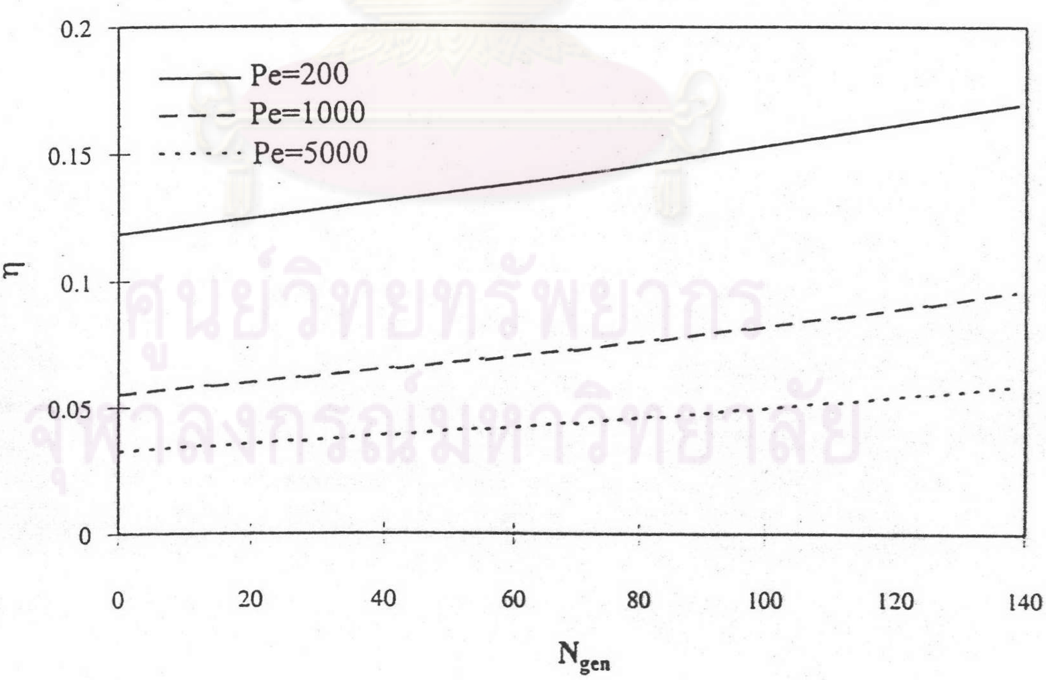

Figure 5.151 Collection efficiency of convective diffusion with Pe as parameter for R=0.1

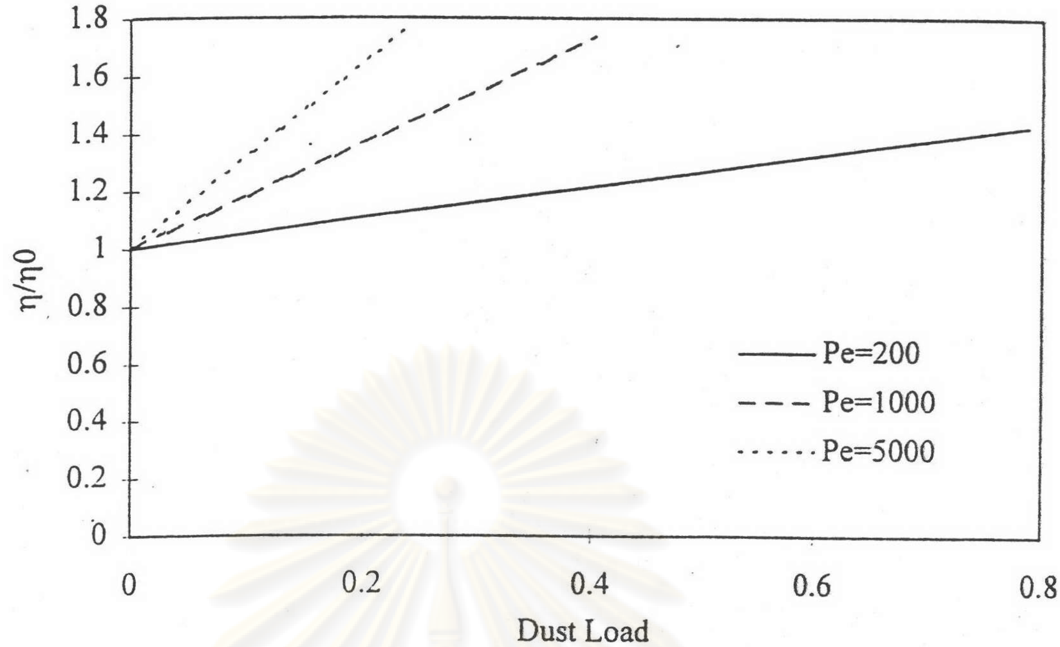

Figure 5.152 Normalized collection efficiency of dust load with Pe as parameter for R=0.1

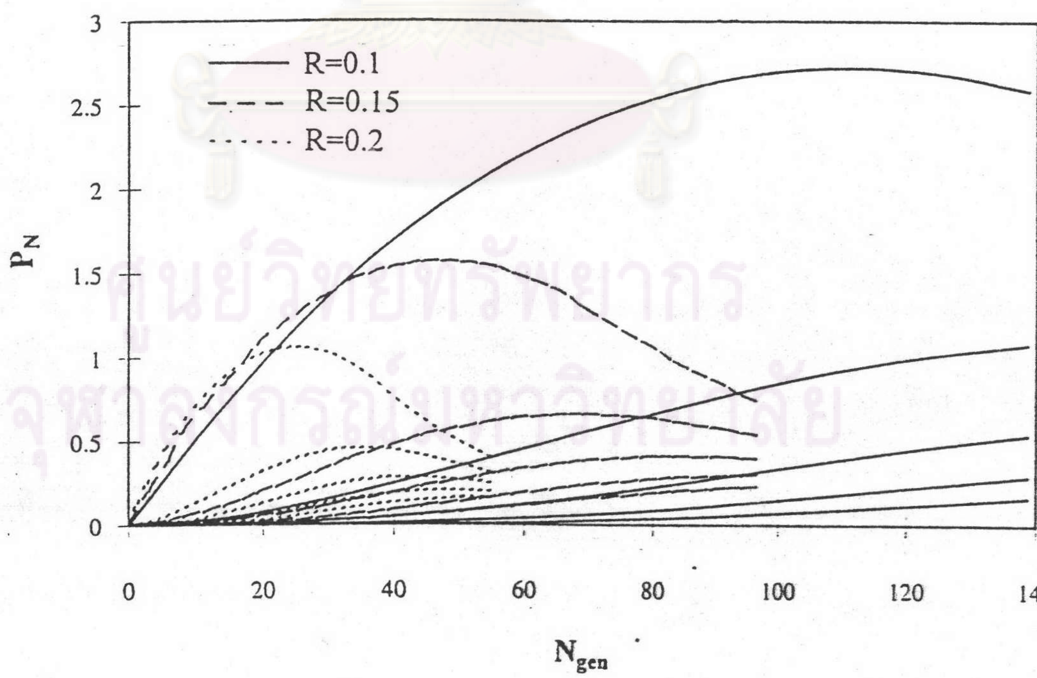

Figure 5.153 Dendrite distribution of convective diffusion with R as parameter for Pe=1000

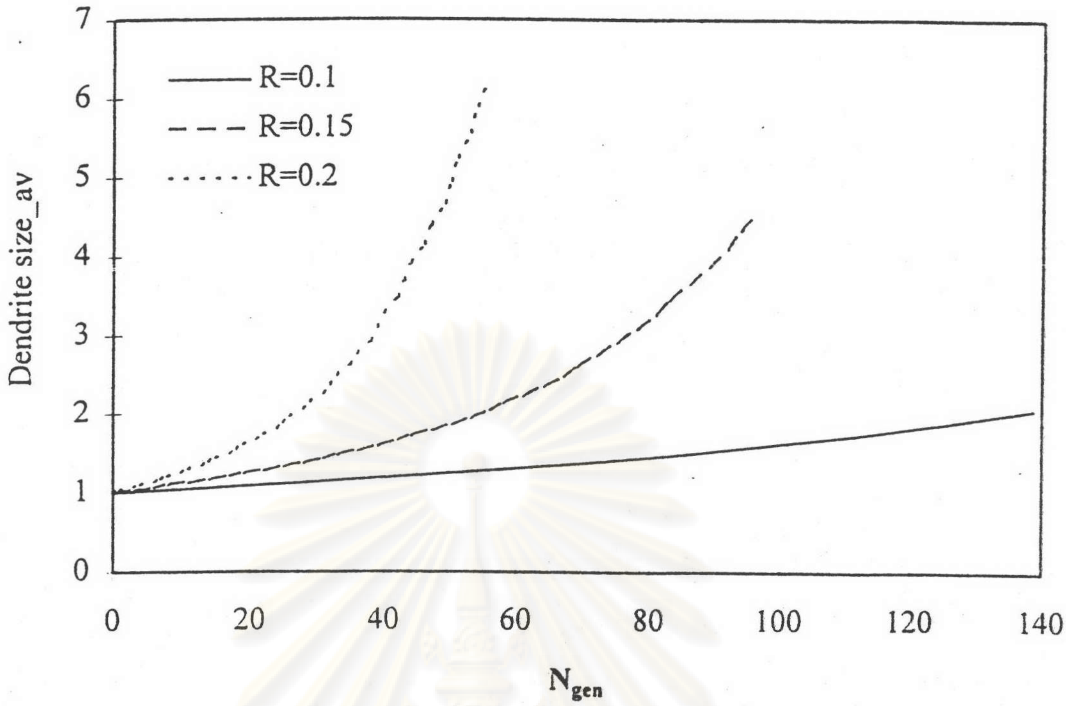

Figure 5.154 Dendrite average size of convective diffusion with R as parameter for Pe=1000

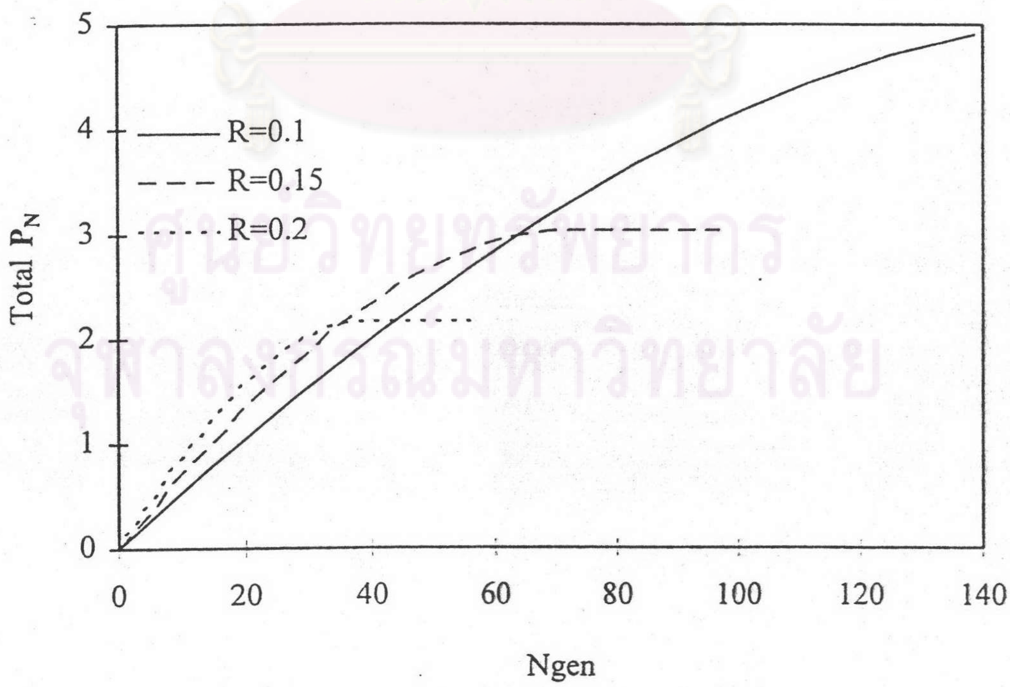

Figure 5.155 Total population of dendrites for convective diffusion (Pe=1000)

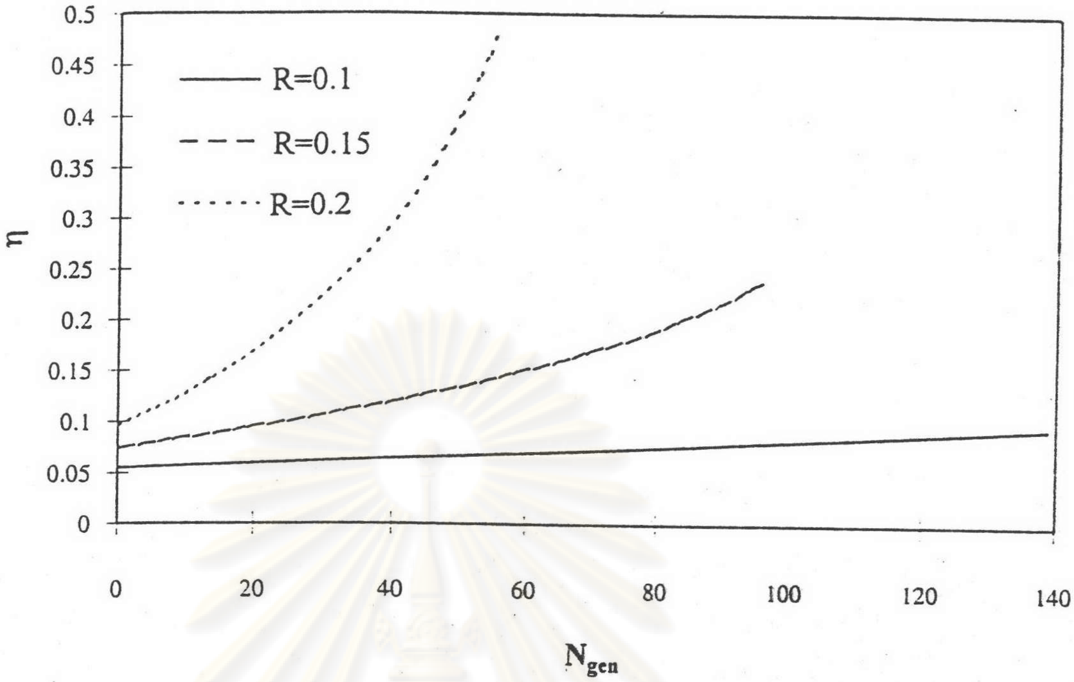

Figure 5.156 Collection efficiency of convective diffusion with R as parameter for Pe=1000

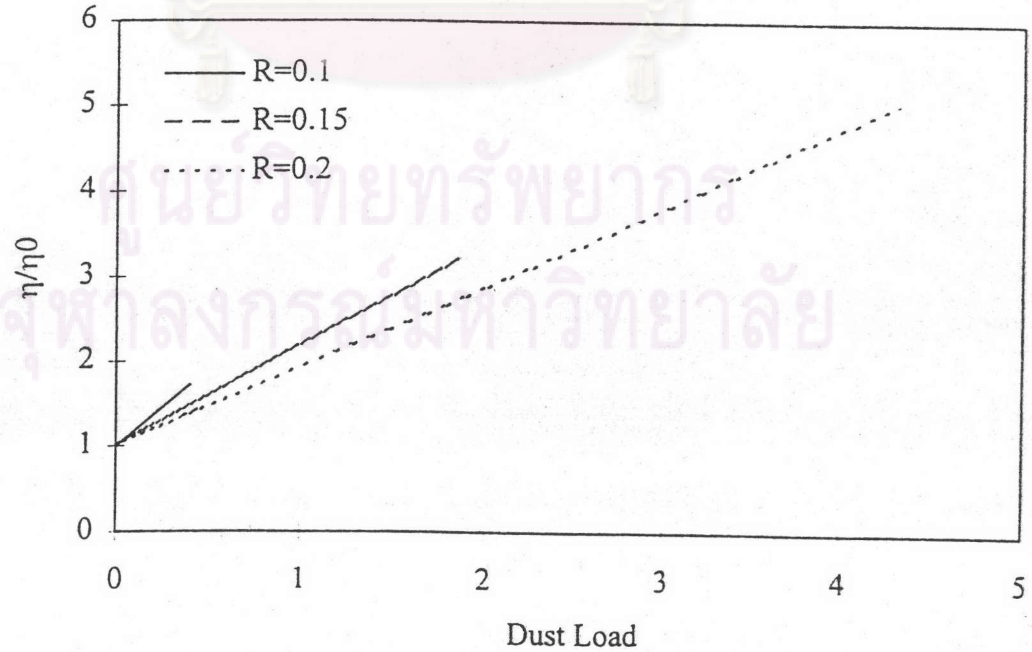

Figure 5.157 Normalized collection efficiency of dust load with R as parameter for Pe=1000

e_N	7	7.499	8
λ	1.562	1.811	2.062

Table 5.13 The collection efficiency raising factor λ for R=0.1 Pe=1000 and e'n=3.877

e'_N	3.4	3.877	4.4
λ	2.05	1.811	1.55

Table 5.14 The collection efficiency raising factor λ for R=0.1 Pe=1000 and en=7.499

Pe	200	1000	5000
e_N	3.159	7.499	12.606
e'_N	2.078	3.877	6.213
λ	0.5405	1.8110	3.1965

Table 5.15 The collection efficiency raising factor λ for R=0.1

R	0.1	0.15	0.2
e_N	7.499	6.234	5.631
e'_N	3.877	2.67	1.906
λ	1.8110	1.1880	0.9313

Table 5.16 The collection efficiency raising factor λ for Pe=1000

'N degraded λ. Figure 5.147 shows the effect of e'_N on η/η_0 vs. dust load. Similarly, e'_N degraded η/η_0 .

5.3.1.3 Effects of Pe

It is well known that the diffusivity and η_0 is inversely proportional to Pe. Here the effects of Pe on the dendrite distribution, the average dendrite size, the total population of dendrites, λ, and η for R=0.1 and the values of e_N and e'_N shown in Table 5.5. Figure 5.148 shows the effect of Pe on the dendrite distribution. As seen from the figure, the concentration of the smaller dendrites decreased when Pe increased. Figure 5.149 shows the effect of Pe on the average dendrite size. As seen from the figure, the average dendrite size increased slightly. Figure 5.150 shows the effect of Pe on the total population of dendrites. As seen from the figure, the population of dendrites becomes much smaller when Pe increases. Table 5.15 show the effect of Pe on λ. λ increased with increasing Pe because of decreasing η_0. Figure 5.151 shows the effect of Pe on η. As soon from the figure, η decreased with increasing Pe. Figure 5.152 shows the effect of Pe on η/η_0 vs. dust-load. η/η_0 increased faster as Pe increased.

5.3.1.4 Effects of R

The effect of R was investigated at Pe=1000 using the values of the parameters e_N and e'_N shown in Table 5.5. When R increased, the particles were larger so more are captured on a fiber. Figure 5.153 shows the effect of R on the dendrite distribution. As seen from the figure, the dendrite concentration P_N was lower and decreased faster as N_{gen} increased. Since the particles were larger, the number of captured particles could be smaller. Figure 5.154 shows the effect of R on the average dendrite size. The average dendrite size increased faster when R was larger. Figure 5.155 shows the effect of R on the total population of dendrites. As seen from the figure, when N_{gen} is still small (less than 30), the total number of dendrites at a lower R is smaller than that at a higher R. However, as time passes, the population of dendrites at a higher R attains a larger asymptotic size. Table 5.16 shows λ the effect of R on λ. λ decreased with increasing R because of increased η_0. Figure 5.156

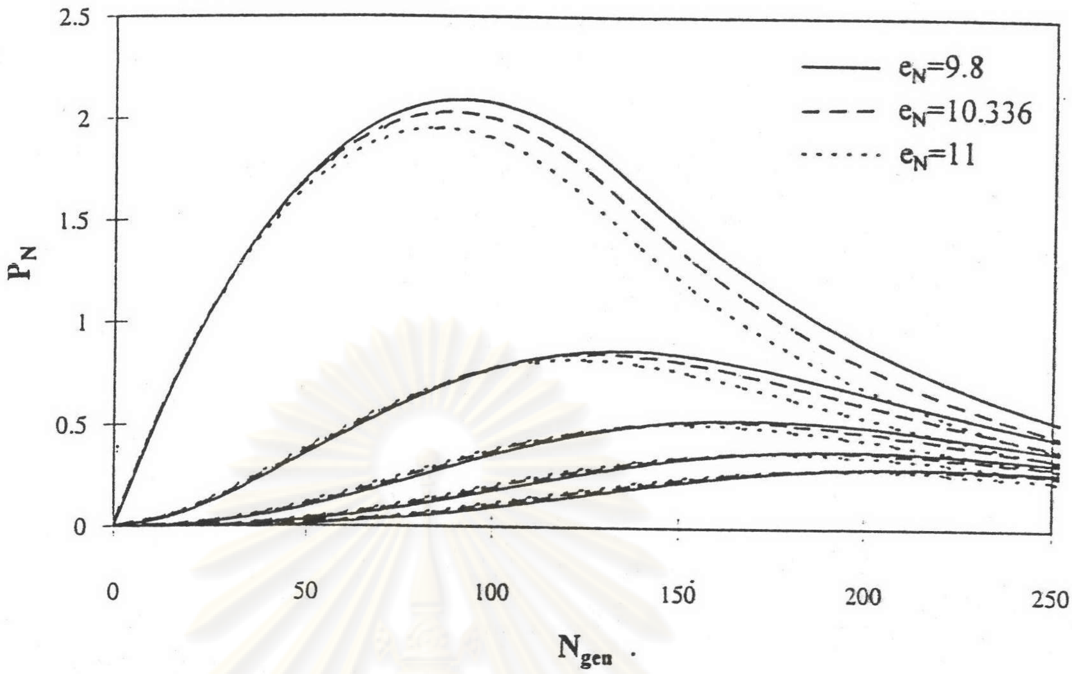

Figure 5.158 Dendrite distribution for inertial impaction of R=0.1, St=1, and e'_N=5.01

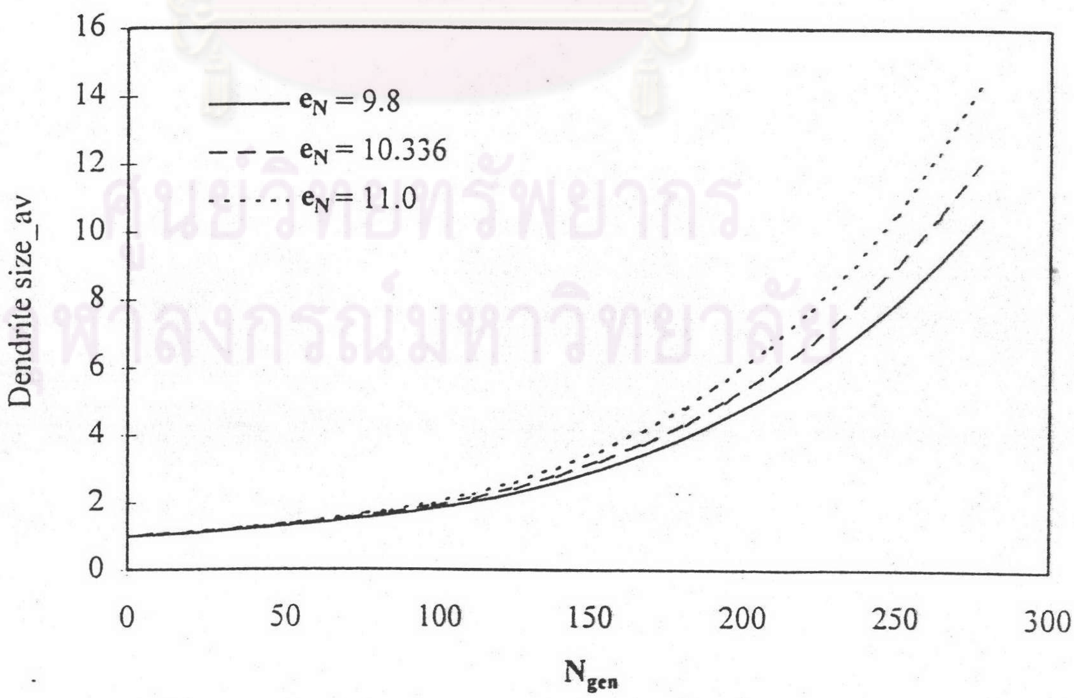

Figure 5.159 Dendrite average size for inertial impaction of R=0.1, St=1, and e'_N=5.01

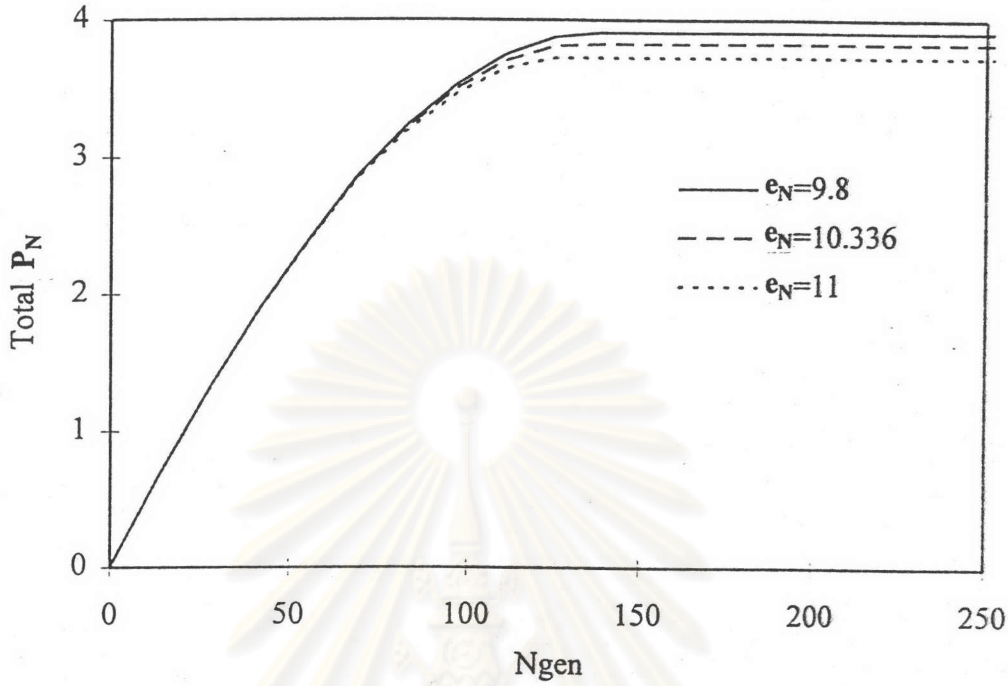

Figure 5.160 Total population of dendrites for inertial impaction (R=0.1, St=1 and e'_N=5.01)

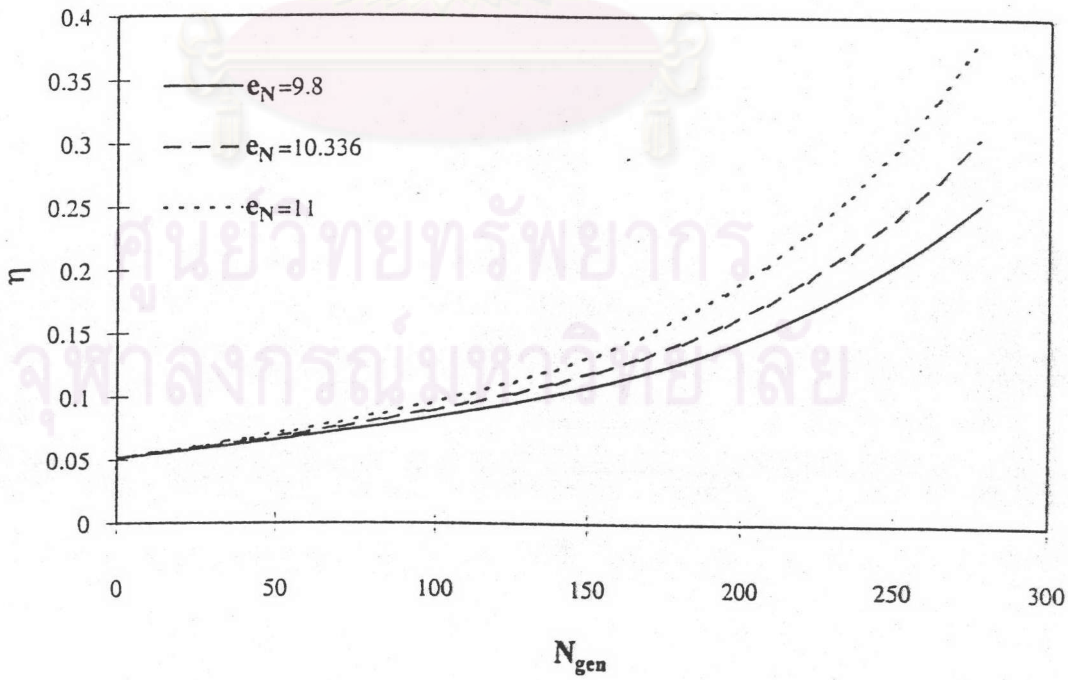

Figure 5.161 Collection efficiency for inertial impaction of R=0.1, St=1, and e'_N=5.01

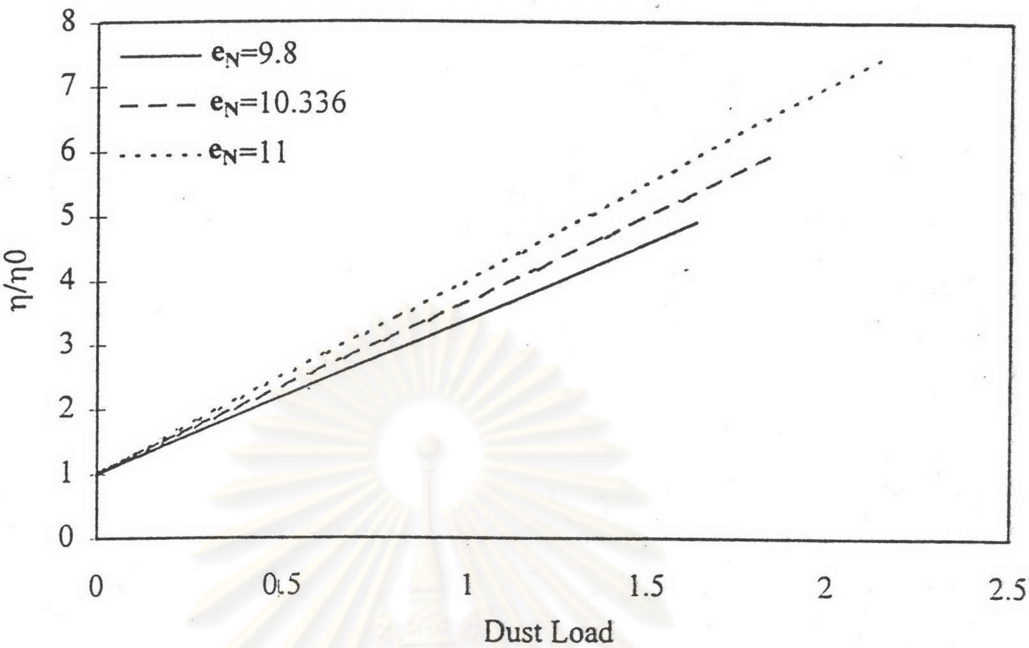

Figure 5.162 Normalized collection efficiency of dust load for R=0.1, St=1, and e'_N=5.01

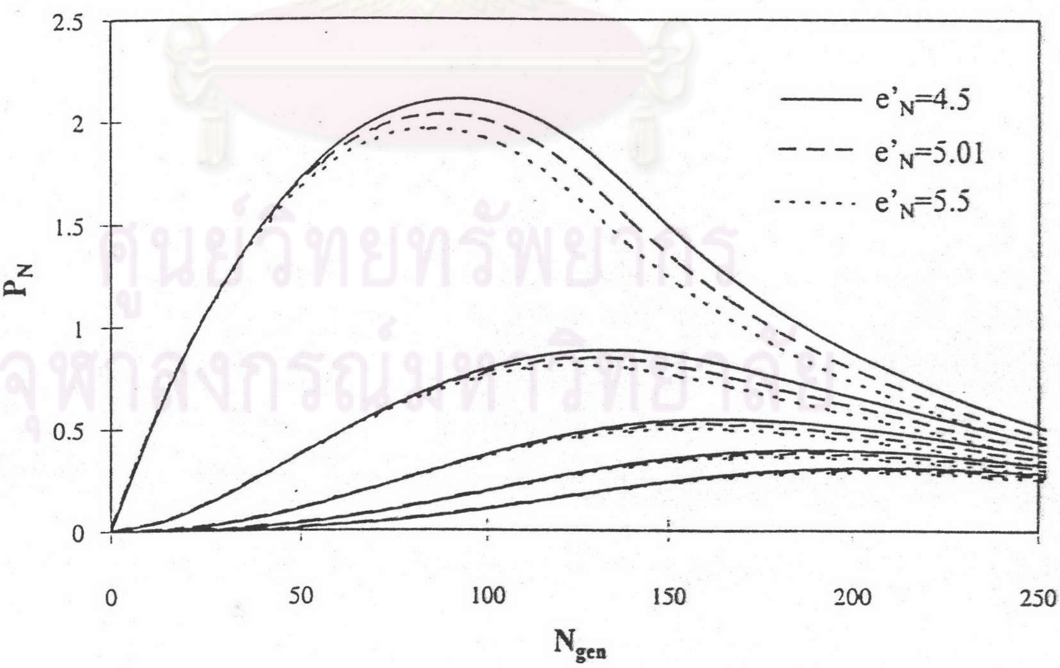

Figure 5.163 Dendrite distribution for inertial impaction of R=0.1, St=1, and e_N=10.336

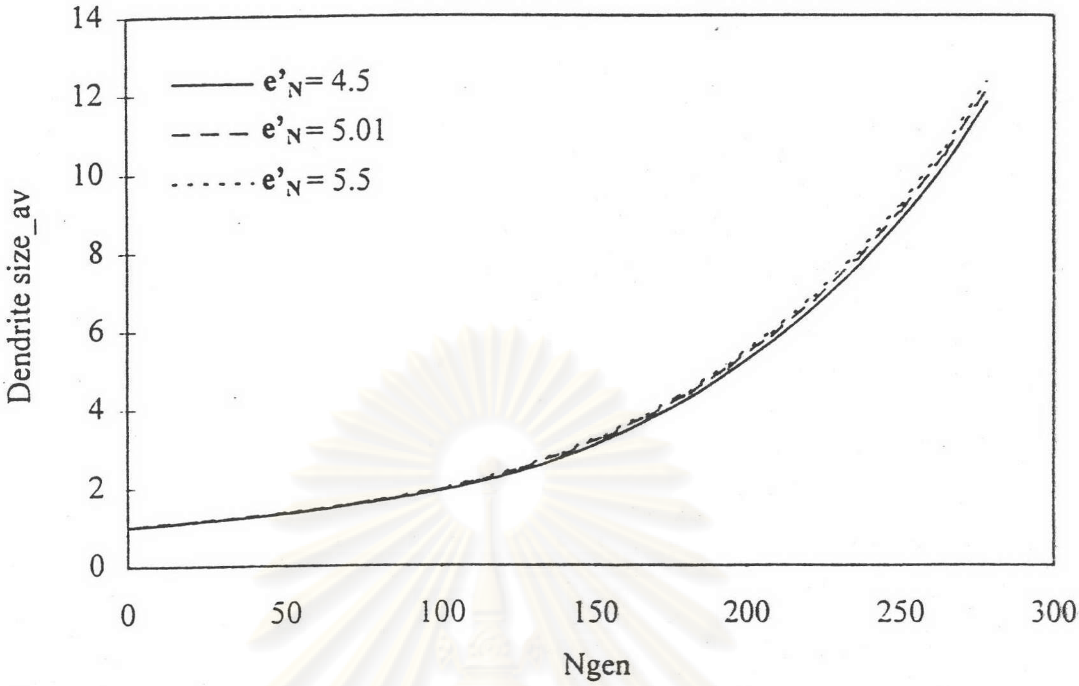

Figure 5.164 Dendrite average size for inertial impaction of R=0.1, St=1, and e_N=10.336

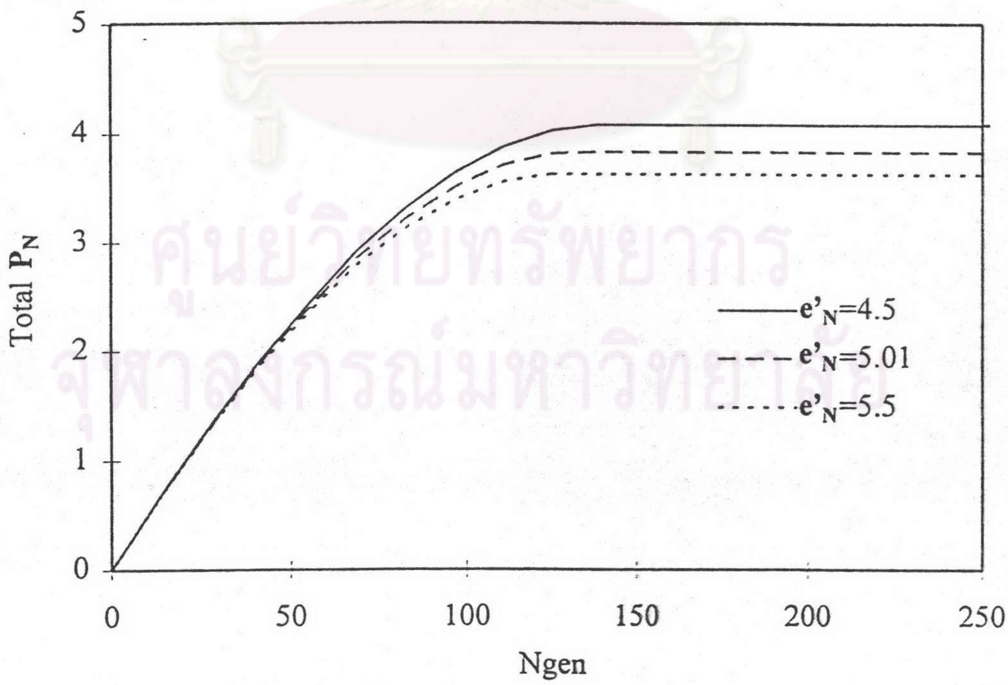

Figure 5.165 Total population of dendrites for inertial impaction (R=0.1, St=1 and e_N=10.336)

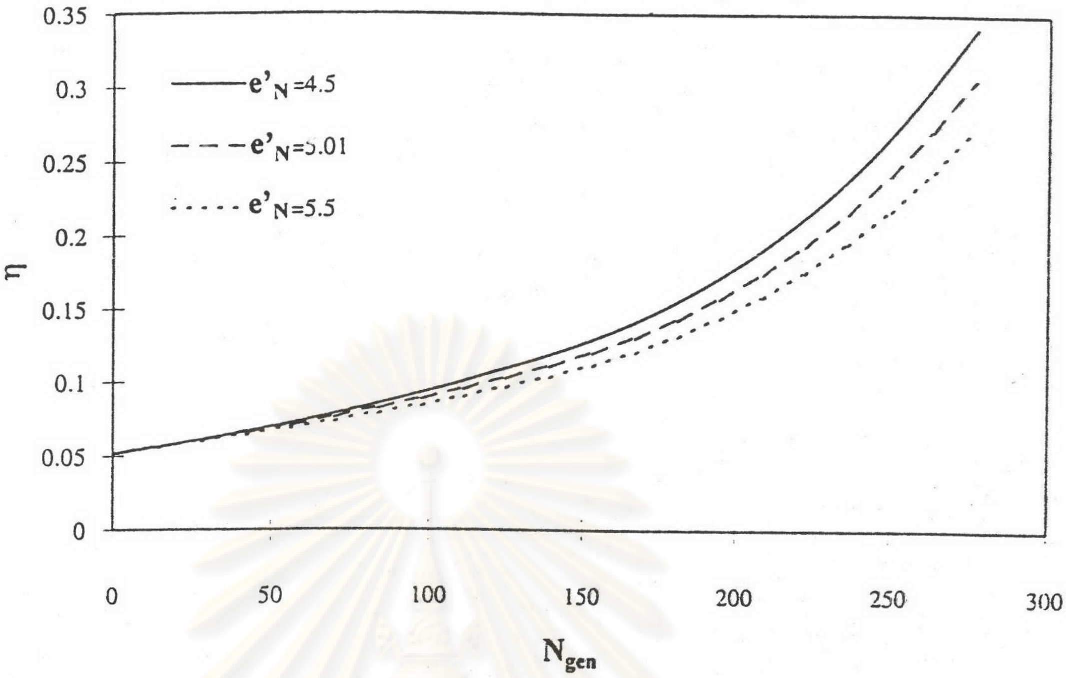

Figure 5.166 Collection efficiency for inertial impaction of R=0.1, St=1, and e_N=10.336

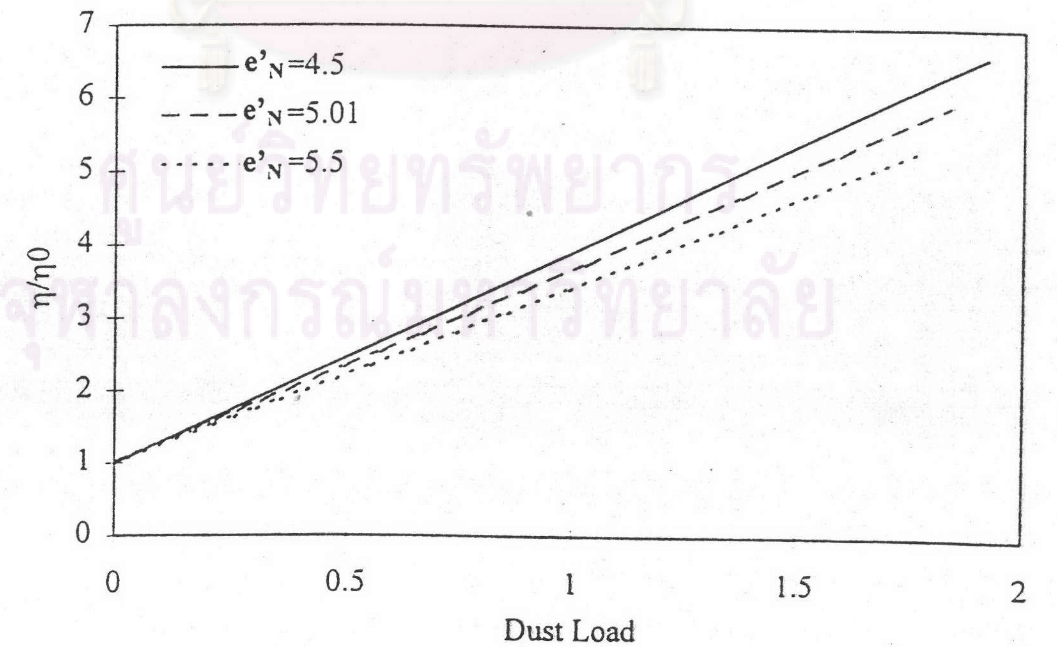

Figure 5.167 Normalized collection efficiency of dust load for R=0.1, St=1, and e_N=10.336

shows the effect of R on η. As seen from the figure, η increased with increasing R. Because the particles were bigger, they were captured more easily. Figure 5.157 shows the effect of R on η/η_0 vs. dust-load. Similarly, η/η_0 increase more slowly as R increased.

5.3.2 Inertial impaction

The dendritic growth was investigated for inertial impaction, the effects of the parameters e_N and e'_N, the Stokes number St, and R on the dendrite distribution, the average dendrite size, the total population of dendrites, λ and η. In this section the effects of the parameters e_N and e'_N for R=0.1 and St=1.0 , the effect of St for R=0.1 , and the effect of R for St=1.0, were investigated.

5.3.2.1 Effects of e_N

When e_N increases, so does the effective capture area. The effect of e_N on the dendrite distribution, the average dendrite size, the total population of dendrites, λ and η were investigated at R=0.1, St=1.0 and e'_N=5.01. Figure 5.158 shows its effect on the dendrite distribution. As seen from the figure, when e_N increased, the dendrite concentration P_N initially increased but subsequently decreased faster. Figure 5.159 shows the effect of e_N on the average dendrite size which increased more rapidly when e_N increased. Figure 5.160 shows the comparative effect of e_N on the total population of dendrites. As seen from the figure, the population number of dendrites becomes smaller when e_N increases. Table 5.17 shows the positive effect of e_N on λ. Figure 5.161 shows its effect on η. As seen from the figure, η increased when e_N increased because its effective capture area increased. Figure 5.162 shows the effect of e_N on η/η_0 vs. dust-load. As seen from the figure, η/η_0 vs. dust load increased also with increasing e_N.

5.3.2.2 Effect of e'_N

Increasing e'_N increases the effective shadow area, so more vacant sites on the fiber surface was shielded. The effects of e'_N on the dendrite distribution, the average dendrite size, the total population of dendrites, λ and η were investigated at R=0.1, St=1.0 and e_N=7.499. Figure 5.163 shows its effect on the dendrite

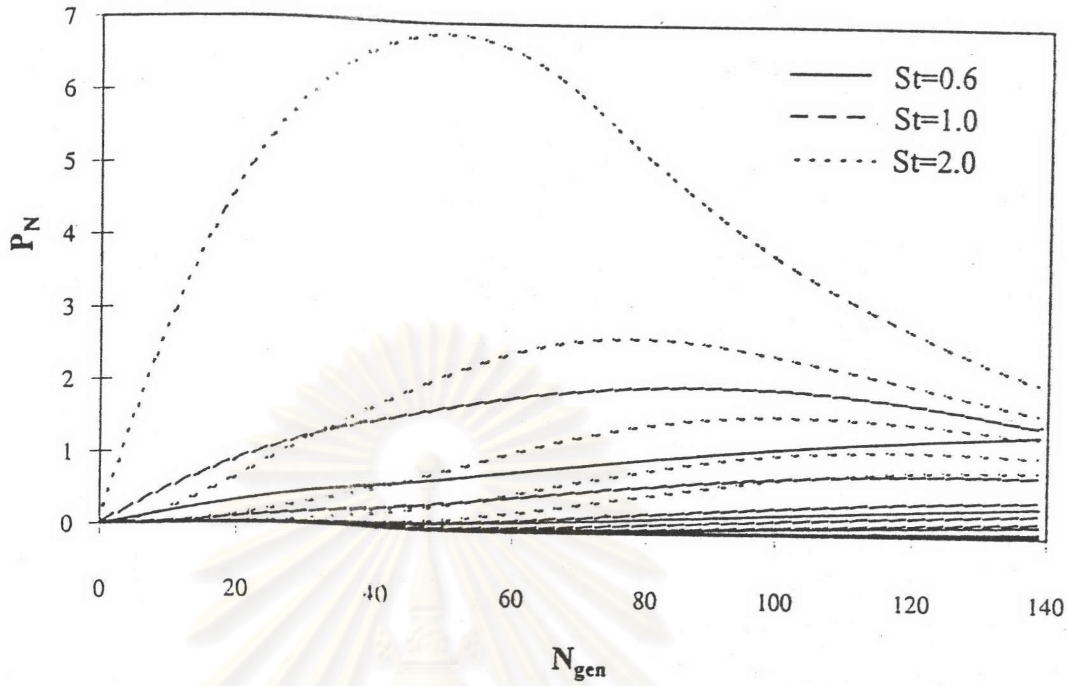

Figure 5.168 Dendrite distribution of inertial impaction with St as parameter for R=0.1

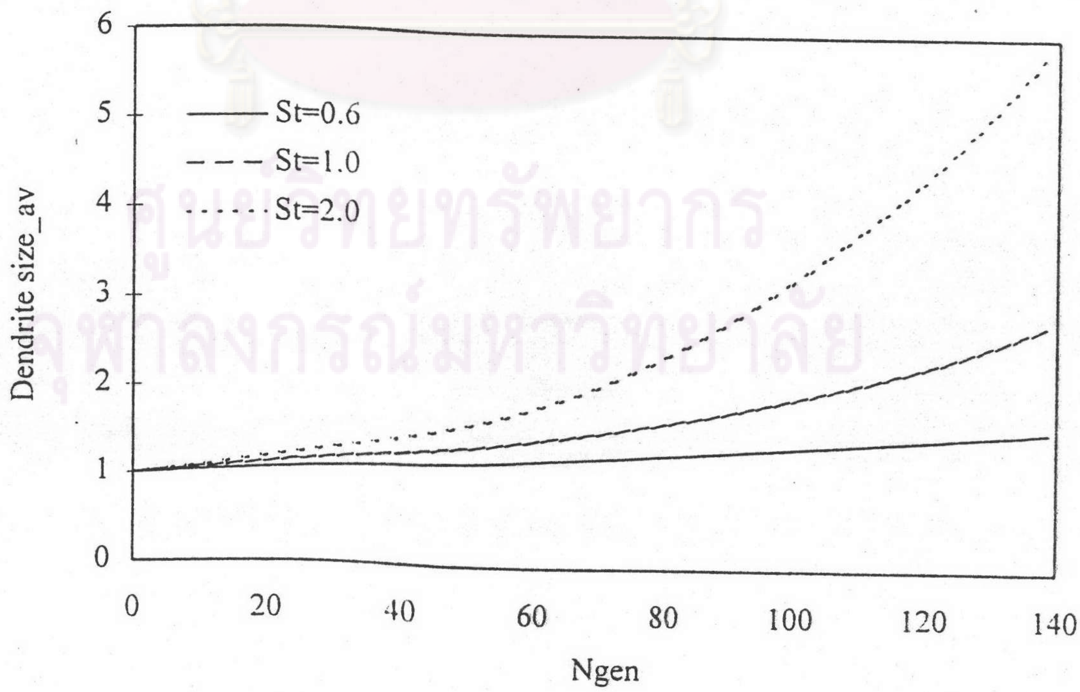

Figure 5.169 Dendrite average size of inertial impaction with St as parameter for R=0.1

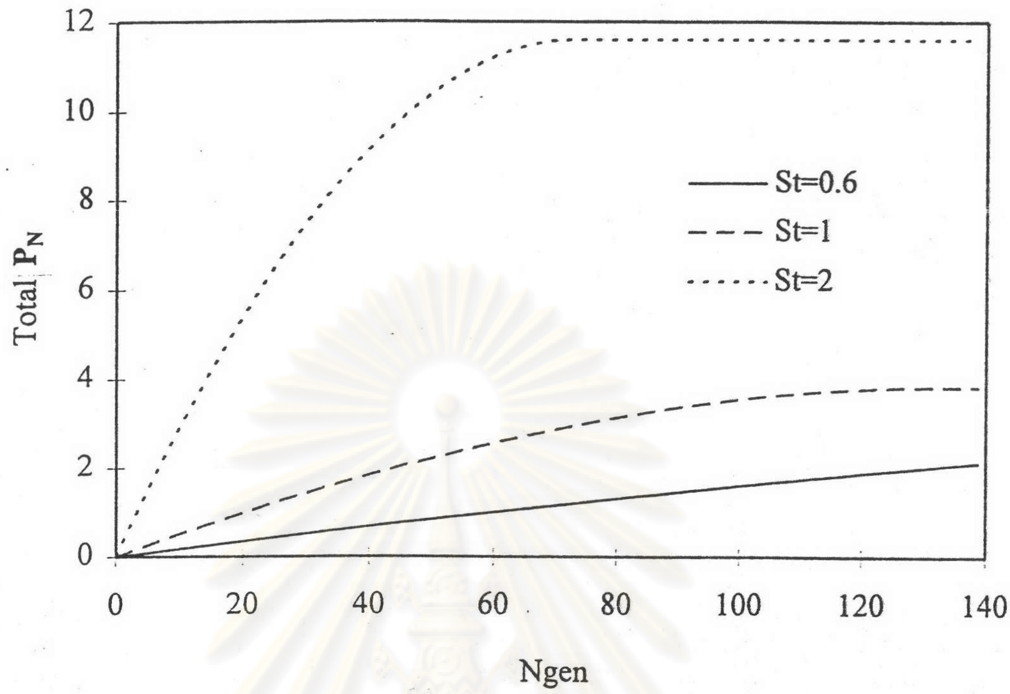

Figure 5.170 Total population of dendrites for inertial impaction (R=0.1)

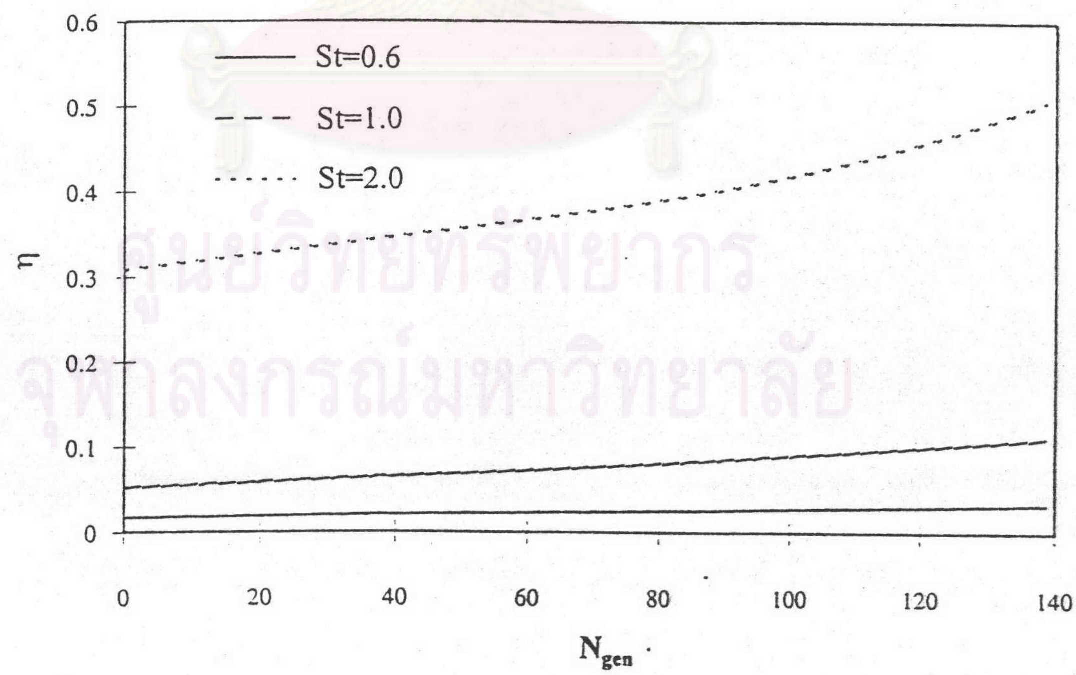

Figure 5.171 Collection efficiency of inertial impaction with St as parameter for R=0.1

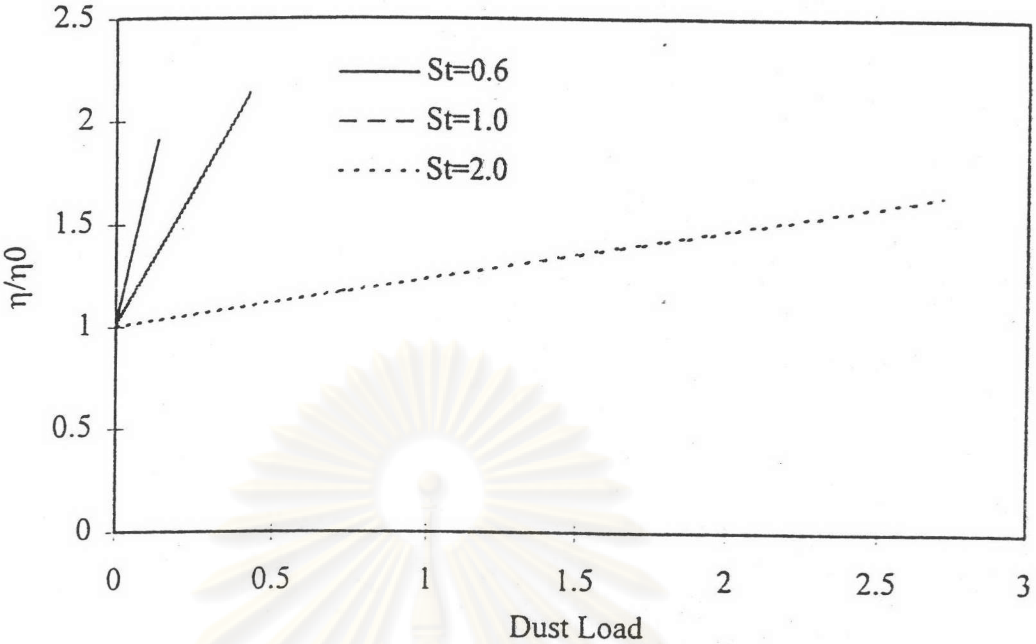

Figure 5.172 Normalized collection efficiency of dust load with St as parameter for R=0.1

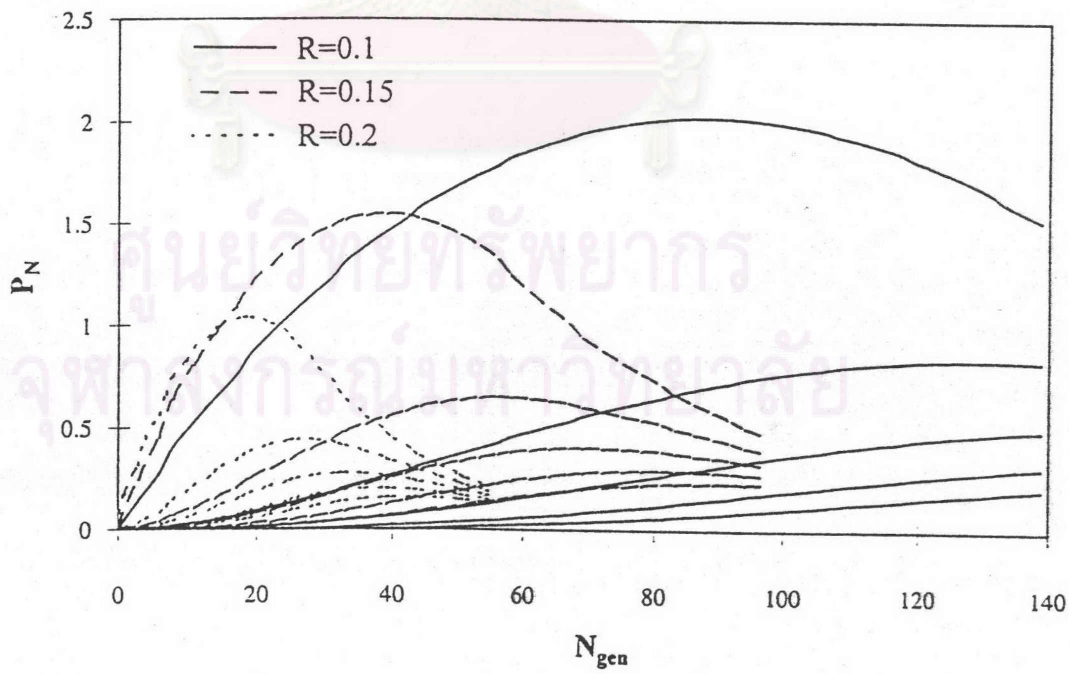

Figure 5.173 Dendrite distribution of inertial impaction with R as parameter for St=1

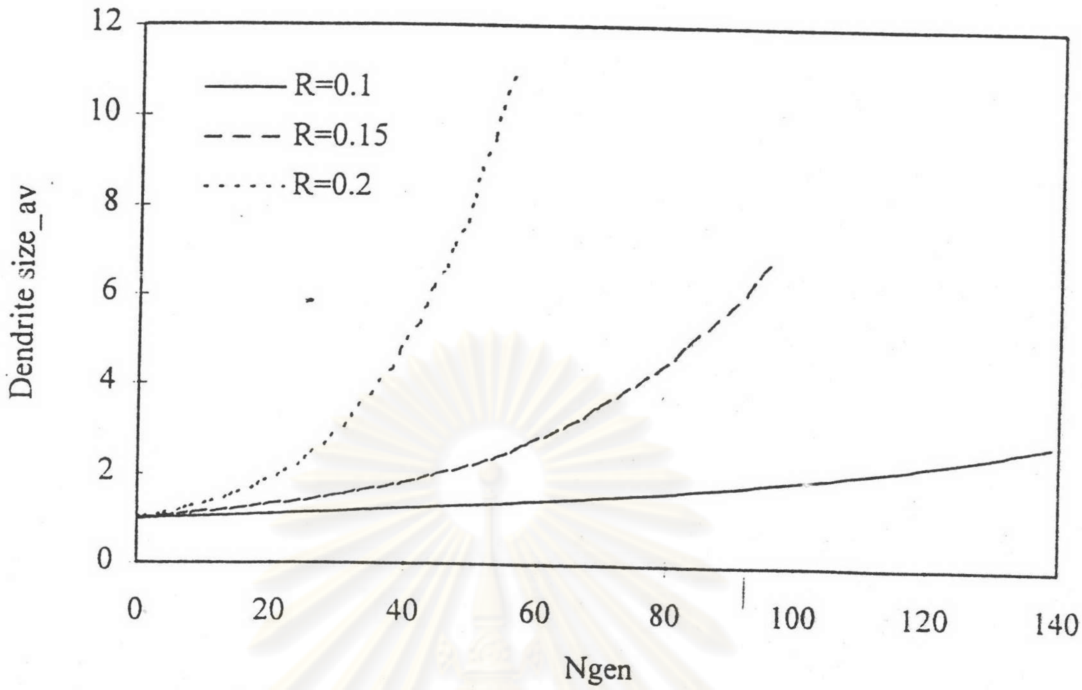

Figure 5.174 Dendrite average size of inertial impaction with R as parameter for St=1

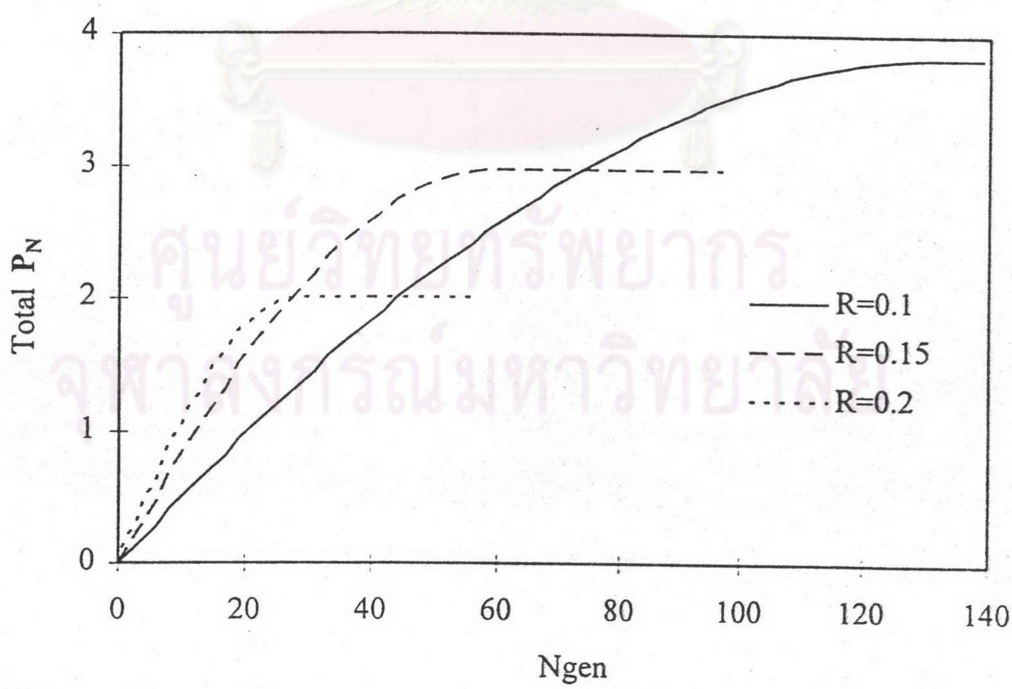

Figure 5.175 Total population of dendrites for inertial impaction (St=1)

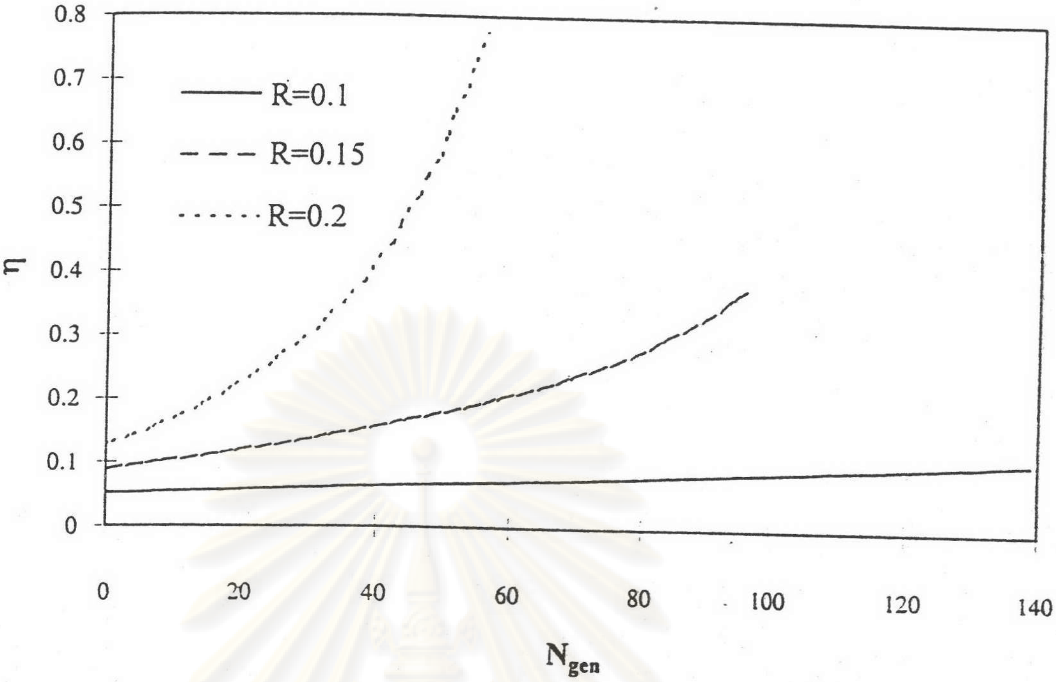

Figure 5.176 Collection efficiency of inertial impaction with R as parameter for St=1

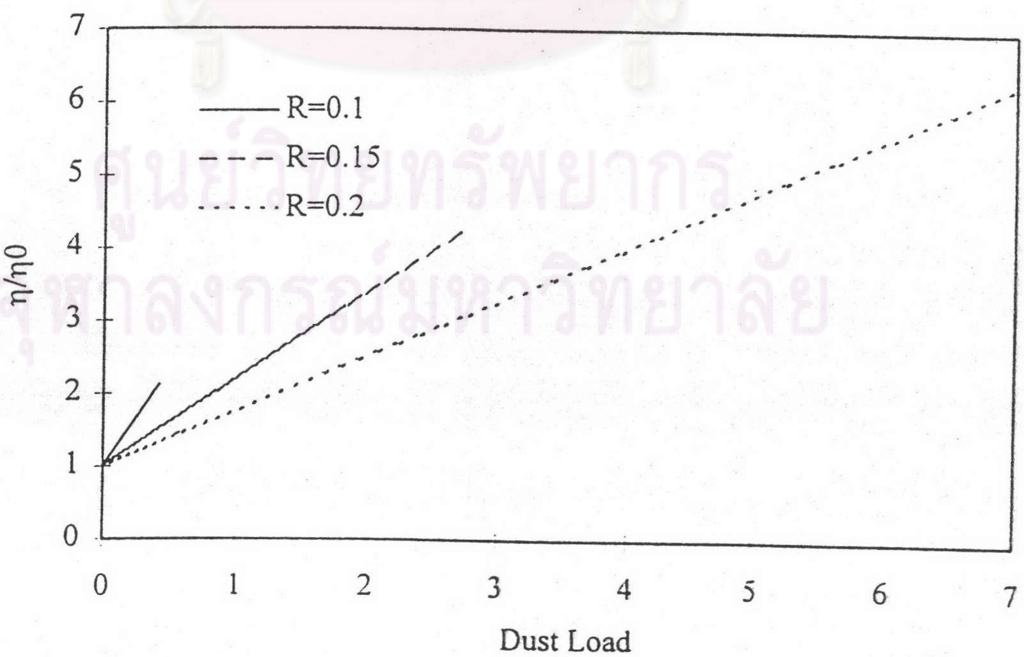

Figure 5.177 Normalized collection efficiency of dust load with R as parameter for St=1

e_N	9.8	10.336	11
λ	2.395	2.663	2.995

Table 5.17 The collection efficiency raising factor λ for R=0.1 St=1 and e'n=5.01

e'_N	4.5	5.01	5.5
λ	2.918	2.663	2.418

Table 5.18 The collection efficiency raising factor λ for R=0.1 St=1 and en=10.336

St	0.6	1	2
e_N	17.453	10.336	2.475
e'_N	3.849	5.01	2.006
λ	6.8020	2.6630	0.2345

Table 5.19 The collection efficiency raising factor λ for R=0.1

R	0.1	0.15	0.2
e_N	10.336	6.299	5.288
e'_N	5.01	2.739	2.287
λ	2.6630	1.1867	0.7503

Table 5.20 The collection efficiency raising factor λ for St=1

distribution. As seen from the figure, the dendrite concentration P_N increase a little initially but subsequently decreased faster. Figure 5.164 shows the effect of e'_N on the average dendrite size. The average dendrite size increased a little faster with increasing e'_N. Figure 5.165 shows the comparative effect of e'_N on the total population of dendrites. As seen from the figure, the population of dendrites also becomes smaller when e'_N increases. Table 5.18 shows the negative effect of e'_N on λ. Figure 5.166 shows the effect of e'_N on η. As seen from the figure, η increased more slowly with increasing e'_N. Figure 5.167 shows the effect of e'_N on η/η_0 vs. dust-load. As seen from the figure, η/η_0 increase more slowly as e'_N increased

5.3.2.3 Effects of St

The effects of St was investigated for R=0.1 and the parameters e_N and e'_N shown in Table 5.6. Figure 5.168 shows the effect of St on the dendrite distribution. The dendrite concentration P_N increased faster as St increased. Figure 5.169 shows effect of St on the average dendrite size. As seen from the figure, the average dendrite size increased a little faster with increasing St. Figure 5.170 shows the effect of St on the total population of dendrites. As seen from the figure, the population of dendrites becomes much larger when St increases. Table 5.19 shows the effect of St on λ. λ decreased because η_0 increased with increasing St. Figure 5.171 shows the effect of St on η. As seen from the figure, η increased faster with increasing St because the particles were captured more easily. Figure 5.172 shows the effect of St on η/η_0 vs. dust-load. As seen from the figure, η/η_0 increased with increasing St.

5.3.2.4 Effect of R on the model

As in the case of convective diffusion, increasign R increased the particle collection efficiency. The effect of R was investigated for St=1.0 and the parameters e_N and e'_N shown in Table 5.6. Figure 5.173 shows the effect of R on the dendrite distribution. As seen from the figure, the dendrite distribution curves packed sooner but lower because it was sufficient to capture lies particles when R was large. Figure 5.174 shows the effect of R on the average dendrite size. The average dendrite size increased faster when R increased. Figure 5.175 shows the effect of R on the total population of dendrites. As seen from the figure, when Ngen is small (less than 20), the total population of dendrites at a lower R is smaller than that at a higher R. However, as times passes, the total population of dendrites at a larger R attains a larger asymptotic size. However. in Table 5.20, λ decreased with increasing R. Figure 5.176 shows the effect of R on η. As seen from the figure, η increased significantly with increasing R because large particles were captured more easily. Figure 5.177 shows the effect of R on η/η_0 vs. dust-load. As seen from the figure, η/η_0 increased faster with increasing R.